AD NUMBER
AD909258
NEW LIMITATION CHANGE

TO

Approved for public release, distribution unlimited

FROM

Distribution authorized to U.S. Gov't. agencies only; test and evaluation; 27 Sept 1972. Other requests shall be referred to AF Flight Dynamicss Laboratory, [FYS], Wright-Patterson Air Force Base, Ohio 45433.
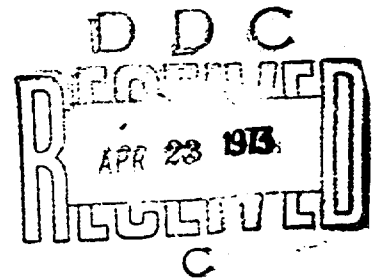
AUTHORITY

AFWAL ltr 1 Mar 1982.

AFFDL-TR-72-116

AD909258

ACTIVE FLUTTER SUPPRESSION SYSTEMS FOR MILITARY AIRCRAFT A FEASIBILITY STUDY

William E. Triplett
Hans-Peter F. Kappus
Robert J. Landy

D D C

APR 23 1973

C

MCDONNELL AIRCRAFT COMPANY
MCDONNELL DOUGLAS CORPORATION
SAINT LOUIS, MISSOURI

TECHNICAL REPORT AFFDL-TR-72-116

FEBRUARY 1973

NOTICE

When Government drawings, specifications, or other data are used for any purpose other than in connection with a definitely related Government procurement operation, the United States Government thereby incurs no responsibility nor any obligation whatsoever; and the fact that the government may have formulated, furnished, or in any way supplied the said drawings, specifications, or other data, is not to be regarded by implication or otherwise as in any manner licensing the holder or any other person or corporation, or conveying any rights or permission to manufacture, use, or sell any patented invention that may in any way be related thereto.

Copies of this report should not be returned unless return is required by security considerations, contractual obligations, or notice on a specific document.

ACTIVE FLUTTER SUPPRESSION SYSTEMS
FOR MILITARY AIRCRAFT
A FEASIBILITY STUDY

William E. Triplett
Hans-Peter F. Kappus
Robert J. Landy

FOREWORD

This report covers work conducted from April 1971 to August 1972.

This report was submitted by the authors on 7 August 1972.

This technical report has been reviewed and is approved.

WALTER J. MYKYTOW
Asst. for Research and Technology
Vehicle Dynamics Division
AF Flight Dynamics Laboratory

ii

ABSTRACT

This analytical study of active flutter suppression systems for military aircraft was directed toward the accomplishment of two broad objectives:

1. Establish flutter modes, configurations, and flight conditions where active flutter control can show an advantage.

2. Formulate design guidelines and criteria to implement and test active flutter suppression systems.

To accomplish these broad objectives the study effort was divided into the three separate investigations listed below:

1. Wing/store flutter control study - to assess the practicality of extension of flutter boundaries for several store combinations.

2. All-movable horizontal tail flutter control study - to investigate both the potential payoff in future aircraft and the unique problems and difficulties when one of the participants in the flutter mechanism is used as the flutter control force producer.

3. Wing flutter control study - to parametrically evaluate the potential payoff in future aircraft by active flutter control of flutter critical primary lifting surfaces.

The studies showed that active flutter suppression systems are feasible and practical for any flutter mode which can be classified as mild or moderate flutter. Nearly all wing/store flutter cases are in this category. The advanced aircraft wing and horizontal tail configurations can be actively controlled if the aeroelastic system is first "tamed" by balance weight. It was found that the flutter control system could work successfully despite realistic hardware limitations and system nonlinearities in a turbulent environment. It was also determined that a fighter aircraft flight control system and the flutter control system can share components and coexist with minimal interference.

TABLE OF CONTENTS

LIST OF ILLUSTRATIONS

LIST OF TABLES

LIST OF ABBREVIATIONS AND SYMBOLS

ABBREVIATIONS

AC	Alternating Current
ACF	Active Control of Flutter
BL	Buttline
CCW	Counter-Clockwise
CPAC	Passive Analog Computer
c.g.	Center of Gravity
CP	Center of Pressure
COPS	Computerized Optimization Procedure for Stabilators
CVU	Computer Voting Units
CW	Clockwise
dB	Decibels $= 20 \log_{10}$ (Amplitude Ratio)
DC	Direct Current
EI	Bending Stiffness
FB	Feedback
GJ	Torsional Stiffness
Hz	Hertz = cycles per second
KEAS	Knots Equivalent Air Speed $= V\sqrt{\rho/\rho_{SL}}$
LVDT	Linear Variable Differential Transformer
MATLOC	Root Locus Computer Program
MAU	Miscellaneous Armament Unit
MER	Multiple Ejector Rack
MIMAC	Acronym for "MIMAC - McDonnell Douglas Automation Company"
MUG	Mass Expressed as (pound - seconds^2)/inch
PC1, PC2	Hydraulic Power Control Systems One and Two
RHP	Right Half Plane
rms	Root Mean Square
SAS	Stability Augmentation System
SFCS	Survivable Flight Control System
SL	Sea Level
T/R	Transformer Rectifier

SYMBOLS

A, A_C	Noncirculatory and circulatory aerodynamic stiffness derivative matrices used in Indicial Lift flutter equations
A_i	Scalar coefficients in Wagner function
A	Complex aerodynamic stiffness derivative matrices used in $(R+iI)$ flutter equations
a_i, a_{ij}	Numerator coefficients of control system transfer functions
a	Speed of sound
B, B_C	Noncirculatory and circulatory aerodynamic damping derivative matrices used in Indicial Lift flutter equations
B_i	Exponent coefficients in Wagner function
B	Complex aerodynamic damping derivative matrices used in the $(R+iI)$ flutter equations
b_i, b_{ij}	Denominator coefficients of control system transfer functions
b	Primary lifting surface reference semichord
C	Viscous damping derivative matrix
$C(k)$	Theodorsen function
$C^{-1}(k)$	Time domain equivalent of the Theodorsen function
C_i	Exponential coefficients in Wagner function $= \frac{V}{b} B_i$
C_{L_α}	Aerodynamic lift curve slope with respect to angle of attack
C_β	Damper coefficient for aileron rotation mode
$\frac{C}{R_i}$	Closed-loop transfer functions
e	Base of Naperian logrithms
F	Excitation force
$F(k)$	Real part of Theodorsen function
$G(k)$	Imaginary part of Theodorsen function
$G_i(S)$	Forward control loop transfer functions
g	Equivalent structural damping coefficient
g	Acceleration of gravity
$H_i(S)$	Feedback control loop transfer functions
h, $\dot{h}$	Deflection vector and rate

I	Aerodynamic inertia derivative matrix
I	Mass moment of inertia
I	Imaginary aerodynamic coefficient matrix in $(R+iI)$ flutter equations
i	$\sqrt{-1}$
J_0, J_1	J Bessel functions of the first and second kind
K	Structural stiffness derivative matrix
K_i	Control system gains
K_β	Stiffness coefficient for aileron rotation mode
k	Reduced frequency parameter in $(R+iI)$ flutter equation $= \dfrac{\omega b}{V}$
L	Aerodynamic lift vector
L, l	Distance measure
M	Inertia derivative matrix
M	Mach Number $= V/a$
M, m	Mass, both discrete and generalized
m'	Mass per unit length
P	Poles of control system open-loop transfer function
Q	Freestream dynamic pressure $= \dfrac{1}{2}\rho V^2$
$\dot{q}$, $\ddot{q}$, q	Generalized coordinates, rates, and accelerations with respect to time for both rigid and flexible modes (also used in the forms q_i and $q(t)$)
q_{F_i}	Coordinates for degrees of freedom used for excitation
$\left\{ \dfrac{\partial F}{\partial q_{F_i}} \right\}$	Column matrices of generalized force in each generalized coordinate mode in response to excitation coordinate q_{F_i}
$\left(\dfrac{\partial out}{q_{F_i}} \right)$	Complex frequency response function of displacement, rate, or acceleration in response to excitation coordinate q_{F_i}
R	Real aerodynamic coefficient matrix in $(R+iI)$ flutter equations
R	Perfect gas constant
R	Effective gain of transfer function $y(s)$

R	Radius vector from the origin in the complex plane
S	Laplace variable used as $i\omega$
s	Nondimensional time $= \dfrac{V}{b} t$
t	Time
T_i	Time constants in transfer functions
V	Aircraft forward velocity
V_F	Flutter onset velocity
X_i	Control system variables
Y_0, Y_1	Y Bessel functions of the first and second kind
y(s)	Transfer function representation of the Wagner function
Z	Zeros of control system characteristic equation
α	Primary surface streamwise angle of attack attributable to twist (also used for total aircraft angle of attack)
β	Control surface flexible deflection angle
γ	Ratio of specific heats
δ	Control surface actuator deflection angle
ζ	Damping coefficient $= g/2$
θ	Angle of radius vector in the complex plane
λ	Normalized eigenvalues in (R+iI) flutter solution
μ	Mass ratio – aerodynamic to structure
ρ	Air density
σ	Nondimensional time $= \dfrac{V}{b} \tau$
σ_0	Normalized inertia derivatives in (R+iI) flutter solution
τ	Time
τ_i	Time constants in transfer functions
$\phi(S)$	Laplace transform of the Wagner function $\phi(t)$
$\phi(s)$	Wagner function $= 1 - A_1 e^{-B_1 s} - A_2 e^{-B_2 s}$
$\phi(t)$	Wagner function $= 1 - A_1 e^{-C_1 t} - A_2 e^{-C_2 t}$
ϕ_i	Participation coefficients (weighting function) for each generalized coordinate in the response function $(0_{out}/q_{F_i})$

ϕ	Aircraft response – general expression
Ω	Normalized stiffness derivatives in (R+iI) flutter solution
ω	Parametric excitation frequency
ω_o	Reference frequency for (R+iI) flutter solution
[ ]	Square and rectangular matrix notation
{ }	Column matrix notation

SUBSCRIPTS

A	Aircraft (full scale)
C	Command
FB	Feedback
i, j	Indices
M	Measured
M	Model
RHP	Right half plane

1. INTRODUCTION

1.1 Background

Considerable progress has been made in the past several years in applying active control principles for the reduction of the responses of "rigid body" and "low frequency" structural modes of large flexible aircraft in atmospheric turbulence. Emphasis has been given to this approach when increased structural loads and fatigue rates were experienced by aircraft flying through turbulent air.

In the mid-1960's, the Air Force initiated several programs to study, design, and flight test an active system that would reduce fatigue damage rates, improve airplane handling qualities, and reduce peak loads. One of these programs developed a stability augmentation system to improve dutch roll damping, reduce structural loads, and improve the controllability of the B-52 aircraft in turbulence. A further extension of these concepts known as LAMS (Load Alleviation and Mode Stabilization-Reference 1) demonstrated by flight tests on the B-52, an active system that alleviated gust loads and controlled the response of some elastic structural modes. Generally, tests indicated that fatigue damage rates were improved while retaining or improving the handling and ride qualities of the aircraft. Another program, References 2 and 3, in this technical area provided a modal suppression system for the XB-70 supersonic aircraft. The ILAF system (Identically Located Accelerometer and Force) employed on the XB-70 was designed to damp the structural motion induced by turbulence and improve the ride qualities at the pilot station. Flight tests on the XB-70 were exploratory but indicated that a flexible-mode stabilization system is operationally feasible.

This study is a logical extension of these concepts. It evaluates the feasibility of active flutter suppression systems for military aircraft. The active flutter control concept employs the features of an automatic feedback control system, possibly in conjunction with more conventional passive methods, to preclude flutter. The flutter onset velocity is delayed with this concept by cycling an aerodynamic force producing element, such as an aileron, in a manner which stabilizes the flutter mechanism. The command to the force producing element is generated by the compensated signal of a sensor, either mechanical or electrical, which detects deformation of the primary surface.

1

1.2 Study Objectives

This analytical study of active flutter suppression systems for military aircraft was directed toward the accomplishment of two broad objectives:

1. Establish flutter modes, configurations, and flight conditions where active flutter control can show an advantage.
2. Formulate design guidelines and criteria to implement and test active flutter suppression systems.

Three basic types of flutter mechanisms were examined: wing/store, horizontal tail, and bare wing. The study vehicles were restricted to supersonic fighter aircraft with moderate aspect ratio surfaces. Conventional all-aluminum as well as advanced composite material structures were analyzed. Factors such as deformation sensor type and location, compensation design, hardware performance requirements, and flight safety were considered in the synthesis of the active flutter control schemes.

2. STUDY CONFIGURATIONS

These studies examine the feasibility of actively suppressing three familiar types of aircraft flutter: 1) wing/store flutter; 2) horizontal tail flutter; 3) bare wing flutter. The configurations analyzed are presented in the following sections.

2.1 Wing/Store Study Configurations

The F-4 aircraft was selected for examining the feasibility of active wing/store flutter control since it carries a large number of different store types exhibiting a wide variation of dynamic properties and flutter mechanisms. Instances of mild wing/store flutter have been documented during flight testing and several stores are currently subject to flutter velocity placards. The specific stores examined in this study are: 370 gallon external fuel tanks - 90%, 62%, and 31% full configurations; MK-84 FO, a 2000 lb laser-guided (smart) bomb; and the MK-82, a 500 pound general purpose bomb. The mass and inertial characteristics of these stores are listed in Table 1. Because of the wide variation in these properties, the general trends determined for these stores should be representative of most wing/store flutter mechanisms encountered on other low-to-moderate aspect ratio fighters with supersonic capability.

2.1.1 _F-4 Wing Description_ - The F-4 wing is constructed entirely of aluminum. Since the wing was strength designed there has been no attempt to weight optimize the wing structure with regard to aeroelastic constraints. A description of the F-4 wing-pylon structural models used in these studies is given in Appendix I. A two-view sketch of the F-4 aircraft with a 370 gallon tank at buttline (BL) 132.5 is shown in Figure 1. The stores under consideration in this study are all carried at the BL 132.5 location. The sketch indicates that the F-4 lateral control surfaces (aileron and spoiler) are situated at precisely the same spanwise location as the stores. These surfaces are, thus, ideally located to suppress a wing/store flutter instability since they can counteract store moments where they are passed into the wing. The leading edge flap is not suitable for active flutter control since it has only two positions (full off-full on) and cannot be cycled at frequencies exceeding 1 Hz.

The flight envelope of the F-4 is given in Figure 2 for the no stores and full stores (60,000 pound gross weight) configurations. Indicated in the envelope is the 550 KEAS flutter placard currently in effect for an F-4

TABLE 1 SUMMARY OF STORE PROPERTIES

Configuration	Mass Mugs	I Pitch[3] Mug-in²	I Yaw[3] Mug-in²	I Roll[3] Mug-in²	Store CG Location FS	Store CG Location BL	Store CG Location WL
370 Gallon Fuel Tank[2]							
90% Full	6.507	12947.2	18480.0	507.0	335.	132.5	-17.2
62% Full	4.737	5003.0	6444.0	411.96	326.9	132.5	-17.1
31% Full	2.672	1728.0	4026.0	245.04	328.5	132.5	-17.2
MK-84 EO Guided Bomb, Max Weight-Min Inertia-Fwd CG	6.086	5642.5	5642.5	291.6	352.	135.3	-16.9
MK-82 500# Bomb[1] MER Rack Locations 3 and 4	3.321	7950.0	7974.0	90.94	341.	126.8	-14.8

NOTES:

1. Bombs 3 and 4 in combination with MER Rack treated as one store.
2. Fuel assumed to be liquid.
3. All inertias are referenced to store CG.
4. FS, BL, WL refer to F-4 aircraft Fuselage Station, Buttline, and Waterline, respectively.

4

Spoiler

Aileron

L.E. Flap

Pylon
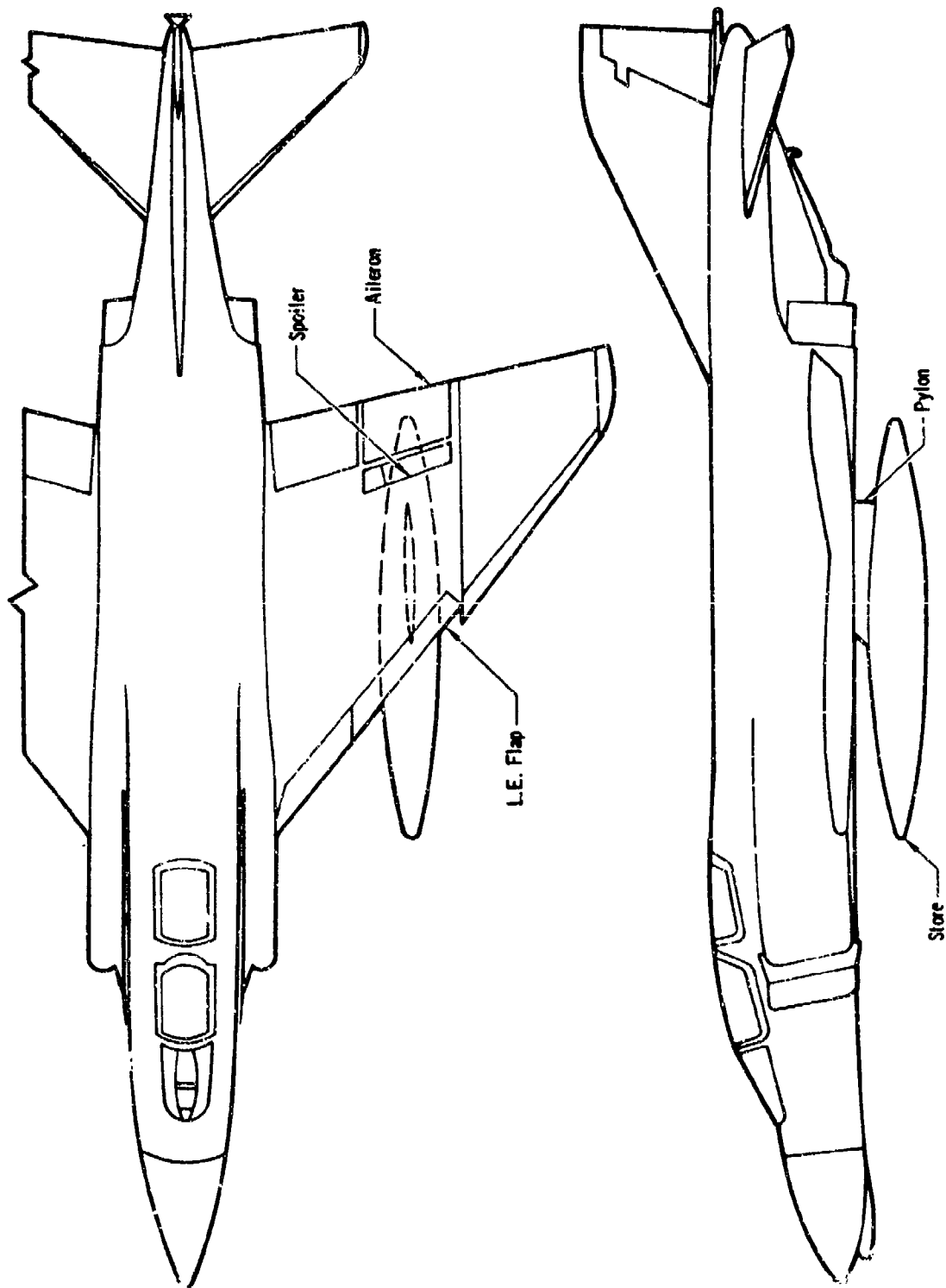
Store

FIGURE 1 F-4 WITH EXTERNAL STORE AT OUTBOARD STORE STATION (BL 132.5)

5
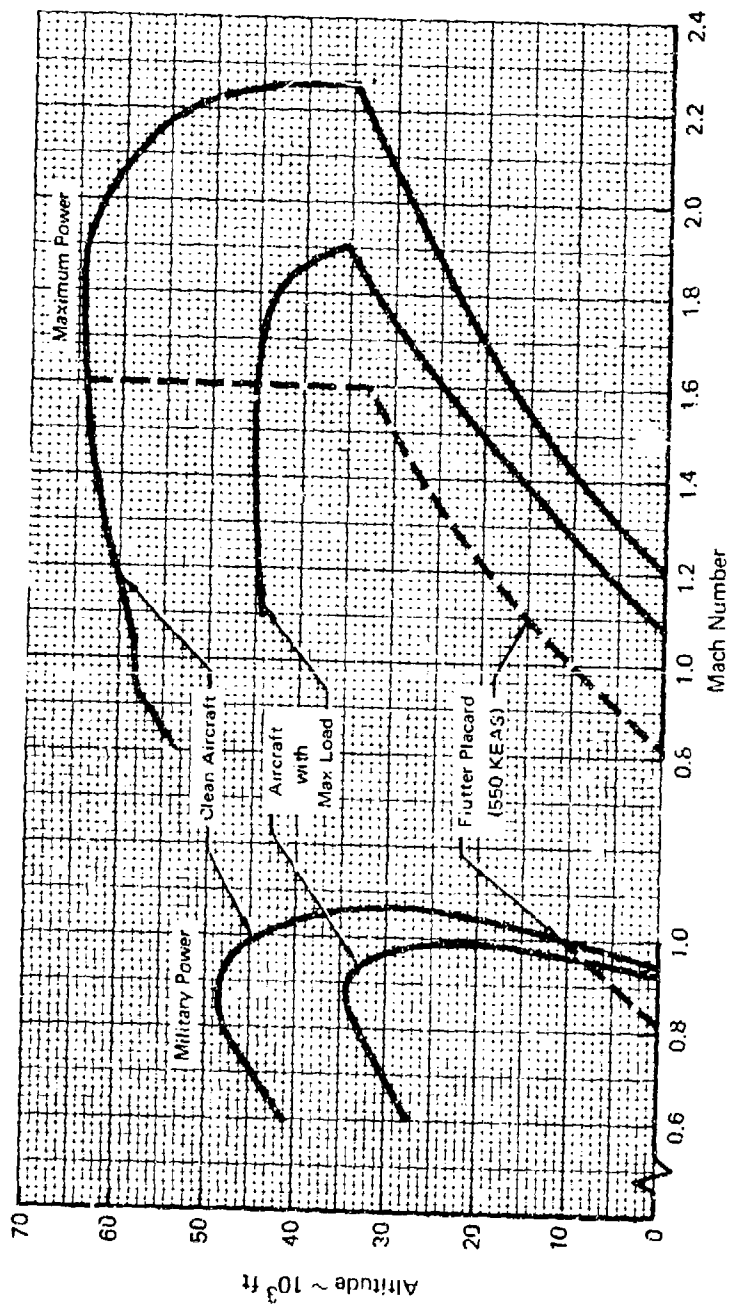
FIGURE 2 F-4 OPERATIONAL FLIGHT ENVELOPE WITH 370 GALLON
EXTERNAL FUEL TANKS

6

with these stores.

2.1.2 **370 Gallon Fuel Tank** – The 370 gallon external tanks are carried during heavy store carry missions which require the use of the afterburner during take-off to shorten ground-roll. The external fuel supply is generally used before the fuselage/internal-wing supply, and the external tanks are jettisoned when empty. The geometry of the 370 gallon-three compartment-external fuel tanks carried as a single store at the BL 132.5 store stations is described in Figure 3. The external tanks are attached to the wing with special tank pylons. Weight information, geometry, and a tabulation of flight and ground tested configurations are given in the figure. The tank fuel loadings: 90%, 62%, and 31% full; are examined in this study.

The 90% configuration was selected for analysis because it is a flight verified minimum flutter velocity case. The 62% and 31% cases are examined also to get a complete picture of how changing inertia and mass characteristics affect the ability to control flutter. The pitch inertia values given in Table 1 have been adjusted to account for fuel slosh effects.

2.1.3 **MK-84 EO** – The MK-84 EO Laser Guided Bomb is used against fixed point targets which are illuminated by a laser beam. The bomb can alter its trajectory with movable steering fins to follow the laser beam. The MK-84 EO, which is carried as a single store by the Miscellaneous Armament Unit (MAU-12) pylon at BL 132.5, is shown in Figure 4. The nose-mounted laser sensing/guidance unit is not shown. The store characteristics given in the figure correspond to the maximum weight, minimum pitch inertia, and most forward c.g. normally encountered in production versions of the MK-84. This particular combination of bomb properties results in a minimum of flutter onset velocity.

2.1.4 **MK-82** – Up to six MK-82, 500 pound bombs can be carried under each wing. The bombs are carried as shown in Figure 5 with the Multiple Ejector Rack (MER) which is in turn attached to the MAU-12 pylon. The rack attaches to the pylon in the forward shifted position. This maintains the aircraft c.g. within specified limits. The bombs can be released one at a time or in a "ripple mode". The numbers in the figure indicate the order of bomb release. Release alternates from wing to wing - i.e., bomb 1/right wing then bomb 1/left wing, etc. The specific configuration analyzed was with bombs 5 and 6 only (inboard MER shoulder) on the left hand wing. This configuration occurs on the left wing near the end of the release sequence whenever a full MK-82 load is carried. This load condition corresponds to the inboard bombs - 3 and 4 - on the right hand wing. A symmetric loading condition was assumed for the flutter analysis.

7

Weight Information (Per Side):

370 gal. Empty Tank and Pylon — Approx. 327 lb.
370 gal. Full Tank and Pylon — Approx. 2856 lb.

FIGURE 3 370 GALLON FUEL TANK MOUNTED AT BL 132.50

Flight Flutter Test Configurations	Ground Vibration Test Configurations
Full Fuel	Full Fuel
81% Full Fuel	
62% Full Fuel	62% Full Fuel
31% Full Fuel	31% Full Fuel
Empty	Empty

FS 370.121
FS 340.126

BS 130.880
BS 77.025
BS 47.025
BS −12.400

A
A

Section A-A

WL 4.053

Wing Moldline

10.7 in.

7.5°

25°

9 in.

10.4 in.

Inboard

2.754 in.
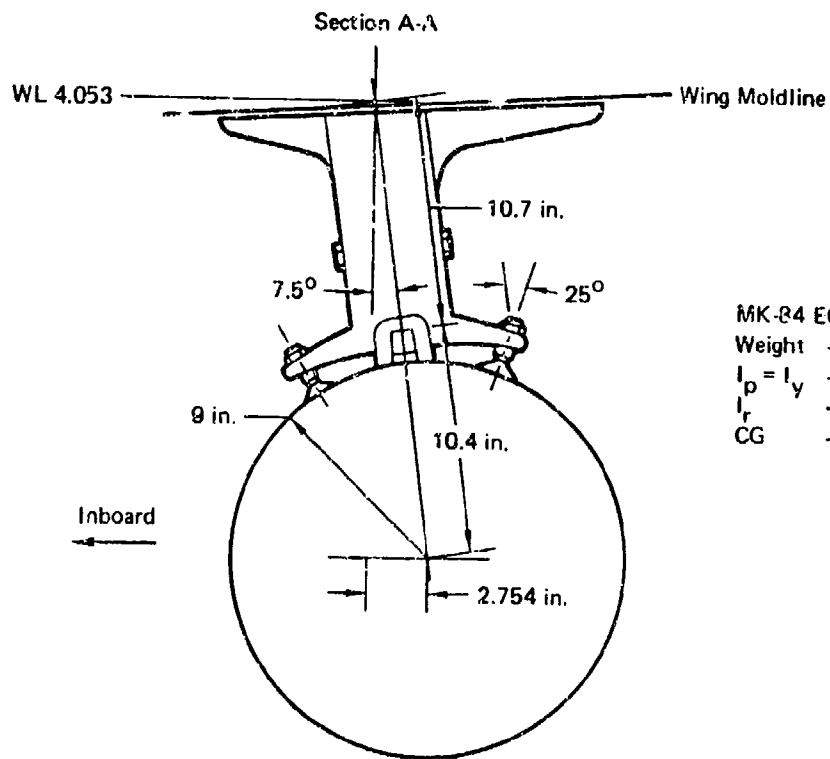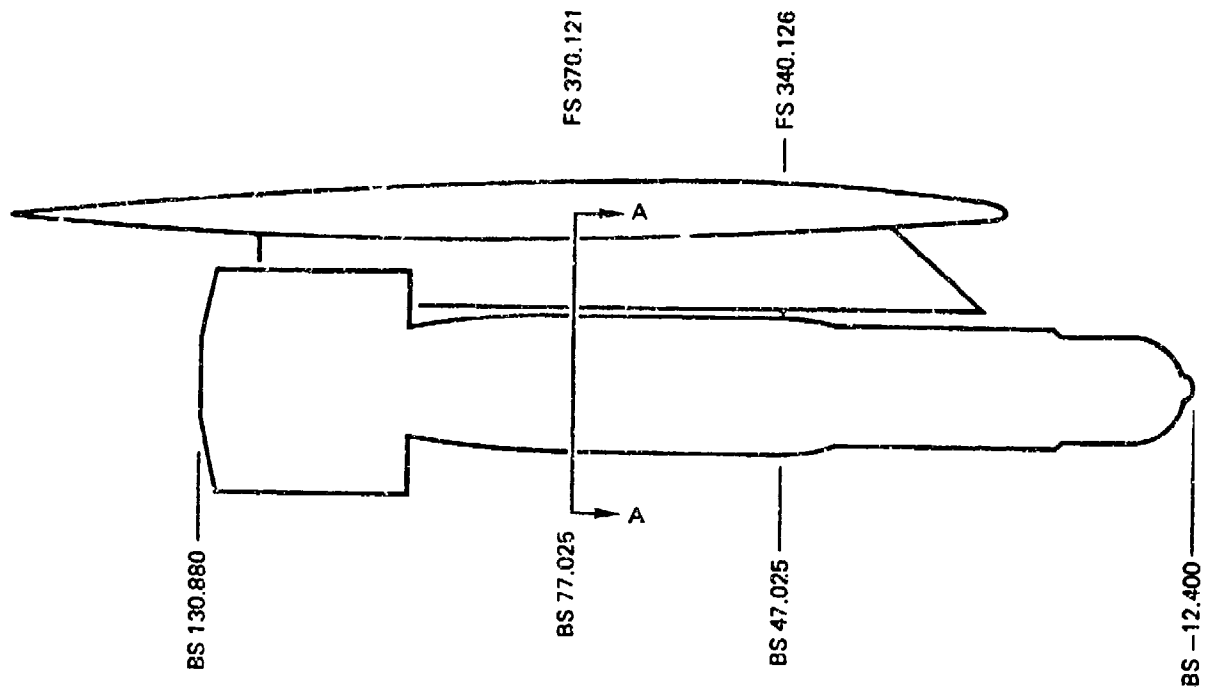
MK-84 EO Study Configuration
Weight - 2351.5 lb
$I_p = I_y$ - 470.21 Slug-ft^2
I_r - 24.3 Slug-ft^2
CG - Bomb Sta. 59.0 in.

FIGURE 4 MK-84 EO GUIDED BOMB MOUNTED ON MAU-12 PYLON AT BL 132.50

9

Store Characteristics
Weight = 531 lb
Moment of Inertia
in Pitch and Yaw = 42.3 Slug-Ft^2

B-B

Inboard

Right Wing

A-A

Forward Shift Lugs

Aft Shift Lugs

15.1

91.3

10.8

36.5

32.5

14.0

$\mathcal{L}$ Store Lugs
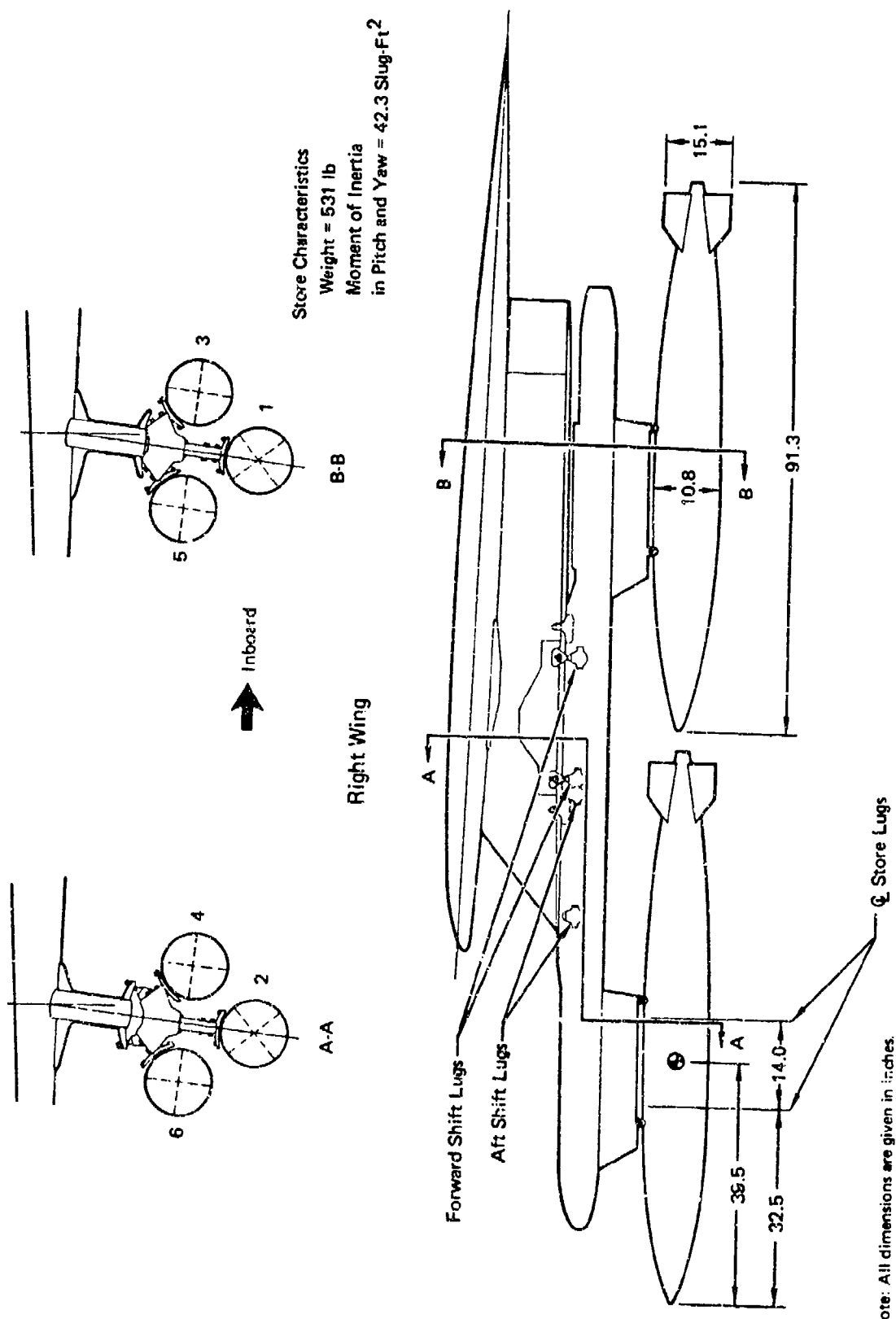
Note: All dimensions are given in inches.

FIGURE 5   MK-82 BOMBS MOUNTED ON FORWARD SHIFTED MER RACK ON MAU-12 PYLON AT BL 132.50

10

This configuration, again, is the most flutter critical.

2.2 Advanced Aircraft Configuration

The advanced fighter aircraft shown in Figure 6 has been chosen as the study vehicle for both the horizontal tail and wing flutter control study efforts. This aircraft anticipates significant improvements in both structure and propulsion. It is also expected that it would have fly-by-wire flight control systems which would be available as a base for cooperative use by flutter control systems.

The basic vehicle design criteria includes a design load factor of 5.0 g (ultimate load factor of 7.5 g) and a dynamic pressure limit which is almost double the maximum dynamic pressure experienced by some fighter aircraft. Composite material will be used for both the wing and the empennage. Aerodynamic controls will include leading edge slats, trailing edge flaps, spoilers, and differential all-movable horizontal tail. The aerodynamic characteristics for the wing and horizontal tail of this aircraft design are given in Table 2.

2.2.1 Advanced Aircraft Horizontal Tail - It has been the common experience with contemporary fighter type aircraft that the design of all-movable horizontal tails is constrained by flutter considerations. Horizontal tails designed to satisfy strength and aerodynamic requirements are usually unable to satisfy the flutter requirements without additional modification. Flutter modifications in the past have always been passive and have employed various combinations of:

1) balance weights

2) pitch restraint

3) torque box stiffening

The weight penalties for passive flutter control of all-movable horizontal tails are significant as shown in Figure 7. This figure, which is based on contemporary aircraft, illustrates that additional weight for flutter will be required in future aircraft even with the use of the highly efficient composite materials.

The total potential reduction in aircraft weight is greater than shown in Figure 7 because of the pronounced sensitivity of overall aircraft weight to small changes in empennage weight. For some advanced aircraft designs

11
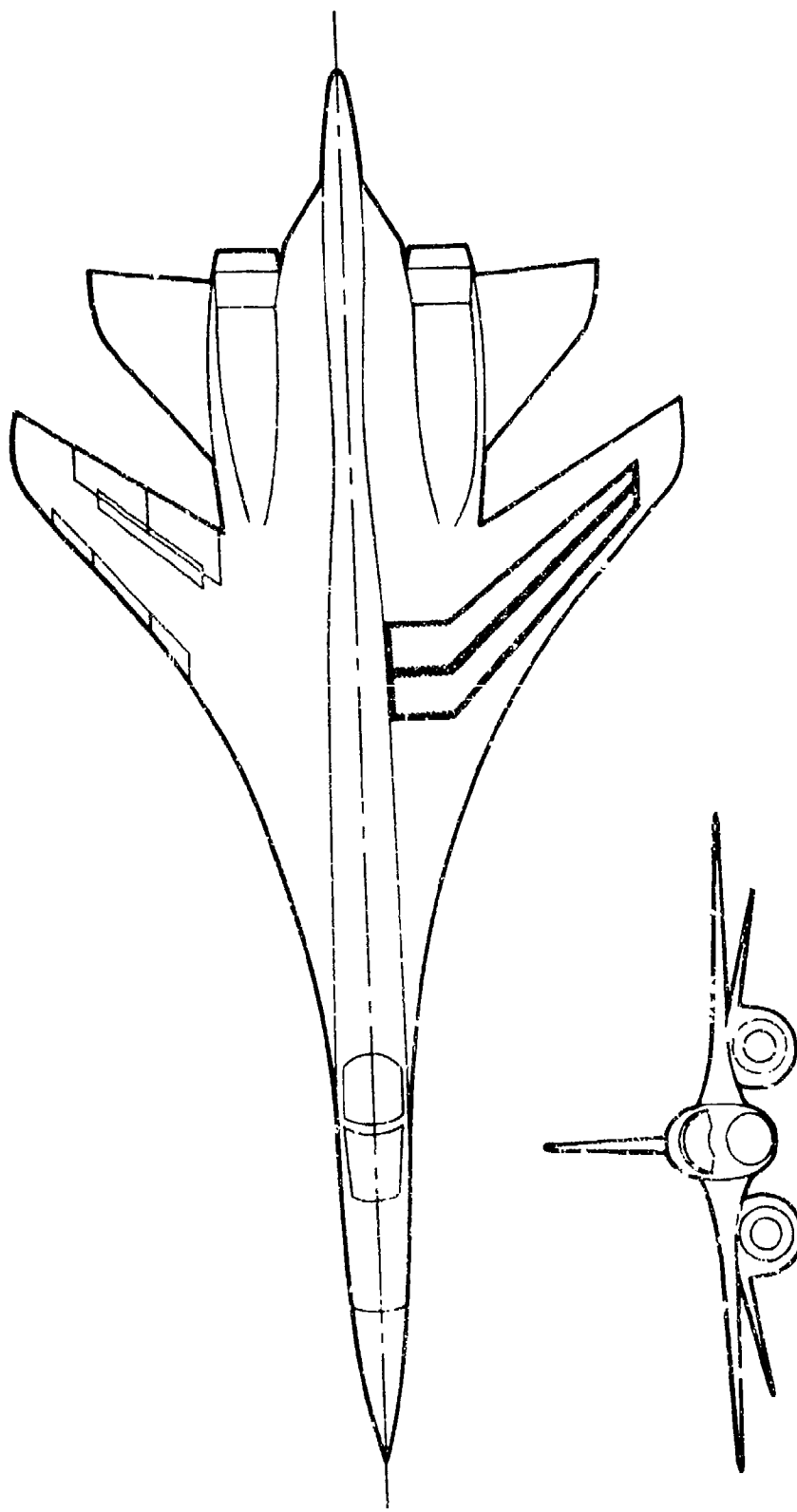
FIGURE 6 WING AND HORIZONTAL TAIL FLUTTER CONTROL STUDY VEHICLE

TABLE 2 ADVANCED AIRCRAFT CHARACTERISTICS

Item		Wing	Horizontal Tail
Area	· ft²	489.2	120.0
Aspect Ratio		4.0	2.01
Taper Ratio		0.233	0.323
Leading Edge Sweep	· deg	52.5	50.0
Thickness Ratio - Root	· %	6.0	3.8
Thickness Ratio - Tip	· %	4.0	2.5
Airfoil		64A00X	64A00X
Incidence	· deg	1.0	0
Span	· ft	44.24	15.53
Span/2	· in	265.4	93.18
Mean Aero. Chord	· in	150.0	100.8
Root Chord	· in	215.3	140.2
Tip Chord	· in	50.2	45.3
Dihedral	· deg	0	10
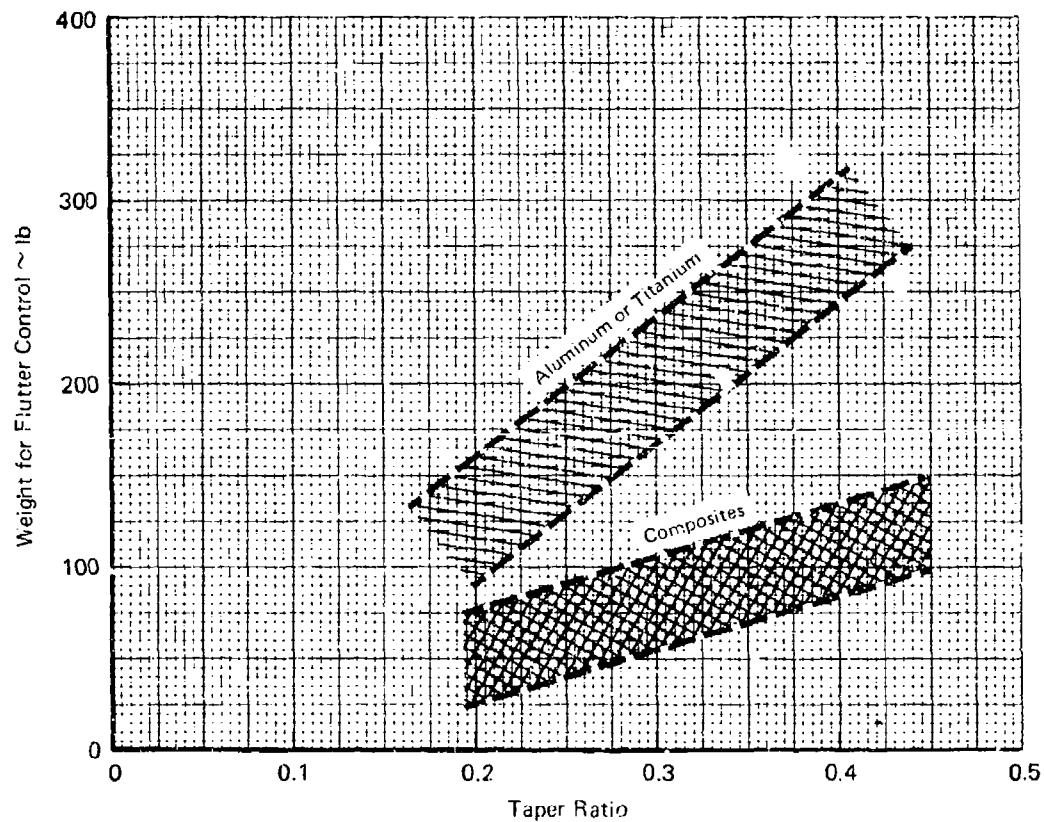
FIGURE 7   TYPICAL PASSIVE FLUTTER CONTROL WEIGHTS FOR
FIGHTER TYPE AIRCRAFT HORIZONTAL TAILS

currently being considered, as much as 15 to 20 pounds of overall weight reduction is possible, in the early design stages, for each pound saved in the empennage.

The Computerized Optimization Procedure for Stabilators (COPS), described in Reference 4, has been used to generate the detailed aeroelastic description for the advanced horizontal tail. The overall aerodynamic characteristics for this control surface, given in Table 2, were used by the COPS program to generate the aeroelastic model shown in Figure 8. The model is a torque box structure idealized by eight discrete rigid chord streamwise sections with three mass points per section. The structural material chosen for this surface is boron/epoxy composite. The composite layup for the feasible strength design torque box is specified with 70% of the fibers at 0 degrees with respect to the elastic axis, 20% at ±45 degrees and 10% at 90 degrees. The total weight for this feasible strength design is 259.45 lbs. The detailed analytical model is given in Appendix II.

2.2.2 Advanced Aircraft Wing - In the past, strength requirements have generally dictated the structural design of fighter aircraft wings. Flutter requirements have been inherently satisfied on such aircraft as the F-4 because the conventional rib-spar wing structure necessary for static air loads has provided enough torsional stiffness to preclude flutter within the flight envelope.

Flutter critical designs are likely, however, for fighters and interceptors planned for 1975 or later. New contemporary fighter aircraft could already be classified as transition aircraft in which both strength and flutter played important roles in the wing structural design. The trend toward flutter critical designs results from the following design trends:

1) The use of materials with high structural efficiency and low structural stiffness

2) low wing load factor designs

3) thin wing designs

The wing stiffness levels which are reduced by each of these trends can create a flutter critical design. Passive flutter control for these advanced aircraft may require so much unnecessary nonstructural weight that active flutter control may become attractive, especially if control surfaces can be
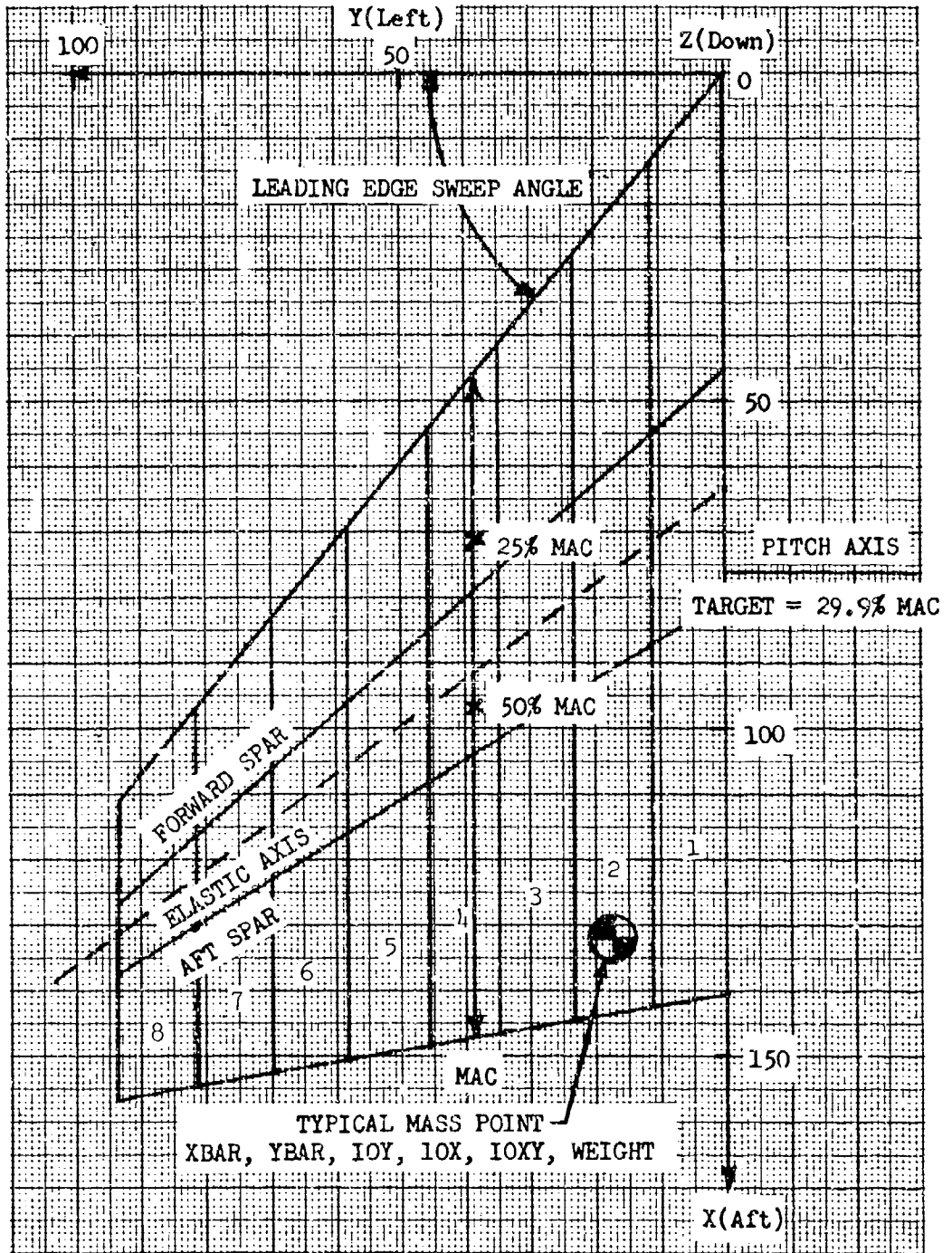
FIGURE 8 AEROELASTIC IDEALIZATION FOR ADVANCED AIRCRAFT
HORIZONTAL TAIL

used for both flutter control and flight control.

Selected modules of the COPS computer program have been used to generate the baseline feasible strength design with no consideration for the aeroelastic constraints. The overall aerodynamic characteristics for this wing, given in Table 2, were used by the COPS program to generate the aeroelastic model shown in Figure 9. The model, which considers only the exposed area of the wing, consists of eight discrete rigid chord streamwise sections with three mass points per section. The structural material chosen for this wing is boron/epoxy composite with 70% of the composite fibers at 0 degrees with respect to the elastic axis, 20% at ± 45 degrees and 10% at 90 degrees. Two weight distributions were calculated. The first weight distribution is for a clean wing with no aerodynamic control surfaces on either the leading or trailing edges. Total weight of this clean version is 918.34 lbs. The second weight distribution is for the wing with both leading and trailing edge control surfaces in each streamwise section. The torque box is the same for both weight versions. Total weight for the second version is 1265.53 lbs. The detailed analytical model is given in Appendix III.
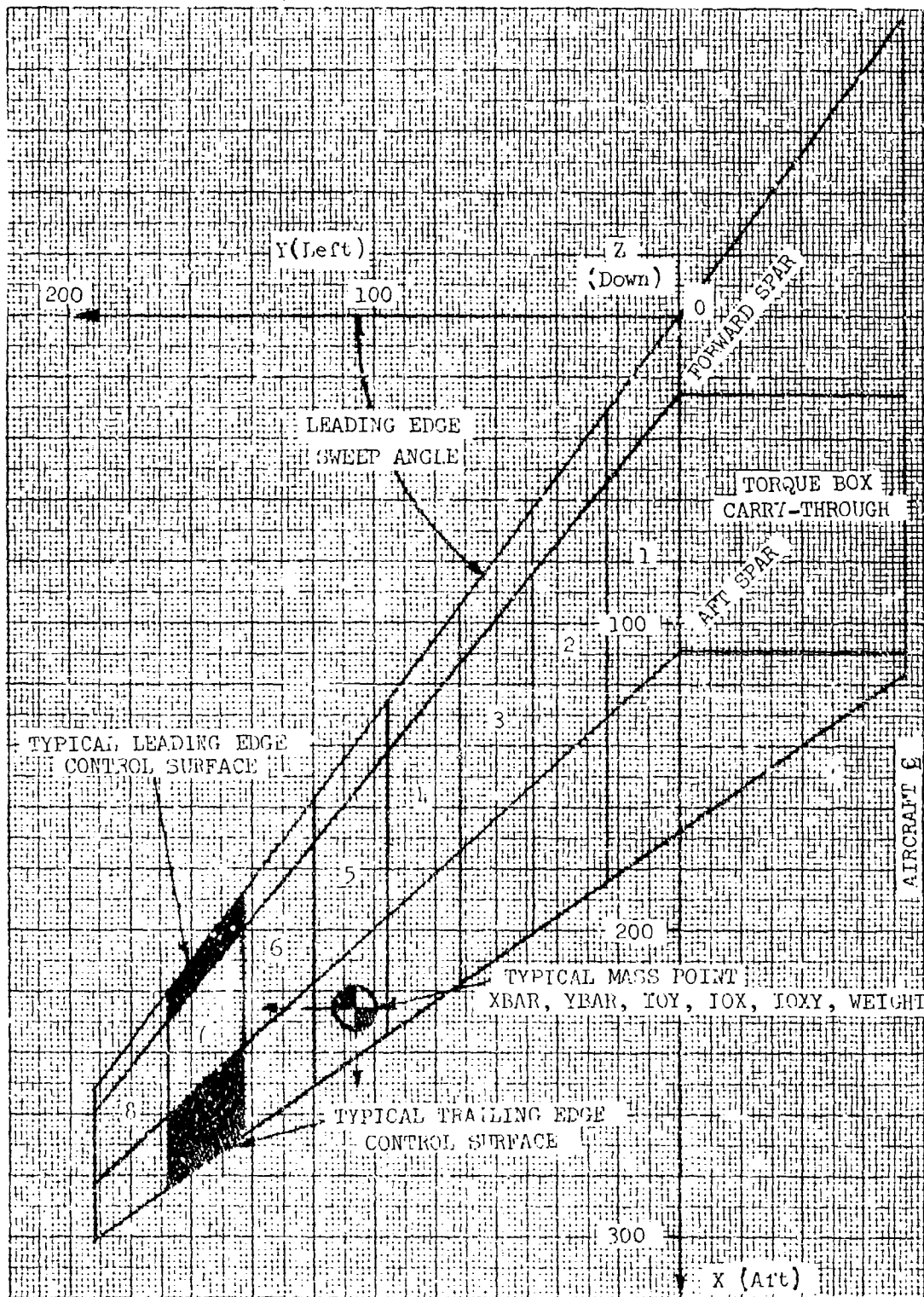
FIGURE 9 AEROELASTIC IDEALIZATION FOR ADVANCED
AIRCRAFT WING

3. TECHNICAL APPROACH

3.1 General Description of Study

3.1.1 Scope - This analytical study of active flutter suppression systems was directed toward the accomplishment of two broad objectives. These objectives are:

- o To establish the potential flutter modes, configurations, and flight conditions where active flutter suppression can show an advantage.
- o To formulate design guidelines and criteria to implement and test acti e flutter suppression systems.

To accomplish these broad objectives the study effort was divided into three separate areas of investigation, wing/store flutter control, all-movable horizontal tail flutter control, and wing flutter control.

The wing/store flutter control study assessed the practicality of extension of flutter boundaries for several store combinations by active control. The vehicle for this study effort was the F-4 Phantom aircraft shown in Figure 1.

The horizontal tail flutter control study investigated both the potential payoff for active control in future aircraft and the unique problems and difficulties encountered when one of the participants in the flutter mode is used as the flutter control force producer. An example of participative control is the pitch actuator being used as the control force producer to suppress pitch-bending flutter. The vehicle for this study effort was the advanced aircraft of Figure 6.

The wing flutter control study parametrically evaluated the potential pay off in future aircraft by active control of flutter critical primary lifting surfaces. The vehicle for this study effort was also the advanced aircraft shown in Figure 6.

3.1.2 Plan of Attack - This discussion presents the general approach which was followed in all three flutter control study efforts. The plan followed is illustrated by the conceptual flow chart of Figure 10. The step numbers in the following paragraphs refer to block numbers in the figure.

Step 1 - A flutter analysis was performed for the candidate configuration to determine a base for subsequent comparisons. For the wing/store studies a flutter analysis was performed for all store combinations being considered.

Step 2 - A choice was made of an active flutter suppression scheme. The

19
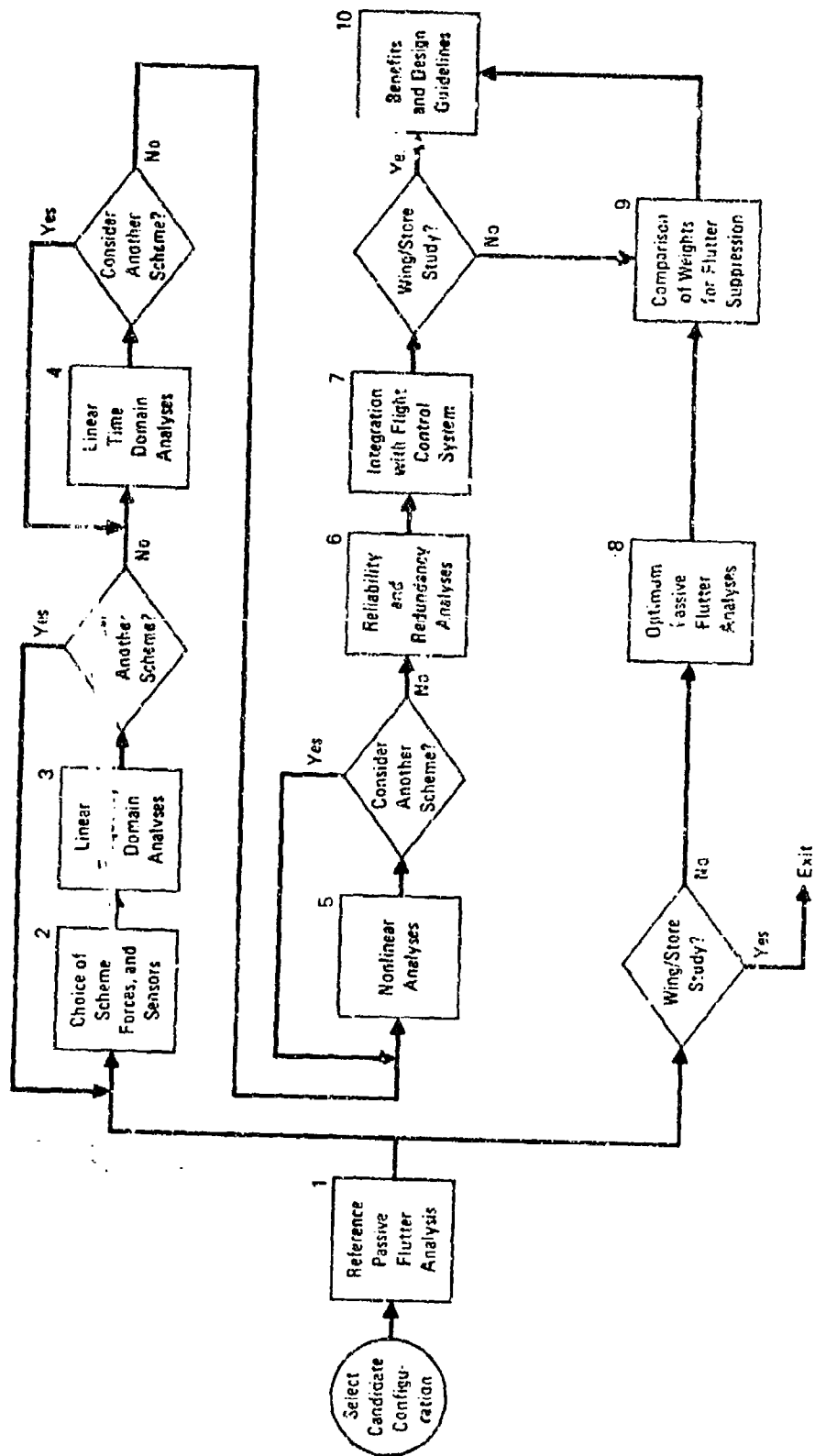
FIGURE 10 GENERAL PLAN OF ATTACK

20

type and location of the force producer or producers were specified. The type and location of the sensor or sensors were specified.

Step 3 - Linear parametric studies were made using appropriate computer programs such as the frequency domain computer program described in Section 3.5.1. Compensation to control flutter was generated by conventional control system design techniques. Compensation networks found suitable for one store configuration or flight condition were then tested on other cases to determine the sensitivity of the design.

Step 4 - Linear time domain studies were made for the most promising design of step 3 using appropriate computer programs such as the time domain computer program described in Section 3.5.2. The control system requirements on rate, displacement, and power were determined for flight both with and without atmospheric turbulence.

Step 5 - The effects of system nonlinearities were determined for the most promising design of step 4 using the time domain computer program.

Step 6 - A reliability and redundancy study was conducted for the most promising candidate system. A significant amount of data from the F-4 SFCS (Survivable Flight Control System, Reference 5) program was used to give credibility to the reliability and weight assessment effort.

Step 7 - The possibility of weight saving by use of a non-dedicated flutter control system was investigated. The Multi-Loop Control Systems computer program (MATLOC) described in Appendix IV was used to evaluate the compatibility of the flutter control system with other flight control systems.

Step 8 - The minimum weight passive flutter solutions were determined for the candidate configurations in the wing and tail flutter study programs. Parametric analyses and engineering judgement, using appropriate computing tools, such as COPS (Computerized Optimization Procedure for Stabilators), described in Reference 4 were used in this assessment.

Step 9 - The minimum weight passive flutter solutions were compared to

the minimum weight active flutter solutions to determine the potential weight payoff of active flutter control for the wing and tail flutter study programs. In the case of the wing/store study, expanded flight envelope is the potential payoff.

3.1.3 Design Guidelines - Certain design constraints and performance objectives were considered as guidelines throughout these studies. These considerations were used to ensure a realistic evaluation of competitive active flutter suppression schemes. Because of the exploratory nature of these studies, however, a failure of any system to rigorously satisfy these design guidelines was not an automatic cause for elimination.

3.1.3.1 Relative Stability - For speeds up to the aircraft limit speed, the design goals for relative stability were the following:

1) Gain margins of ± 6 dB

2) Phase margins of ± 60 degrees

3) Effective structural damping coefficient of $g = 0.03$ ($\zeta = 0.015$) on time history traces.

In addition, the flutter control systems were required to be stable for all elastic modes other than the flutter mode being controlled.

3.1.3.2 Turbulence and Maneuver Environment - The flutter control systems were expected to withstand the following gusts and maneuver loads:

1) Random gust with rms of 13 ft/sec.

2) Discrete gust of the form $(1 - \cos \omega t)$ for 30 ft/sec peak amplitude.

3) Limit load factor maneuvers.

3.1.3.3 Reliability - Control surface actuators were sized for continuous control in the specified turbulence and maneuver environments. The design objective was to use a minimum number of redundant control system components to ensure system reliability, with a failure rate of less than one catastrophic failure (loss of aircraft) per million flight hours.

3.2 Solution Techniques

3.2.1 The Active Flutter Control Concept - Flutter is a self-excited mechanism whereby energy is absorbed by the lifting surface from the airstream. The critical flutter mode is characterized by a unique flutter frequency of oscillation in which the motion consists of both bending and torsion (twist) components. The oscillation is essentially simple harmonic. The bending and the torsion motions are not in phase with each other; in fact the torsion motion lags considerably behind the bending motion at

22

flutter. If either the bending or torsion motion is suppressed this classical coupled bending-torsion flutter will not occur. The flutter may also be controlled by changing the phasing of the two motions to change the energy flow so that the net work is done on the airstream instead of on the wing. The flutter onset speed may also be increased by delaying the coalescence of participating modes with increasing airspeed.

Let us examine in more detail one cycle of motion when flutter is occurring. For this purpose consider only a single discrete wing streamwise section and plot its displacement versus time as shown in Figure 11. The lift vector is in phase with the torsion motion. The small lag angle due to lift build-up delays is not necessary for this development and has been eliminated for clarity. Bending leads torsion 90 degrees so that positive work is being done on the wing. The lift vector is in the direction of the deflection change. The work is thus positive during each quarter cycle.

For a real-world wing the net work will be the summation over the entire wing surface. Generally during each cycle of oscillation lift forces attributable to torsion will do positive work on the wing during a portion of the cycle and negative work during the remainder of the cycle. The motion will just maintain itself when such net positive work is balanced by damping or dissipative forces in the system. The motion will diverge (flutter will occur) when the balance of work on the wing is positive.

Ideal flutter control of this example wing section is described in Figure 12. No flutter will occur if either type of motion is suppressed or if the phasing is such that the net work is zero or negative. Aerodynamic control surfaces offer a convenient means for generating flutter control forces. Figure 13 shows a trailing edge control surface producing a stabilizing moment which tends to oppose the torsion motion. This surface could be either existing or specifically dedicated for active flutter control.

An alternate, and more enlightening, description of the flutter motion is shown in Figure 14. Consider the work done by the lift vector during one cycle of motion.

$$
\text{Work/Cycle} = \int_0^{t = \frac{2\pi}{\omega}} (\text{POWER}) dt = \int_0^{\frac{2\pi}{\omega}} L(-\dot{h}) dt
$$

The power input to the system is positive for $-L\dot{h} \cos \sigma > 0$ or when $\cos \sigma < 0$.
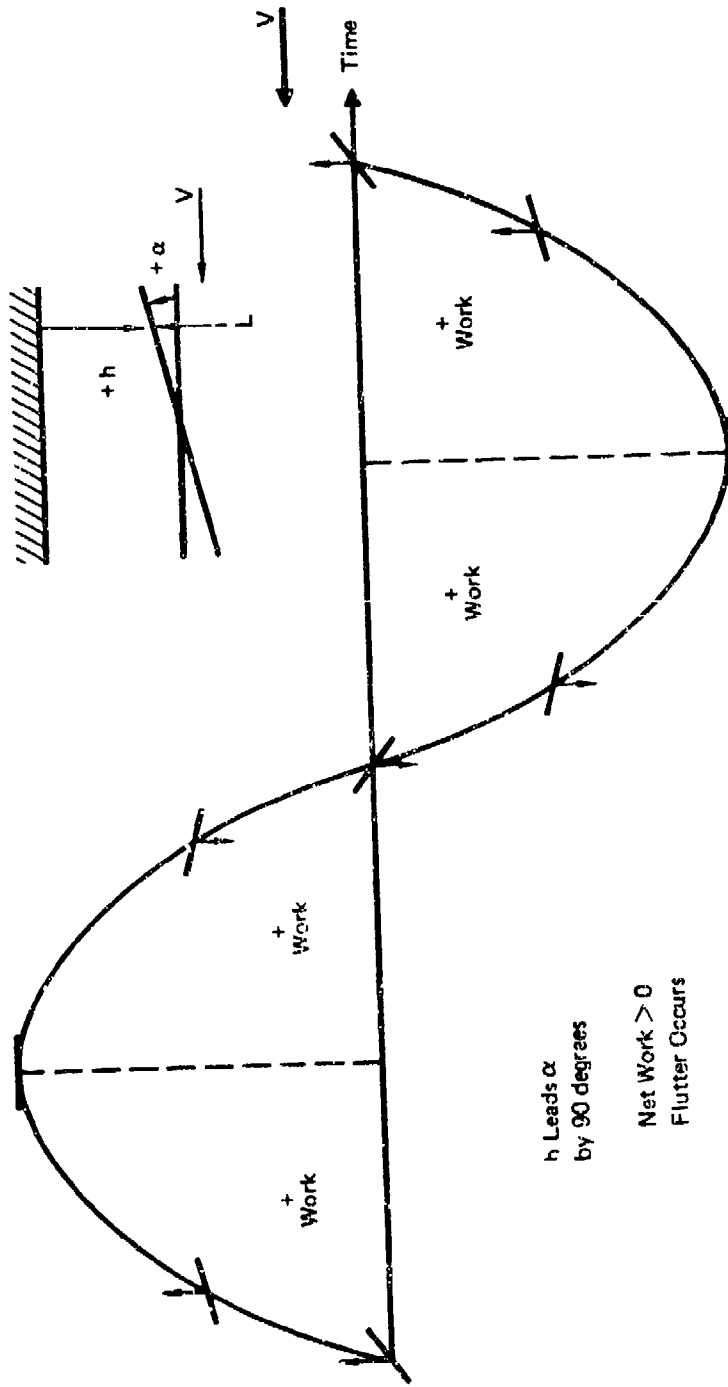
FIGURE 11 SCHEMATIC REPRESENTATION OF FLUTTER MECHANISM WITH MAXIMUM ABSORPTION OF AIRSTREAM ENERGY

Total Suppression of Angle of Twist - $\alpha = 0$

No Flutter

h Leads α by 180°

No Flutter
Net Work = 0

+ Work   — Work

+ Work   — Work
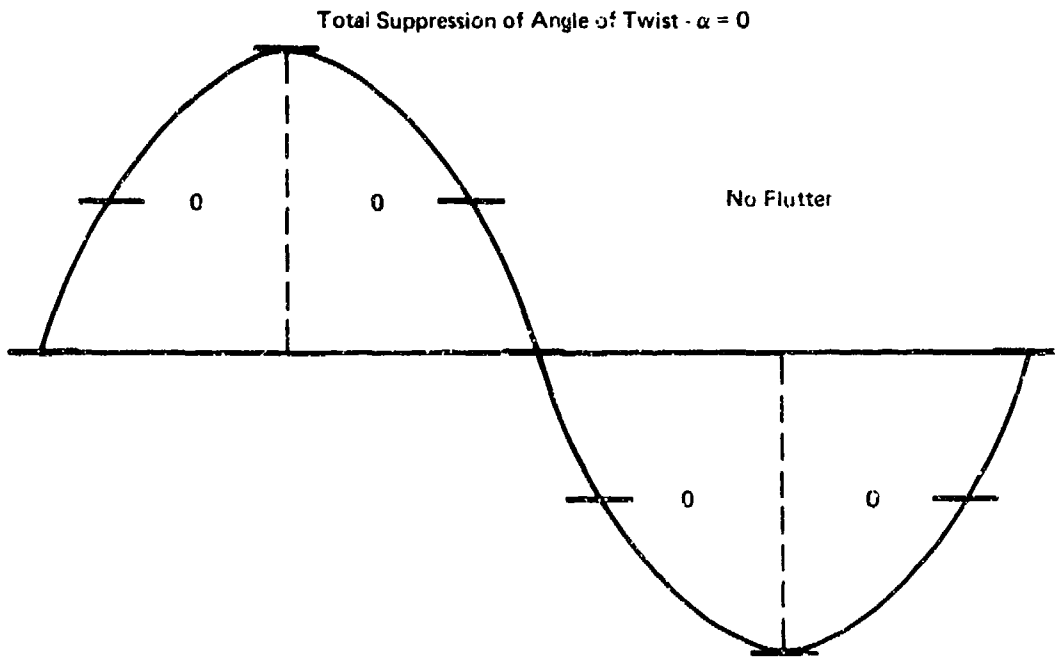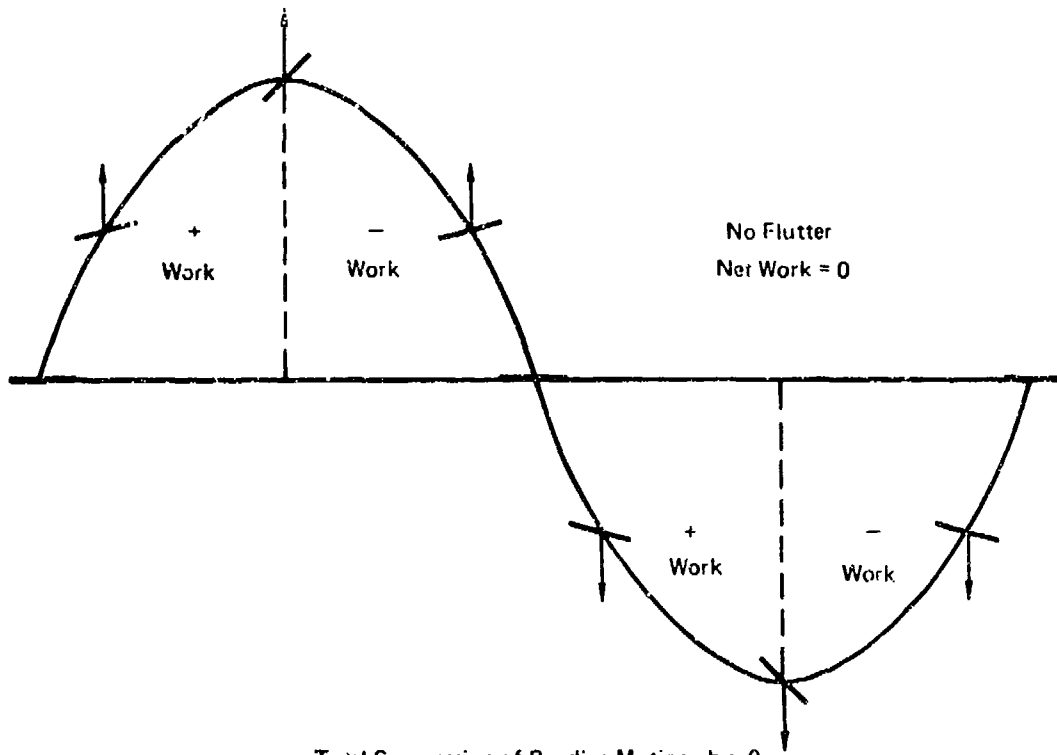
Total Suppression of Bending Motion - $h = 0$

No Flutter

FIGURE 12 EXAMPLES OF IDEAL FLUTTER CONTROL

25
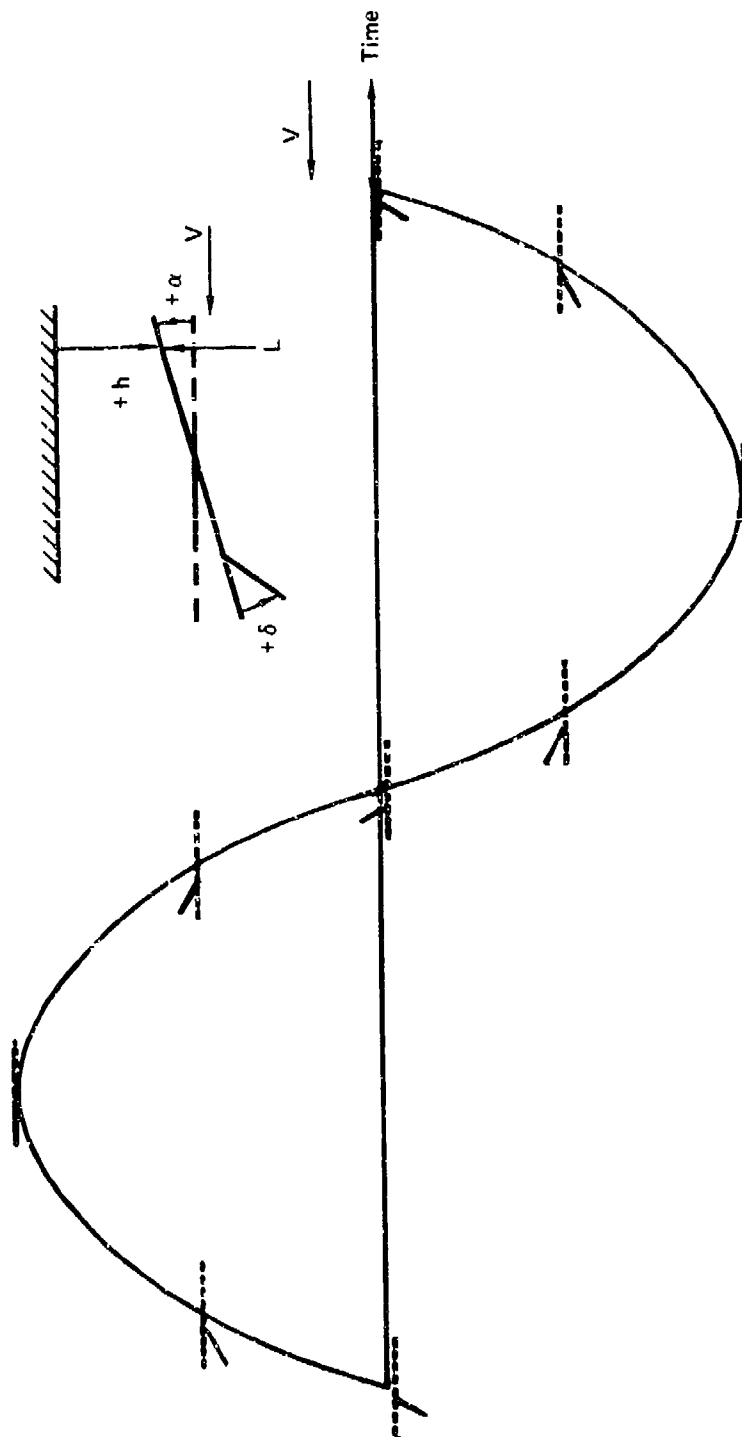
FIGURE 13 CONTROL SURFACE DEFLECTION TO STABILIZE
FLUTTER MECHANISM
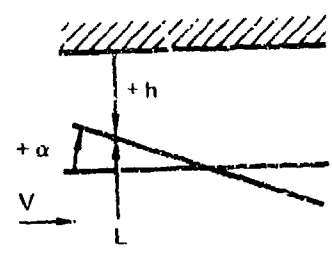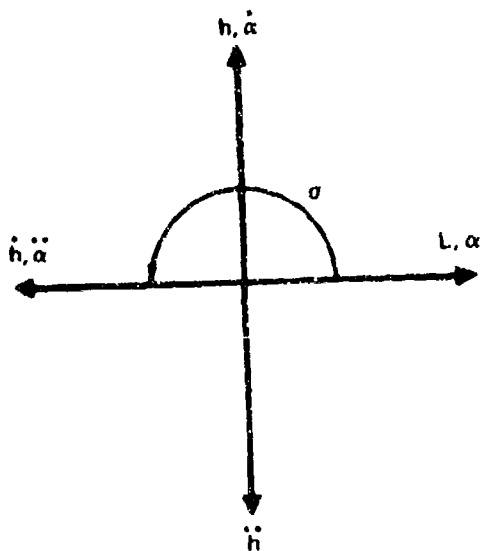
σ is the Angle between L and $\overset{\cdot}{h}$
Flutter Occurs for $90^0 < \sigma < 270^0$
Explosive Flutter Occurs for $\sigma = 180^0$

FIGURE 14   PHASE PLANE DESCRIPTION OF FLUTTER
MECHANISM

The maximum power occurs when $\cos \sigma = -1$ or $\sigma = 180°$ as shown.

In the light of the preceding discussion, several choices for flutter control feedback signals appear promising. Both individual and blended feedback signals are considered in these studies to competitively evaluate these various possibilities. The individual feedback signals tested include all of the variations of torsion motion such as,

$$\pm\, K_A \alpha, \quad \pm K_A \dot{\alpha}, \quad \pm K_A \ddot{\alpha}$$

and bending motion such as,

$$\pm K_A h, \quad \pm K_A \dot{h}, \quad \pm K_A \ddot{h}$$

The blended feedback signals tested include the following combinations,

$$\pm\, K_A \,(\alpha \pm K_B \,\dot{\alpha})$$

$$\pm\, K_A \,(\dot{\alpha} \pm K_B \,\ddot{\alpha})$$

$$\pm\, K_A \,(\ddot{\alpha} \pm K_B \,\ddot{h})$$

where K_A and K_B are arbitrary constants.

3.2.2 Flutter Control Schemes - In general there are three separate operations which must be performed by any practical flutter control system. These are,

1) Sensing
2) Feedback compensation
3) Control force production

Sensing may be done by transducers which produce either an electrical signal or a physical displacement. Feedback compensation may also be accomplished by either electrical or mechanical components. The production of forces and moments to control flutter may be done in many different ways, such as by electro-hydraulic or mechanical actuation of control surfaces, reaction jets, or jet flaps.

3.2.2.1 Electrical Feedback - This general concept for flutter control is illustrated in Figure 15. Sensing and compensation are both performed by electrical components. Control force production is by a hydraulically

Airframe

R = ϕ_c +/−   K Gain   S Servo   C δ ϕ/δ ϕ

ϕ_{FB}

F High Pass Filter   C Compen-sation ϕ_M G Sensor
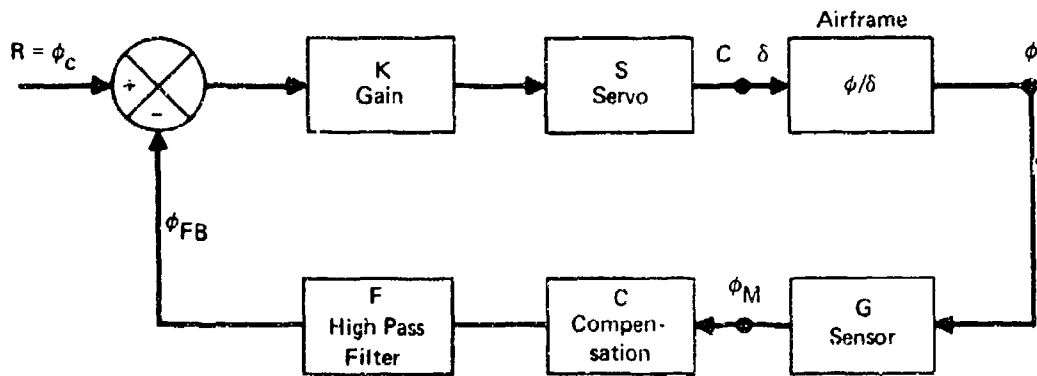
δ = Control Surface Deflection ϕ – Airframe Response

$$\frac{C}{R} = \frac{\delta}{\phi_c} = \frac{KS}{1 + KS\left(\frac{\phi}{\delta}\right)GCF}$$

$$\frac{\phi}{R} = \frac{KS\left(\frac{\phi}{\delta}\right)}{1 + KS\left(\frac{\phi}{\delta}\right)GCF}$$

Loop Characteristic Equation = $1 + KS\left(\frac{\phi}{\delta}\right)GCF$

**FIGURE 15 BLOCK DIAGRAM ILLUSTRATING ELECTRICAL FEEDBACK FLUTTER
CONTROL SCHEME**

actuated control surface. The basic scheme shown in this figure has been applied in one form or another to each of the study configurations.

The reference signal for the control loop of Figure 15 is a command for the airframe response to be zero. A sensor, which gives an electrical output signal, is used to measure the airframe response at the location of the sensor. The total airframe response signal includes components for all aeroelastic modes in the bandwidth of the sensor. These signals are fed back through electronic compensation networks and hydraulic actuators to command the rotation of the control surface. The control surface produces aerodynamic forces which can potentially modify the airframe response to ensure the stability of the system. If the airframe response is continuously nullified, the flutter instability can be precluded. The high pass filter, shown in the figure, has been introduced to filter out the static and low frequency response signals associated with the normal aircraft maneuvering and rigid body short period mode so that only the higher frequency flutter modes are suppressed. The control system design procedure here is to create the proper forces in both amplitude and phase to control this airframe response motion which varies with airspeed, altitude, and other flight parameters.

3.2.2.2 Structural Feedback - Active flutter control can also be achieved through structural feedback. A conceptual sketch of a particular structural feedback scheme is shown in Figure 16. The scheme uses a structural link to sense wing twist at one end and to actuate a control surface at the other end. Mechanical compensators such as springs, masses, and/or dampers can be incorporated in the link to achieve the phasing of aileron deflection to wing twist angle required for active stability.

The wing twist angle sensing concept is similar to that employed by a torque wrench. The outside shaft (Shaft A) represents the wing torsional stiffness elements while the internal shaft (Shaft B) is fixed to the fuselage with the outer shaft free to rotate about it. Thus, under aerodynamic moments Shaft A twists relative to Shaft B and the wing twist angle, α, is sensed. The arm connected to Shaft B is used to actuate the control surface as shown in the figures. The connection shown results in an aileron angle which, without further compensation, is 180° out of phase with the wing twist angle. In-phase forcing can be achieved by means of a "top to top" connection. The control surface could be an aileron shared with the lateral control

30

Structural Link

Wing Arm

Compensation Module

Wing Torsion Member (Shaft A)

Wing Twist Sensing Member (Shaft B) Located at Elastic Axis

Aileron Pivot

Aileron Arm

d_1

Structural Link

EA

d_2

Wing Arm

Aileron Arm

No Wing Twist

α

Wing Centerline

β

Wing Twist LE Up

β

$-\alpha$

Wing Centerline

Wing Twist LE Down
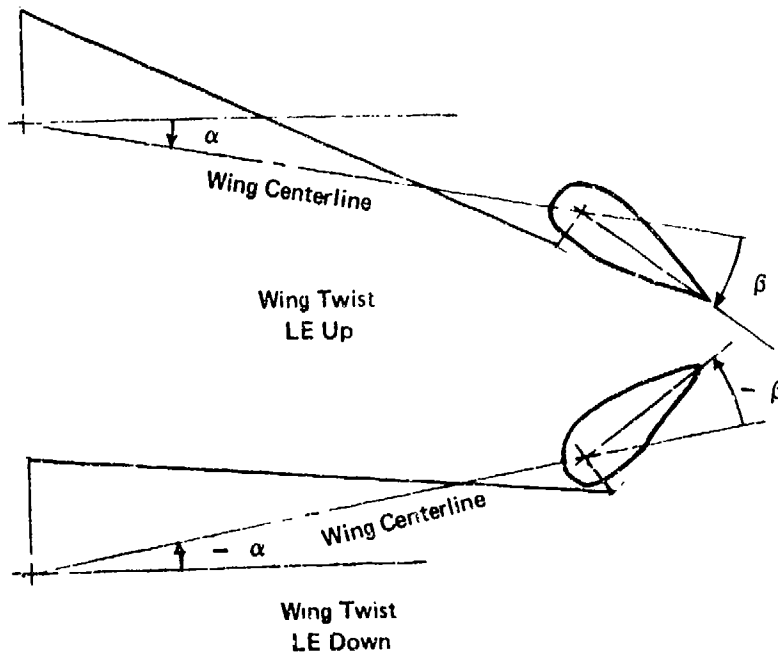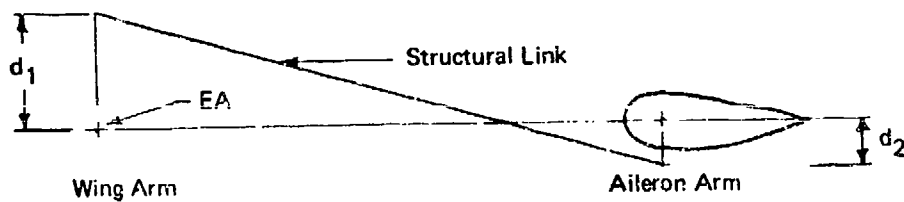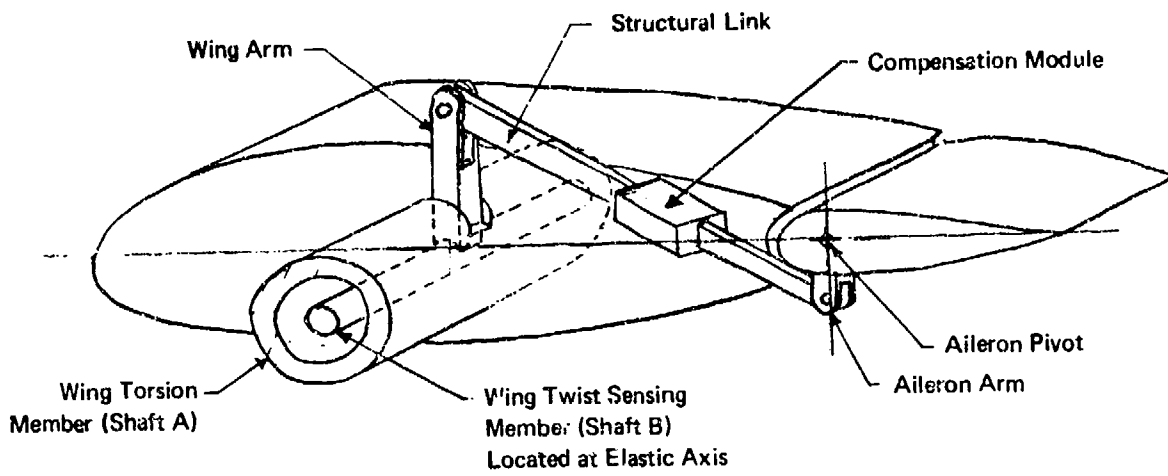
FIGURE 16 CONCEPTUAL STRUCTURAL FEEDBACK SCHEME

31

system or it could be an auxiliary surface specifically for active flutter control. An auxiliary surface could be incorporated in the wing or on the store pylon.

3.2.2.3 Load Suppression for Wing/Store Flutter Control - There is one feature common to all wing/external stores flutter mechanisms. The crux of that feature s illustrated in Figure 17. The store loads, P and Q, are transmitted into the wing and adversely affect the wing flutter speed. If these store loads were nullified, the wing/store configuration would be effectively decoupled and the wing would revert to the bare wing flutter mechanism and speed.

Even with a wide variety of stores, we can suppress or nullify the vibratory store loads transmitted into the wing. This might be accomplished, for example, by replacing the passive load transmitting members by active members, i.e., support-actuators as shown in the figure. These support-actuators would suppress the vibratory load components P_V and Q_V and pass the steady load components P_S and Q_S. These "steady load components" also include the quasi-steady or low frequency maneuver loads. The suppression system might consist of:

- o Load cells to sense P and Q
- o High pass filters to filter out the steady (low frequency) load signals leaving only the vibratory load signals
- o Support-actuators driven by the vibratory load signals to nullify the vibratory loads F_V and Q_V.

This is a promising scheme also if only the vibratory pitching moment transmitted to the wing, $P_V a - Q_V b$, is suppressed.

3.3 Hardware Considerations

There are many practical considerations which enter into the design and development of a successful active flutter control system for a high performance type aircraft. Some of the more important of these are listed below:

- o The requirement for the system to operate with changing flight condition parameters such as velocity, altitude, and maneuver loads.
- o The requirement for acceptable interactions among stability augmentation systems, gust alleviation systems, and flutter control systems if control loops are shared.
- o The requirement for reliable hardware which is able to satisfy the demands of the flutter control system.

A) Wing/store configuration

Load transmitting members

Wing

Pylon

A   B

Store

B) Equivalent idealization

Bare wing

$\odot$

$\leftarrow$ b $\rightarrow$ a $\rightarrow$

Q

P

Store loads into wing
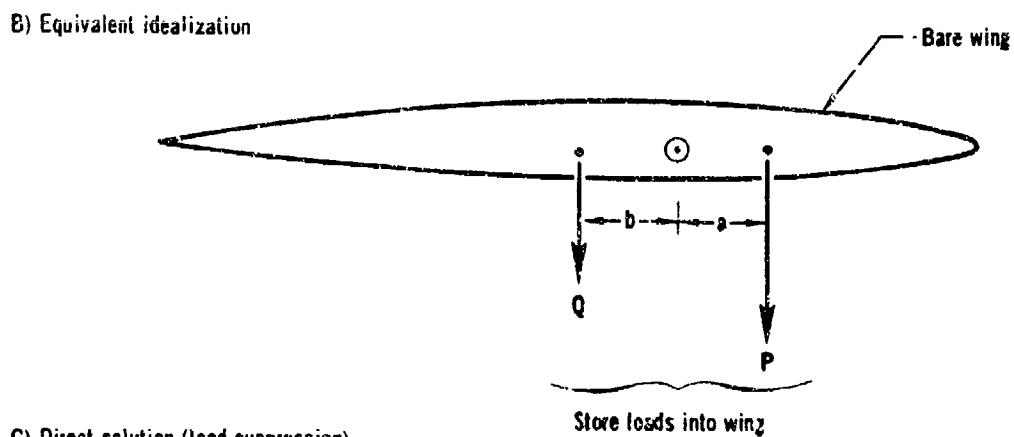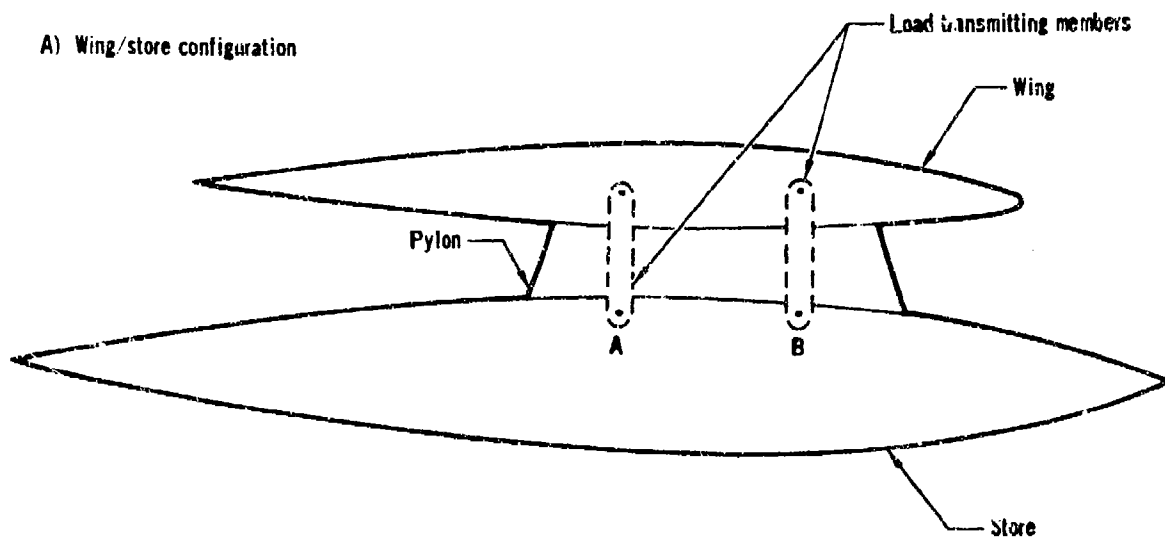
C) Direct solution (load suppression)

Total load = Steady load + vibration load

$$P = P_s + P_v$$
$$Q = Q_s + Q_v$$

Support actuators { Suppress P_v and Q_v
at A and B { Pass P_s and Q_s

FIGURE 17 CRUX OF WING/EXTERNAL STORES FLUTTER MECHANISM
AND A DIRECT FLUTTER ELIMINATION APPROACH

33

o The requirement for continuous control of flutter when deep in the flutter region since, particularly in the case of explosive flutter, once flutter motion builds up it is doubtful that any active system can control it.

3.3.1 Variable Flight Conditions - The requirement to operate over variable flight conditions is one of the major design considerations in the development of a successful active flutter control system. A high performance aircraft experiences elastic deformations as a result of turbulence and maneuver loads which occur during flight. A flutter control system must be able to prevent the unstable buildup of these deformations even when the aircraft is in a flutter critical region of the flight envelope. This requirement to control a potentially unstable dynamic system in a turbulent environment is distinctly more demanding than the normal requirements for control of stable dynamic systems. The successful control of flutter requires the use of sensors, compensation networks, and force producers in such a way that the resulting design is relatively insensitive to the variable flight condition parameters such as velocity, altitude, Mach No., and disturbance level. In the particular case of wing/store flutter control the active system must also be able to accommodate variable dynamic configurations as the store loading changes.

3.3.2 Control System Integration - Another significant design consideration is the possibility of the integration of flutter control systems with other systems for flight control, stability augmentation, and gust and load alleviation. Integration of an active flutter control system with other flight control systems is desirable from a weight saving standpoint. It is especially desirable in fighter aircraft since both the number and location of feasible control surfaces is limited. Two possible arrangements are: mechanical linked series servo integration, and complete electronic integration.

A mechanically linked series servo arrangement is used in contemporary aircraft. This system adds the pilot's mechanical inputs to electronic inputs from the automatic feedback control system such as those for stability augmentation and flutter control. The resultant combined signal drives the control valve of a hydraulic power actuator.

Complete electronic integration combines the separate signals from the primary flight control systems and the flutter control system electronically

to command integrated fly-by-wire electro-hydraulic power actuators. This type of control system integration is likely in future aircraft.

3.3.3 Hardware Capabilities - Significant difficulties in the implementation of active flutter control occur in the area of hardware. The control system components whether mechanical, electrical, or hydraulic are, in general, sensitive to the frequency of operation. They must be designed for the specific application since the design guidelines and criteria for one range of frequencies, such as for rigid aircraft control, are not appropriate for other frequency ranges, such as for flutter.

It is relatively easy to fabricate sensors and electronic components into very precise, highly redundant units which will reliably perform over a wide range of frequencies. It is a significantly more difficult design problem to satisfy the force producer frequency requirements.

The force producer rate limit is another critical design constraint and affects the system gain and available power for flutter control. The force producer, whether mechanical, electrical,or hydraulic, must be designed for high rates.

3.3.4 Continuous Control - Continuous control of flutter is required when deep in the unstable flutter region in order to preclude the buildup of flutter forces and motions to an uncontrollable level. The danger of loss of control is very real for explosive flutter such as pitch-bending flutter of a stabilator or bending-torsion flutter of a wing. The energy extracted from the airstream when a well developed flutter mode is occurring is enough to overpower any practical hydraulic actuator or other force producer.

Loss of continuous control is possible because of excessive deflection or rate demands on the control system in an environment of severe turbulence or excessive maneuver. This may demand the use of dedicated flutter control force producers on some aircraft. In an integrated control loop, where a control surface is shared by two systems, limits on deflection may have to be imposed on each of the systems. These limits could be imposed electronically for the case of a completely integrated system. The limits could be mechanical for a series servo arrangement.

The requirement for continuous control demands the use of redundant control system elements. The F-4 fly-by-wire (SFCS, Reference 5) program is developing redundant hydraulic actuators, servo valves,and electronics to ensure continuous control.

3.4 Analytical Considerations

A complete model of both the control system and the aeroelastic airframe is necessary for the design of a system for the active control of flutter. Traditional control dynamics and structural dynamics analyses seldom include such an integrated model. The practical design of the control system requires these coordinated studies in both the frequency and the time domains, and each of these domains is preferred for certain aspects of the total analytical job.

3.4.1 **Frequency Domain Analyses** - The frequency domain is appropriate for use in determining dynamic stability. In addition, using power spectral density techniques, the frequency domain can be used to evaluate the environmental response (deflections, loads, stresses, etc.). Frequency domain analyses allow for:

o The assessment of aeroelastic airframe/control system dynamic stability, including both the low frequency effects and flutter.

o The generation of data which is useful for gaining insight into the dynamic stability problem including modal data such as mode shape, frequency, and damping, as well as the identification of the mechanism causing the instability.

o The use of frequency dependent unsteady aerodynamic representations.

o The use of the many tools of classical control theory for the design of the control system.

o The generation of data in a format suitable for PSD gust response and ride quality analyses.

In addition, the frequency response approach is readily and efficiently adaptable to computers. Results can be obtained quickly and cheaply using frequency domain techniques.

3.4.2 **Time Domain Analyses** - Time domain analyses were used in the study for certain aspects of active flutter control not readily treated by the frequency domain analyses. The time domain was used for:

o The evaluation of the rate, displacement, and power demands of the control system.

o The evaluation of the total and complete effect of nonlinearities on both stability and response.

o The assessment of the required power to avoid control system saturation during flight through severe turbulence.

36

3.4.3 _Aerodynamic Theory_ - The principal area of the aeroelastic analyses in which a choice of approaches is required is in the representation of the unsteady aerodynamics, where some of the analytical tools are deficient. Computer programs are not available to accurately assess the unsteady aerodynamics on control surfaces for the high subsonic and transonic region.

The approach used in these studies was to rely heavily on strip theory aerodynamic derivatives modified for finite aspect ratio and compressibility based on wind tunnel data. This procedure is justified for several reasons:

o Believable flutter trends are obtained from strip theory for wings and tails with moderate aspect ratios.

o Curve fit difficulties and inaccuracies quite often compromise the promised accuracy of the more sophisticated lifting surface theories.

o The many parametric variations required make primary use of lifting surface theory economically prohibitive because of excessive computation time per case.

o The strip theory derivatives for control surfaces are consistent with the strip theory derivatives for primary surfaces and can be specified to match measured hinge moment data.

o The data from strip theory may be used in terms of velocity and frequency as separate values rather than being tied to reduced frequency k as required by lifting surface theory, thus allowing an approach to flutter analysis that is similar to flight flutter testing.

3.4.4 _Control System Design Procedures_ - The classical frequency domain design procedures are suitable tools for the study of active flutter control. These conventional approaches to the control system design were chosen in preference to the Optimal Control Theory (OCT) procedures for the following reasons:

o The gains for each of the state variables which are determined by the OCT must be implemented by practical hardware. This implementation usually requires the subsequent use of an analog computer.

o Compensation network design must still be performed after the OCT has determined the optimum state variable gains.

o OCT is formulated in the time domain and thus is inherently very expensive to use for the high frequency systems characteristic of flutter.

37

3.5 Principal Analytical Tools

Recently developed computer programs for integrated control/structural dynamics analyses in both the frequency domain and the time domain have been used in these studies. Both programs are designed to evaluate the dynamic stability of a general aeroelastic system considered as an integral part of a multi-loop feedback control system. Detailed descriptions of these programs are given in Appendix IV; the highlights are covered in the subsequent paragraphs.

3.5.1 <u>Active Control of Flutter (ACF) Computer Program - Frequency Domain</u> - This computer program is designed specifically for general application to the study of active flutter control. It represents an effort at the integration of the technologies of control dynamics and structural dynamics into a single computerized package. The dynamic stability of the combined general aeroelastic system is evaluated both passively and as an integral part of the active multi-loop feedback control system. Freedom of choice is allowed in the assignment of control system components. Sensor types and locations may also be specified in an arbitrary fashion.

The current idealization for this computer program is described by the two loop control system block diagram shown in Figure 18. Both control system blocks and aeroelastic airframe blocks are shown in the figure.

3.5.1.1 <u>Control System Blocks</u> - The transfer function blocks other than blocks 5, 9, and 10 are designed to represent the control system. These control system blocks will accept a linear representation of the control system and sensor components. Dimensions in the program allow for a fourth order ratio of transforms in each block. These transforms are of the form

$$\frac{a_0 S^0 + a_1 S^1 + a_2 S^2 + a_3 S^3 + a_4 S^4}{b_0 S^0 + b_1 S^1 + b_2 S^2 + b_3 S^3 + b_4 S^4}$$

Control system nonlinearities such as dead band, free play, saturation, and backlash may be specified for these control blocks by the Describing Function Technique of control theory.

3.5.1.2 <u>Aeroelastic Airframe Blocks</u> - Transfer function blocks 5, 9, and 10 are designed to represent the aeroelastic airframe. These blocks contain calculated frequency response functions obtained by simultaneous solution of the forced aeroelastic equations of motion.

38

- Blocks 5, 9, 10 are Calculated Aeroelastic Airframe Frequency Response Functions
- All Other Blocks Represent Control System Transfer Functions
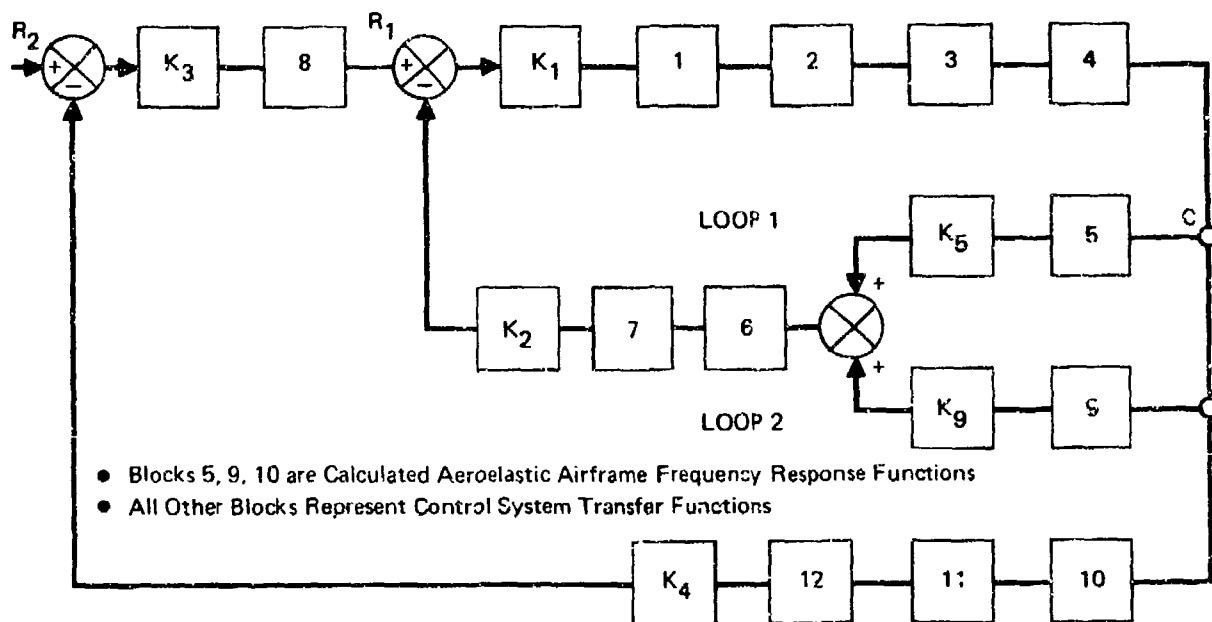
FIGURE 18 CONCEPTUAL FLOW DIAGRAM - ACTIVE CONTROL OF FLUTTER
COMPUTER PROGRAM-FREQUENCY DOMAIN

Aeroelastic Equations of Motion

The aeroelastic equations, for both rigid and flexible motion, are expressed in generalized coordinates to fit the symbolic linear equation,

$$M \ddot{q} + C \dot{q} + K q$$

$$= -Q \left[(A + A_c C^{-1}(k)) q + (B + B_c C^{-1}(k)) \frac{\dot{q}}{V} + I \frac{\ddot{q}}{V^2} \right]$$

where $C^{-1}(k)$ is an equivalent time domain representation for the Theodorsen function of reduced frequency k. This formulation, as well as an alternate formulation based on the classical aerodynamic derivatives $(R + i I)$, is described in Appendix IV.

These equations of motion are transformed to the frequency domain by the harmonic motion constraint,

$$q_j = q_{j_0} e^{i\omega t} \qquad i = \sqrt{-1}$$

The Theodorsen function is expressed as

$$C(k) = F(k) + i G(k)$$

where

$$F(k) = \frac{J_1 (J_1 + Y_0) + Y_1 (Y_1 - J_0)}{(J_1 + Y_0)^2 + (Y_1 - J_0)^2}$$

$$G(k) = \frac{J_0 J_1 + Y_0 Y_1}{(J_1 + Y_0)^2 + (Y_1 - J_0)^2}$$

and J_0, J_1, Y_0, Y_1 are the J and Y Bessel Functions of the first and second kind. The equations of motion then become,

$$\left(-\omega^2 \left[M + \frac{Q}{V^2} I \right] + \left[K + Q(A + A_c C(k)) \right] + i\omega \left[C + \frac{Q}{V} (B + B_c C(k)) \right] \right) \{q\}$$

$$= \left\{ \frac{\partial F}{\partial q_{F_1}} \right\} q_{F_1} + \left\{ \frac{\partial F}{\partial q_{F_2}} \right\} q_{F_2} + \cdots$$

where the column matrices added on the right are used for the forcing function degrees of freedom. The forcing functions may or may not involve

40

aerodynamics as the user chooses. When the program is used for a linear study superposition applies, and more than one forcing function may be evaluated.

Frequency Response Functions

The complex equations of motion are solved simultaneously for a specified airspeed (V) and frequency (ω) to obtain the response of each generalized coordinate to the forcing function. The complex frequency response functions are sensed by sensors located at arbitrary points on this aeroelastic system. The sensor output response functions are calculated by the general symbolic equation,

$$\left(\frac{\theta_{out}}{q_{F_1}}\right) = S^n \left[\phi_1 \frac{q_1}{q_{F_1}} + \phi_2 \frac{q_2}{q_{F_1}} + \cdots\right]$$

n is the response type

    $n = 0$ gives deflection response

    $n = 1$ gives rate response

    $n = 2$ gives acceleration response

The participation coefficients ϕ_i specify the relative amounts for each generalized coordinate in the general response equation. For the elastic degrees of freedom the participation coefficients are the modal data at the location where the response is being calculated.

These sensor signals represent the airframe dynamics in blocks 5, 9, and 10 of the two-loop aircraft control system shown in Figure 18. This idealization is easily modified to apply to more complicated systems, if necessary, by minor changes in the main FORTRAN calling program. The current idealization is based on the premise that unused generality in a computer program is costly in terms of both turn-around-time and money.

3.5.1.3 Control Loop Calculations - Frequency response transfer function data is calculated for control loops 1 and 2 of Figure 18 for each specified V and ω.

F r loop 1 the forward transfer function is evaluated as,

    $G_1(S) = K_1$ (1) (2) (3) (4)

where (1) etc. are symbolic references to block numbers in the figure. The feedback transfer function is evaluated as,

    $H_1(S) = K_2$ (6) (7) $\left[K_5 (5) + K_9 (9)\right]$

Then, the closed-loop transfer function for loop 1 is evaluated as,

$$\frac{C}{R_1} = \frac{G_1 (S)}{1 + G_1 (S) H_1 (S)}$$

The denominator of this expression is the characteristic equation for control loop 1. The stability of the loop may be assessed by examination of this characteristic equation. Certain other data such as bandwidth, peak response, and rise time may also be determined.

Similar calculations are performed for loop 2. The forward transfer function for loop 2 is,

$$G_2 (S) = K_3 (9) \frac{C}{R_1}$$

The feedback transfer function is,

$$H_2 (S) = K_4 (10) (11) (12)$$

The closed-loop transfer function is then,

$$\frac{C}{R_2} = \frac{G_2 (S)}{1 + G_2 (S) H_2 (S)}$$

3.5.1.4 Stability Assessment – Dynamic stability is assessed for both the passive aeroelastic system, represented by the left hand side of the equations of motion, and the closed-loop feedback control system.

Passive Dynamic Stability

The stability of the aeroelastic equations of motion, for a typical nine degree-of-freedom representation of the F-4 with external stores, is shown in Figures 19 and 20. These figures are generated by the computer program. They allow stability to be assessed at a glance with no manual effort. The procedure is thus ideal for a computer graphics application.

Stability is sensed by the Mikhailov stability criterion of Reference 6 which states that the characteristic equation of the equations of motion has only roots with negative real parts (i.e., stable) if, and only if, the Mikhailov response diagram (the plot of the characteristic equation in the complex plane for $0 < \omega < \infty$) passes through exactly n multiples of π degrees in the positive sense (counter-clockwise), where n is the number of the complex roots in the characteristic equation. An equivalent criterion for

42
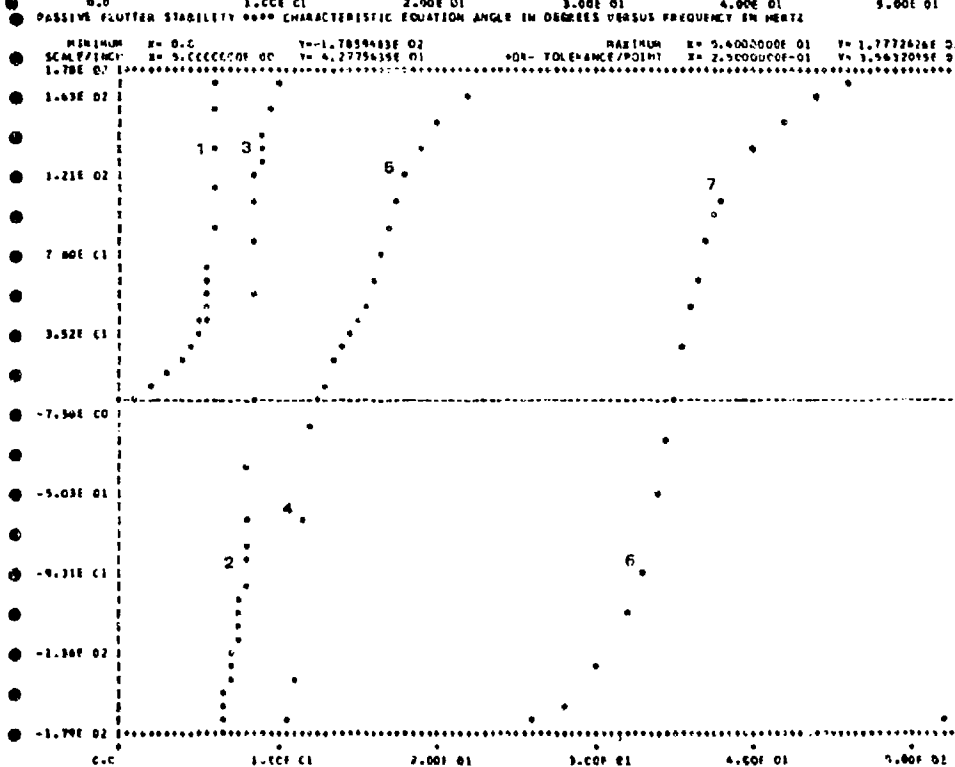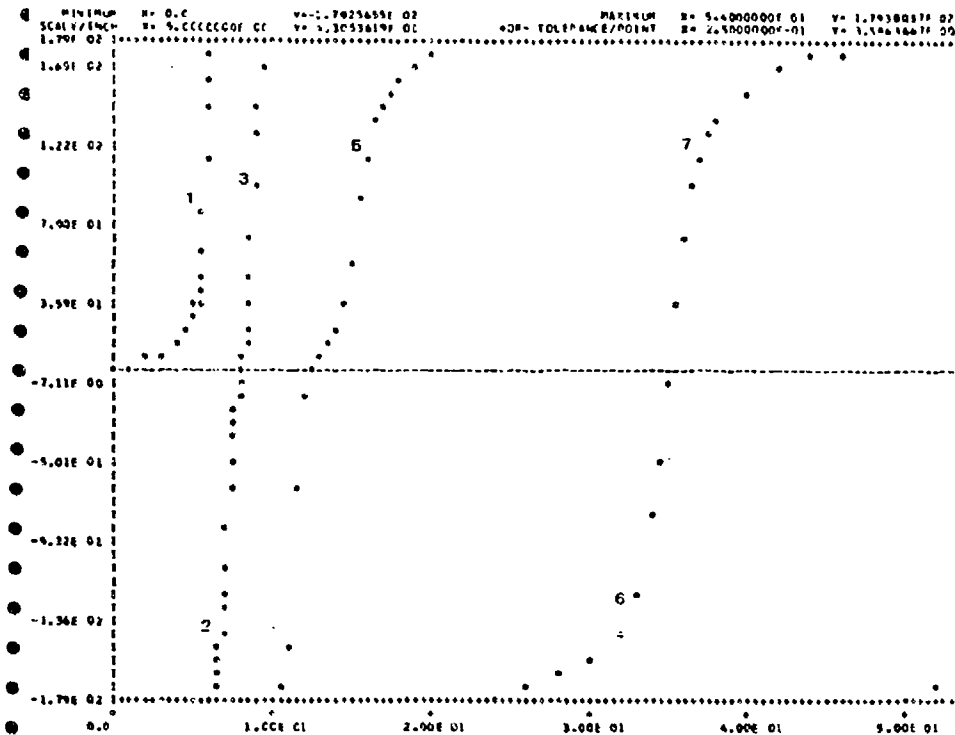
FIGURE 19 VARIATION OF PHASE WITH FREQUENCY FOR TYPICAL AEROELASTIC
EQUATIONS - V = 200 AND 550 KEAS

43
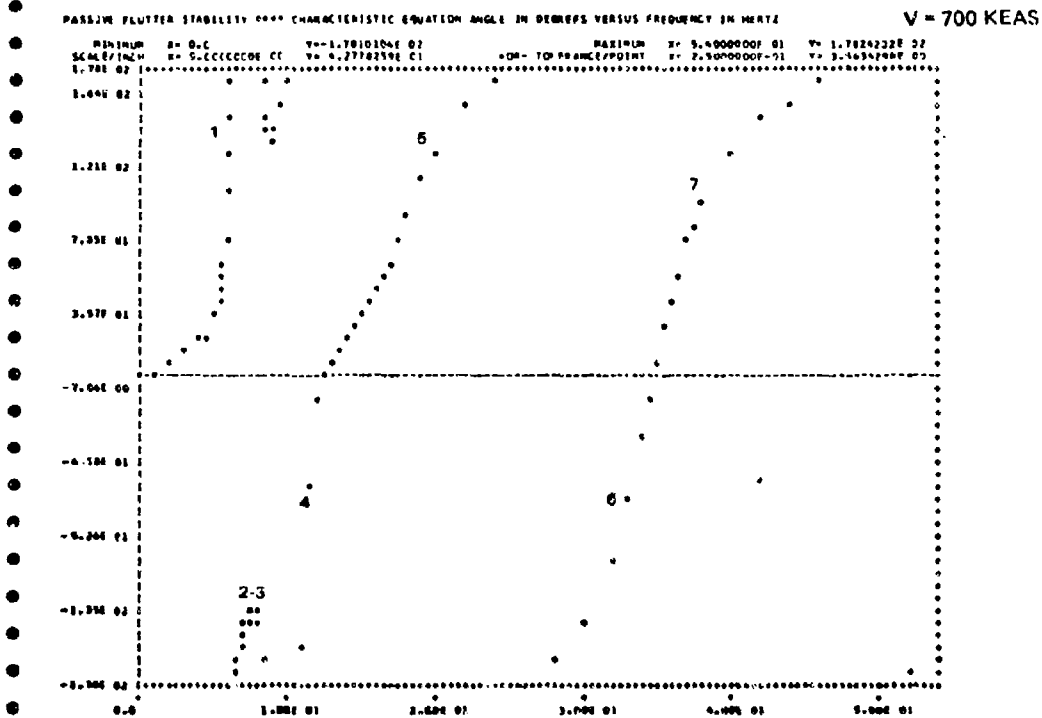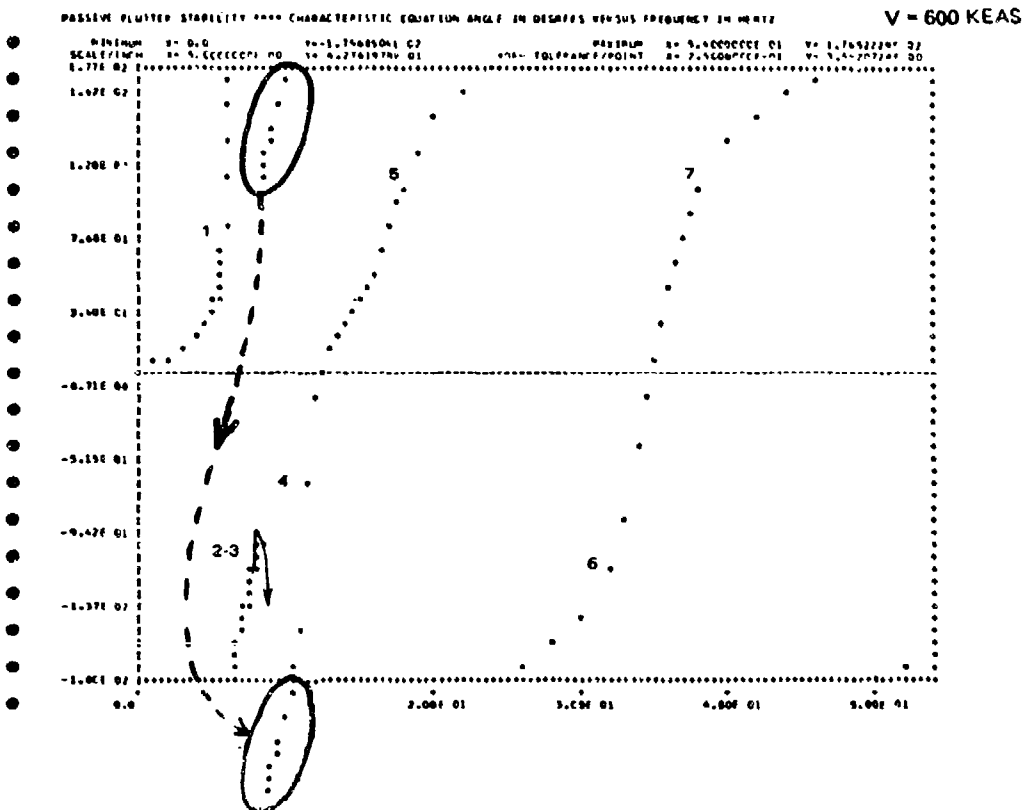
FIGURE 20 VARIATION OF PHASE WITH FREQUENCY FOR TYPICAL AEROELASTIC
EQUATIONS - V = 600 AND 700 KEAS

the assessment of passive stability is described by Landahl in Reference 7. The upper half of Figure 19 shows the variation of the phase angle of the characteristic equation in degrees versus the excitation frequency in Hertz when the velocity is 200 KEAS (Knots Equivalent Airspeed). Traces are shown for the 7 lowest vibration modes. The traces are continually increasing and each trace sweeps out a 180 degree phase change in the positive sense indicating a stable system. The equivalent structural damping in each mode for this case is $g = 0.04$. A stable system is also indicated for a velocity of 550 KEAS as shown by Figure 19.

At a velocity of 600 KEAS an instability is indicated by a barely detectable reversal in the direction of the trace in the neighborhood of 8 Hertz as shown in the upper half of Figure 20. Figure 20 also shows the unstable system when deep in the flutter region at 700 KEAS. The phase reversal is easily recognized at 700 KEAS. Flutter has occurred at a velocity between 550 and 600 KEAS. A vernier of velocity increments can be used to establish the velocity of flutter occurrence within a smaller range.

For conventional flutter analyses, the structural damping can be specified as $g = 0.0$ to obtain data corresponding to the crossings of traditional V-g studies.

Closed-Loop Stability

The stability of the closed-loop system is determined by a modified form of the Nyquist criterion of Reference 8. The characteristic equation for the closed-loop system is plotted in the complex plane so that the origin replaces the -1 point of the classical criterion. The Nyquist stability criterion determines the existence of zeros in the right half plane of the closed-loop characteristic equation $1 + G(S) H(S) = 0$, by tracing out the trajectory of $1 + G(S) H(S)$ as S encircles the entire right half plane. For each pole in the right half plane, the Nyquist trajectory will encircle the origin in the CCW (counter-clockwise) direction. For each zero, the encirclement will be in the CW (clockwise) direction. To ensure a stable closed-loop system, which requires that there are no zeros of the characteristic equation in the right half plane, the net number of encirclements, if any, must be both CCW and equal to the number of open-loop poles in the right half plane. An example of a stable multiple degree of freedom system with two poles in the right half plane is shown in Figure 21. As the frequency varies from 0^+ to $+\infty$ and from $-\infty$ to 0^-, there are two net CCW encirclements.

Unstable Passive System - Stable Active System

NO POLES AT ORIGIN
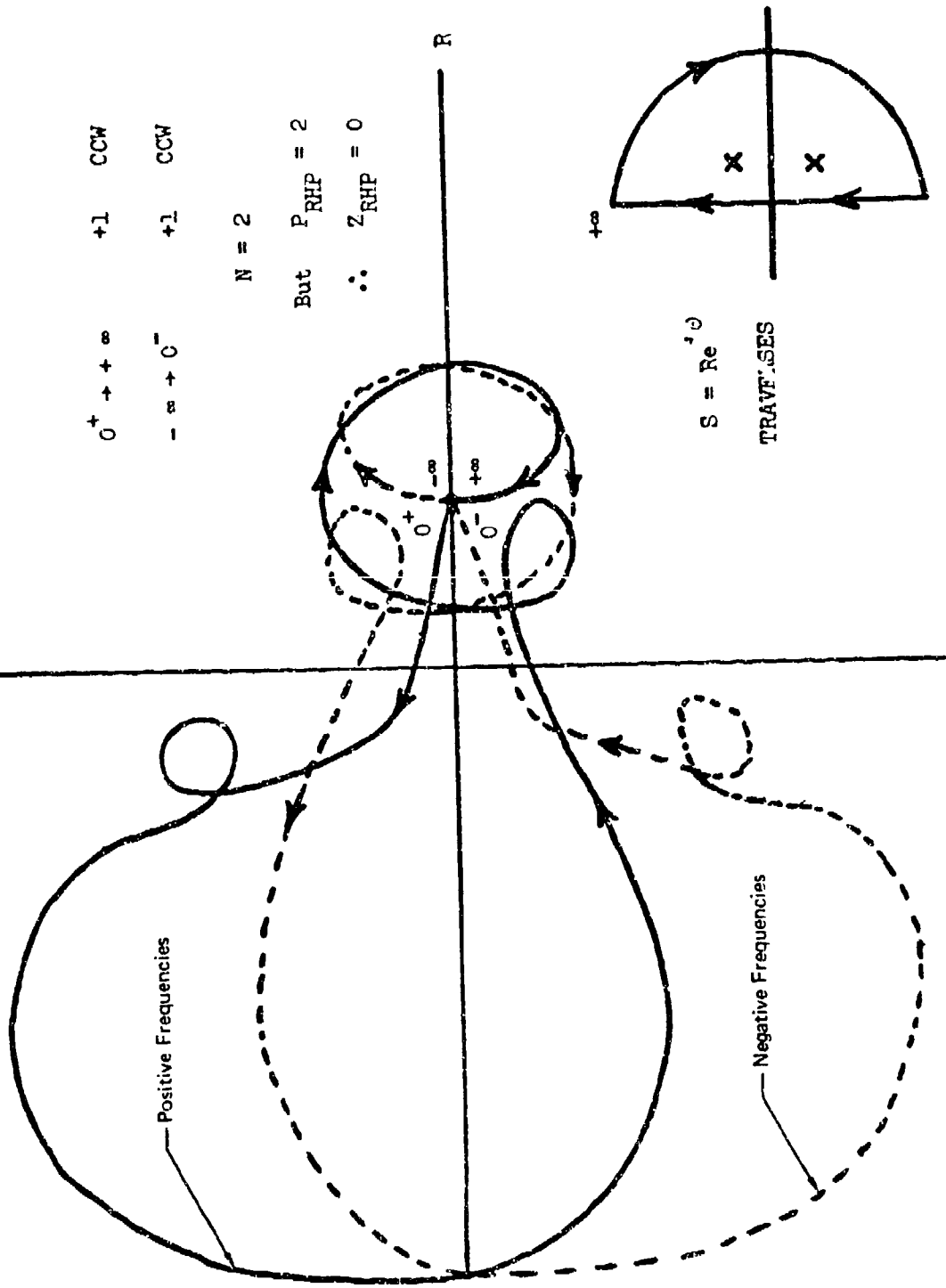
$0^+ \to +\infty$ $+1$ CCW

$-\infty \to 0^-$ $+1$ CCW

$N = 2$

But $P_{RHP} = 2$

$\therefore$ $Z_{RHP} = 0$

$S = Re^{j\theta}$

TRAVERSES

Positive Frequencies

Negative Frequencies
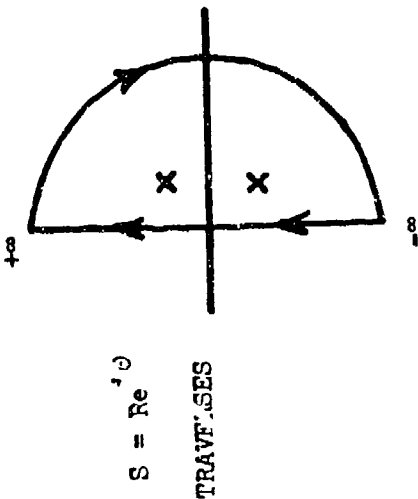
FIGURE 21 EXAMPLE OF STABILITY ASSESSMENT USING THE NYQUIST CRITERION

46

The variation from $+\infty$ to $-\infty$ around the infinitely large semi-circle is represented by the single point at 1.0, and since there are no poles at the origin O^+ and O^- are the same point. The two net CCW encirclements are equal to the number of poles in the right half plane, therefore the number of ι s in the right half plane is zero, and the system is stable.

Modified Nyquist plots are shown in Figure 22 for the characteristic equation of the closed-loop system of an example case when a sensor picks up only the angle-of-twist acceleration of the unstable flutter mode. The open-loop gain for the inner loop of Figure 18 is $K_1 = 250.$, block 7 has form $(S/1+S)$, block 1 has the form $(1/1+.1S)$, block 5 senses the acceleration of the unstable flutter mode, $K_1 = 0.0$, and all other blocks are unity. The system is stable at 200 KEAS but a control system instability at approximat 8.3 Hz is indicated for a velocity of 500 KEAS. Note that this instability, which is indicated by the clockwise encirclement of the origin, occurs at a lower speed than the passive flutter velocity of 575 KEAS. The control system has been driven unstable by the relatively high open-loop gain and the cumulative effect of phase lags in the control loop. The situation is similar at 550 KEAS where clockwise encirclement of the origin is still indicated. Passive flutter has occurred for the speed of 600 KEAS as indicated he change in the direction of closure for the trajectory. The phase change of the Nyquist trajectory is clockwise (CW) below flutter onset and counterclockwise (CCW) above flutter onset. The flutter roots are in the denominator of the expression for the characteristic equation so that when flutter occurs, there are two poles (one for both positive and negative frequencies) in the complex right half plane. For the velocities of 600 and 700 KEAS in Figure 22 the number of net encirclements of the origin is zero. The closed-loop system is unstable since the number of zeros in the right half plane is $Z = N = 0+2 = 2.$

3.5.2 <u>Active Control of Flutter Computer Program - Time Domain</u> - This computer program is designed for general application to the study of active flutter control in the time domain. The program, which is written using the McDonnell MIMAC simulation language (a modification of the AFFDL MIMIC system) is intended to complement the frequency domain program.

The MIMAC system is a digital equivalent to an analog computer. The input language enables a user to prepare program statements describing a physical system, starting from either a block diagram or a differential equation representation of that system.
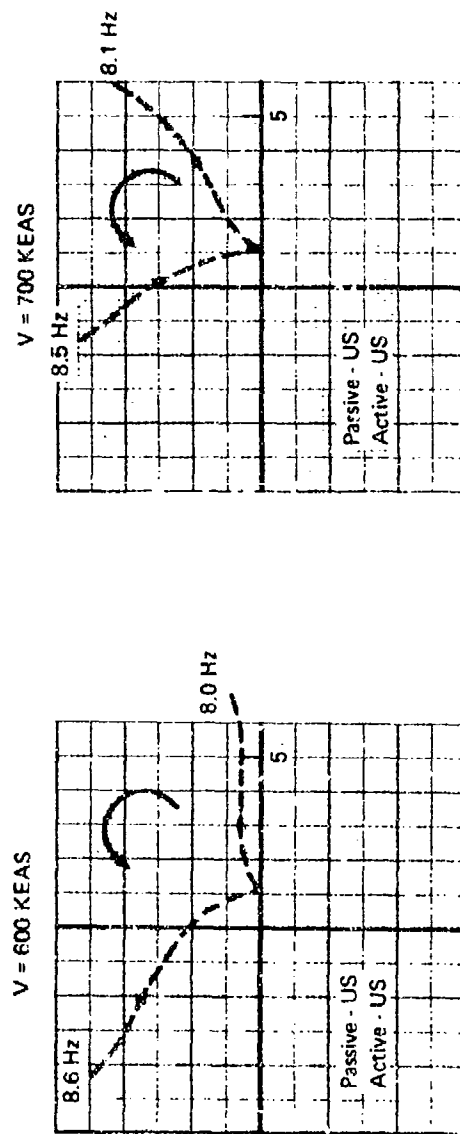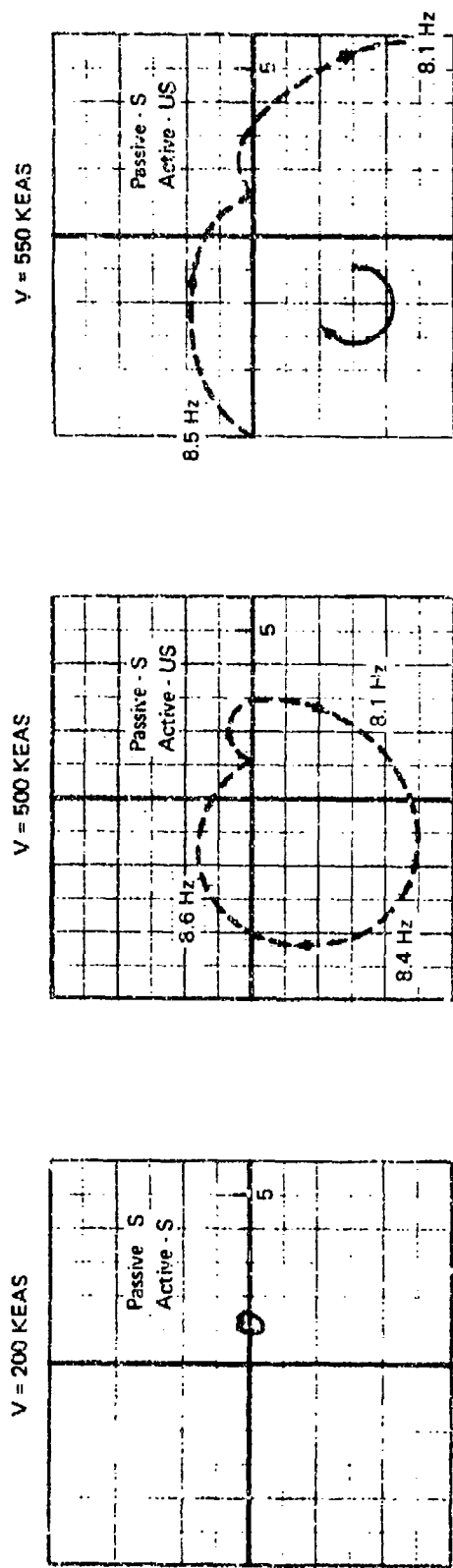
FIGURE 22 MODIFIED NYQUIST PLOTS AT VARIOUS FREESTREAM VELOCITIES
FOR CLOSED-LOOP SYSTEM
(Origin Replaces the −1 Point)

48

The current idealization for this computer program is described by the control system block diagram shown in Figure 23. The model consists of two gains, nine control system transfer function blocks, and an aeroelastic airframe block.

3.5.2.1 Control System Blocks - The control system blocks can accept a second order ratio of transforms for each block of the form

$$\frac{a_{10} + a_{11} S + a_{12} S^2}{b_{10} + b_{11} S + b_{12} S^2}$$

The solution technique requires a formulation (standard form) with the highest derivative of each variable expressed in terms of lower derivatives of the same variable and other known variables. Because of this solution technique, the coefficients b_{i2} may not be equal to zero. If, for example, a block is to be unity it must be expressed as

$$\frac{a_{12} S^2}{b_{12} S^2}$$

where $a_{12} = b_{12} = 1.0$
Similar logic applies for other transfer functions.

3.5.2.2 Aeroelastic Airframe Blocks

Aeroelastic Equations of Motion

The specific MIMAC program used in these studies expresses the aeroelastic equations to fit the symbolic equations

$$M \ddot{q} + C \dot{q} + K q + Q A q + \frac{Q}{V} B \dot{q} + \frac{Q}{V^2} I \ddot{q}$$

$$+ Q A_c [q(0) \phi(s) + \int_o^s \frac{dq}{d\sigma} \phi(s - \sigma) \, d\sigma]$$

$$= \frac{Q}{V} B_c [\dot{q}(0) \phi(s) + \int_o^s \frac{d^2 q}{d\sigma^2} \phi (s - \sigma) \, d\sigma]$$

$$= \{\frac{\partial F}{\partial q_{F_1}}\} q_{F_1} + \{\frac{\partial F}{\partial q_{F_2}}\} q_{F_2} + \ldots$$
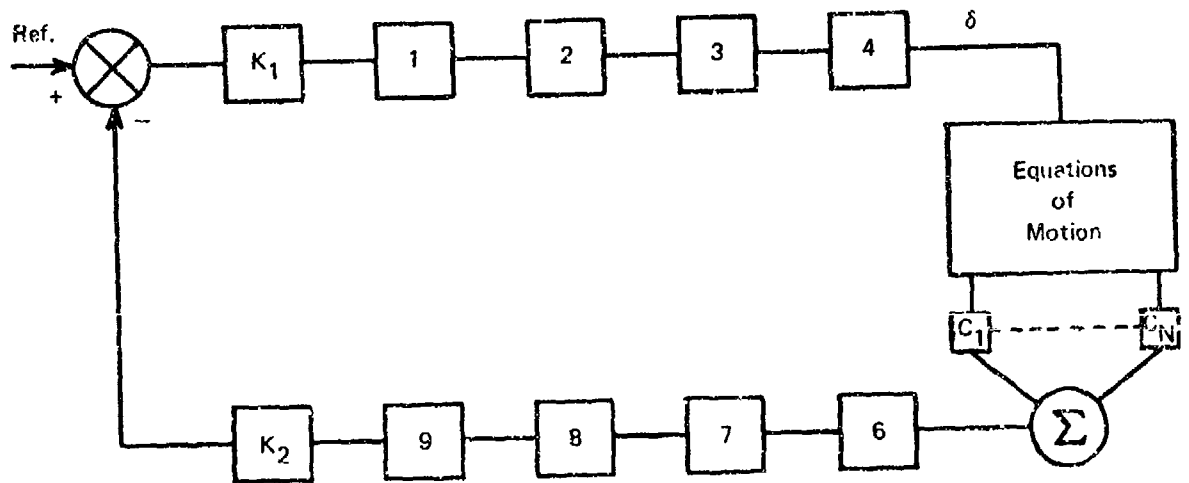
FIGURE 23 CONCEPTUAL FLOW DIAGRAM-ACTIVE CONTROL
OF FLUTTER COMPUTER PROGRAM-TIME DOMAIN

This time domain program is designed to match the frequency domain program as closely as possible. The convolution integral, based on the Wagner function, is used to represent the unsteady indicial aerodynamics in the time domain program. The Theodorsen function represents the equivalent unsteady effect in the frequency domain program. Other than this difference there is a one-to-one correspondence between the two programs. The final form of the equations of motion, as programmed, are developed in Appendix IV.

Aeroelastic Transfer Function

The transfer function block for the aeroelastic airframe allows for the feedback of a linear combination of the generalized coordinates and their derivatives obtained by a solution of the forced aeroelastic equations of motion. This linear combination transforms the generalized coordinates back into physical coordinates. The numerator of control system block 6 is used to indicate the order of the response being sensed; acceleration, rate, or deflection.

3.5.2.3 Control Loop Calculations

Closed-Loop Time History

The primary purpose of this time based computer program is to evaluate those aspects of the study of active flutter control for which the frequency domain data is questionable or deficient. The program may be used to verify the relative effectiveness, in terms of damping, of active flutter control systems designed in the frequency domain. The time history printouts also give the displacement and rate requirements for the control system for various types and amplitudes of excitation. In general, the data required is the same as that for the frequency domain program described in Section 3.5.1. Current dimensioning allows for the evaluation of up to 10 generalized coordinates.

Nonlinear Effects

The MIMAC format allows the user to program nonlinear or time-variant problems. The existing MIMAC program library includes special purpose function generators for effects such as dead space, free play and saturation. Switching type functions such as relays, flip-flops, and quantizers are also available for use. The functions available in the MIMAC library are supplemented by the FORTRAN library and any specific function programmed in FORTRAN by the user.

51

Passive Dynamic Stability

The MIMAC program may be used to evaluate the passive stability of the aeroelastic equations of motion. To do this the control system is decoupled from the aeroelastic airframe by deleting all terms which involve the control surface rigid actuator deflection. The resulting equations may then be forced with whatever forcing function the user desires.

4. FLUTTER CONTROL STUDIES

4.1 Wing/Store Flutter Control

The design of an active flutter suppression system consists of the following steps:

1. Analytical description of the flutter mechanism (from passive flutter studies)
2. Selection of deformation sensor location and type
3. Selection of the suppression scheme
4. Definition of system hardware requirements

This section describes each of these areas. Passive solution techniques, involving mass additions to the wing or stores and pylon stiffening, are also discussed so that the desirability of employing an active flutter suppression system can be properly evaluated. The target flutter onset speed for these wing/store studies was assumed to be 730 knots at sea level (corresponding to the maximum dynamic pressure capability of the F-4 aircraft with stores). Reference 9 discusses the problems associated with a wide gamut of passive wing/store flutter fixes, including pylon stiffness adjustments and mass additions to the wing.

4.1.1 Passive Flutter Studies

4.1.1.1 Baseline Design — The analytical models for the wing/store configurations considered in this study are described in Appendix I. Each model consists of a truncated set of wing/store modes: the first nine normal modes plus an aileron rotation mode. These data are used in F-4 flutter analyses for external stores. Modified strip theory aerodynamics with experimental coefficients were used in the analysis. The Indicial Lift flutter program, described in Appendix IV, was used to determine passive flutter velocities and mechanisms. The program was also used to generate the aerodynamic matrices needed for the subsequently run active stability programs.

F-4 wind tunnel test data, shown in Figure 24, from Reference 10 was used to obtain values for the lift curve slope (C_{L_α}) and the location of the center of pressure (CP). Two aerodynamic conditions were chosen for this study:

- $M = 0.9$ $C_{L_\alpha} = 4.6/\text{radian}$ $CP = 25\%$
- $M = 1.2$ $C_{L_\alpha} = 4.08/\text{radian}$ $CP = 37\%$

53
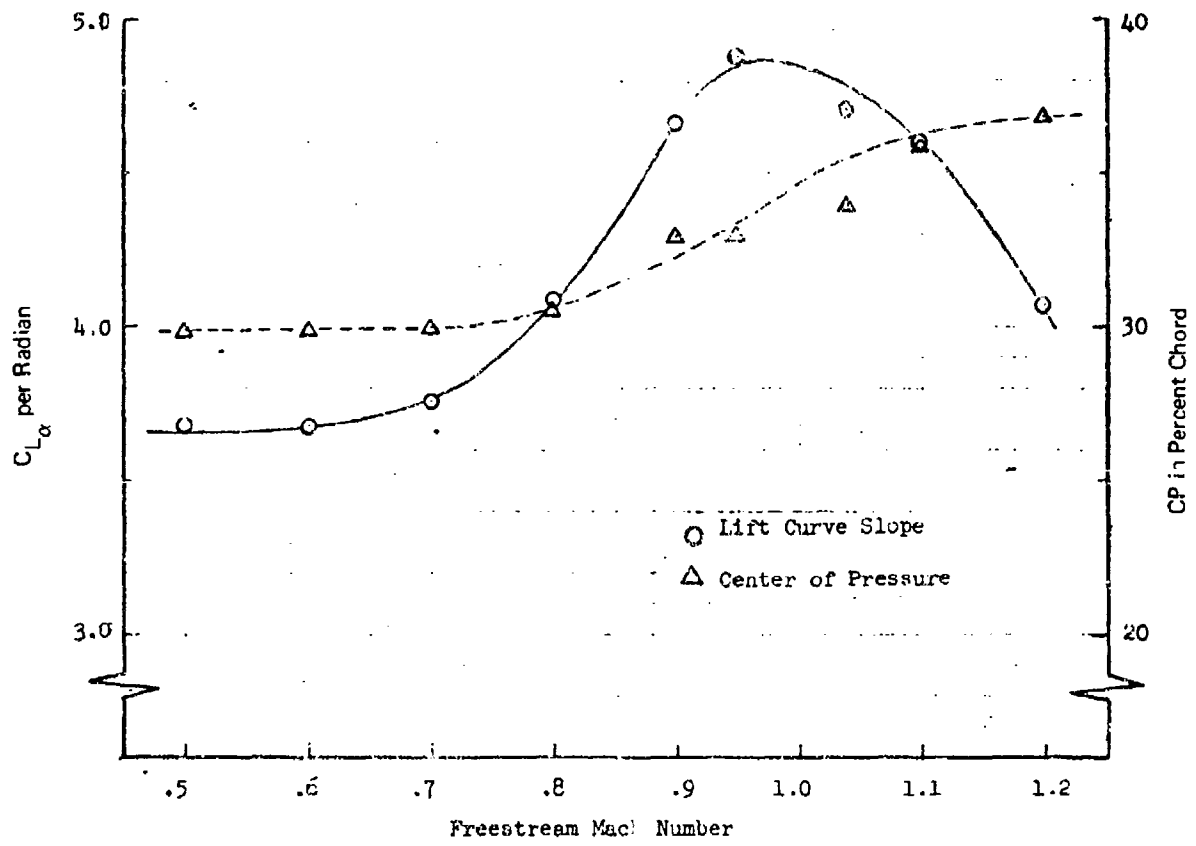
FIGURE 24 VARIATION OF C_{L_α} AND CP WITH MACH NUMBER FOR THE F-4 WING

The Mach 0.9 CP was assumed at the 25% chord rather than the 33% chord shown in the figure to ensure minimum flutter velocities. The two Mach Number conditions were selected to bracket the region of the F-4 flight envelope in which wing/store flutter normally occurs. All of the baseline passive flutter studies were run at sea level air density. The eight section wing shown in Figure 25 was used as the aerodynamic model. The control points indicated in the figure were used to compute the wing twist and vertical displacement at each section. Displacement data interpolated from the adjoining sections was used for the two sections, 4 and 7, which lack control points.

The classical V-g and frequency coalescense plot for the 90% full 370 gallon tank wing/store study configuration, using M = 0.9 data, is given in Figure 26. The primary instability occurs at 603 knots resulting from the coalescense of the 2nd and 3rd vibration modes at 8.33 Hz. The unstable mode, the 3rd, as indicated by the V-g plot, is the tank pitch - 1st wing torsion mode at zero airspeed. At velocities near flutter, however, the unstable mode as defined by the eigenvector may have significantly different characteristics. (For example, the 62% full-370 gallon tank case flutters in the third mode, also, but its characteristics at flutter onset most closely resemble those of the second still-air mode.) Flutter of the 90% full-370 gallon tank configuration has actually been detected during flight test. The flutter occurrence, reported in Reference 11, was recorded during a 618 knots equivalent airspeed (KEAS) flight at 5,000 feet while fuel in the 370 gallon external tank was being used. Figure 27 is a plot of the external tank theoretical flutter onset velocity as a function of fuel loading. Superimposed on the plot is the test flight line indicating flutter onset at 91% fuel load and termination at 81%.

A complete summary of flutter onset data for all of the wing/store cases under study is given in Table 3 for subsonic and supersonic aerodynamic data. The columns labeled g/V give the change in effective structural damping coefficient during a 100 knot velocity increment centered at the flutter onset velocity. This parameter is a measure of the severity of flutter. The larger the value the more explosive the flutter. The table shows that in every instance, supersonic aerodynamics increases the flutter speed. Only in one instance, the 31% full 370 gallon tank case, is the
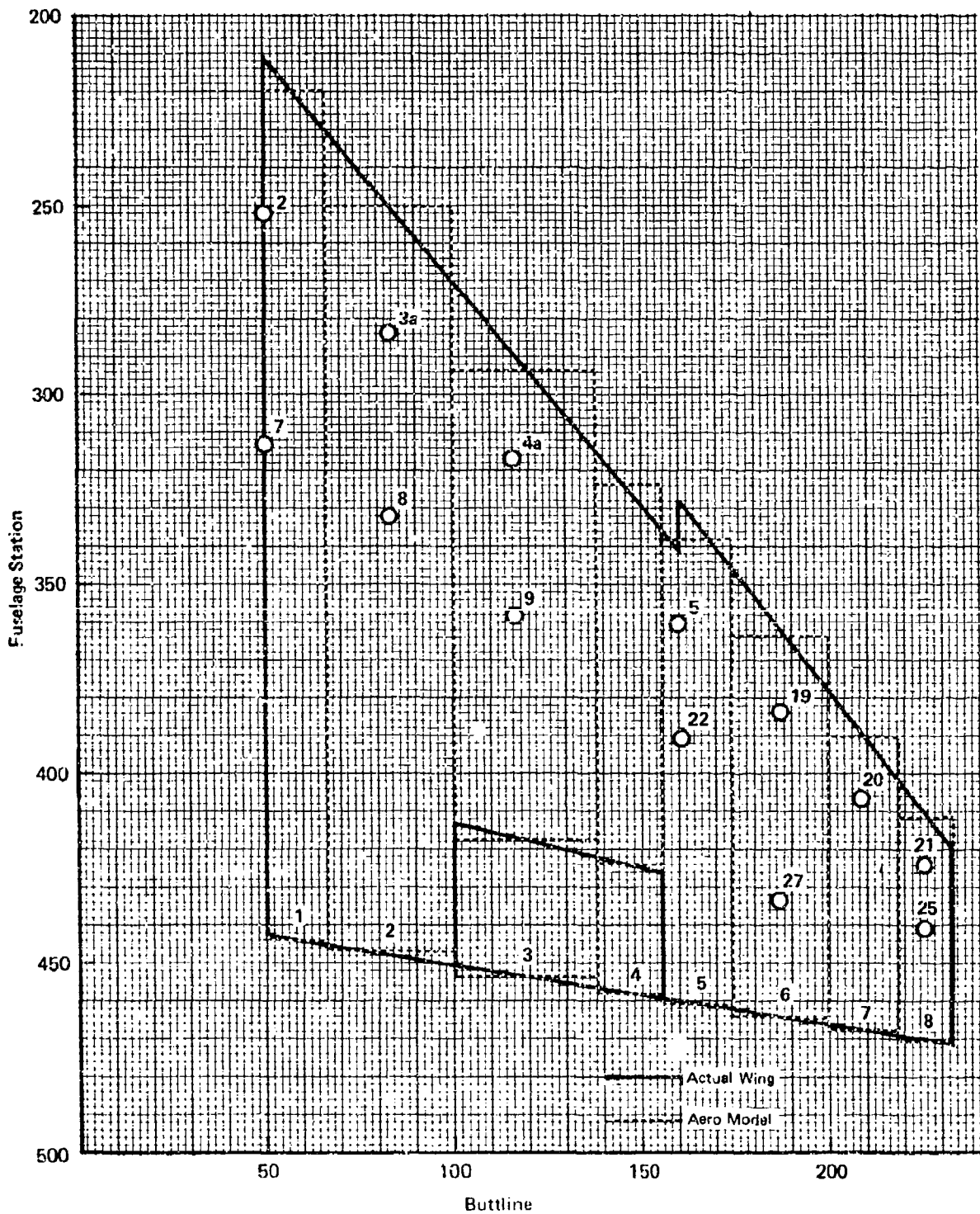
FIGURE 25 AERODYNAMIC IDEALIZATION
OF F-4 WING
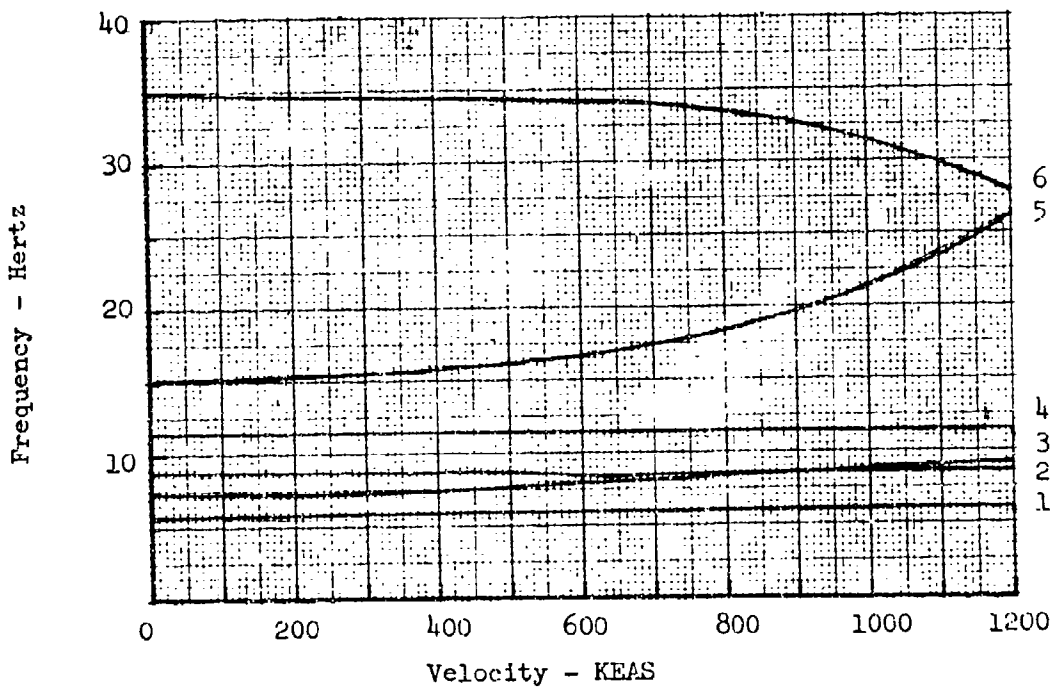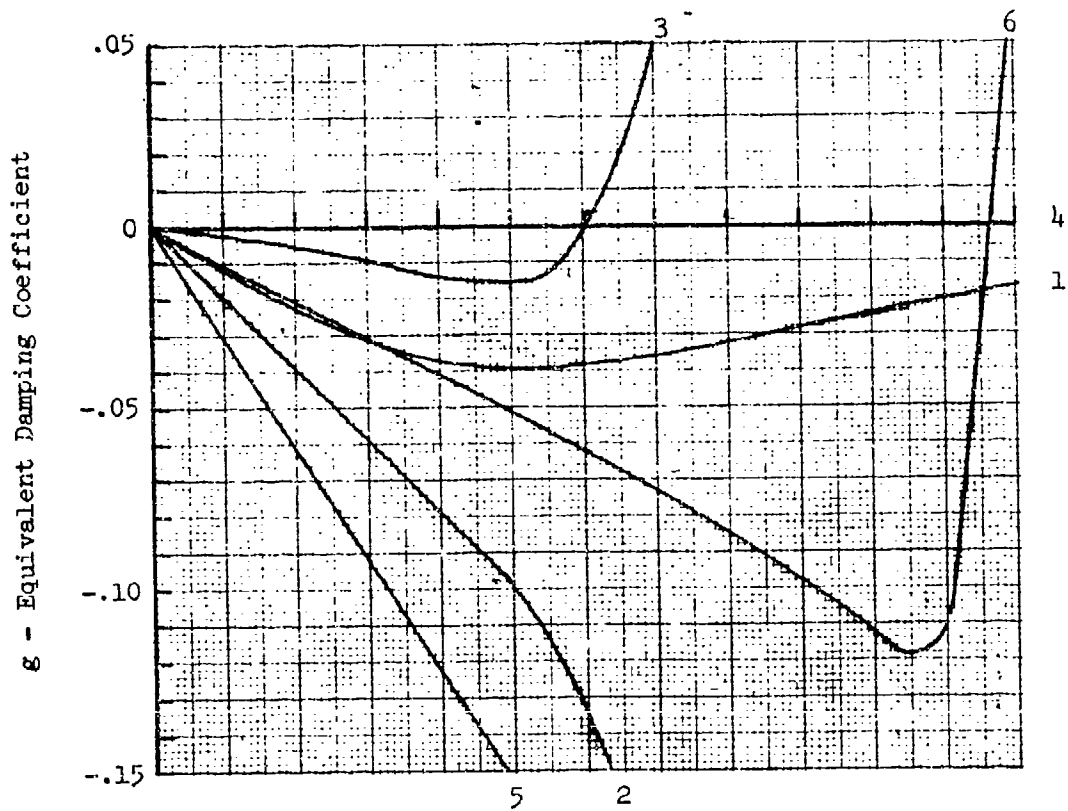
FIGURE 26 DAMPING AND FREQUENCY vs VELOCITY - F-4 WING WITH
370 GALLON TANK 90% FULL WITH LIQUID FUEL INERTIA CHARACTERISTICS

Lift Curve Slope Equal to 4.60/Radian
Center of Pressure at Quarter Chord
Data Shown is for Zero Equivalent Damping Coefficient
Sea Level Conditions
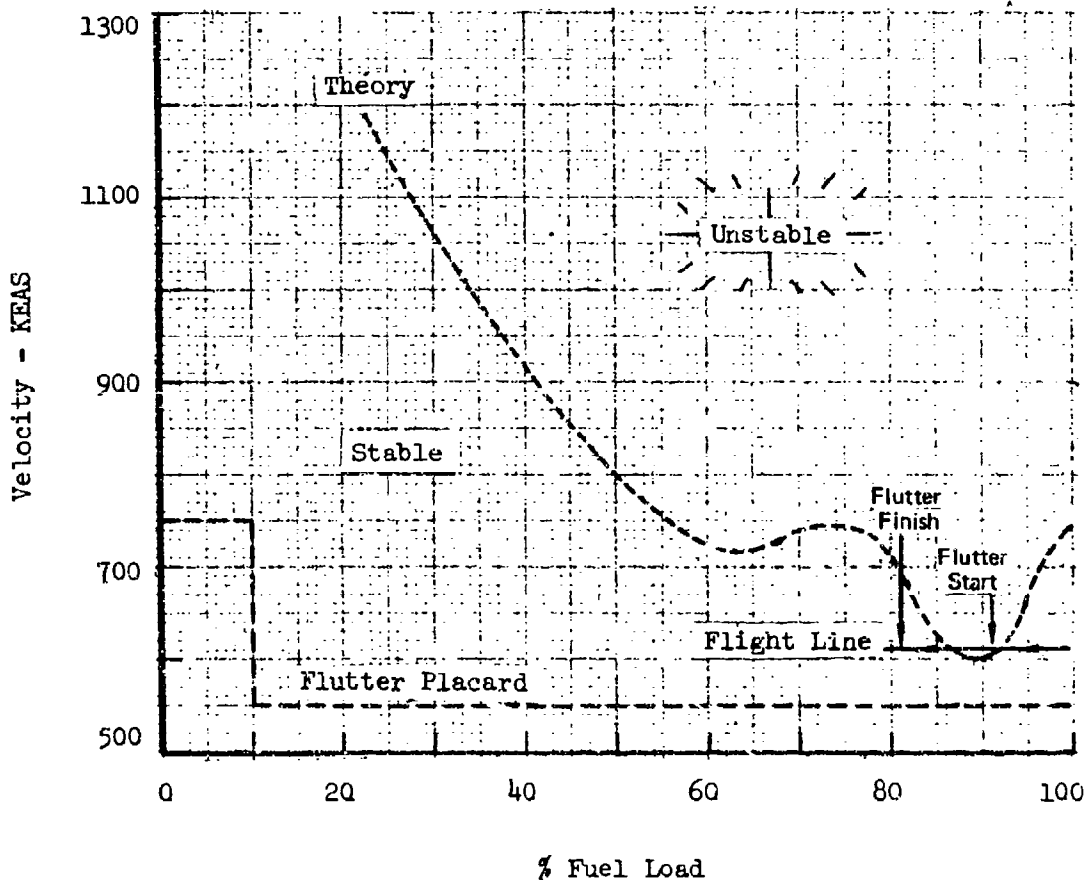
FIGURE 27 FLUTTER BOUNDARY - F-4 WITH 370 GALLON TANK

TABLE 3 SUMMARY OF WING/STORE FLUTTER ANALYSES BASED ON
THE CORNELL AERODYNAMIC DATA

	M = 0.9				M = 1.2			
	Analysis using C_{L_α} = 4.6, CP at 25% Chord				Analysis using C_{L_α} = 4.08, CP at 37/% Chord			
	Flutter Velocity KEAS	Frequency Hz	g/V 1/100 KEAS	Modal Interaction	Flutter Velocity KEAS	Frequency Hz	g/V 1/100 KEAS	Modal Interaction
370 Gal. Tank 90% Full	600	8.33	.051	2, 3	621	8.45	.0471	2, 3
370 Gal. Tank 62% Full	713	10.13	.042	2, 3	987	10.09	.0318	2, 3
370 Gal. Tank 31% Full	1050	12.88	.272	2, 3	1475	28.21	.157	5, 6*
MK-84 EO/ MAU Pylon	683	10.71	.024	2, 3	731	11.09	.0092	2, 3
MK-82 (3,4) MER/MAU	371	7.67	.0078	2, 3	377	7.67	.0064	2, 3

*The 2, 3 mode occurs for this case at 1510 KEAS and 12.91 Hz.

flutter mechanism changed during the transition from subsonic to supersonic aerodynamic coefficients. All of the other mechanisms involve coalescence of the 2nd and 3rd still-air modes. The 31% full-370 gallon tank configuration was eliminated from further study at this stage because the flutter onset velocity exceeds 730 knots.

Offhand, the flutter analysis appears to be unnecessarily complicated by including nine vibration modes when the mechanism is a coalescense of modes 2 and 3. The usual rule-of-thumb is to include all of the lower modes up to one more than the highest mode participating in the flutter mechanism. Thus, an analysis which included only the first four modes should have given reasonably accurate flutter predictions. The higher modes, though unnecessary in the flutter analysis, are important in the active stability analysis because their inclusion permits a realistic simulation of a wing motion sensor. Such a sensor is required by a flutter control system to generate the signal which, when compensated, commands the aileron motion that suppresses flutter. Any wing mounted sensor picks up a cumulative displacement resulting from the summation of the displacements due to each vibration mode. Modes near the flutter mode frequency make significant contributions to the total displacement and, thus, may have a profound effect on the relative phase and amplitude of the wing motion at the sensor location. Hence, any implied mode filtering through the elimination of the lower non-flutter vibration modes could cause completely erroneous conclusions concerning the active stability of the system.

4.1.1.2 Passive Flutter Fixes - Mass additions were tried at various store locations in an effort to raise all of the wing/store flutter speeds to 730 knots. Wing mass ballasts and pylon stiffening were also considered.

Store Mass Additions

Store mass ballasts are practical only if they can be located within the existing envelope. Altering the external store geometry to achieve a favorable mass distribution would affect store carriage capability and drop characteristics possibly resulting in a redesign of pylons and/or racks. Hopefully, the ballast weights could be located within the store envelope without displacing payload. Such a payload reduction would degrade the store's performance either as a bomb, fuel tank, or ECM (Electronic Counter-Measures) pod.

370 Gallon Tank - 90% Full - The 20 foot length dimension of the 370 gallon tank allows large translations of the c.g. through store mass addition. For these passive studies mass was added 50 inches aft of the nominal c.g. at the store centerline. This places the balance weight in the aft compartment of the fuel tank. Figure 28 shows the effect of adding mass at this location. About 500 lbs per store or 1000 lbs per aircraft are required to raise the flutter speed to 730 knots. Mass additions forward of the c.g. also improved the flutter velocity, though not as effectively as the aft mass conditions.

370 Gallon Tank - 62% Full - The flutter velocity of the 370 gallon tank - 62% full case showed no clear-cut trends with mass additions 50 inches aft of the c.g. at the store centerline. Figure 29 shows the erratic be-havior of this store's flutter velocity when mass is added. The flutter velocity is actually degraded for wide ranges of mass additions. The flutter speed cannot be increased to 730 knots for the 50 inch aft mass addition scheme for less than a 1000 lb addition. Weight additions forward of the c.g. drastically lower the flutter onset velocity of this store. The addi-tion of 500 lbs 50 inches forward of the c.g. lowers the onset velocity to 155 knots (8.32 Hz).

MK-84 EO - Two passive schemes were tried for the MK-84 EO:

1. Mass addition at the store c.g. with no pitch or yaw inertia change.
2. Mass addition at the store centerline 30 inches aft of the nominal c.g.

30 inch aft dimension for the second scheme was chosen since this placed the mass balance weight within the existing MK-84 EO casing while still permitting a sizeable aft shift in the store c.g.

The first scheme, pure mass addition, was ineffectual - no flutter vel-ocity increase even for weights exceeding 300 pounds.

The second scheme, however, did have a favorable effect on the flutter onset velocity. Figure 30 shows the variation of the two lowest flutter modes with weight addition according to scheme two. The figure shows that approximately 200 lbs per side or 400 lbs per airplane are required to raise the flutter onset speed to 730 knots. It is interesting to note that this weight addition scheme raises the third mode flutter speed but lowers that of the fourth mode. The result is that the cross-over at 300 pounds added weight determines the maximum flutter onset speed (840 knots) possible with this scheme.

Lift Curve Slope Equal to 4.6/Radian

Center of Pressure at the Quarter Chord

Data Shown is for Zero Equivalent Damping Coefficient

Sea Level Conditions
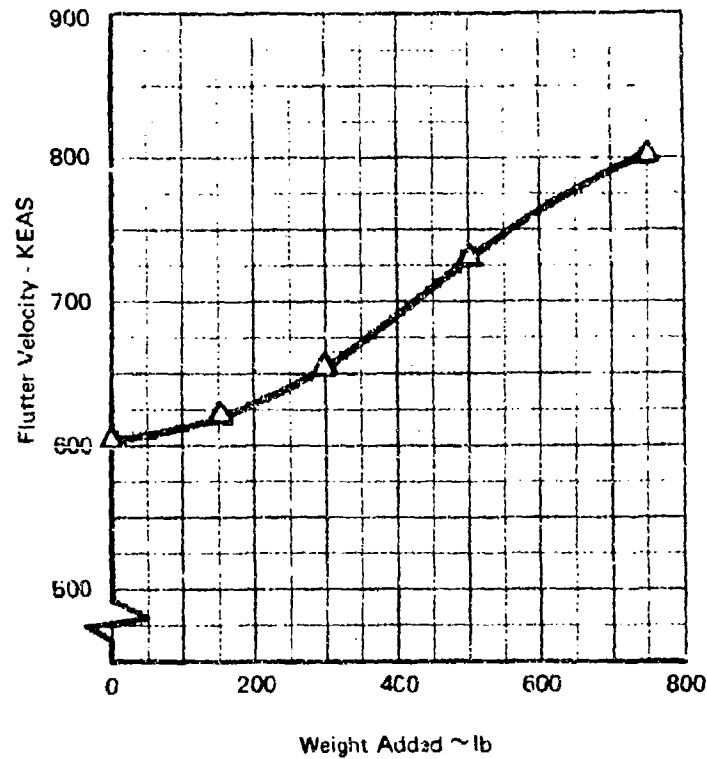
Weight Added ~lb

Note: Weight added 50 in. aft of store C.G.

FIGURE 28 EFFECT OF STORE MASS ADDITION ON THE FLUTTER VELOCITY OF THE 370 GALLON TANK - 90% FULL

Lift Curve Slope Equal to 4.60/Radian
Center of Pressure at Quarter Chord
Data Shown is for Zero Equivalent Damping Coefficient
Sea Level Conditions
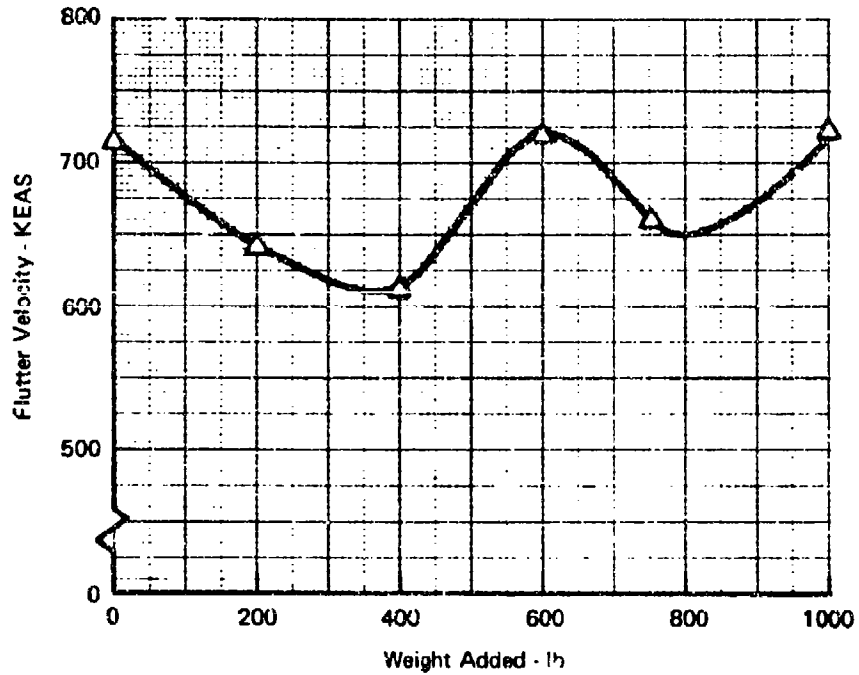
Note: Weight added 50 in. aft of store C.G.

FIGURE 29 EFFECT OF STORE MASS ADDITION ON THE FLUTTER VELOCITY OF THE 370 GALLON TANK - 62% FULL

Lift Curve Slope Equal to 4.60/Radian
Center of Pressure at Quarter Chord
Data Shown is for Zero Equivalent Damping Coefficient
Sea Level Conditions
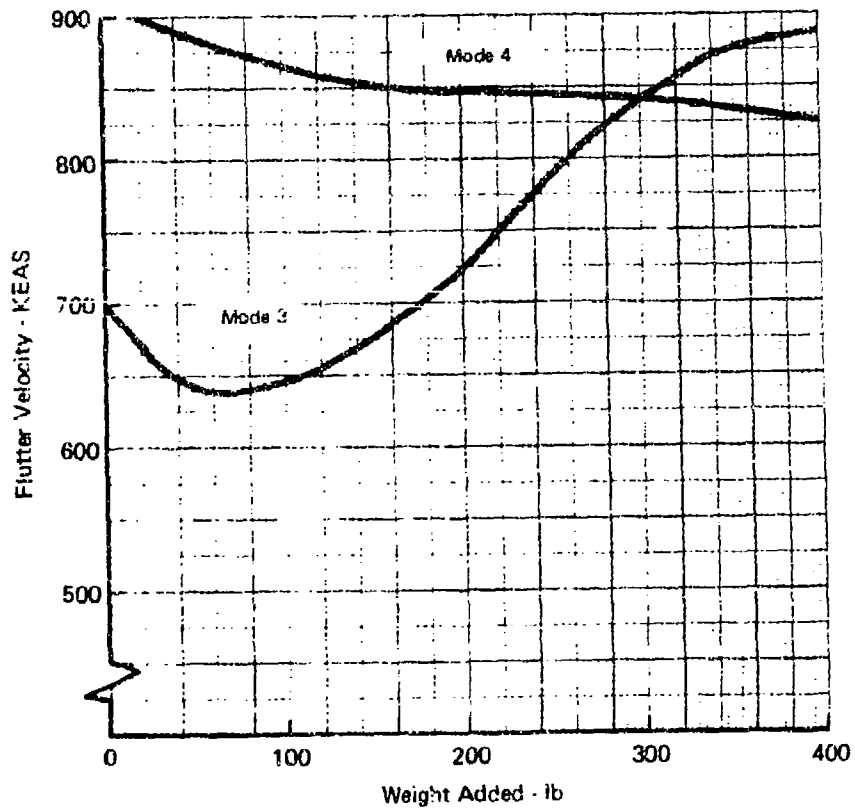
Note: Weight added 30 in. aft of store C.G.

**FIGURE 30 EFFECT OF STORE MASS ADDITION ON THE
FLUTTER VELOCITY OF THE MK-84 EO**

MK-82 (Bombs 3, 4) - Two passive solutions were tried for this case:

1. Concentrated mass addition at each individual store c.g.

2. Concentrated mass addition 15 inches aft of the individual store c.g. centerline.

Figure 31 shows the flutter velocity as a function of store mass addition. The flutter velocity is limited to less than 650 knots for practical mass additions. (Since the store weighs only 520 lbs, it hardly makes sense to add more than 300 lbs to the store.)

It is interesting to note the diminishing improvement of flutter velocity with store mass addition exceeding 150 lbs for the case when the mass is added 15 inches aft of the c.g. The situation here, similar to the MK-84 case, again involves transition from one flutter mechanism to another. In this instance the primary flutter mode changes from a rack vertical bending-wing bending interaction to a pylon pitch - wing bending interaction.

Pylon Stiffness Variation

The elimination of wing/store flutter through pylon stiffness adjustment is a thankless task because of the narrow range of stiffness available to the designer. The stiffness is bracketed on the high side by pylon physical dimensions and backup structure and on the low side by the divergence speed. Normally this stiffness range is insufficient to eliminate flutter, particularly, as is the case in these studies, when multiple stores with fundamentally different flutter mechanisms are carried by the same pylon.

Mass Addition to Wing

No F-4 wing mass additions were tested as passive flutter fixes. Wing mass additions really are not practical unless a single distribution of balance weights solves the flutter problem for all store carriages. In view of the store balance weight results this seems highly unlikely. Two of the store configurations, the MK-82 and MK-84, have large store motions which wing mass ballast cannot affect. The tank flutter modes resemble each other but the wing twist at 62% full is 180° out of phase with that at 90% full. Thus, it is highly probable that a wing ballast optimized for the 90% configuration will actually worsen the 62% situation.

It is interesting to note that the large mass ballasts examined for the store mass ballast trials had an almost negligible impact on the "bare wing" flutter velocity at 28 Hz. Even with 1000 lb store mass ballasts

65

Lift Curve Slope Equal to 4.60/Radian
Center of Pressure at Quarter Chord
Data Shown is for Zero Equivalent Damping Coefficient
Sea Level Conditions

□ Weight Added 16 in. aft of C.G.
○ Weight Added at C.G.
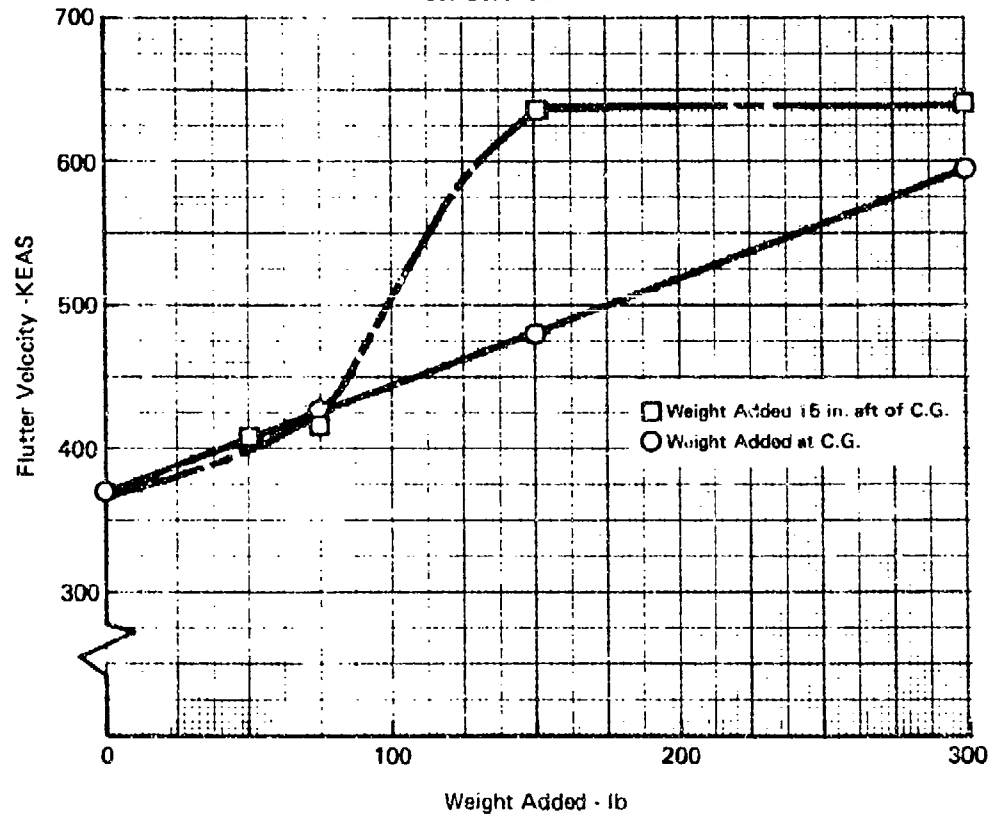
FIGURE 31 EFFECT OF STORE MASS ADDITION ON THE FLUTTER VELOCITY OF THE MK-82 (BOMBS 3, 4)

the flutter onset velocity of this mode varied by only ±10 knots from the unballasted 1140 knot value.

4.1.2 Active Flutter Studies

4.1.2.1 Sensor Selection – There are three variables which must be specified to determine the optimum sensors:

1. Sensor location

2. Displacement coordinate measured by the sensor

3. Number of integrations of sensor output

Sensor location is the primary determinant of the phase margins that can be achieved by a flutter control system. The upper Nyquist plot in Figure 32 was obtained with the 370 gallon tank 90% full data at 800 knots with an uncompensated wing twist angle feedback (two integrations of an angular accelerometer). The wing twist was measured just upstream of the aileron at BL 132.5. The lower plot is for the same configuration but with a sensor which detects pitch of the store pylon relative to the wing. The unstable (counter-clockwise) loop in the lower plot is significantly larger. The larger loop promises better phase margins and lower feedback gain requirements to achieve active stability. The maximum possible phase margins can be determined from uncompensated Nyquist plots by constructing the angle, with its vertex at the +1 real axis point, which is tangent to the sides of the unstable loop. This angle (50 degrees in the lower plot of the figure) is equal to twice the maximum balanced phase margins possible for the selected sensor location. The size of this angle is affected by sensor location because the sensor detects a cumulative summation of all modes – stable and unstable. The complex value of this summation will vary with sensor location. In order to function as an active flutter control sensor, the pickup should measure the unstable mode response to the maximum exclusion of the stable modes. Any sizeable stable mode responses will only "muddy the water" and make the job of the flutter suppression system more difficult.

Wing response acceleration at the sensor location can be represented mathematically as:

$$\ddot{\alpha} = -\omega^2 \sum_{i=1}^{N} \emptyset_i \frac{q_i}{\delta} \delta$$

where: $\ddot{\alpha}$ is the wing twist acceleration

ω is the frequency parameter

N is the number of wing/store still-air modes

$\emptyset_i$ is the participation coefficient for each still-air mode at the sensor location

67

Top plot labels:
370 Gallon Tank - 90% Full
Sense Wing Twist Just Upstream of Aileron
800 KEAS, No Structural Damping , SL
Subsonic Aerodynamics
All Control System Transfer Functions Removed
No Elements in the Feedback Loop
Feedback Gain: 5.0

11.4 Hz, 7.7 Hz, 8.2 Hz, 8.3 Hz, 6.4 Hz, 0.1 Hz, 8.5 Hz

Bottom plot labels:
370 Gallon Tank - 90% Full
Sense Relative Pylon Pitch
800 KEAS, No Structural Damping , SL
Subsonic Aerodynamics
All Control System Transfer Functions Removed
No Elements in the Feedback Loop
Feedback Gain: 5.0

8.2 Hz, 7.3 Hz, 6.2 Hz, 8.3 Hz, 60°, 10.0 Hz, 8.4 Hz, 11.4 Hz

FIGURE 32 NYQUIST PLOTS SHOWING EFFECT OF SENSOR LOCATION

$\dfrac{q_i}{\delta}$ is the generalized coord nat response of each still-air mode to a unit angular deflection of the control surface

δ is the control surface deflection.

Note that the weighted sum

$$\sum_{i=1}^{N} (\emptyset_i) \frac{q_i}{\delta}$$

determines the phase of $\ddot{\alpha}$ since this sum contains the only complex quantities in the equations. The participation coefficients, $\emptyset_i$ are the single amplitude displacements of the "ith" still-air mode at the sensor location. The response vector, consisting of all the q_i/δ terms, is the collection of all complex generalized coordinates at airspeed. These q_i/δ terms vary with frequency but are independent of sensor location. At the flutter frequency the largest generalized coordinate defines which still-air mode is most characteristic of the flutter mode. Thus, if q_3/δ is the largest generalized coordinate at the flutter frequency, a sensor which undergoes large deflections in the 3rd still-air mode but has minimal deformation in the other modes should be selected for the flutter control system. A typical example of how this works is given in Figure 33. The individual modal response vector components are plotted for two 370 gallon tank configurations, 90% and 62% full. The unstable mode of the 90% configuration primarily resembles the 3rd still-air mode while that of the 62% configuration is a 2nd mode. The $\emptyset_i$ values shown below the plots are the still-air mode participation coefficients measuring pylon pitch relative to the wing. The pylon location is satisfactory for the 90% tank configuration since the 3rd mode is emphasized. This location is bad for the 62% configuration since the 3rd mode (stable) is emphasized almost 10 times more than the 2nd mode (unstable). Figure 33 illustrates two interesting points:

1. Sensor location affects phase and gain characteristics of the sensed motion

2. Different mass loadings of the same store result in different flutter mechanisms.

The first point can be explained with the weighted summation given above where the $\emptyset_j$'s, though real, affect the manner in which the q_i/δ's are summed and, thus, differing locations alter the instantaneous value of $\ddot{\alpha}$.
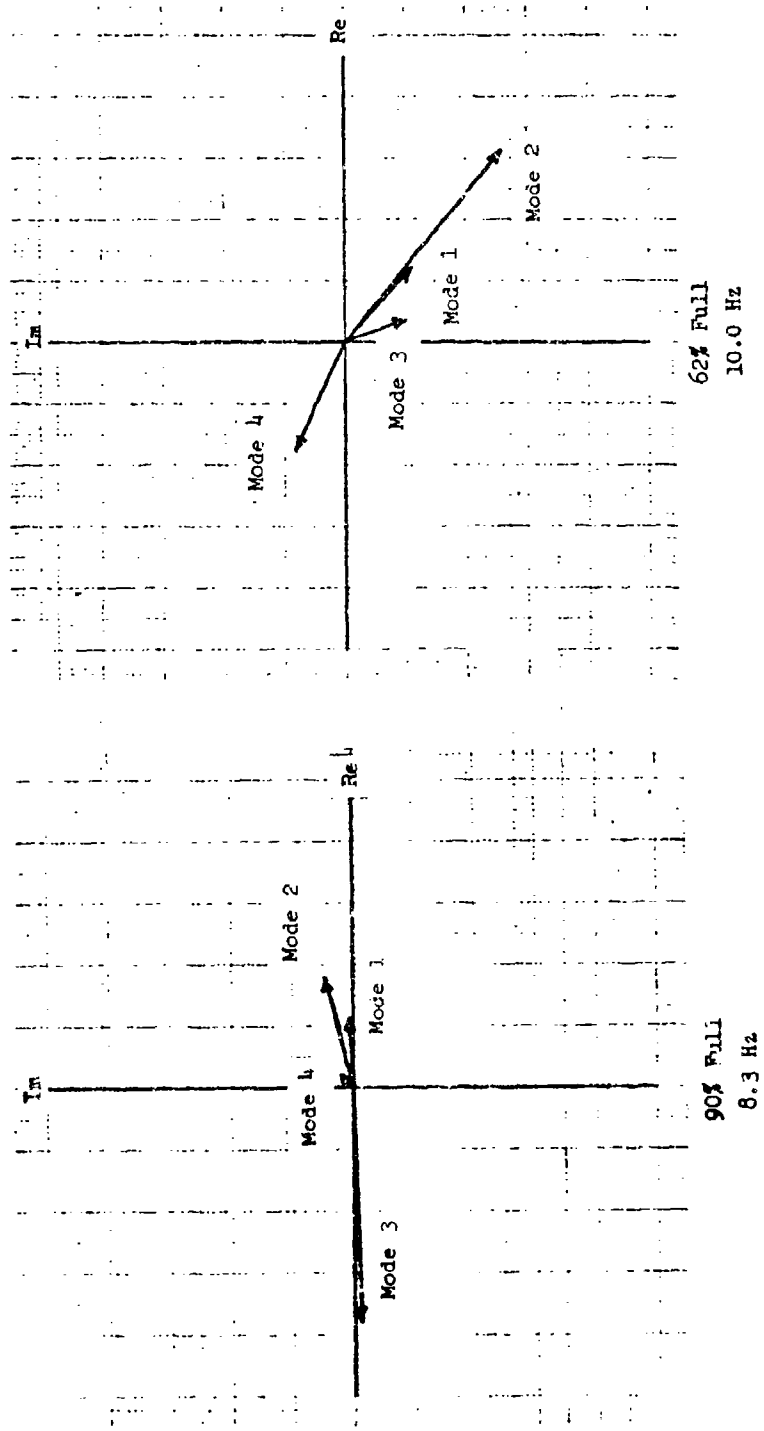
FIGURE 33 MODAL RESPONSE VECTORS AT THE FLUTTER FREQUENCY FOR THE 370 GALLON TANK - 90% AND 62% CASES AT 800 KEAS

In the frequency domain (Nyquist plot) this translates into a difference in phase and gain at all frequencies. Hence, the appearance of the Nyquist plot in terms of the angular size and orientation of the resonant loops is altered by changing the sensor location. This, in turn, affects the maximum possible phase margins and the compensation required for active stability. The second point—different mass loadings of the same store result in different flutter mechanisms—is obvious from the magnitudes of the generalized coordinates and participation coefficients shown in the figure. The change in fuel loading has resulted in what amounts to a new store requiring its unique compensation to achieve active stability. Any change in store/pylon mass would thus be expected to change the compensation requirements. Similar reasoning would also apply to pylon stiffness changes.

The question of what acceleration quantity to measure with the sensor is again a function of the unstable mode characteristics. If, for example, the unstable mode has large wing bending with little store pitch, wing bending acceleration is the better coordinate to measure.

The number of accelerometer output integrations affects the phase and gain characteristics of the sensed coordinate: No integration – acceleration; one integration – velocity; two integrations – displacement. Each integration adds a 1/S term in the feedback and thus cuts the gain at 20 dB per frequency decade and adds 90 degrees of phase lag. Thus, the effect of each integration is to shrink the Nyquist plot size and pivot the entire plot 90 degrees clockwise about the +1 real axis point. The rotation of the plot may or may not lessen the phase compensation angle necessary to achieve stability. The integrations act as low pass filters and eliminate high frequency non-flutter resonances which could result in control system instabilities. For the wing/store cases considered in these studies it was necessary to use two integrations (displacement feedback) to eliminate a troublesome resonance of the secondary actuator at 36 Hz.

Table 4 summarizes the included phase angle and gain amplitude of the unstable loop at several sensor locations for the wing/store configurations under study. The gain amplitude shown in the table is the magnitude of the vector drawn from the +1 real axis point to the farthest extremity of the unstable loop. There is a good probability that each wing/store configuration could be stabilized individually without phase compensation if there was free choice of sensor location and feedback gain. However, none of these

TABLE 4 VARIATION OF UNSTABLE LOOP INCLUDED PHASE ANGLE AND GAIN AMPLITUDE WITH SENSOR LOCATION

	Sensed Deformation							
	Sense Twist Just Ahead of Aileron		Sense Twist at Wing Tip		Sense Relative Pylon Pitch Angle		Sense Wing Bending Angle at Wing Tip	
	Included Phase Angle	Gain Amplitude	Included Phase Angle	Gain Amplitude	Included Phase Angle	Gain Amplitude	Included Phase Angle	Gain Amplitude
370 Gallon Tank								
90%	30°	.33	46°	.63	54°	.85	29°	.73
62%	36°	.37	35°	.74	65°	.32	32°	.30
MK-82 (3,4)	140°	.15	145°	1.18	97°	2.08	62°	3.22
MK-84 EO	103°	1.62	83°	2.24	>180°	6.4	50°	5.6

Loop characteristics with V = 800 knots, g = 0.0, subsonic aerodynamic conditions, sea level.

Given included phase angle value occurs when gain margins are balanced.

separately optimized sensor locations would be identical. This would force the completely impractical situation of locating many multiply-redundant sensors (to achieve necessary reliability) on the wing and pylon with a switching mechanism to allow connection with the proper sensor depending on store carriage. Probably the biggest disadvantage of many sensor locations without phase compensation versus one sensor location with phase compensation is the inability of the multiple location concept to respond to inaccuracies between the wing/store model and the actual flight hardware. If the system in flight requires a 30 degree phase lag compensation rather than a 100 degree prediction, the single sensor with phase compensation adjustment capability could make the adjustment and survive while the multiple location scheme without phase adjustment capability could not. Based on these considerations alone the relative pylon pitch angle sensor signal appears the best choice. It was not chosen for the subsequent control system designs, however, because of the practical difficulties of implementation and logistical support when compared with permanently installed wing mounted systems. The next best choice without this difficulty is the wing tip mounted twist angle sensor. This sensor was therefore used in designing the compensations for all the wing/store configurations under study.

4.1.2.2 <u>Generalized Procedure for Design of Electronic Compensation</u> - The compensation design procedure can begin once the sensor type and location have been specified. All through the sensor selection studies the flutter control system was considered only as an airframe experiencing airloads, forced by an aileron deflection which was commanded by the feedback signal originating with the motion sensor. At this stage it is necessary to incorporate transfer functions in the control loop to approximate the aileron actuation hardware. Two elements in the F-4 hydraulic system, the power actuator and servo actuator, translate an aileron command into an aileron deflection. These elements are less effective for high frequency commands than for low frequency commands and may also suffer output distortion at their respective mechanical resonances. Thus, the output of these aileron actuation elements may deviate considerably in phase and gain from the input command. A structural feedback flutter control system simulation requires no transfer functions for aileron actuation hardware since this scheme employs a rigid link rather than hydraulics to actuate the aileron. Similarly, the response characteristics of an accelerometer must be accounted for. An

73

active flutter suppression system must also incorporate a high pass filter in the feedback loop to decouple the system from pilot induced wing deformations. When the pilot deflects the aileron the wing twists and bends with the redistribution of air loads. Without a high pass filter for decoupling, the system would attempt to negate the wing deformation with a command equal to but 180 degrees out of phase with the pilot's command. The flutter control system would, thus, be continuously resisting the pilot in his attempts to maneuver the aircraft. Fortunately, pilot commands are generally at such a low frequency that they can be filtered out of the feedback signal without compromising control of flutter modes whose frequencies exceed 5.0 Hertz. The final control system with the added elements and a compensation block in the feedback loop is shown in Figure 34.

The transfer functions for the secondary actuator and accelerometer were chosen to simulate actual hardware.

$$\text{Secondary Actuator} = \frac{1}{1 + \frac{2(.86)}{226} S + \frac{S^2}{(226)^2}}$$
(36 Hz resonance)

$$\text{Accelerometer} = \frac{1}{1 + \frac{2(.6)}{502} S + \frac{S^2}{(502)^2}}$$
(80 Hz resonance)

The form of these transfer functions is recognizable as that of a parallel spring and damper forcing a mass. Figure 35 shows gain and phase characteristics of such transfer functions with variable damping (ζ) and normalized frequency. Fortunately the resonant frequency of either element is far enough removed from the flutter frequencies (less than 11.0 Hz in all cases) that the resonances can be attenuated (with low pass filters) without interfering with control of the flutter mode. The other elements in the control loop (power actuator, high pass filter, and compensation) can be selected to give the desired Bode plot shape shown in Figure 36 without the secondary actuator or accelerometer transfer functions. Maximum gain is selected to occur at the flutter frequency. The gain is constant for several Hertz on each side of the flutter frequency to permit active control even when the flutter frequency is only known approximately. A notch filter may be necessary to suppress feedback of resonating non-flutter modes which occur near the flutter frequency. A high pass filter with a 20 dB/decade buildup provides minimal interference
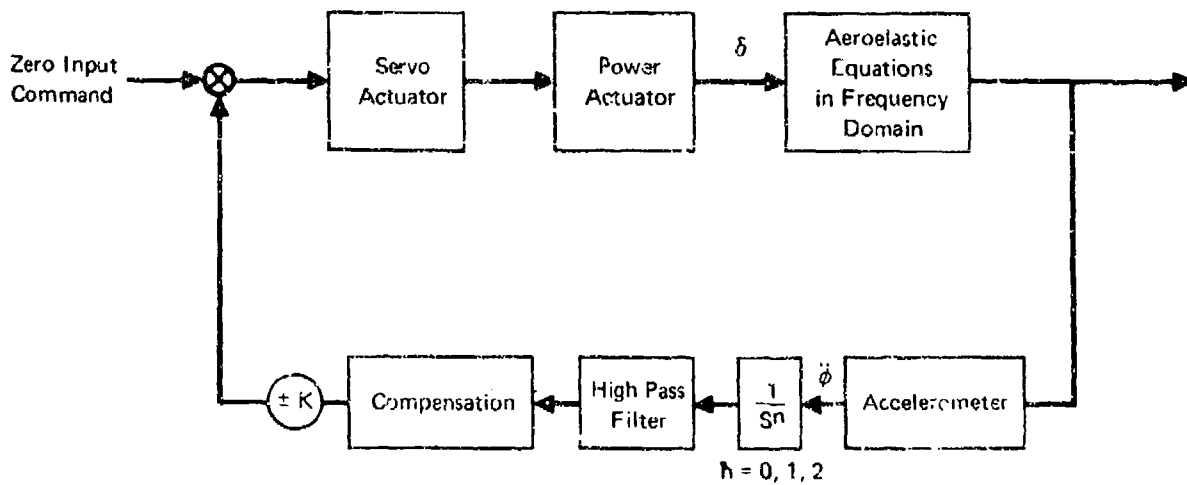
$\delta \sim$ Aileron Deflection
$\ddot{\phi} \sim$ Sensed Feedback Acceleration

FIGURE 34 BLOCK DIAGRAM SHOWING GENERALIZED
ACTIVE FLUTTER CONTROL LOOP
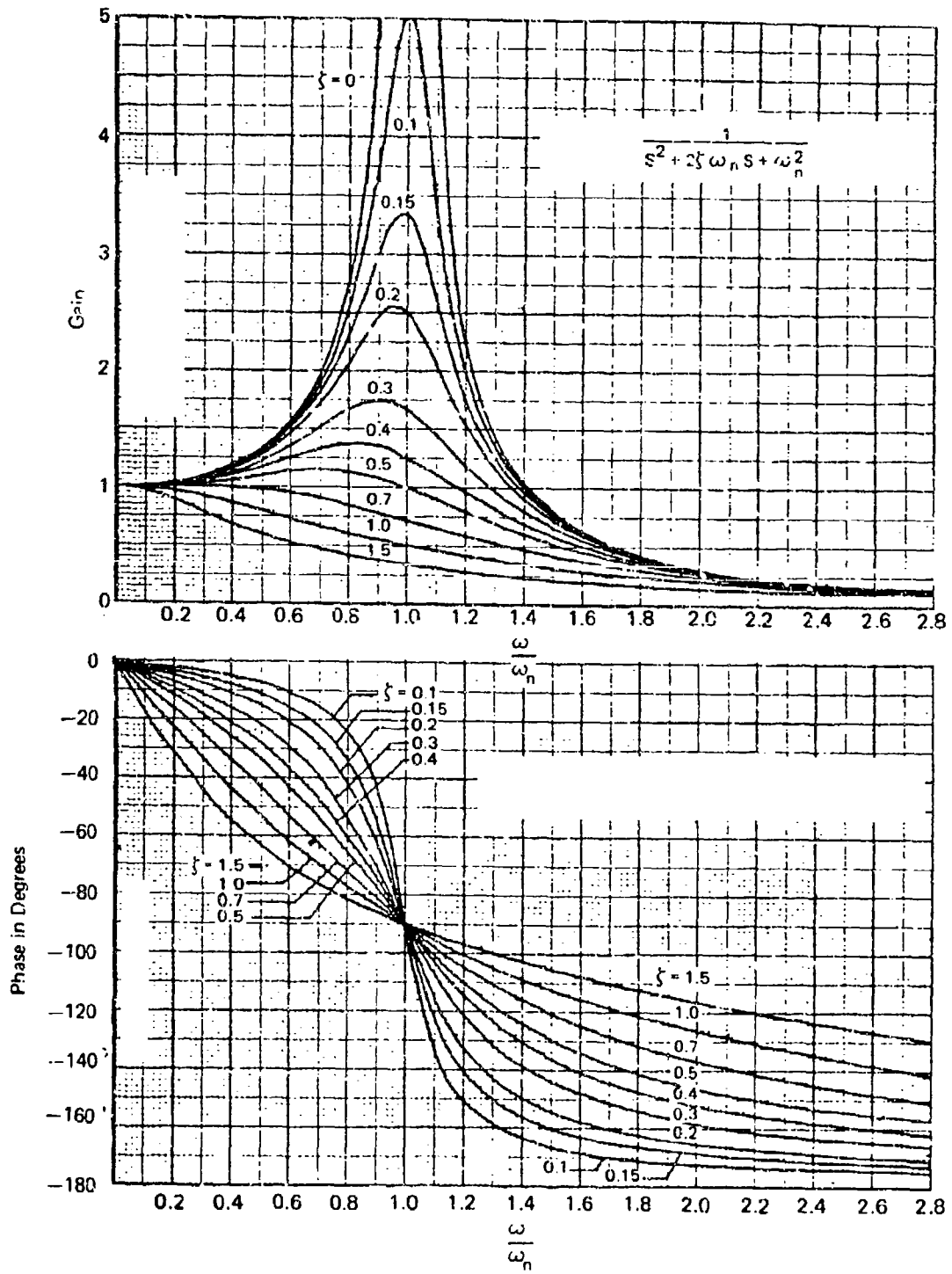
FIGURE 35 GAIN AND PHASE CHARACTERISTICS FOR A SECOND ORDER
DENOMINATOR TRANSFER FUNCTION

76
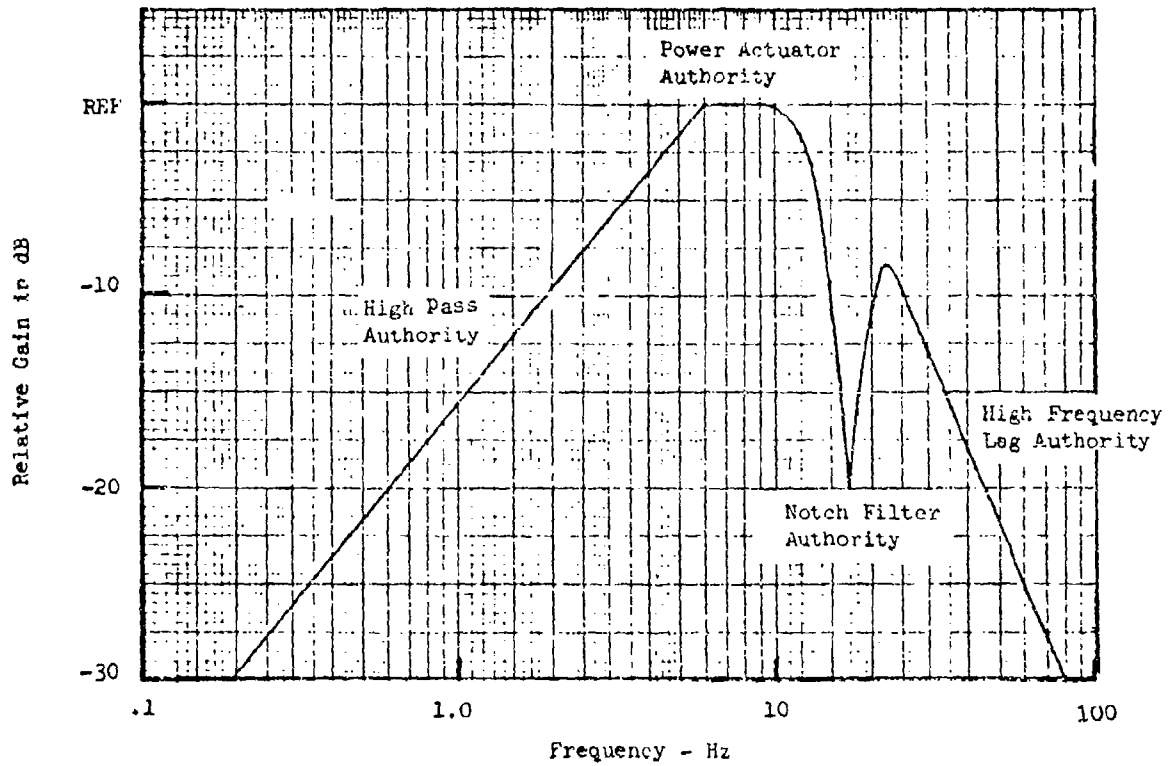
FIGURE 36 TYPICAL BODE GAIN DIAGRAM FOR GENERAL ACTIVE FLUTTER
COMPENSATION SCHEME

with pilot control inputs. The low frequency shoulder of the "flutter control plateau" occurs at the high pass filter break frequency. The sharp drop-off at the high frequency shoulder is caused by the notch filter and the successive effects of the power actuator and high frequency lag breaks. This gain drop-off eliminates potential high frequency resonance problems.

Some compromises are in order to simplify problems associated with flying different store configurations with the same active control system. As few control system elements as possible should require adjustment from one store configuration to another. To provide this commonality it was decided to use the same accelerometers, secondary actuators, power actuators, and high pass filters for all wing/store configurations. Compensation elements can be adjusted to provide the required phase compensation. The selected high pass filter and power actuator transfer functions are given below:

$$\text{High Pass Filter} - \frac{.0265S}{1 + .0265S}$$
(6 Hz break)

$$\text{Power Actuator} - \frac{1}{1 + .016S}$$
(10 Hz break)

The break frequencies for these elements were selected to locate the "flutter control plateau" to cover the range of expected flutter frequencies. The power actuator break frequency at 10 Hz represents a significant improvement over the existing F-4 actuator which gives a flat response to 1.6 Hz. The power actuator break frequency determines the high frequency shoulder of the "flutter control plateau". This was a compromise value selected to minimize the effects of a resonating 11.5 Hz mode which occurred for several of the wing/ store configurations. Ideally this break should have been located beyond the maximum flutter frequency of 10.6 Hz.

Some phase compensation can be obtained by means of a high frequency (break frequency higher than flutter frequency) lag term of the form: $\frac{1}{1 + T_3S}$. The 20 dB/decade gain roll off beyond the break frequency also helps to preclude control system instabilities. Additional phase compensation is achieved by incorporating a pure phase lag network of the form:

$$\frac{1 - T_2S}{1 + T_2S}$$

This type of network has been used extensively in operational analog simulations to verify control system phase margins. It is ideal for this use because large phase angles are possible with no gain change. It may therefore be inserted in a control loop without affecting the basic characteristics of the loop. The phase angle achieved is twice the angle of either numerator or denominator, as seen by the expressions

$$\frac{1 - T_2 S}{1 + T_2 S} = \frac{A \angle -\phi}{A \angle + \phi} = 1.0 \angle -2\phi$$

The network is also suitable for use in flutter control systems. The interpretation of the Nyquist plots is the same for systems with this network as for systems with any of the more conventional compensation networks. The open-loop zero of the phase lag network is of no consequence in the Nyquist stability criterion since only the open-loop poles in the right half plane must be known. And we still have the situation where the flutter roots are the only open-loop poles in the right half plane. The electronic realization of this network is described in Section 5.3.3.

The complete generalized compensation used in these studies is given below with a summary of the function of each element.

HIGH PASS FILTER	PHASE LAG NETWORK	NOTCH FILTER	HIGH FREQ. LAG
$\pm K \left(\dfrac{T_1 S}{1 + T_1 S}\right)$	$\left(\dfrac{1 - T_2 S}{1 + T_2 S}\right)$	$\left(\dfrac{\omega_N^2 + 2\zeta_N \omega_N S + S^2}{\omega_D^2 + 2\zeta_D \omega_D S + S^2}\right)$	$\left(\dfrac{1}{1 + T_3 S}\right)$

High Pass Filter   – decouples flutter control loop from the pilot's flight control loop

Phase Lag Network – gives required phase control with no gain reduction

Notch Filter   – gain stabilizes non-flutter modes which occur at frequencies near the flutter frequency

High Frequency Lag – gain stabilizes modes well separated from the flutter mode.

The algebraic sign on K, the feedback gain, is to ensure that the system requires phase lag for stability. If the Nyquist plot, for example,

requires 30 degrees lead for stability, compensation can be achieved by changing the sign on the feedback gain and applying 150 degrees of phase lag. Figures 37 through 39 show gain and phase plots for first order denominator terms, first order numerator terms, and a typical notch filter. These three figures can be used to determine gain and phase characteristics of all the compensation terms.

It was mentioned earlier, in Section 4.1.2.1 that compensation elements could not be used to expand the unstable loop in the sense that the enclosing angle is increased. It was stated that sensor location, almost exclusively, determines the size of the enclosing angle and hence the achievable control system phase margins. It would appear from Figure 39 that such second order transfer functions with very rapidly changing phase characteristics could be used to expand the unstable loop angularly by centering the transfer function at the flutter frequency. It would then be possible to, for example, add 40 degrees phase lag at 1/2 Hz less than the flutter frequency and add 40 degrees phase lead at 1/2 Hz greater than the flutter frequency. This would effectively increase the enclosing angle by 80 degrees. The adverse gain characteristic of a notch filter can be eliminated by inverting the transfer function so that the numerator has a high damping and the denominator a low damping. This results in a gain "peak" rather than a "notch". Unfortunately the inversion of the damping coefficients results in phase lead at frequencies below the center frequency and phase lag at higher frequencies. Thus, the included angle of the unstable loop (increasing frequency in the counter-clockwise direction) is actually reduced. Even if such an element were practical it would be very difficult to implement since it requires a very precise knowledge of the flutter frequency. A slight inaccuracy in predicting this frequency results in an undesired phase compensation which could cause the recurrence of the instability the system was designed to control.

The stabilizing compensation is specified by first obtaining a Nyquist plot incorporating everything in the control loop except the compensation elements; accelerometer, power actuator, secondary actuator, high pass filter, and, of course, the aeroelastic equations of motion in the frequency domain. The Nyquist plot shape, size, and orientation for a given configuration vary with airspeed, damping, and altitude; so these parameters must be fixed before any compensation is attempted.
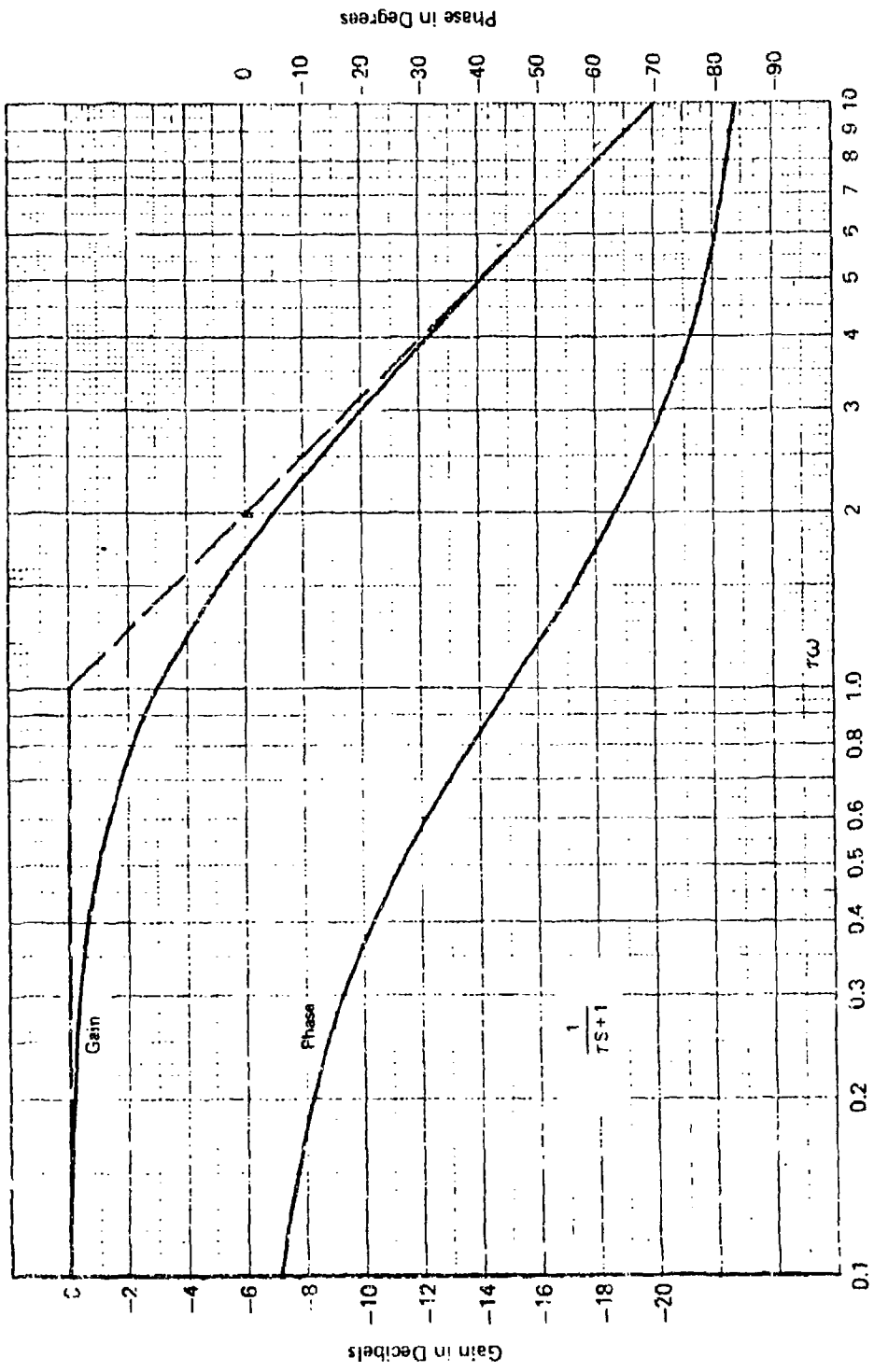
FIGURE 37 GAIN AND PHASE CHARACTERISTICS FOR A FIRST ORDER
DENOMINATOR TRANSFER FUNCTION

81
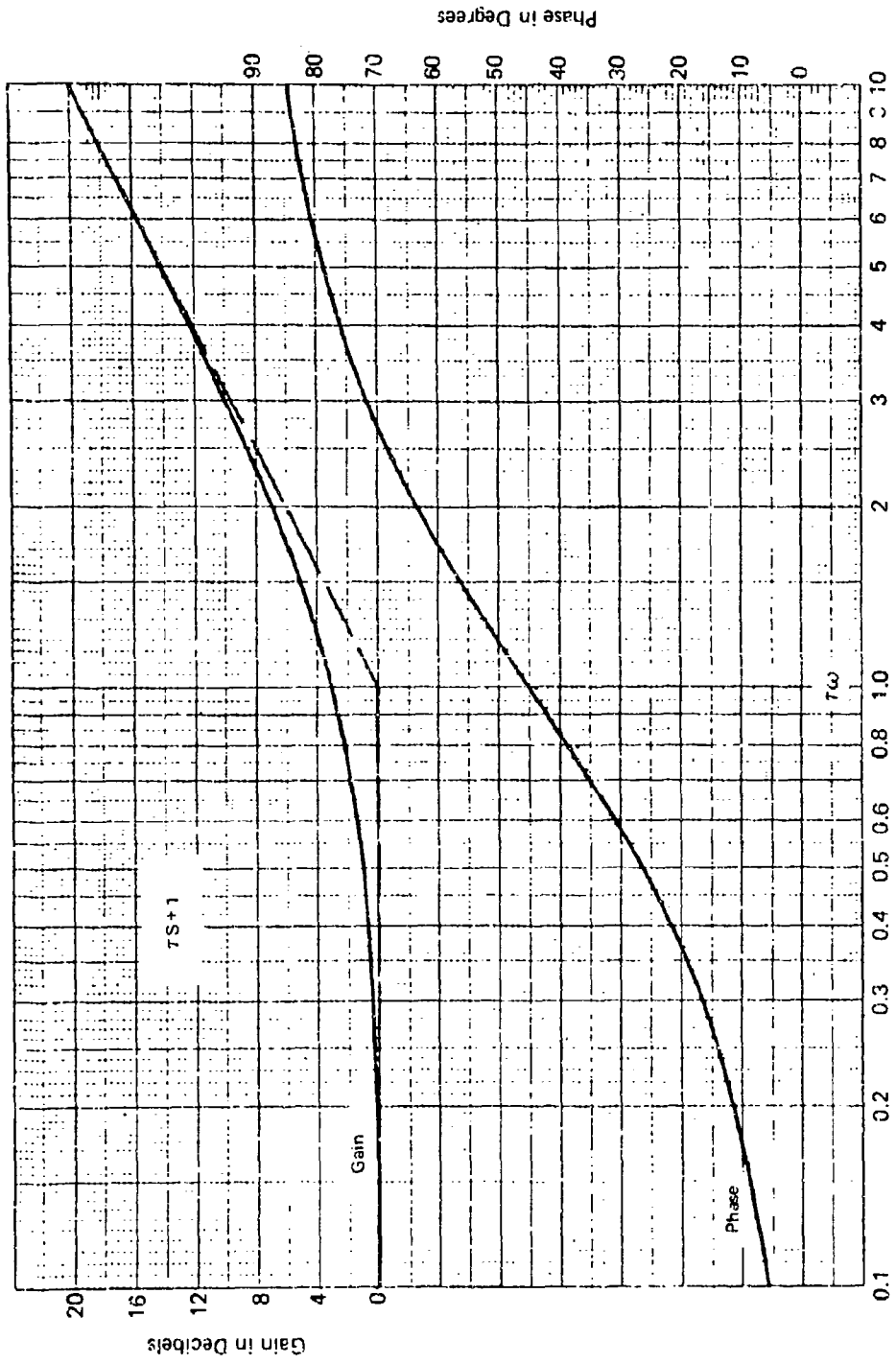
FIGURE 38 GAIN AND PHASE CHARACTERISTICS FOR A FIRST ORDER
NUMERATOR TRANSFER FUNCTION

82

$$\frac{S^2 + 2\,(.1)\omega_n S + \omega_n{}^2}{S^2 + 2\,(.7)\omega_n S + \omega_n{}^2}$$
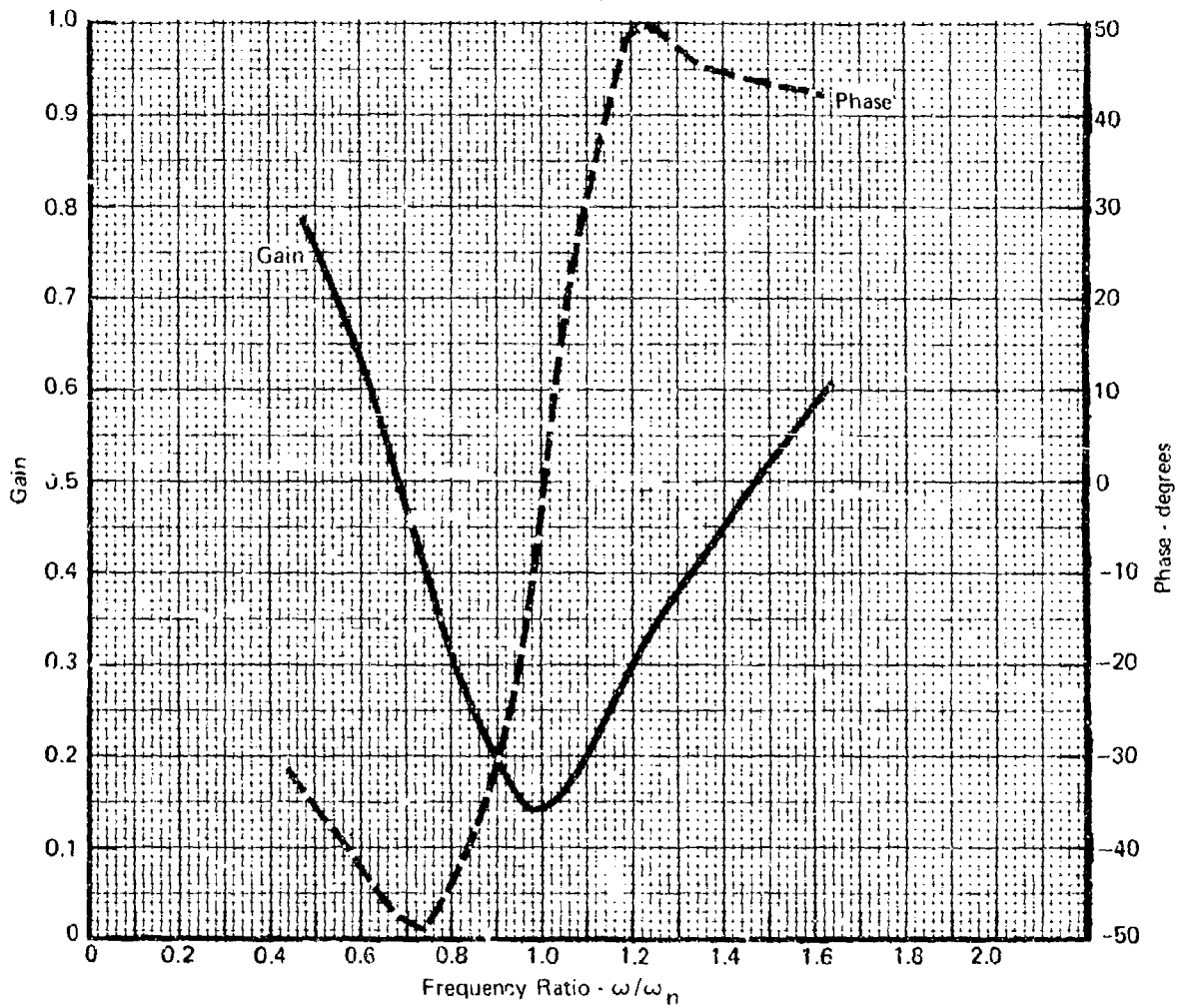
FIGURE 39 GAIN AND PHASE CHARACTERISTICS FOR A TYPICAL NOTCH FILTER

Conditions of Airspeed, Structural Damping, and Altitude

To ensure that the flutter control system can effectively maintain flutter control over the desired flight regime the compensation should be designed for the most conservative conditions of velocity and structural damping. The altitude should be selected as a design condition governed by where the system is expected to operate. For most of these wing/store studies the altitude was set at sea level. Sea level air density is a reasonable choice since most of the anticipated benefits of active flutter control are restricted to low-level, high-speed attack missions. As will be discussed in the following section no one feedback gain setting can ensure wing/store stability within the entire F-4 flight envelope with the required gain and phase margins. Stability margins against flutter decrease with increasing velocity (discounting the transonic Mach effect on aerodynamics) and decreasing structural damping. Therefore, conditions were conservatively set at the max Q condition for the F-4, approximately 800 knots, (730 knots with a margin) and minimum damping, g = 0.0 for the compensation determination runs on the Active Control of Flutter (ACF) computer program. The effects of freestream velocity and structural damping will be discussed in the subsequent section in more detail.

Determination of Stability Margins

With velocity, damping, and altitude specified the phase angle addition required for stability is the angle between the negative real axis and the line drawn through the +1 real axis point bisecting the unstable loop of the Nyquist plot. The required phase lag is obtained after accounting for the phase contributions of the notch filter, if necessary, by setting the time constants in the pure lag and high frequency lag terms. Once the system has been phase compensated the feedback gain is increased or decreased to provide balanced gain margins. The compensation design procedure is illustrated in Figures 40 and 41. Figure 40 shows the Nyquist plot for the uncompensated MK-84 EO configuration for 800 knots, g = 0.0, sea level conditions. Since 800 knots is greater than the passive flutter speed, a counter-clockwise encirclement of the origin is required for stability. 65 degrees of phase lag are required to align the principal axis of the unstable loop with the negative real axis for maximum phase stability. Figure 41 shows the compensated Nyquist plot with a feedback gain of 1.81. The single counter-clockwise (CCW) encirclement of the origin indicates
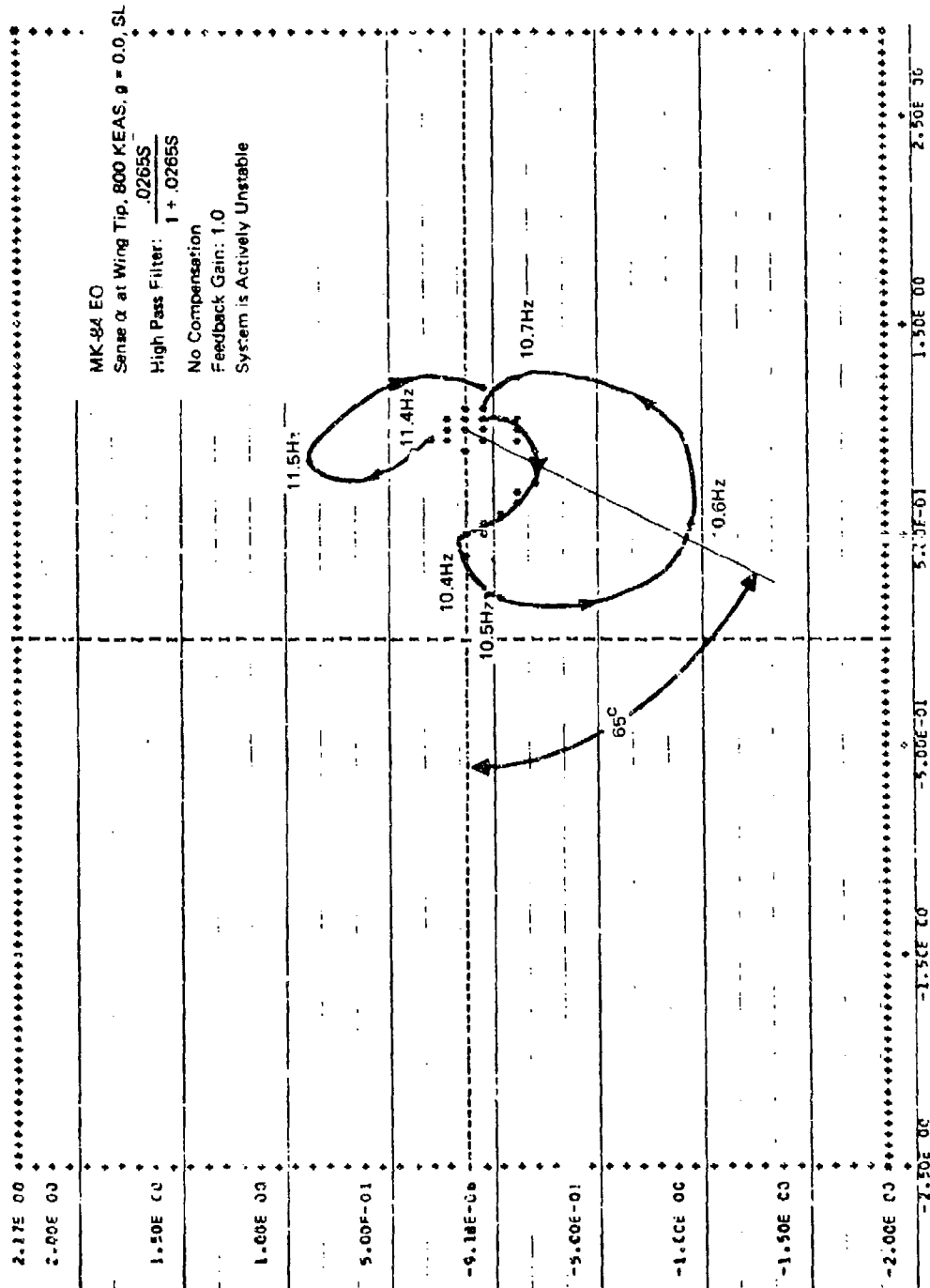
FIGURE 40 NYQUIST PLOT FOR MK-84E0, UNCOMPENSATED

MK-84 EO
Sense α at Wing Tip, 800 KEAS, g = 0.0, SL

High Pass Filter: $\frac{.0265S}{1 + .0265S}$

No Compensation
Feedback Gain: 1.0
System is Actively Unstable

MK-84 EO
Sense α: α: Wing Tip, 800 KEAS, g = 0.0, SL

High Pass Filter: $\dfrac{.0265S}{1 + .0265S}$

Compensation: $\left\{\dfrac{1}{1 + .04447S}\right\}\left\{\dfrac{1 - .0032S}{1 + .0032S}\right\}$

Feedback Gain: 1.81

Phase Margins: $+55^\circ$ Gain Margin $+5.23$dB
-39° -3.20dB

11.5 Hz
11.4 Hz
9.5 Hz°
10.5 Hz
10.7 Hz
55°
39°
10.6 Hz
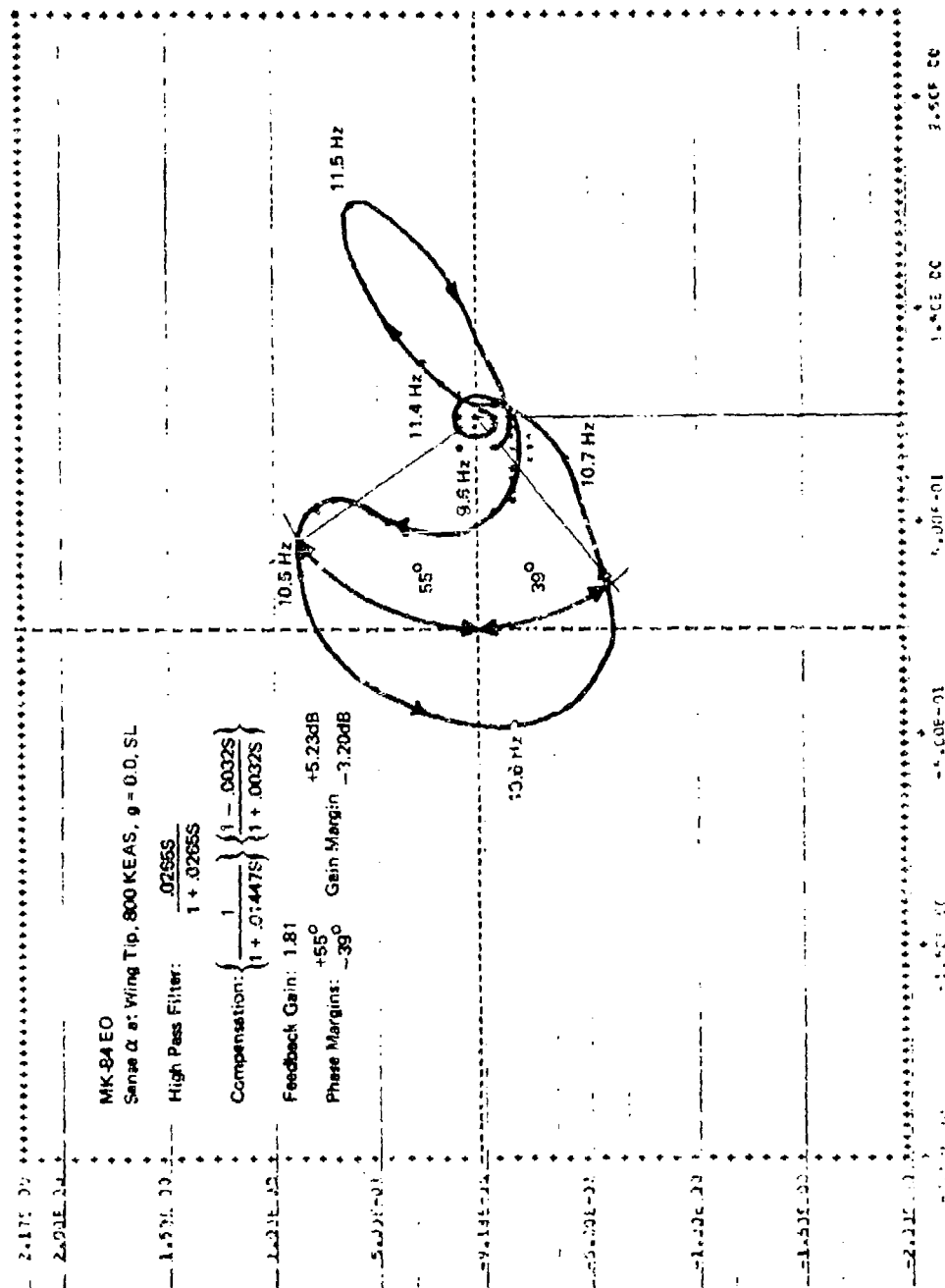
FIGURE 41 NYQUIST PLOT FOR MK-84 EO, COMPENSATED

86

stability since there is only one passive flutter mode at this speed. The phase margins may be determined by constructing a circular arc of unit radius centered on the +1 point until it intersects the plot as in Figure 41. The subtended angle between the corresponding ray and the negative real axis determines the phase margin. In this figure there are two such angles, a positive (upper) phase margin of 55 degrees and a nega ive (lower) phase margin of 39 degrees. The absolute sum of these is the phase margin range, in this case 55 + 3 = 94 degrees. If the cumulative adverse summation of the control loop ment phase uncertainties exceeds either of the phase margins an instab. ty can result.

Gain margins, similar to phase margins, are either the maximum decrease or increase in feedback gain which still retains a single CCW encirclement of the origin. Generally, gain margins are expressed in decibels, this is 20 times the log to the base 10 of the maximum or minimum stable gain divided by the compensation gain. Thus, gain margins of ±6dB indicate that stability can be maintained even though the feedback gain is halved or doubled.

4.1.2.3 Active Control of Flutter Schemes - The flutter control schemes considered in these wing/store studies can be lumped into two broad categories acco. ling to how the compensating forces are generated:

o Control surface deflection

o Store support pylon movement

All of the suppression schemes, with the exception of structural feedback, have control loops of the form shown in Figure 34. The structural feedback concept does not include blocks for the secondary actuator, power actuator, integrator, or accelerometer. The aileron hydraulic actuators are eliminated because the aileron is deflected directly through a rigid member connecting a wing point with the aileron. The integrator and accelerometer are not required since motion sensing is accomplished mechanically. All of the suppression schemes require a high pass filter in the feedback loop to filter out structural responses resulting from pilot lateral control commands.

Control with Electronic Compensation for Particular Systems

Compensations were designed for each of the wing/store configurations using the previously discussed procedure. The particular compensations are listed below:

87

90% Full: $\qquad -5.34 \; (\dfrac{1}{1 + .01768S}) \; (\dfrac{1 - .02875S}{1 + .02875S})$

62% Full: $\qquad 5.46 \; (\dfrac{1}{1 + .01326S}) \; (\dfrac{1 - .242S}{1 + .242S})(\dfrac{(122.5)^2 + 2(.1)(122.5) \, S + S^2}{(122.5)^2 + 2(.7)(122.5) \, S + S^2})$

MK-84 EO: $\qquad 1.81 \; (\dfrac{1}{1 + .01447S}) \; (\dfrac{1 - .0032S}{1 + .0032S})$

MK-82 (3,4): $\quad 15.21 \; (\dfrac{1}{1 + .01768S}) \; (\dfrac{1 - .124S}{1 + .124S})(\dfrac{100^2 + 2(.1)(100) \, S + S^2}{100^2 + 2(.7)(100) \, S + S^2})$

As stated before the compensations were selected to yield approximately balanced phase margins at the design condition: 800 knots, $g = 0.0$, and sea level density. For some of the configurations phase margins were adjusted slightly toward the positive or negative side to achieve reasonable gain margins. The compensations, as expected, are different for every case. Before and after compensation Nyquist plots are given in Figures 42 through 44 for the 90% tank, 62% tank, and MK-82 cases, respectively. Figures 40 and 41 discussed in the previous section, present the MK-84 EO Nyquist plots at the design condition.

Effect of Velocity and Structural Damping on Stability Margins - Figures 45 and 46 summarize the gain and phase margins versus aircraft velocity for the cases studied using the listed compensations. Subsonic aerodynamics employing the C_{L_α} and CP of Section 4.1.1.1 were used in obtaining the plots. Structural damping values of $g = 0.0$, 0.02, and 0.04 are shown. The stable gain variation shown on the plots translates into gain margins greater than ± 6 dB for zero structural damping for each of the stores at velocities up to the maximum sea level velocity of the F-4 with stores (730 knots). This is a significant improvement over the indicated flutter onset velocities. Phase margins of ± 60 degrees or greater are shown for zero structural damping for each of the stores except the 370 gallon tank. For that particular store the inclusion of structural damping, $g = 0.02$, creates phase margins of approximately ± 45 degrees when 90% full and more than ± 60 degrees when 62% full. The general characteristic evident from the figures is an improvement in stability margins with decreasing velocity and/or increasing structural damping. The data given in the stability plots is dependent on the value of feedback gain. Generally, a gain decrease will improve phase margins while gain increases will degrade phase margins. The 62% full, 370 gallon tank case demonstrates this behavior. Nyquist plots for this store at 750 knots

370 Gallon Tank, 90% Full
Sense α at the Wing Tip, 800 KEAS, g = 0.0, SL

High Pass Filter: $\dfrac{.0265S}{1 + .0265S}$

No Compensation
Feedback Gain: 1.0
System is Actively Unstable

8Hz   7.9Hz
8.6Hz

370 gal. Tank, 90% Full
Sense α at Wing Tip, 800 KEAS, g = 0.0, SL

High Pass Filter: $\dfrac{.0265S}{1 + .0265S}$

Compensation: $\left(\dfrac{1}{1+.01768S}\right)\left(\dfrac{1-.0287S}{1+.0287S}\right)$

Feedback Gain −5.34

Phase Margins: +19° −15°   Gain Margins: +3.78dB −3.3dB

7.7Hz   18Hz   11.40Hz
8.2Hz
7.0Hz
8.4Hz
8.7Hz

FIGURE 42 NYQUIST PLOTS FOR 370 GALLON TANK - 90% FULL,
BEFORE AND AFTER COMPENSATION

370 Gallon Tank, 62% Full
Sense α at Wing Tip, 800 KEAS, g = 0.0, SL

High Pass Filter: $\dfrac{.0265S}{1 + .0265S}$

No Compensation
Feedback Gain: 1.0
System is Actively Unstable

34°

10.11 Hz
21 Hz
10.0 Hz
9.9 Hz
12 Hz

370 Gallon Tank, 62% Full
Sense α at Wing Tip, 800 KEAS, g = 0.0, SL

High Pass Filter: $\dfrac{.0265S}{1 + .0265S}$

Compensation: $\left\{\dfrac{S^2 + 2(.1)(122.52)S + (122.52)^2}{S^2 + 2(.7)(122.52)S + (122.52)^2}\right\}\left\{\dfrac{1}{1 + .01326S}\right\}\left\{\dfrac{1 - .242S}{1 + .242S}\right\}$

Feedback Gain: 5.46

Phase Margins: $\begin{matrix}+11°\\-19°\end{matrix}$ Gain Margins: $\begin{matrix}+2.09dB\\-2.3dB\end{matrix}$

4.8 Hz   11 Hz
10 Hz   9.6 Hz
10.3 Hz
10.1 Hz
10.2 Hz

FIGURE 43 NYQUIST PLOTS FOR 370 GALLON TANK - 62%
FULL, BEFORE AND AFTER COMPENSATION

90

MK-82
Sense α at Wing Tip, 800 KEAS, g = 0.0, SL

High Pass Filter: $\dfrac{.0265S}{1 + .0265S}$

Feedback Gain: 1.0
System is Actively Unstable

7.7 Hz
9.4 Hz   18 Hz
9.2 Hz
9.1 Hz   9.0 Hz

MK-82
Sense α at the Wing Tip, 800 KEAS, g = 0.0, SL

High Pass $\dfrac{.0265S}{1 + .0265S}$

Compensation: $\left\{\dfrac{100^2 + 2\,(.1)(100)S + S^2}{100^2 + 2\,(.7)(100)S + S^2}\right\}\left\{\dfrac{1}{1 + .017684S}\right\}\left\{\dfrac{1 - .124S}{1 + .124S}\right\}$

Feedback Gain: 15.21

Phase Margin: $\begin{array}{c}+90^\circ\\-49^\circ\end{array}$ Gain Margin: $\begin{array}{c}+10.8\ dB\\-4.6\ dB\end{array}$

7.6 Hz
9.0 Hz
16 Hz
2.7 Hz
Notch Filter
7.7 Hz
8.0 Hz
9.2 Hz

**FIGURE 44 NYQUIST PLOTS FOR MK-82, BEFORE
AND AFTER COMPENSATION**

91
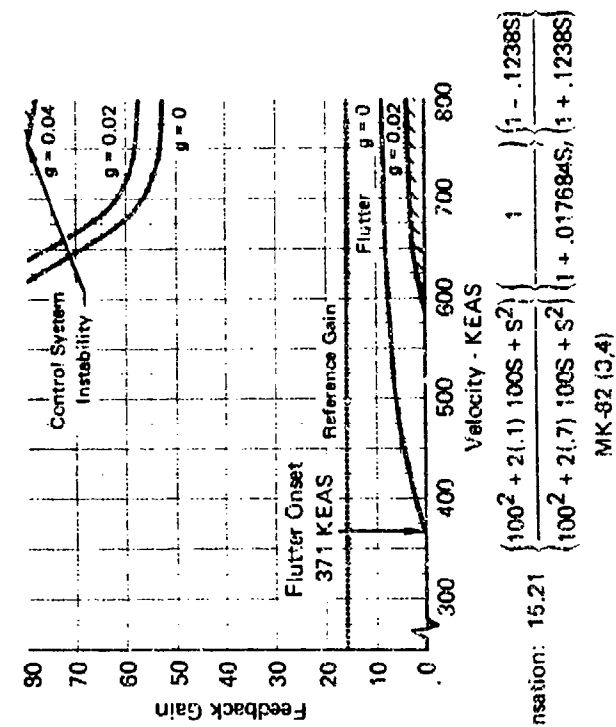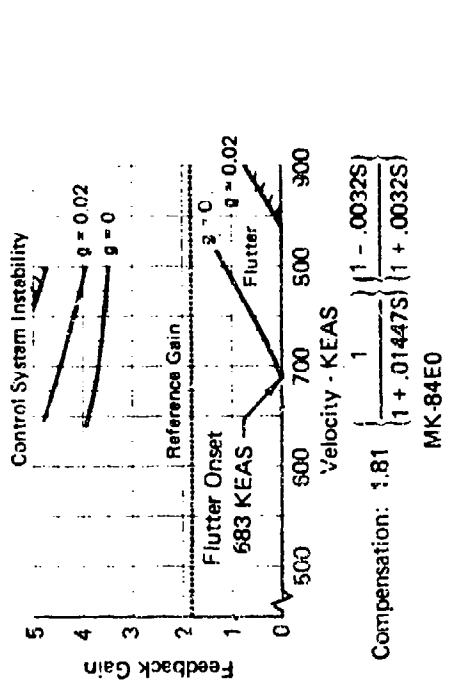
FIGURE 45 RANGE OF STABLE GAIN VALUES FOR COMPENSATED WING/STORE
CONFIGURATIONS - SUBSONIC DATA
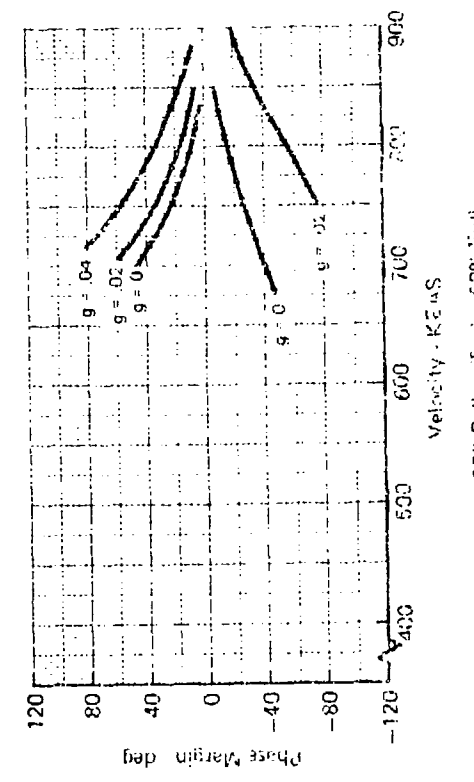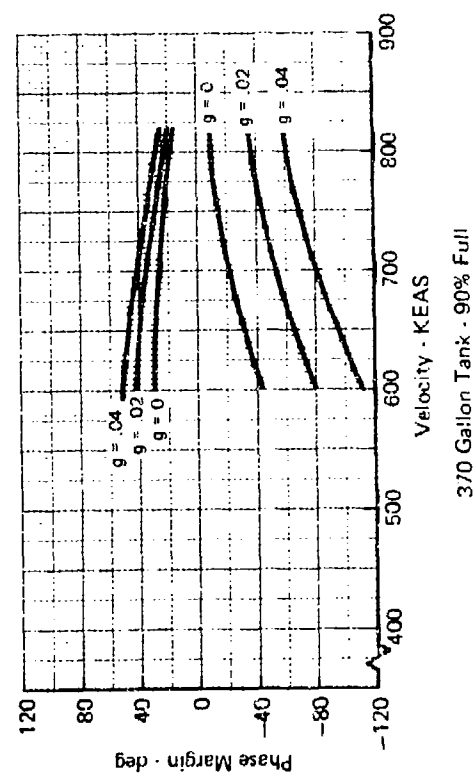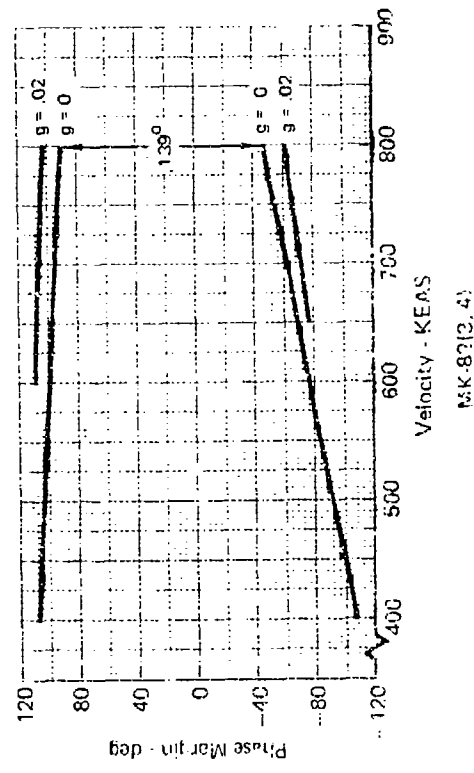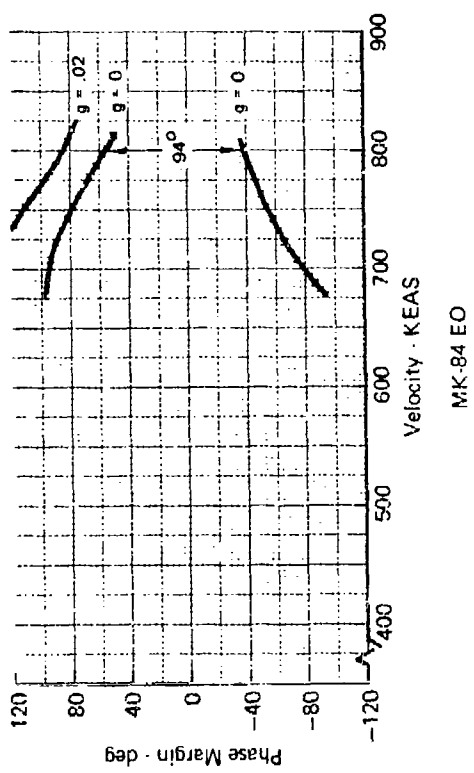
FIGURE 46 PHASE MARGINS FOR COMPENSATED WING/STORE
CONFIGURATIONS - SUBSONIC DATA

are given in Figure 47 for feedback gains of 5.46 and 2.73. Halving the gain increases the phase margins from +21 and -28 degrees to +50 and -24 degrees. The increased phase margin, however, is obtained at the expense of the minimum stable gain value. Flutter for the halved gain occurs at a gain decrease margin of -4.8 dB rather than -10.5 dB. Thus, it makes sense to improve the phase margin by gain decreases only if the accompanying gain margin degradation is acceptable.

Figure 48 shows the effects of an increasing velocity on the Nyquist plots for the compensated 90% full 370 gallon tank configuration. As the freestream velocity increases the Nyquist plot enlarges until the unstable loop is infinitely large at precisely the flutter onset speed. Thereafter the plot decreases in size with increasing velocities. Notice how the unstable loop changes phase by 180 degrees and changes direction (CW to CCW) as the flutter onset velocity, at slightly more than 600 knots, is passed. At sub-flutter velocities an increasing Nyquist plot size indicates an increasing tendency toward control system instability (lower margin with respect to gain increase). Beyond flutter onset a diminishing Nyquist plot size (with any system parameters) indicates decreasing flutter control capability. Both the gain and phase margins decrease with velocity. Hence the shape of the stability plots, Figures 45 and 46. Notice that the ever diminishing gain margins with increasing velocity imply that there is some velocity beyond which the gain margins are zero. This velocity is the absolute limit velocity for active flutter control with the particular scheme under consideration.

The addition of structural damping is always stabilizing—decreasing the loop sizes at sub-flutter velocities and increasing the loop sizes at post-flutter velocities. Figure 49 and 50 show the 90% full tank for the various damping values at a sub-flutter and post-flutter velocity, respectively.

Effect of Supersonic Aerodynamics - The stability data given in Figures 45 and 46 was obtained with subsonic lift curve slope and center of pressure experimental data. Since it is questionable whether subsonic, $M = 0.9$, data applies at velocities exceeding 661 knots all of the wing/store cases were rerun with compensations unchanged but with supersonic aerodynamics. The supersonic data, $C_{L_\alpha} = 4.08$/radian and $CP = 37\%$, is shown in Figure 24 for $M = 1.2$ flow conditions. Phase and gain margin plots for the wing/store

370 gal. Tank, 62% Full

Sense α at Wing Tip, 750 KEAS, $q = 0.0$, SL

Compensations:
$$\left\{ \frac{S^2 + 2\,(0.1)\,(122.52)\,S + (122.52)^2}{S^2 + 2\,(0.7)\,(122.52)\,S + (122.52)^2} \right\} \left\{ \frac{1}{1 + 0.01326S} \right\} \left\{ \frac{1 - 0.242S}{1 + 0.242S} \right\}$$

.... Feedback Gain: 5.46   + 2.04dB

               Phase Margin: +21   Gain Margin: − 10.5 dB

                                    −28

——— Feedback Gain: 2.73   + 7.95dB

                          + 50   Gain Margin: − 4.8dB

               Phase Margin: −24

10.0 Hz

10.21 Hz

10.1Hz
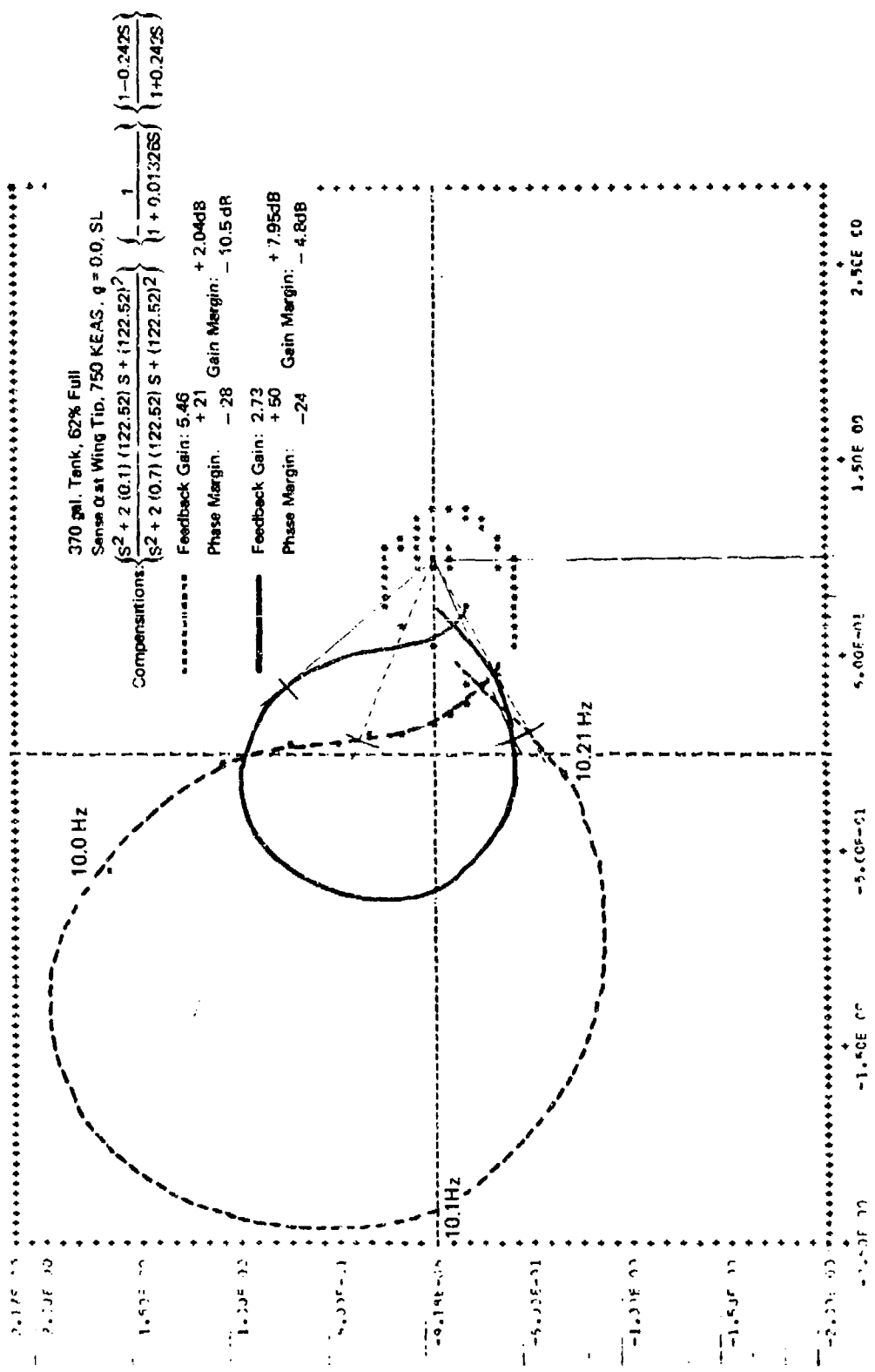
FIGURE 47 NYQUIST PLOT FOR COMPENSATED 62% CASE SHOWING EFFECT OF GAIN CHANGE

370 Gallon Tank, 90% Full
Sense α at Wing Tip,   g = 0.0, SL

High Pass Filter:

$$\frac{.0265S}{1 + .0265S}$$

$$\text{Compensation:} \left\{\frac{1}{1 + .01768S}\right\} \left\{\frac{1 - .0287S}{1 + .0287S}\right\}$$
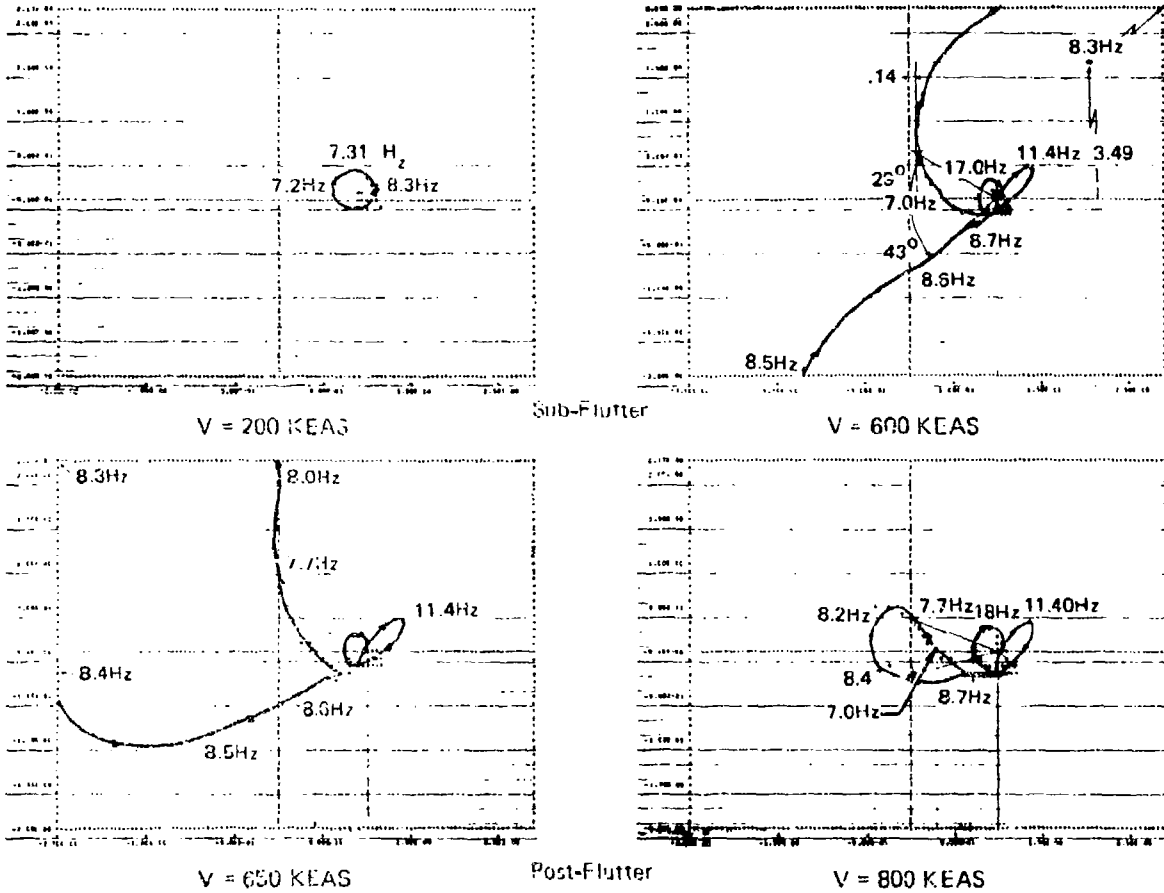
Feedback Gain. ~5.34

FIGURE 48 NYQUIST PLOTS SHOWING EFFECT OF
INCREASING VELOCITY AT CONSTANT DAMPING

96

370 Gallon Tank, 90% Full
Sense α at Wing Tip, 600 KEAS, SL
High pass Filter: $\dfrac{.0265S}{1 + .0265S}$

Compensation: $\left\{\dfrac{1}{1 + .01768S}\right\}\left\{\dfrac{1 - .0287S}{1 + .0287S}\right\}$

Feedback Gain: -5.34

g = 0.00

g = 0.02

g = 0.04
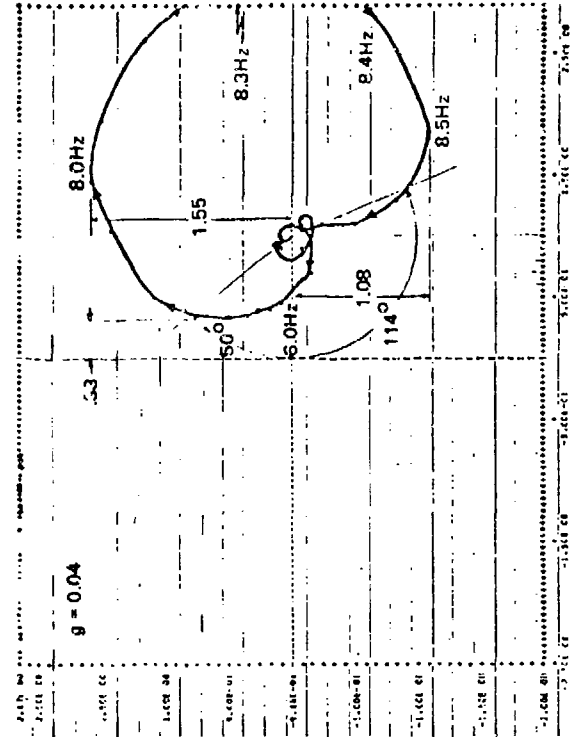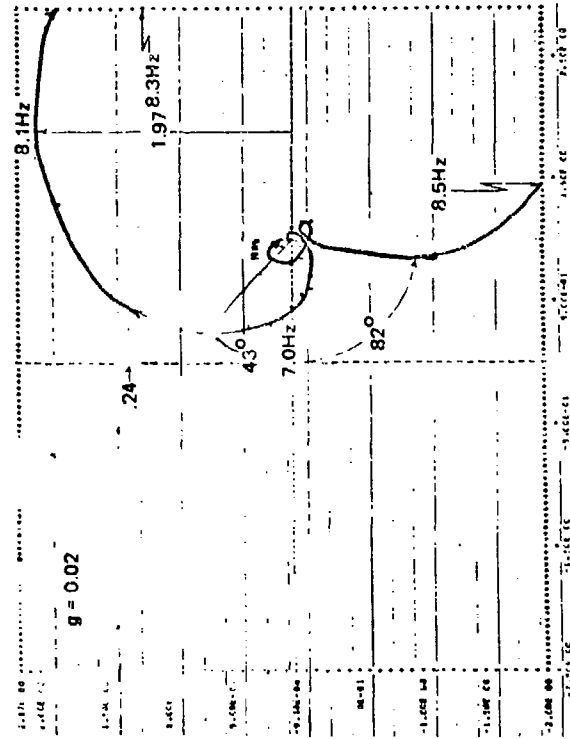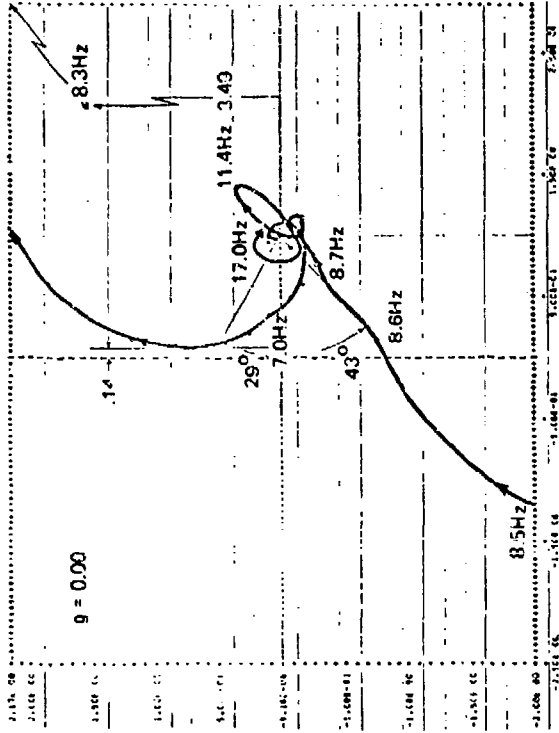
FIGURE 49 NYQUIST PLOTS SHOWING EFFECT OF STRUCTURAL DAMPING
AT A SUB-FLUTTER VELOCITY

370 Gal. Tank, 90% Full

Sense α at Wing Tip. 800 KEAS, SL

High Pass Filter: $\dfrac{.0265S}{1 + .0265S}$

Compensation: $\left\{\dfrac{1}{1 + .01768S}\right\}\left\{\dfrac{1 - .0287S}{1 + .0297S}\right\}$

Feedback Gain: –5.34

g = 0.00

11.40Hz

19Hz

7.7Hz

70Hz

8.2Hz

8.7Hz

8.4Hz

g = 0.04

19.0Hz

8.8Hz

7.8Hz

7Hz

+16°

–64°

8.4Hz

8.3Hz

g = 0.02

19.0Hz

8.7Hz

7.7Hz

7.0Hz

+23°

–40°

8.5Hz

8.3Hz
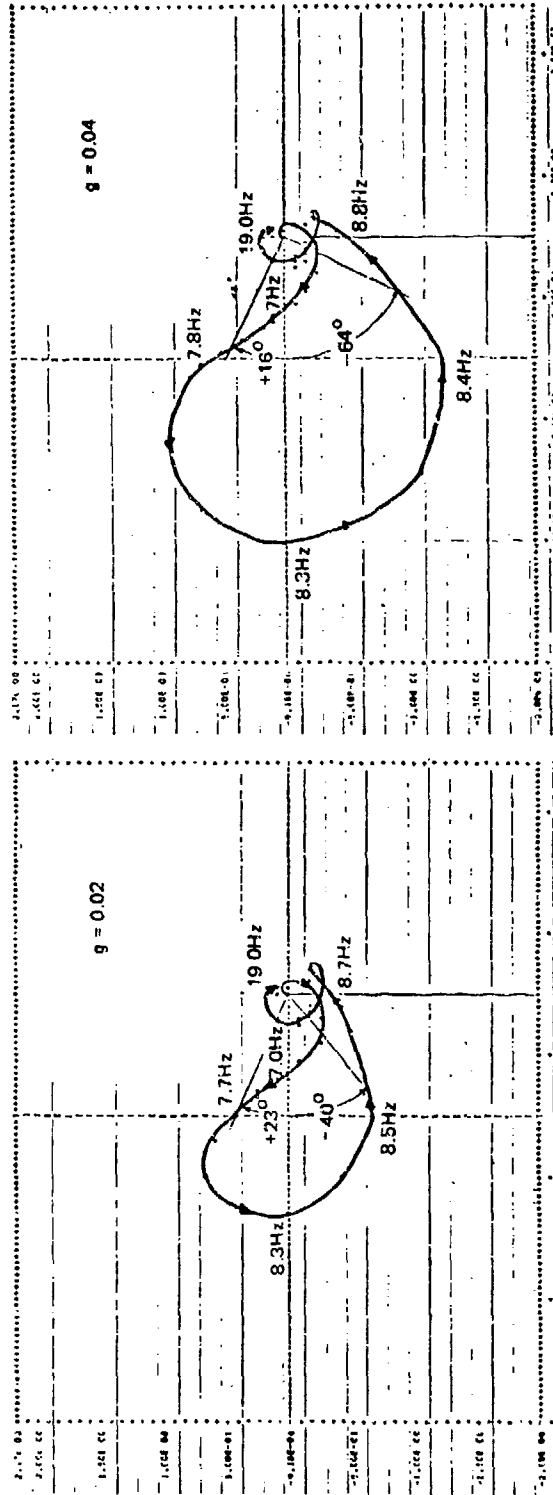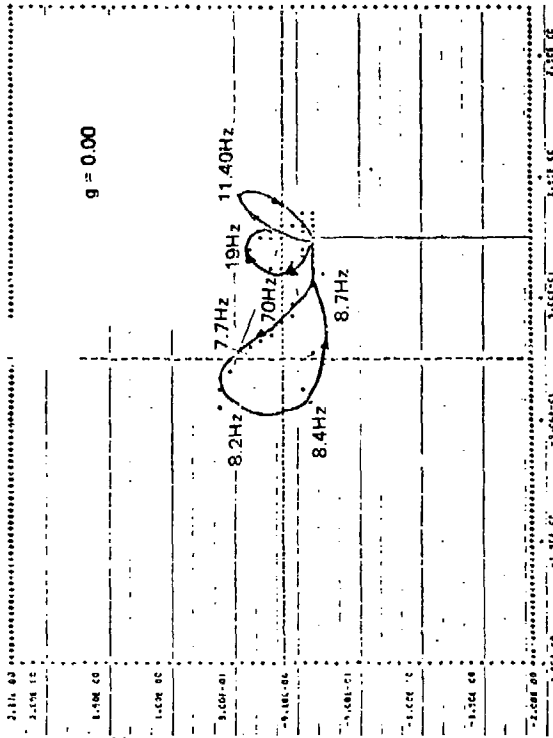
FIGURE 50 NYQUIST PLOTS SHOWING EFFECT OF STRUCTURAL DAMPING
AT A POST-FLUTTER VELOCITY

98

configurations with feedback compensation and supersonic aerodynamics are shown in Figures 51 and 52. (The cases with subsonic aerodynamics are superimposed for comparison.) These analyses were performed with structural damping set equal to zero. The 62% full 370 gallon tank case is the only configuration which no longer flutters at 800 knots. The phase margins obtained with supersonic aerodynamics were slightly larger than the corresponding subsonic phase margins. The very slight degradation in stable gain range experienced by the 90% full 370 gallon tank and MK-84 EO cases can be eliminated by fine-tuning the feedback gain.

Effect of Altitude Variation - Decreasing air density degrades stability margins. The effect can be traced to the aerodynamic damping which decreases with increasing altitude for a constant equivalent airspeed. Thus, similar to the effect of decreasing the structural damping, increasing altitude will decrease gain margins at sub-flutter velocities and will decrease both gain and phase margins at post-flutter velocities.

The MK-84 EO wing/store configuration is a good example of what occurs with increasing altitudes at sub-flutter velocities. With this configuration flutter occurs within the F-4 flight envelope only at altitudes below approximately 6000 feet. Figure 53 is a plot of MK-84 EO gain margins superimposed on the F-4 flight envelope. Gain margins of ± 6 dB are possible only below 2,500 feet. Control is lost (zero gain margins) at about 30,000 feet. If the gain in the previously designed compensation,

$$1.81 \ (\frac{1}{1 + .01447S}) \ (\frac{1 - .0032S}{1 + .0032S}) \ ,$$

is adjusted for $V = 730$ knots, the maximum F-4 sea level velocity with stores, rather than 800 knots, the gain is reduced from 1.81 to 1.56. The plot to match that in the previous figure for the revised gain is given in Figure 54. The maximum ± 6 dB control limit altitude has been increased to 6000 feet and the maximum control altitude has been increased to about 40,000 feet by the gain reduction. The flutter control system can give satisfactory performance for this particular store throughout the F-4 envelope by reducing the feedback gain at high altitudes.

The 90% full-370 gallon tank case demonstrates the effects of increasing altitude on phase margins during operation at a post-flutter velocity. This particular wing/store combination flutters within the F-4 envelope
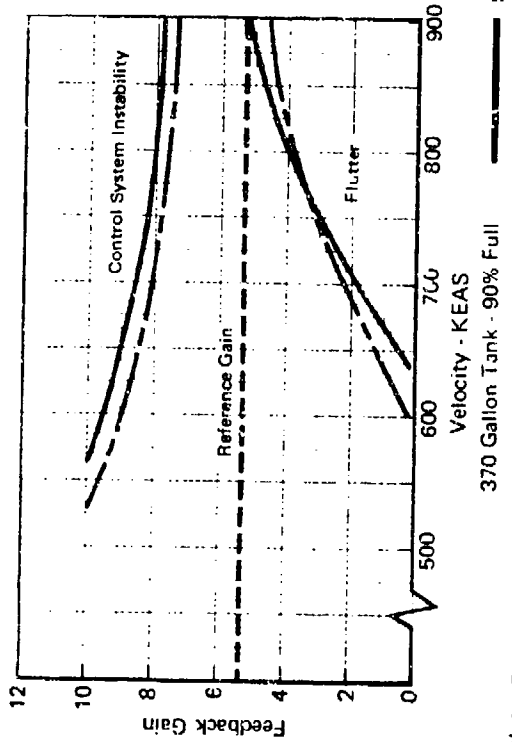
99
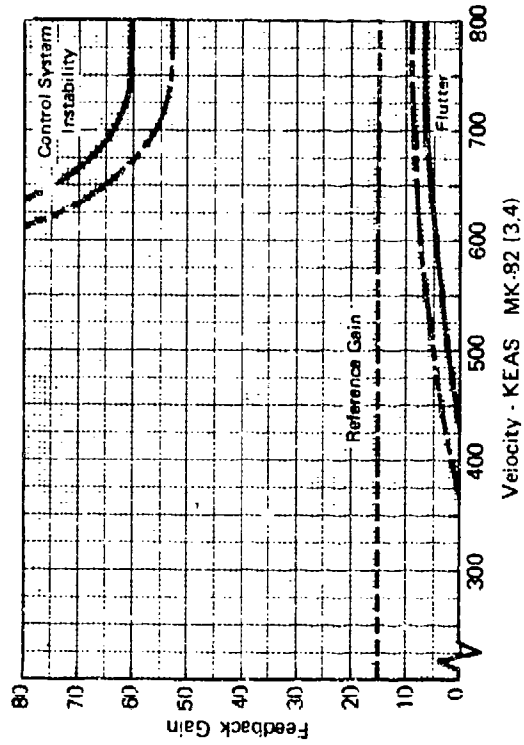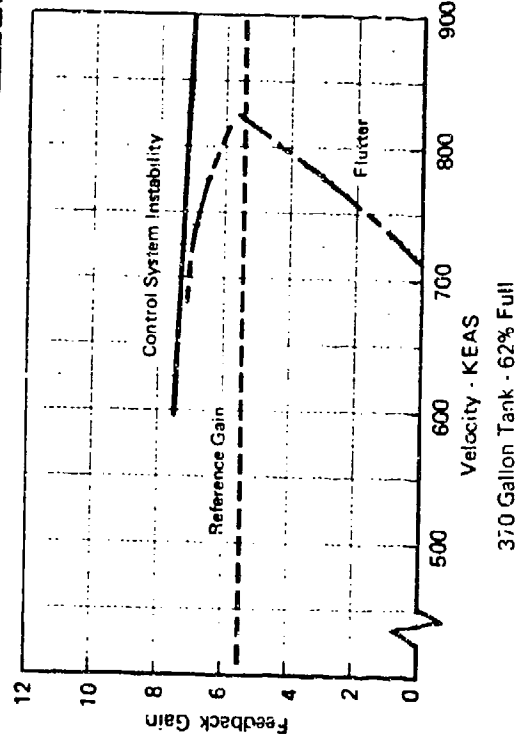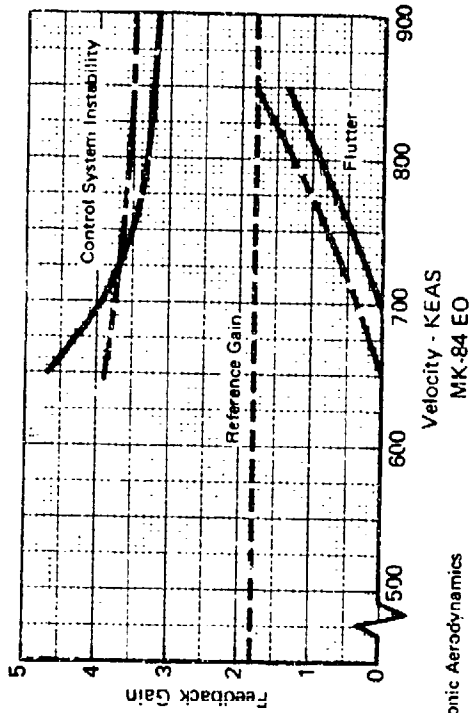
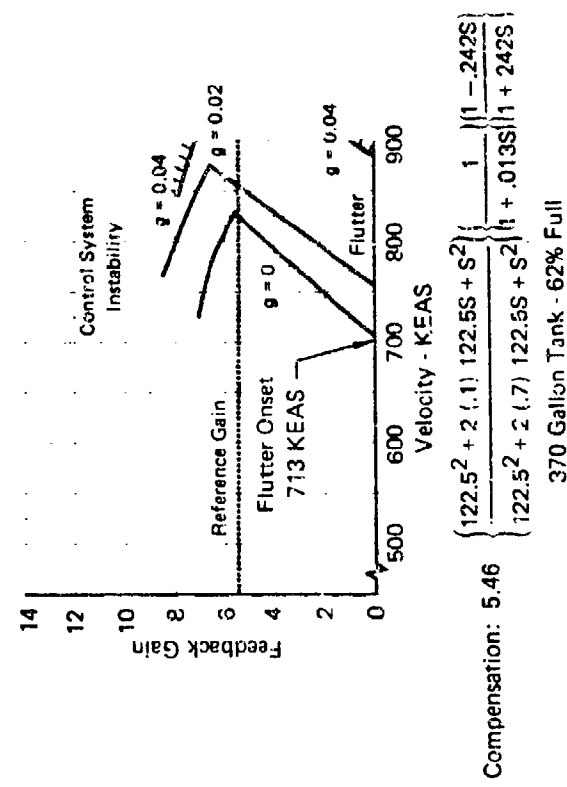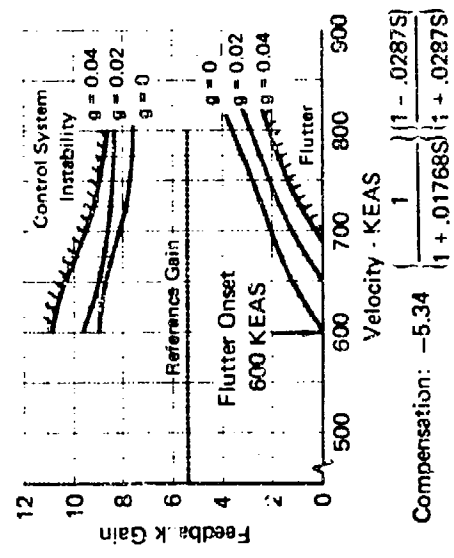FIGURE 51 RANGE OF STABLE GAIN VALUES FOR COMPENSATED WING/STORE CONFIGURATIONS — COMPARISONS OF SUBSONIC AND SUPERSONIC DATA

100
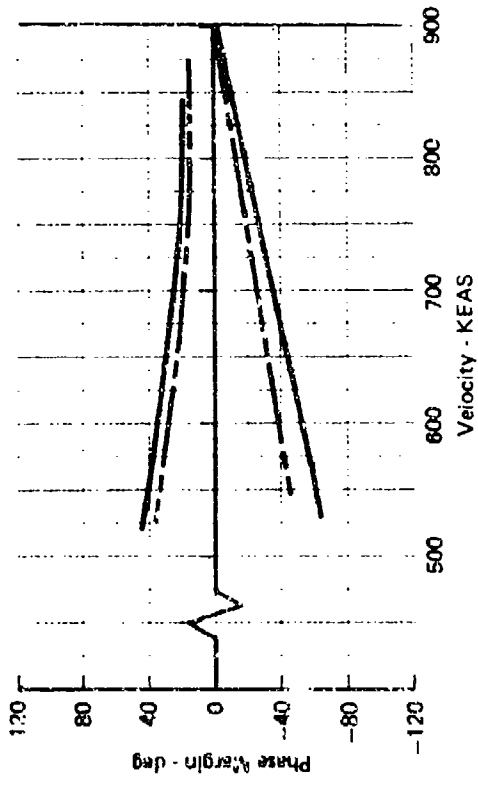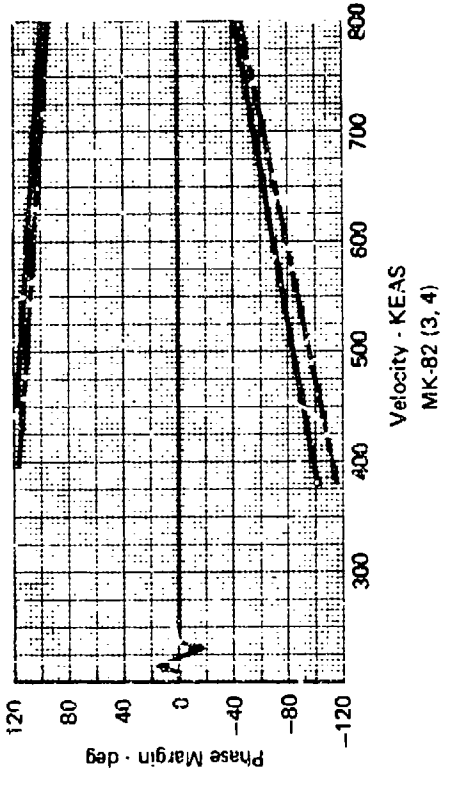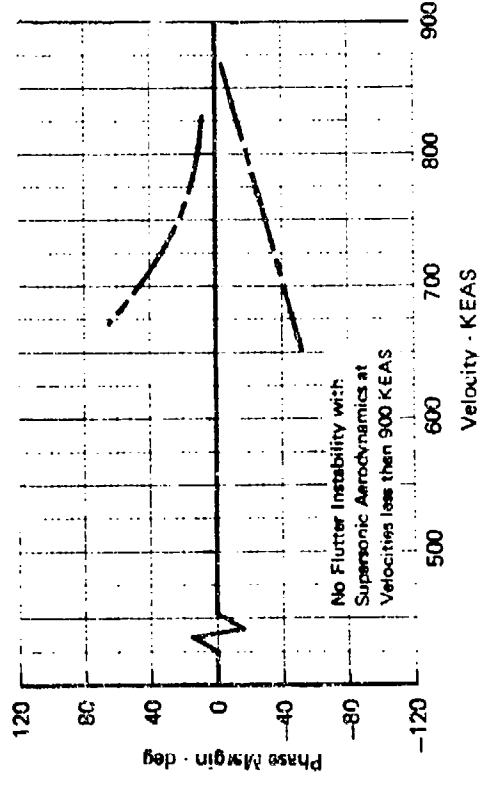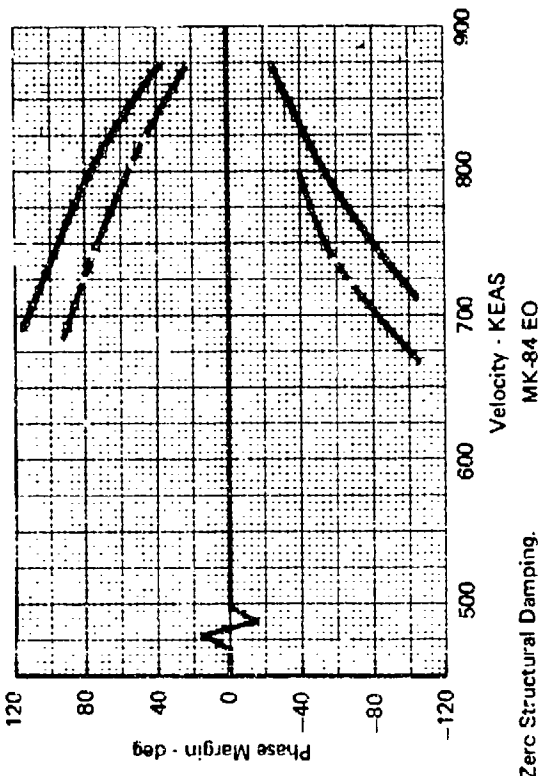
FIGURE 52 PHASE MARGINS FOR COMPENSATED WING/STORE CONFIGURATIONS
- COMPARISONS OF SUBSONIC AND SUPERSONIC DATA

Feedback Gain = 1.81
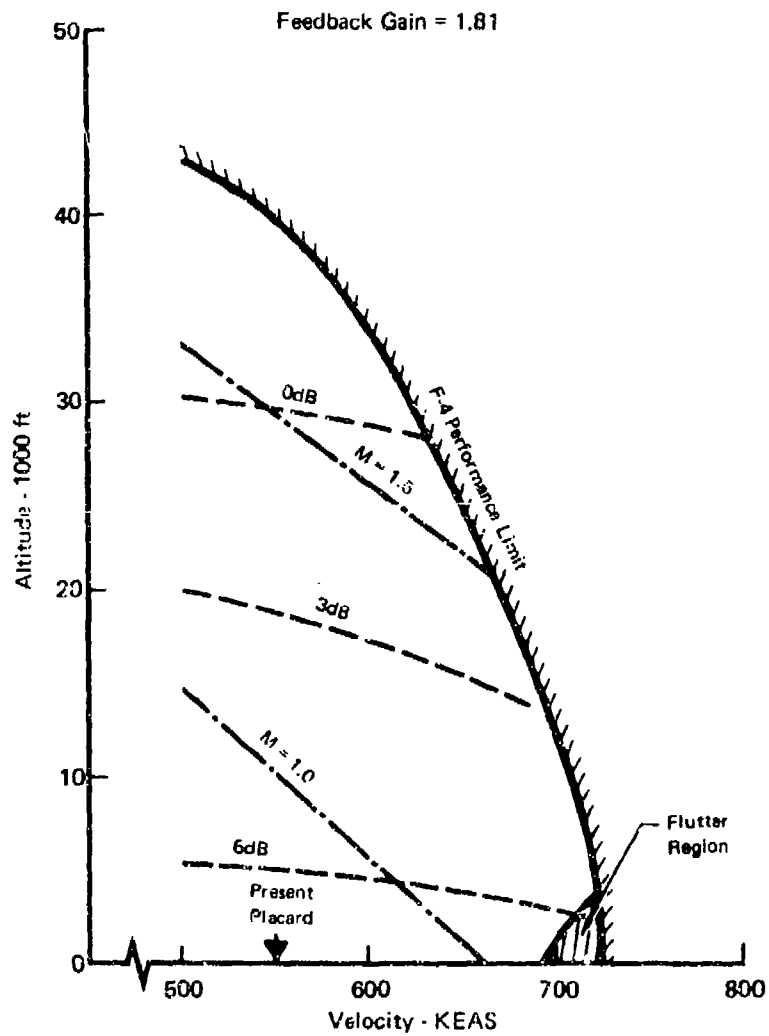
FIGURE 53 VARIATION OF GAIN MARGIN WITH
ALTITUDE AND VELOCITY
MK-84 EO CASE - NOMINAL GAIN

Feedback Gain = 1.56
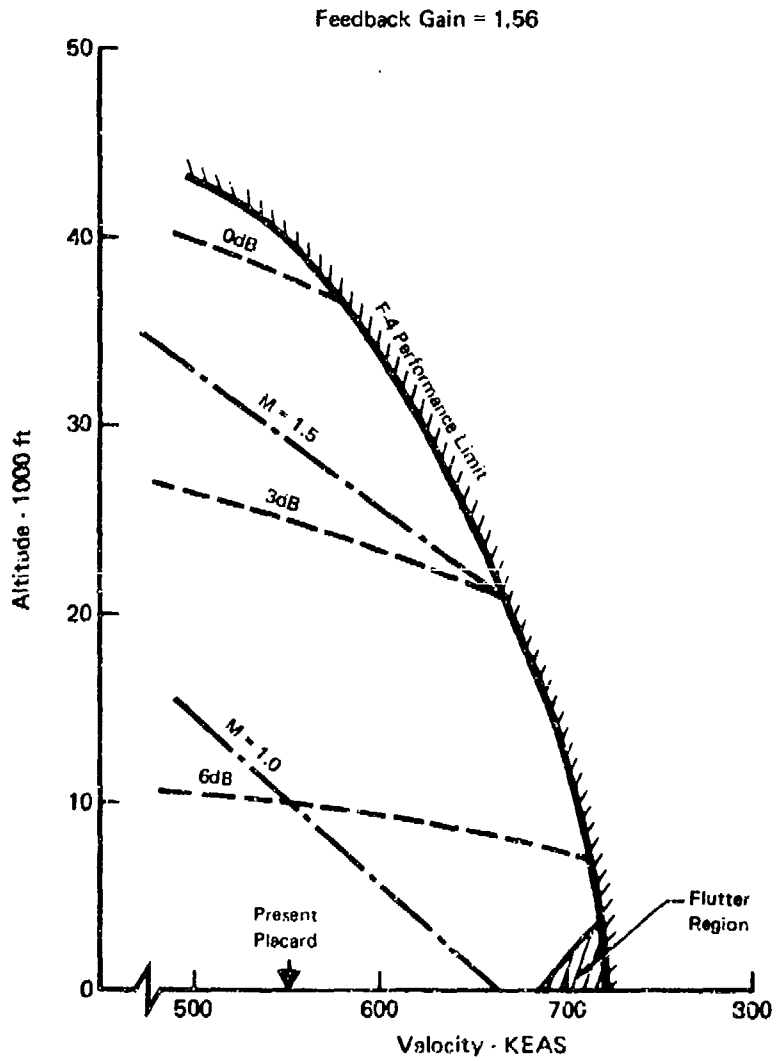
FIGURE 54 VARIATION OF GAIN MARGIN WITH
ALTITUDE AND VELOCITY
MK-84 EO CASE - REDUCED GAIN

right up to the maximum altitude of 45,000 feet. The previously developed feedback compensation for this case is listed below:

$$-5.34 \; \frac{1}{1 + .01768S} \; \frac{1 - .02875S}{1 + .02875S} \; \frac{.0265S}{1 + .0265S}$$

Figure 55 shows the variation of phase angle range (twice the phase margin for balanced phase angles) with velocity and altitude for zero structural damping and subsonic aerodynamics. The plot indicates a substantial degradation of phase margins with increasing altitude. Even if the feedback compensation could be varied with altitude, phase margins at zero damping are limited to ± 20 degrees at altitudes exceeding 10,000 feet. The inclusion of structural damping improves these phase margins slightly.

Control with Common Compensation Elements - The previously reported stability studies assumed complete freedom in the selection of compensation elements. If the difference in compensation elements could be limited to the pure lag term and feedback gain, only two adjustments would be necessary when store carriage was altered. The notch filter and high frequency lag would remain fixed regardless of store carriage. Trial runs were made on the ACF program with the 90% and 62% tank cases. Identical notch filters and high frequency lags were used in the compensations. Stability was again achieved with margins identical to those presented previously. With a broader notch filter similar results could be obtained for the other two stores: MK-84 EO and MK-82.

Wing/Store Flutter Control by Store Moment Cancellation

One means of negating store pitch moments transmitted into the wing is to actuate the aileron to create a wing aerodynamic moment which is always equal and opposite to the store pitching moment. This effectively eliminates the store pitch degree of freedom from the flutter equations and the flutter speed would revert to that of a bare wing with a point mass lumped at the store attachment point.

A static aerodynamic analysis of the model sketched in Figure 56 was used to derive an expression for the aileron deflection angle, β, which would eliminate all aerodynamic pitch moments at the store attachment point. The pitch torque due to store action was expressed as the product of the pylon pitch spring constant, $K_{\emptyset}$, and the relative store pitch angle $\emptyset$.
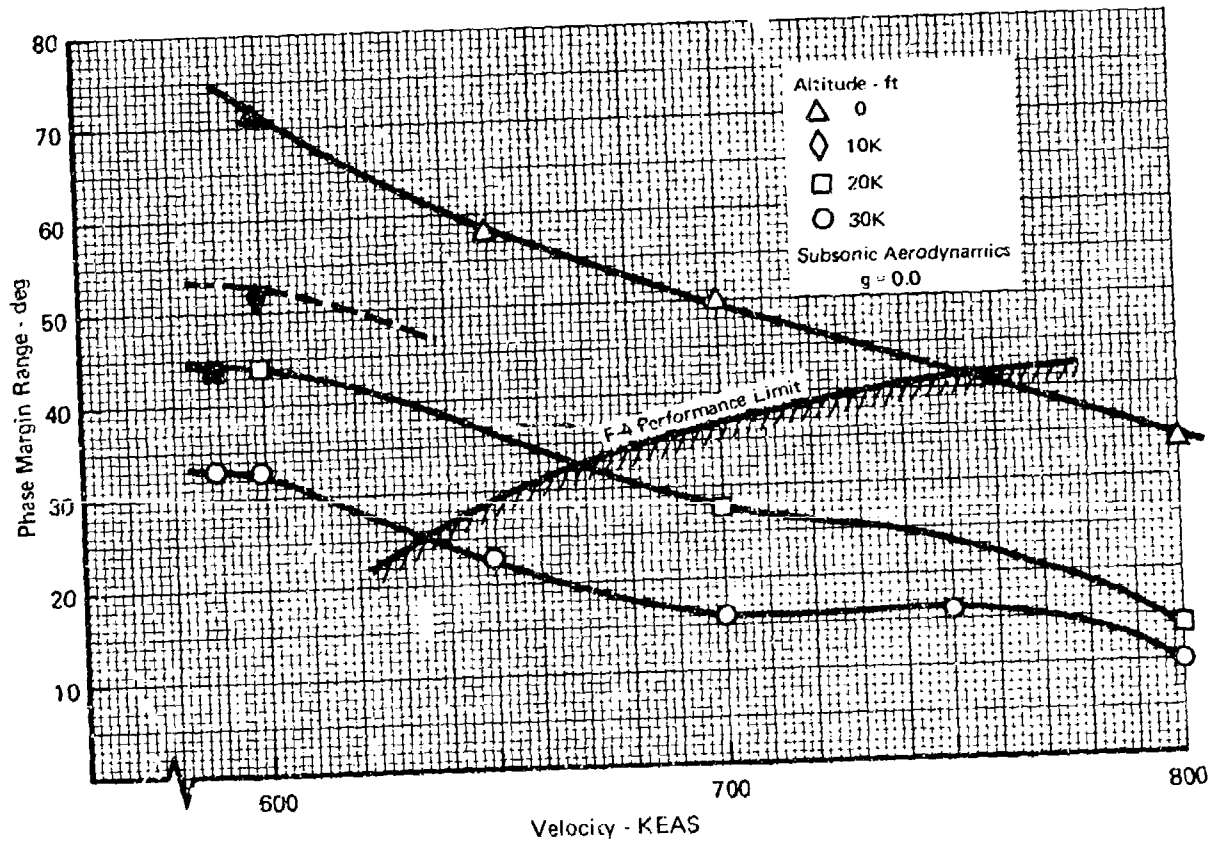
Note: Shaded symbols are sub-flutter data points
Phase Margin Range is the absolute value summation
of the positive and negative phase angle stability margins

FIGURE 55   VARIATION OF PHASE MARGIN RANGE WITH VELOCITY AND
ALTITUDE FOR THE 370 GALLON TANK - 90% FULL
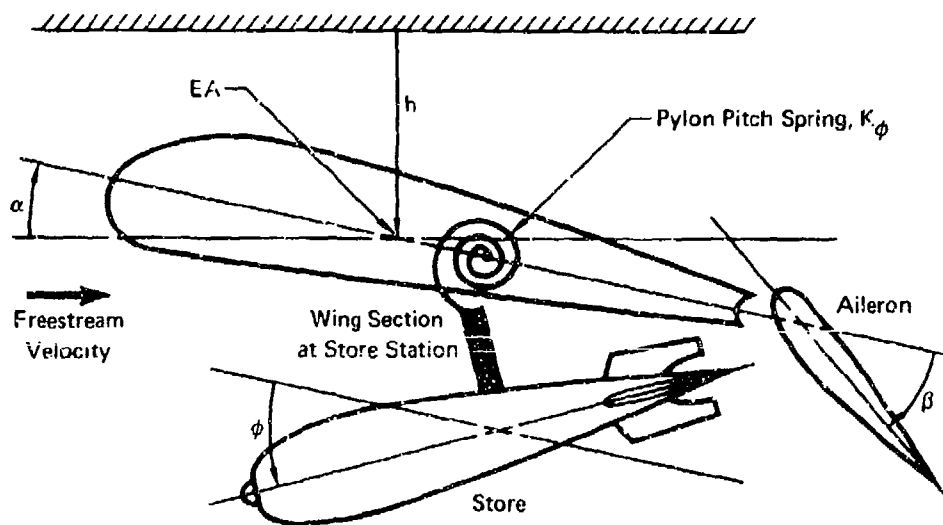
FIGURE 56 WING/ STORE MODEL FOR STORE MOMENT CANCELLATION SCHEME

Several simplifying assumptions were made in the analysis which could affect the magnitude of β required to nullify the store pitch torque. These assumptions include omitting effects due to the following:

1. All aerodynamic damping terms
2. All wing structural and aerodynamic inertia terms
3. Aileron flexure due to airloads
4. Contributions to the wing twist angle from non-flutter modes

With these assumptions the required β was found to be a linear function of α and $\emptyset$. The coefficients of α and $\emptyset$ are the gains which should be applied to the feedback signals, α and $\emptyset$, to eliminate the effects of store pitch torque. These coefficients are functions of the wing geometry, $K_\emptyset$, dynamic pressure, and the wing aerodynamic derivatives. Since the coefficients in this analysis are independent of the store properties, it would be expected that the flutter of different stores carried by identical pylons could be stabilized by feeding back α and $\emptyset$ with unaltered gain settings.

This scheme was applied to the 370 gallon tank - 90% and 62% full cases. The 90% case was stable at 800 knots, but it was stable already with either a pure $\emptyset$ or α feedback. The 62% case, however, required additional compensation amounting to more than 90 degrees of phase lag. Thus, the 62% full case was stabilizeable for a specific ratio of α gain to $\emptyset$ gain, but the gain ratio was different from that required for the 90% full case. This indicates that store characteristics do affect the compensation necessary for flutter stabilization. Apparently a static analysis cannot adequately describe the dynamic situation.

Active Flutter Control Through Structural Feedback

Section 3.2.2.2 discussed conceptually how a structural feedback scheme could be implemented. Structural feedback uses a rigid link to sense wing twist at one end and to actuate a control surface at the other end. Mechanical compensators such as springs, masses, and/or dampers can be incorporated in the link to achieve the phasing of aileron deflection to wing twist angle required for active stability.

In order to demonstrate the feasibility of suppressing flutter through structural feedback a test case was run with the ACF Program using MK-84 EO wing/store data. Compensation of the mechanically sensed wing twist was accomplished by incorporating a mechanical compensation module into the wing-aileron link arm. The mechanical compensations which were considered

for this demonstration study are presented in Figure 57. The parallel
spring and damper forcing a mass (#4) was selected as the most promising
compensation configuration because of the large phase lags which are possible
and the favorable gain amplification at the resonant frequency. If the
resonant frequency coincides with the flutter frequency about 90 degrees of
phase lag can be obtained at a high gain. The gain peak serves to decouple
the flutter frequency from its surrounding frequencies. A host of other
possible structural compensation modules are discussed on pages 10.7 through
10.15 of the Shock and Vibration handbook, Reference 12.

The damper used in the selected compensation module (parallel spring
and damper forcing a mass) is similar to that currently in use with the F-4
rudder. Mass and spring constant values were chosen to match the flutter
frequency and the phase lag required for active stability. The mass weight
was 91.5 pounds and the spring constant was 1036 lb/in. Nyquist plots of the
resultant wing/store feedback control equations at 750 knots are given in
Figure 58 for the uncompensated and compensated control loops. The effects
of the compensation elements on the free-vibration characteristics of the
aileron were not included in this first-cut analysis. The single counter-
clockwise encirclement of the origin in the lower plot of Figure 58 indicates
that active stability has been achieved. Unfortunately insufficient phase
lag was added by the mechanical compensation resulting in only a 20 degree
phase margin in lead. This points out the limited phase compensation capa-
bility of the mechanical compensator - about 110 degrees maximum in lag.
This example required about $135°$ in lag, which explains the restricted phase
margin.

Gain and phase versus frequency for the example mechanical compensation
are given in Figure 59. The broken lines show the improvement possible when
the damper coefficient is halved. The phase lag at the flutter frequency is
improved by 10 degrees and the gain is doubled.

The feedback gain of a structural feedback scheme can be altered by
adjusting the length of the aileron actuator arm relative to the wing twist
sensing arm. (See Figure 16 - length d_2 and d_1, respectively.) If the
twist arm length is fixed, decreasing the aileron arm length will increase
the aileron deflection angle per unit of wing twist.

1. Mass and Damper in Series

$$\beta/\alpha = \frac{c}{MS + c}$$
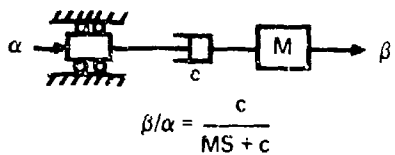
Phase Lag Compensation
No Low Frequency Decoupling
Very Low Break at $\omega = c/M$
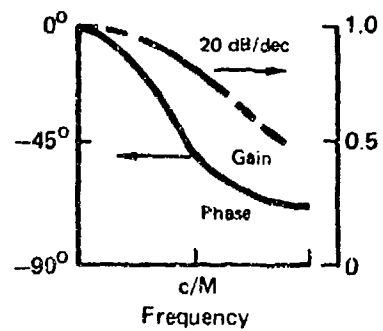
2. Mass and Spring in Series
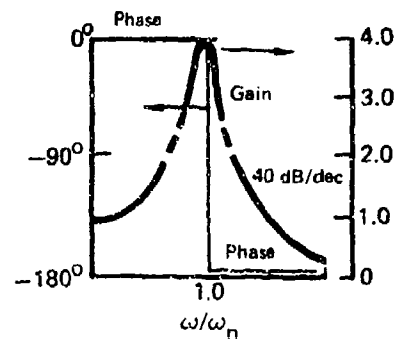
$$\beta/\alpha = \frac{1}{S^2/\omega_n^2 + 1}$$

$$\omega_n = \sqrt{K/M}$$

No Low Frequency Decoupling

3. Mass, Spring, and Damper in Series

$$\beta/\alpha = \frac{1}{S^2/\omega_n^2 + 2\xi_{eq} S/\omega_n + 1}$$

$$\omega_n = \sqrt{K/M} , \quad \xi_{eq} = \frac{\sqrt{K/M}}{2c} \rightarrow \text{Always Large}$$
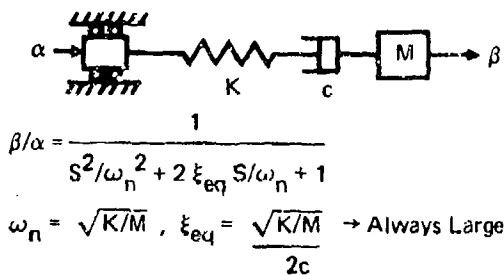
Large Phase Lag Compensation
No Low Frequency Decoupling
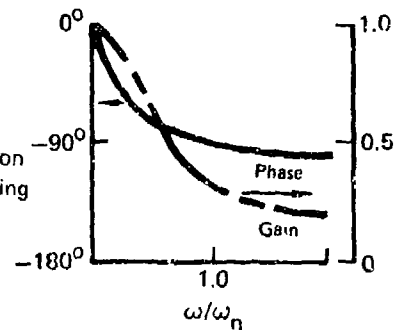
4. Parallel Spring and Damper in Series with Mass

$$\beta/\alpha = \frac{1 + c S/K}{S^2/\omega_n^2 + 2\xi_{eq} S/\omega_n + 1}$$

$$\omega_n = \sqrt{K/M} , \quad \xi_{eq} = \frac{c}{2\sqrt{K/M}} \rightarrow \text{Always Small}$$
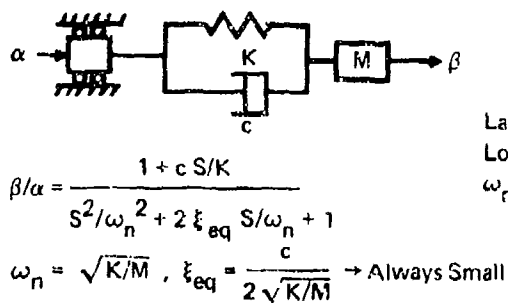
Large Phase Lag Compensation
Low Frequency Decoupling
ω_n is Adjustable
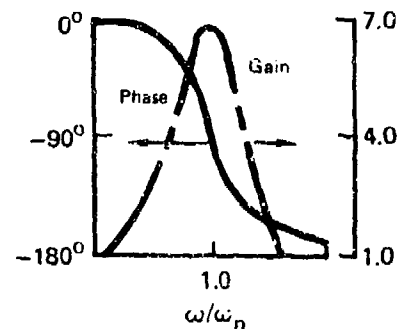
FIGURE 57   MECHANICAL COMPENSATIONS UNDER CONSIDERATION FOR
STRUCTURAL FEEDBACK SCHEME

109

Top plot labels:

MK-84 EO
Sense α Store Section,750 KEAS, g = 0.0, SL
No Compensation, No Hydraulics
Gain: 5.0
Case is Actively Unstable

11.6 Hz
10.8 Hz
11.5 Hz
10.7 Hz
9.3 Hz
10.5 Hz
10.6Hz

Bottom plot labels:

MK-84 EO
Sense α at Store Section,750 KEAS, g = 0.0, SL
Structural Compensation:

$$\frac{1 + 9.65 \times 10^{-3}\,S}{1 + 9.65 \times 10^{-3}\,S + 2.539 \times 10^{-4}\,S^2}$$

Gain: .641
Phase Margins: $^{+20^{\circ}}_{-113^{\circ}}$
Gain Margins: $^{+6dB}_{-3.5dB}$
Case is Actively Stable

11.5 Hz
10.6Hz
11.6Hz
10.7 Hz

FIGURE 58   NYQUIST PLOTS ILLUSTRATING ACTIVE CONTROL BY
STRUCTURAL FEEDBACK SCHEME

110

$$Y(S) = \frac{1 + c/K \, S}{S^2/\omega_n^2 + 2\zeta \, S/\omega_n + 1}$$

where $\omega_n = \sqrt{K/M}$, $\zeta = \dfrac{C}{2\sqrt{KM}}$, $K = 1036\text{lb/in.}$, $M = 0.266 \text{ mugs}$
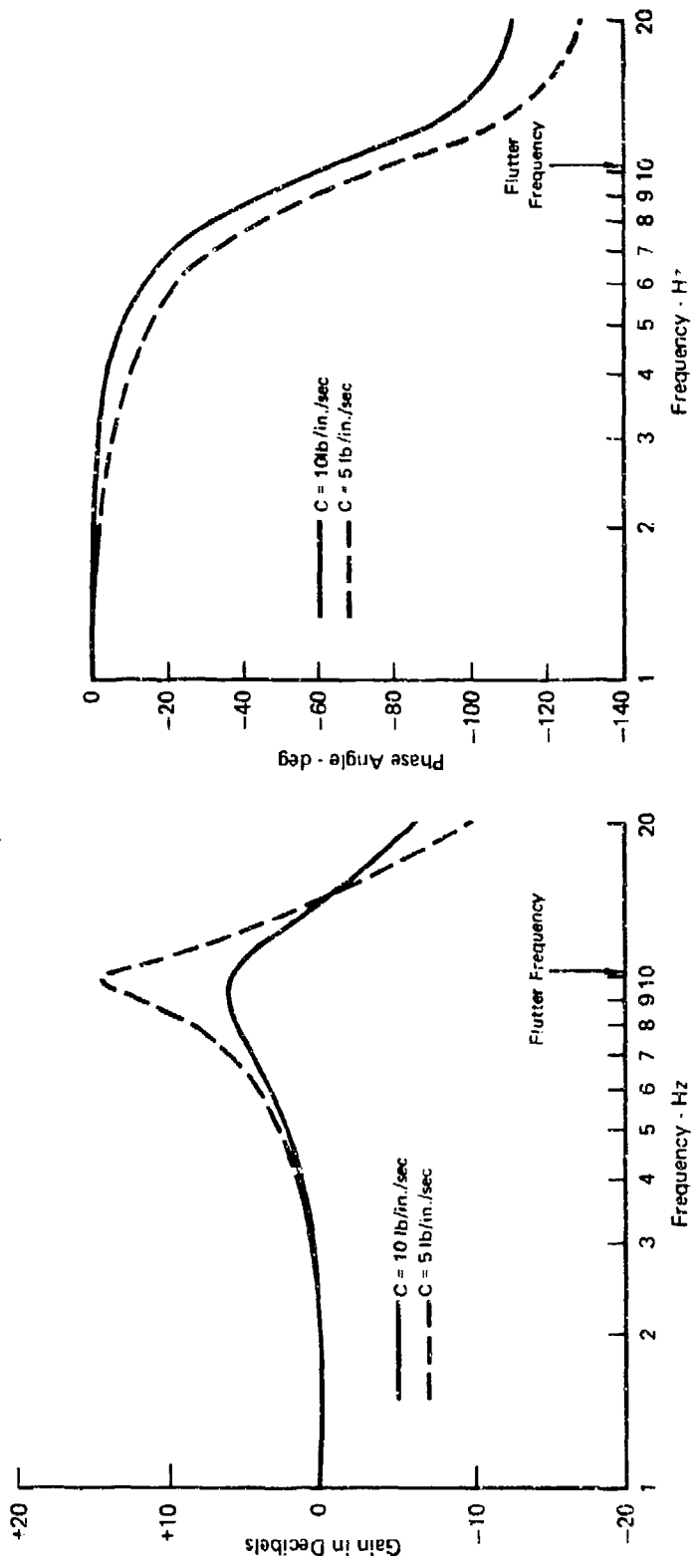
FIGURE 59 GAIN AND PHASE CHARACTERISTICS OF EXAMPLE MECHANICAL COMPENSATION

The potential advantages of a structural feedback flutter suppression scheme over an electronic compensation - hydraulic actuation scheme result from the elimination of all hydraulic and electronic components. This drastically lowers cost and improves reliability. Since structural feedback is not dependent on hydraulic actuators it does not suffer performance limitations at high frequencies.

The shortcomings of structural feedback, however, are serious when compared with electronic compensation-hydraulic actuation schemes. Structural feedback lacks:

1. Versatility in handling different stores
2. Phase characteristics which vary gradually with frequency
3. Total decoupling of low frequencies or non-flutter modes

A store configuration change necessitates switching heavy weights and springs while an electronic compensation may be adjusted through a potentiometer setting. The desirability of achieving a gain "peak" at the flutter frequency forces small equivalent damping for structural feedback compensation. This in turn causes large phase angle changes in the vicinity of the flutter frequency as shown in Figure 59. Large phase margins are thus required to accommodate flutter frequency uncertainty. The gain "peaking" at the flutter frequency does not decouple low frequencies from the flutter control loop nearly as effectively as the high pass filter in an electronic compensation which passes zero signal at zero frequency. Greater interferences with pilot control would thus result with a structural compensation scheme. Finally, the presence of resonating non-flutter modes would require the difficult (if not impossible) task of generating the mechanical analog of an electronic notch filter.

The structural feedback concept has been tested analytically for a wing/store configuration. It is equally suitable, however, for bare wing flutter control. For that application the control system components could be designed specifically and permanently for a single well-defined control requirement.

Flutter Control Through Sensor Output Combinations

As discussed in Section 3.2, two out-of-phase wing motions can be added together in such a manner that when the sum is used as a feedback signal - active stability occurs. It is possible, for example, to control flutter by using a feedback signal of the form $\pm B$ $(\alpha \pm A\dot{\alpha})$ where α and $\dot{\alpha}$ are the wing twist angle and rate, and A and B are constants. However, additional

electronic networks, such as high pass filters, notch filters, and high frequency lags, are still required for a practical control system design. The variable signs on the feedback gain constants B and A are necessary to account for the different phase requirements of different stores for stability. The four possible combinations of sign are illustrated in Figure 60.

Figure 61 illustrates the design procedure. The uncompensated Nyquist plots with displacement and velocity feedback are determined individually. A vector is constructed on each of the plots from the +1 point on the real axis to the flutter frequency point (Step 1). The constant A is equal to the negative of the imaginary part of the displacement feedback vector divided by the imaginary part of the velocity feedback vector, $A = -\dfrac{I_1}{I_2}$. This ensures that the weighted vector sum ($\alpha + A\dot{\alpha}$ for plot type 1, see Figure 60) lies along the real axis, since the imaginary parts of the two vectors have been equated (Step 2). The constant B is increased until an encirclement of the origin is achieved with the desired gain margins (Step 3). A Nyquist plot for the 370 gallon tank 90% full case compensated in this manner is shown in Figure 62.

Load Suppression with Active Pylons

This potentially promising scheme for wing/store flutter control, described conceptually in Section 3.2.2.3, has been investigated. Passive flutter analyses were conducted with the subsonic aerodynamic data, for the 370 gallon tank-90% full configuration. These runs were made to demonstrate that decoupling the wing/store system can cause the wing to revert to the bare wing flutter mechanism and speed. The results, shown in Figure 63, indicate that for total suppression of the tank pitch inertia the wing does, indeed, revert to approximately its bare wing flutter velocity. For partial suppression of the tank inertia, however, the bare wing flutter velocity is not achieved.

Additional studies were made to determine the hardware requirements for total suppression of the pitching moment for the 370 gallon tank - 90% full. Support-actuators were assumed to act as shown in Figure 17. The total hydraulic fluid flow rate required for four such actuators per aircraft is shown in Figure 64 as a function of the amplitude and frequency of the store pitching motion being controlled. It is seen that only very small amplitude - low frequency motion can be achieved even using the total hydraulic flow rate capacity of an operational F-4 (100 gals/min). Store inertial
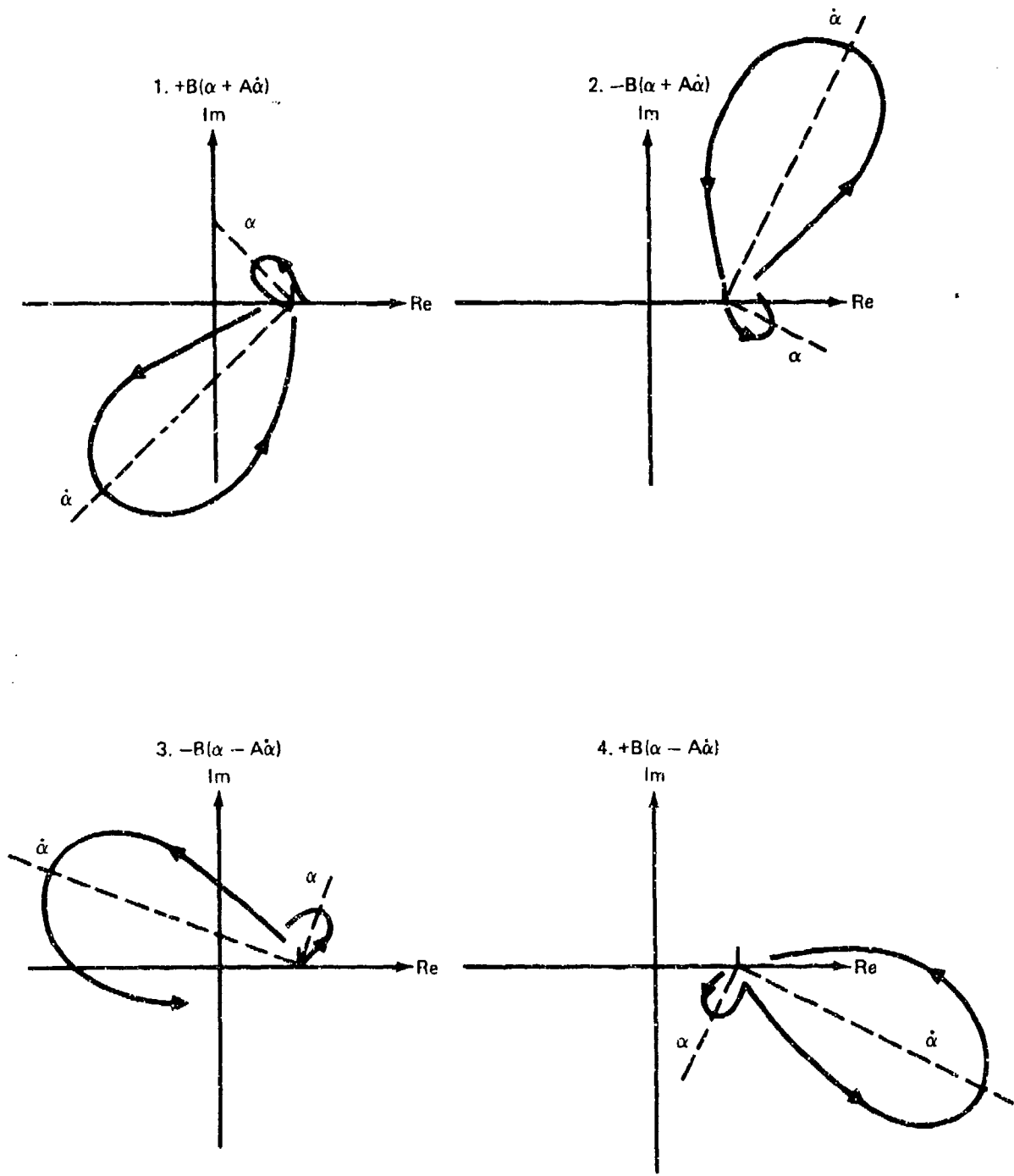
FIGURE 60 ALGEBRAIC SIGN DETERMINATION FOR COMBINED DISPLACEMENT
- VELOCITY FEEDBACK SCHEME

114

Nyquist Plot: α Feedback

Step 1

Nyquist Plot: $\dot{\alpha}$ Feedback

Nyquist Plot: α + A$\dot{\alpha}$ Feedback

$$A = -\frac{I_1}{I_2}$$

Step 2

Nyquist Plot: +B(α + A$\dot{\alpha}$) Feedback

Step 3
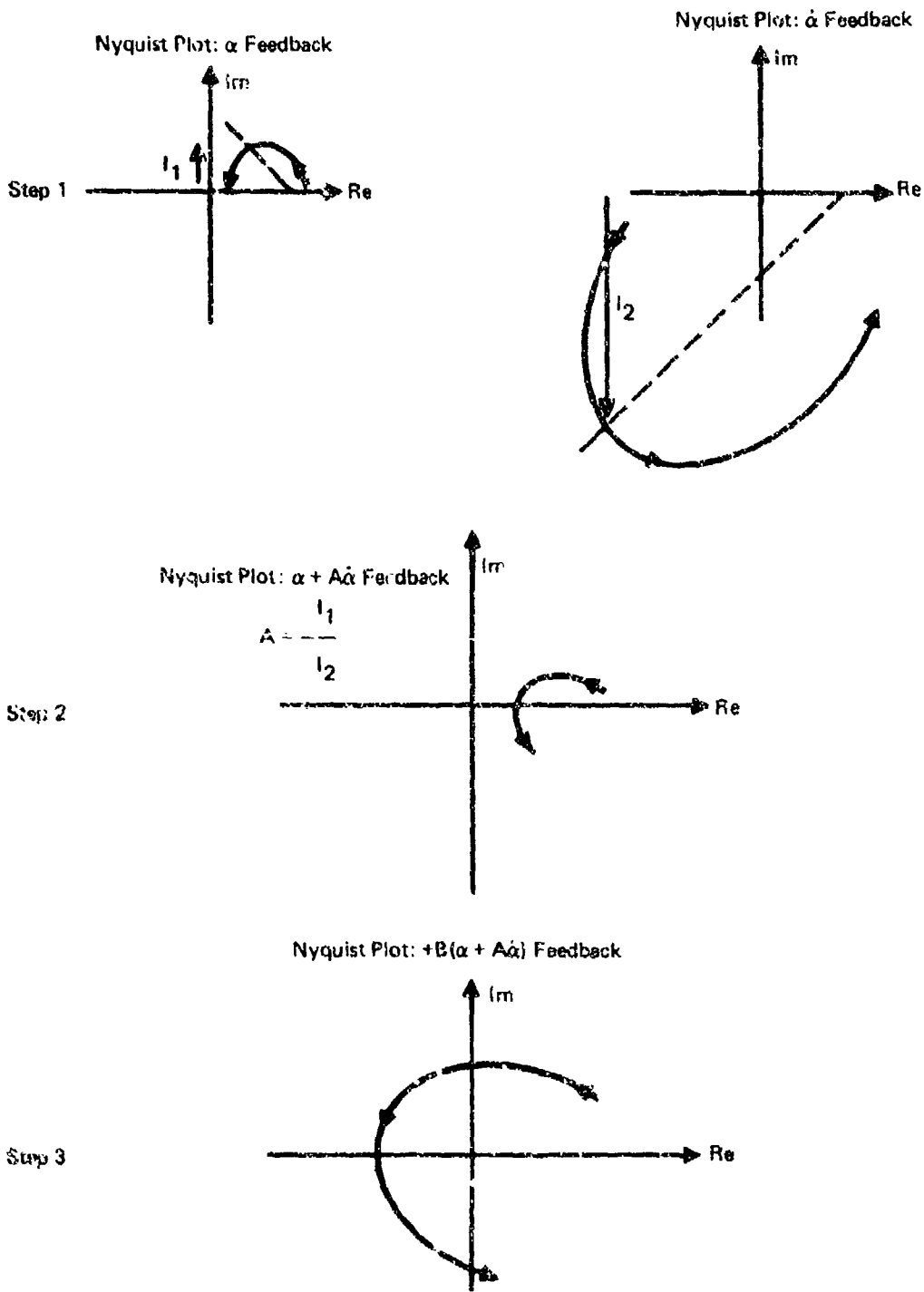
FIGURE 61 PROCEDURE FOR DETERMINING THE COEFFICIENTS A AND B
IN A COMBINED DISPLACEMENT - VELOCITY FEEDBACK SCHEME

115

370 Gallon Tank, 30% Full
g = 0.0 V = 800 KEAS
Sensor: Just Ahead of Aileron

High Pass Filter: $\dfrac{.05S}{1+.05S}$

Compensation: $\alpha + .0267\dot{\alpha}$ feedback
Feedback Gain: 3.4

Phase Margin: $+12^0$ Gain Margin: $+6.9$ dB
-15^0 -2.3 dB

11.4 Hz
7.8 Hz
8.2 Hz
3.4 Hz
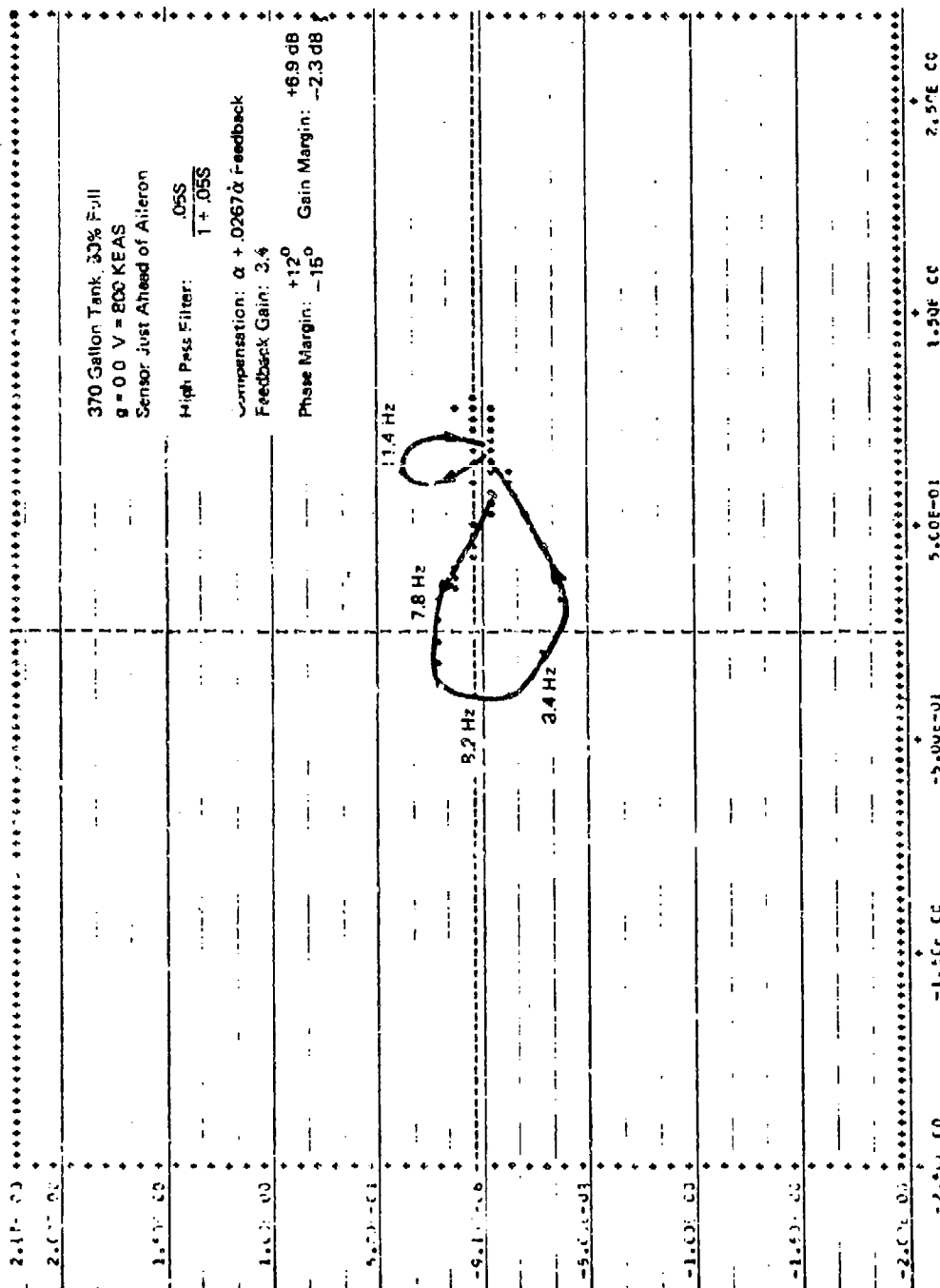
FIGURE 62 NYQUIST PLOT ILLUSTRATING ACTIVE CONTROL BY COMBINED
DISPLACEMENT-VELOCITY FEEDBACK SCHEME

116
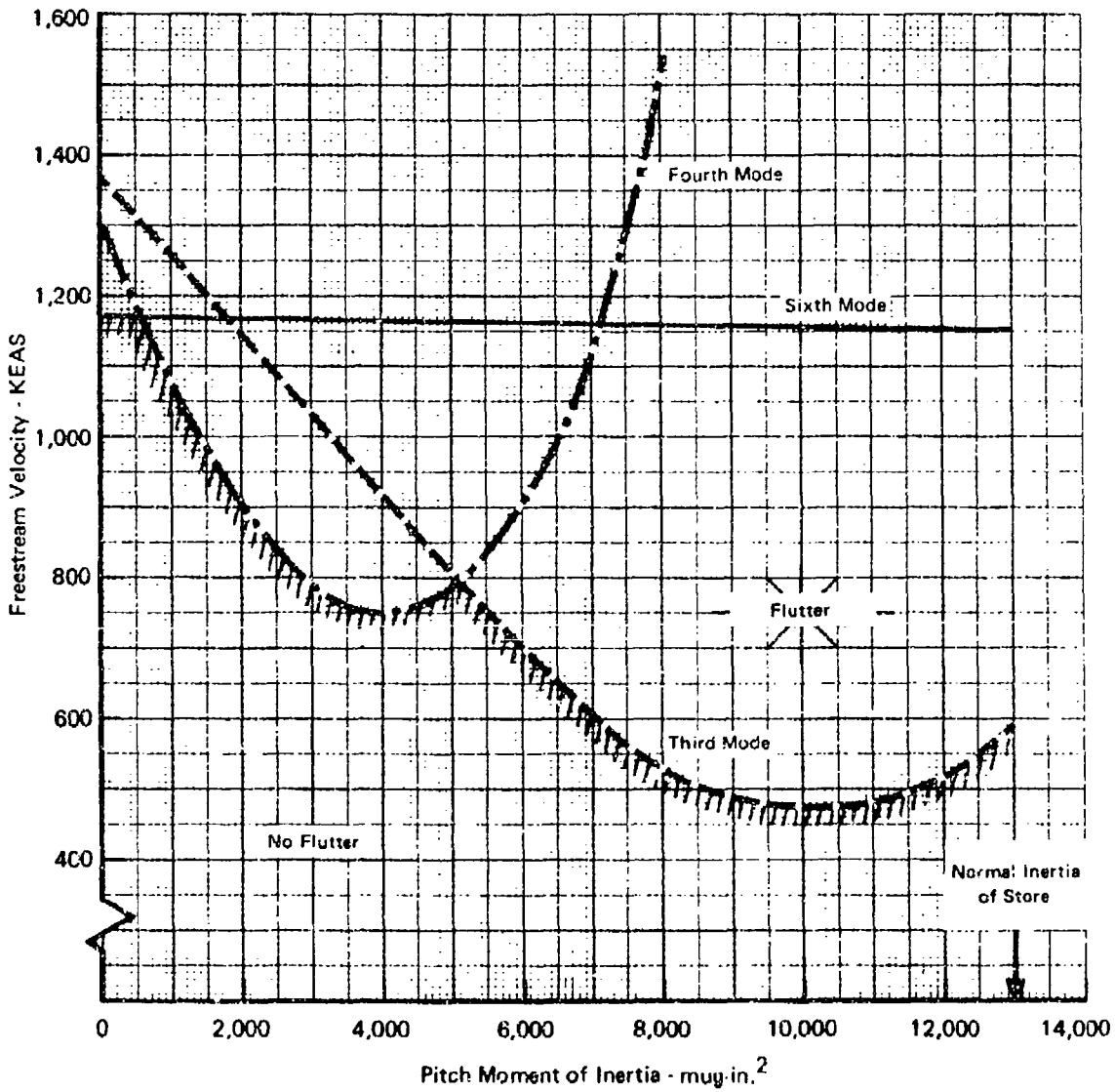
FIGURE 63   EFFECT OF STORE PITCH INERTIA ON 370 GALLON TANK
—90% FULL FLUTTER SPEED
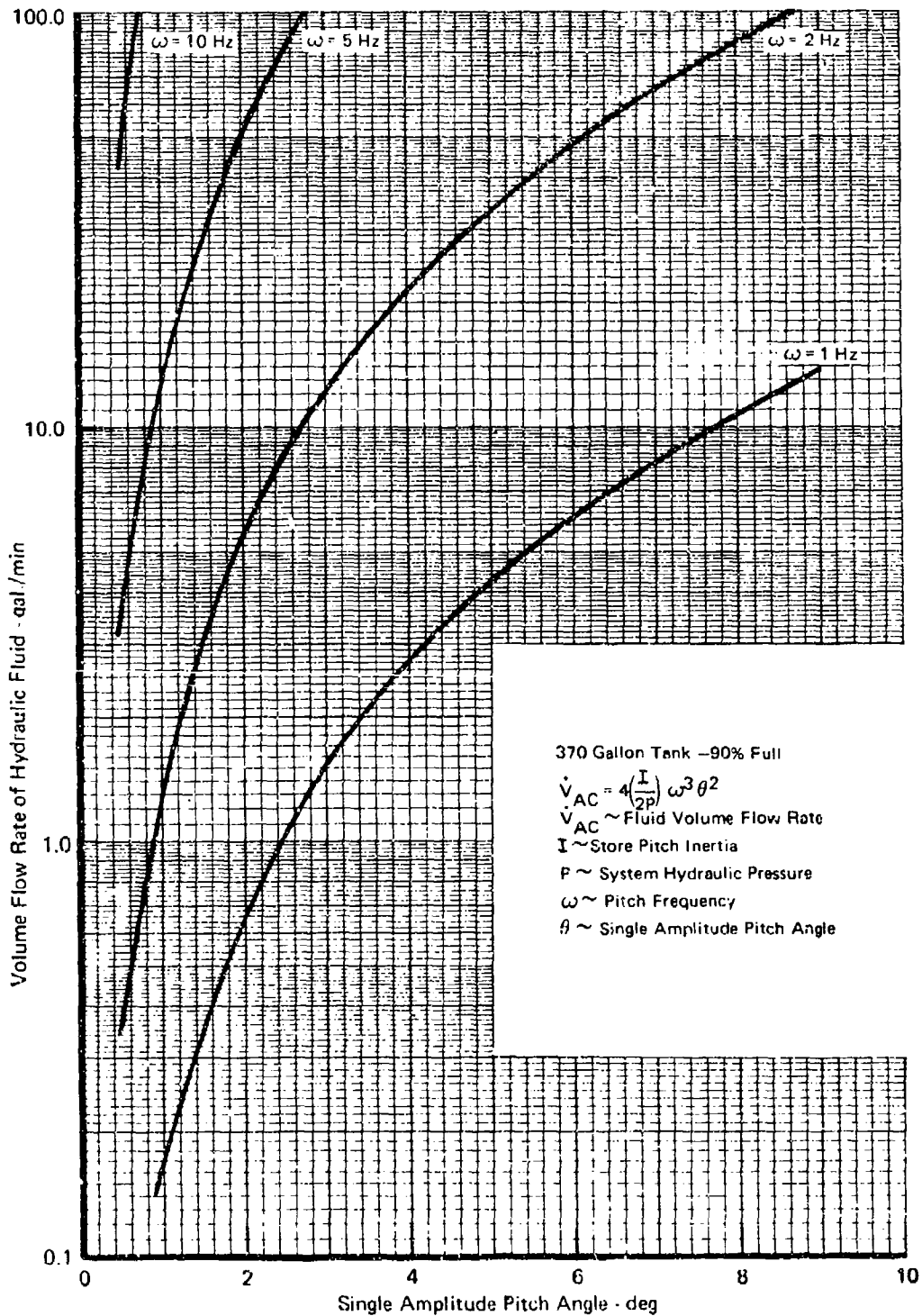
FIGURE 64 TOTAL AIRCRAFT ACTUATOR VOLUME FLOW RATE FOR ACTIVE
CONTROL BY LOAD SUPPRESSION SCHEME

loads in the frequency range of flutter would thus be passed into the wing and the promised benefits of load suppression would not be realized.

4.1.2.4 Time Domain Studies – Time domain studies were conducted using the compensated control loops listed in Section 4.1.2.3. Such time domain studies are useful not only in verifying the stability predictions of the frequency domain analysis but also they yield the following new information:

o Actuator hardware requirements for active stability

o The effects of hardware limitations on system performance.

The previous frequency domain studies have presumed unlimited aileron rate and displacement capabilities. Once the feedback gain was determined it was assumed that the aileron power actuator and secondary actuator could deliver the commanded deflection at the flutter frequency. Practically, however, both the aileron displacement and velocity (displacement-frequency product) are restricted. The first question, then, is "are the aileron rate and displacement capabilities higher than the maximum values commanded?" If so, there is no problem. If not, then the question becomes, "Can active stability be maintained even though the aileron actuators are rate and/or displacement limited during some portion of their deflection cycle?" In addition to rate or displacement saturation, the effect of other non-linear phenomena on active control can be evaluated, such as:

o Aileron-Spoi   Flutter Control

o Actuator Dead Space

o Aileron Free Play

Time domain studies, thus, considerably enhance the realism of the simulation.

Linear Studies

As discussed in Section 3.5.2 and Appendix IV, a special computer program was developed for simulating the flutter control loop equations in the time domain. Aerodynamic data generated by an Indicial Lift program was used in the programs. The time domain studies were limited to four wing/store modes: the first three vibration modes and an aileron rotation mode. Recall that the basic flutter mechanism involved the interaction of the 2nd and 3rd modes. The number of modes was limited for two reasons:

1. To avoid excessive computer time usage

2. To avoid integration errors arising from the presence of high frequency modes.

Excitation of the time domain equations was achieved by means of a gust force of the form:

$$(10000/2) \ (1 - \cos \ ((2\pi)(\omega_F) \ t)) \ \text{pounds}$$

This gust force represents the equivalent force excitation at the flutter frequency, ω_F, experienced by a minimum weight F-4 flying through a thunderstorm at Mach 1.0, sea level conditions. The 10,000 pound amplitude was obtained by integrating under a power spectral density curve for a 13.38 ft/sec (rms velocity) thunderstorm over the half power bandwidth of the flutter mode frequency (8.0 to 8.7 Hz for the 90% full 370 gallon tank). The PSD plot for this thunderstorm, presented in Reference 13, is typical in that its energy content is constant for low frequencies and falls off rapidly after about 1 Hz. Discrete gusts derived for the same thunderstorm at sub-flutter frequencies as well as aircraft maneuver loads produced rather mild system responses when compared with the flutter frequency gust as reported in Reference 14. Thus, only the flutter frequency gust results are reported here.

Verification of System Stability - The stability of the aeroelastic active control loop equations can be verified by obtaining a printout of mode response as a function of time from the time domain computer program. Stability is indicated by a response whose amplitude diminishes with time after the initial transient response. Such time history printouts were obtained for each of the four compensated wing/store configurations at 700 knots, $g = 0.02$, sea level conditions. The 10,000 pound gust loading at the flutter frequency was used to excite the structure. All responses were found to be stable. Additional runs were also made to check the gain margins previously derived from the frequency domain studies. That is, feedback gain was set at its predicted maximum and minimum stable values. The gain margins for each store were verified in this manner.

Aileron Rates and Displacements with No Limits - Aileron rate and displacement as a function of time is an output of the time domain computer program. Thus, if it is assumed that the aileron response is not restricted in rate or displacement, maximum values can be read from the time history plots. Figures 65 through 68 are time history plots for each of the wing store configurations. The data shown includes response of each vibration
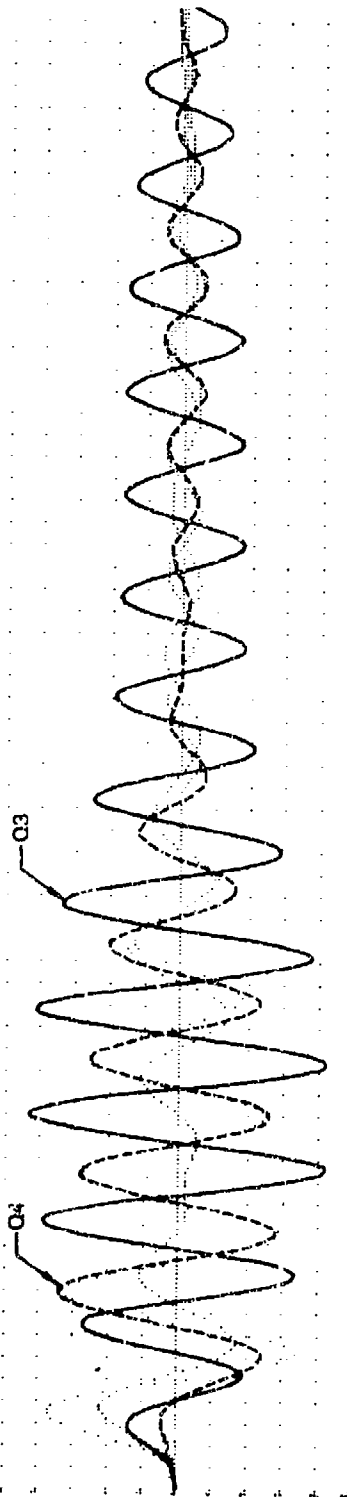
120

FIGURE 65 DYNAMIC RESPONSE TO (1 - COS) GUST AT THE FLUTTER FREQUENCY - INCLUDING AILERON FLEXIBILITY - 370 GALLON TANK - 90% FULL
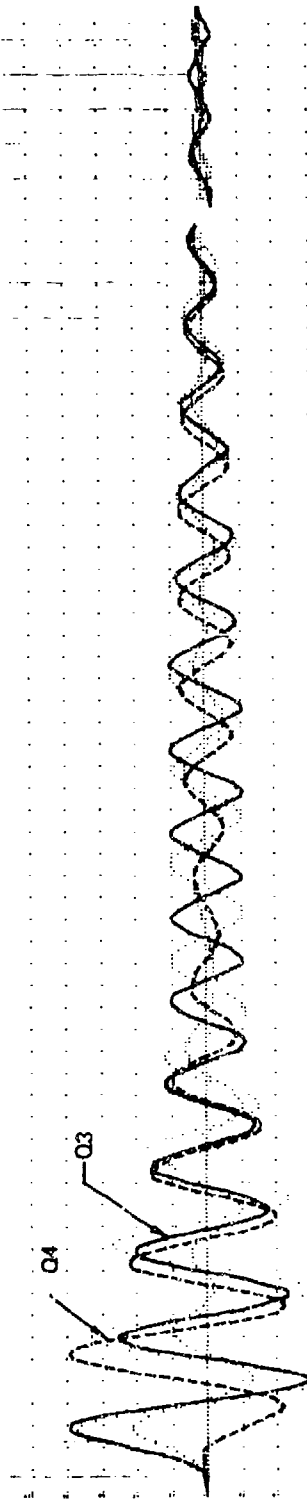
FIGURE 66 DYNAMIC RESPONSE TO (1 - COS) GUST AT THE FLUTTER FREQUENCY - INCLUDING AILERON FLEXIBILITY - 370 GALLON TANK - 62% FULL

122

F-4 MK-84 EO V = 700 KEAS g = 0.0₂ Gust RMS = 13 ft/sec
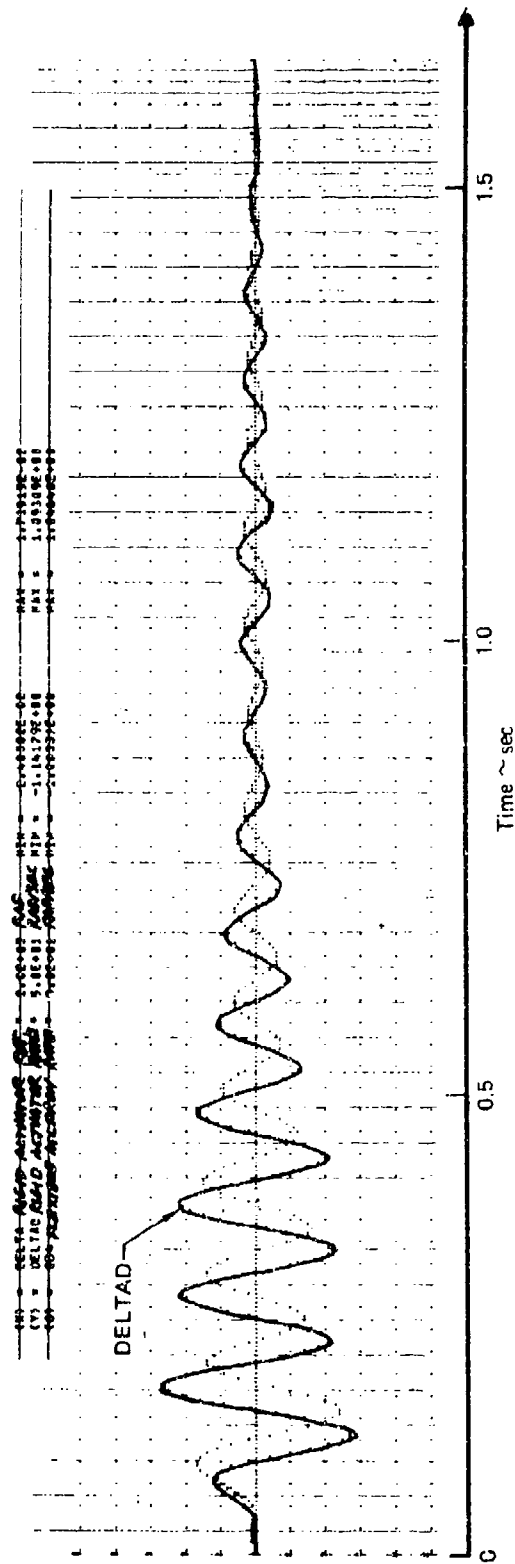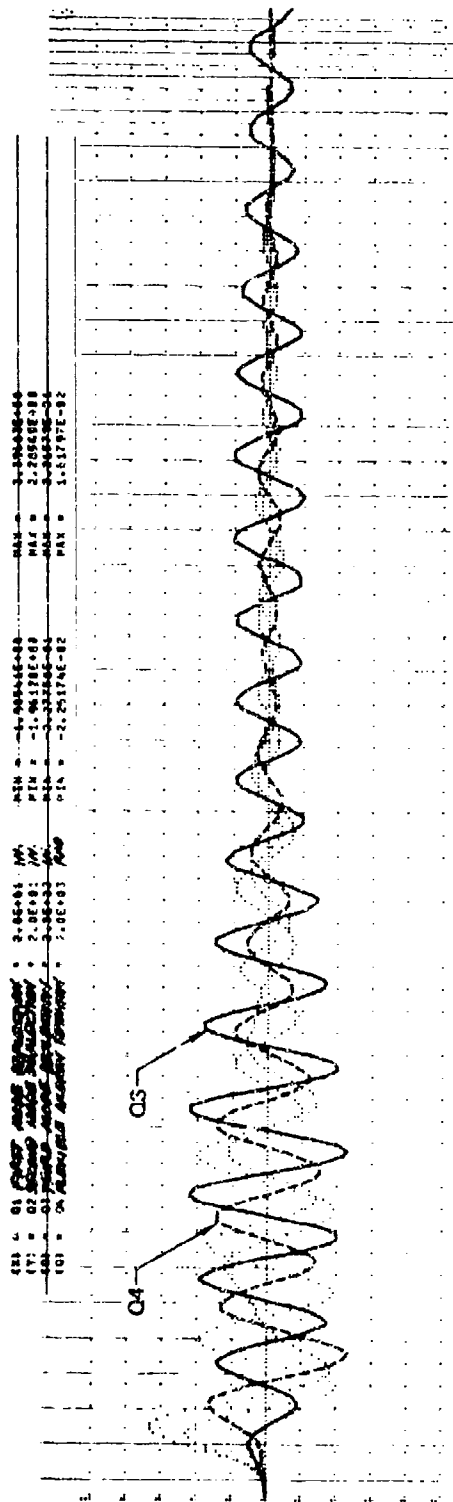
FIGURE 67 DYNAMIC RESPONSE TO (1 - COS) GUST AT THE FLUTTER FREQUENCY - INCLUDING AILERON FLEXIBILITY - MK-84 EO

Time ~ sec

123

F-4 MK-82(3, 4) V= 700 KEAS g = 0.02 Gust RMS = 13 ft/sec
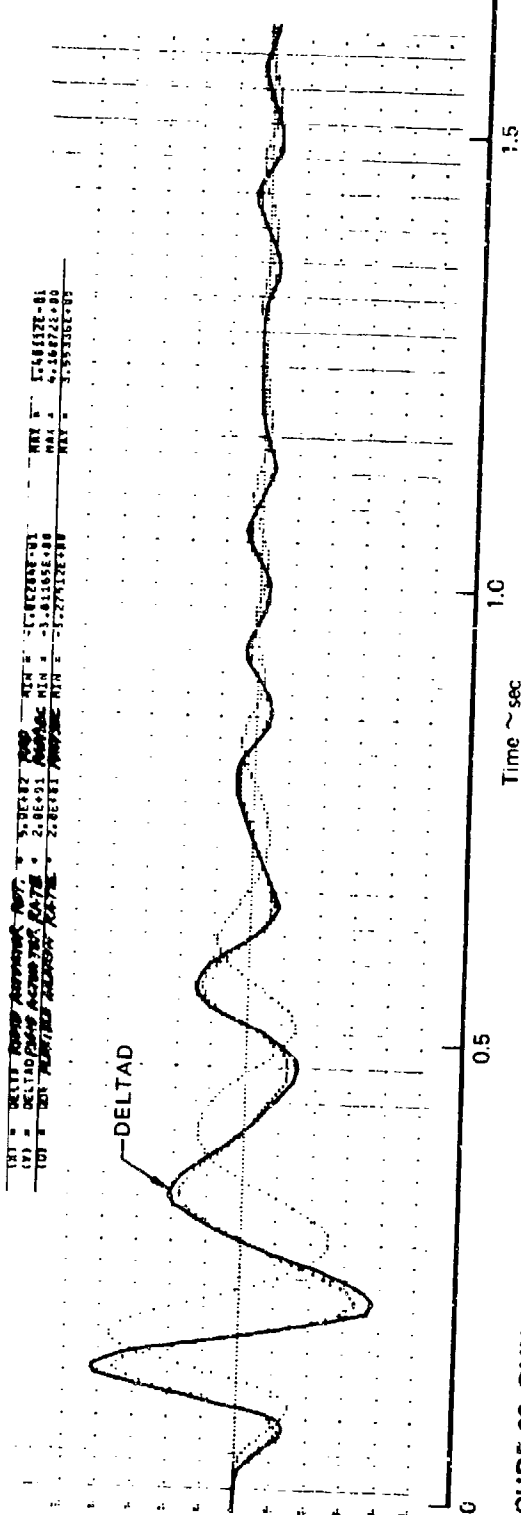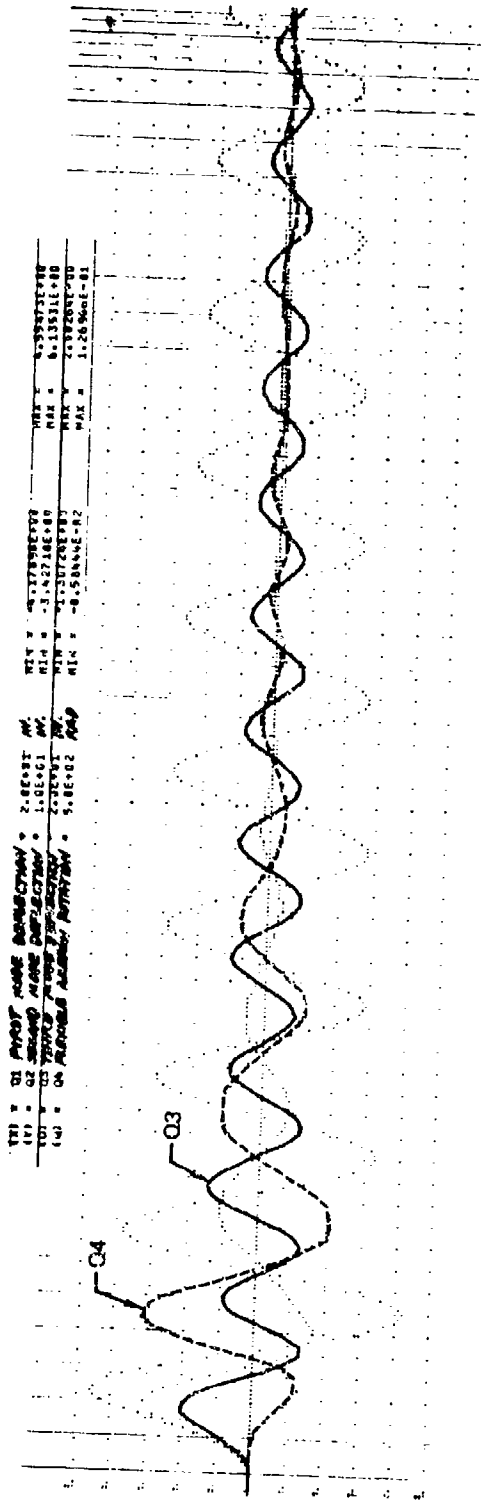
FIGURE 68 DYNAMIC RESPONSE TO (1 - COS) GUST AT THE FLUTTER FREQUENCY - INCLUDING AILERON FLEXIBILITY - MK-82 (3,4)

124

mode, actuator displacement and rate, and aileron rate. Again the 10,000 pound 1-cosine gust at the flutter frequency is used for excitation. In each case the maximum flexible aileron rate is in phase with but slightly less than the maximum actuator rate. This results because the flexible aileron "gives" under airloads and so is not as effective as a rigid aileron. All of the configurations are stable at the 700 knots, g = 0.02, sea level condition as evidenced by the converging flutter mode (3rd mode) response. Control system instabilities are also non-existent since all traces possess converging characteristics. Figure 69 summarizes maximum aileron actuator rates and the equivalent damping of the flutter mode obtained from the previously shown figures. Recall the feedback gain used in compensating each wing/store:

    90% - 370 gallon tank - 5.34
    60% - 370 gallon tank - 5.46
    MK-84 EO   - 1.81
    MK-82 (3,4)   - 15.21

The figure shows that the store with maximum'feedback gain, the MK-82 (3,4), also has the maximum aileron actuator rate. This makes sense because the power actuator is asked to respond to a higher feedback displacement command. Rate is the product of displacement and frequency. Hence an amplified displacement signal results in a higher aileron rate requirement. The rates shown in the figure, however, indicate that the maximum rate required for one store relative to another is not just equal to the ratio of feedback gains. Other factors such as the relative explosiveness of the flutter mode also came into play - the more violent the flutter mode, the higher the aileron rate and displacement requirements. Rates decrease drastically for all configurations if the system is designed to ±6 dB gain margins at g = 0.02 rather than g = 0.0. Increasing structural damping increases the maximum gain margins for a constant gain setting. Thus, a smaller gain is required to obtain the 6 dB margin.

For a given store the maximum aileron rate is proportional to the feedback gain. The aileron rate also varies linearly with the rms gust velocity, provided that the gust velocity is small when compared to the aircraft velocity. When these two facts are known a plot showing aileron rate as a function of feedback gain and rms gust velocity can be constructed based on one gain-gust velocity design condition. This has been verified by test runs with the time domain program. Such a plot is shown in Figure 70
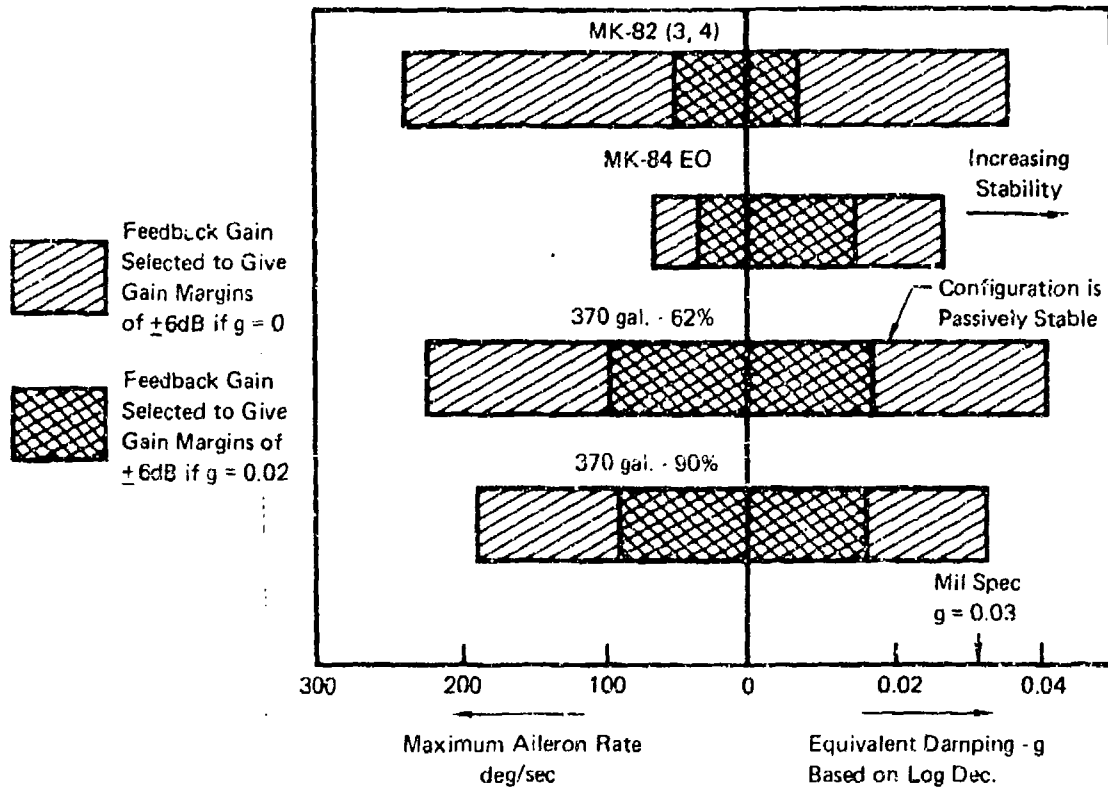
V = 700 KEAS   Structural Damping g = 0.02   Gust RMS = 13 Ft/Sec

FIGURE 69   AILERON RATE AND EQUIVALENT DAMPING IN FLUTTER
MODE FOR WING/STORE STUDY CONFIGURATIONS
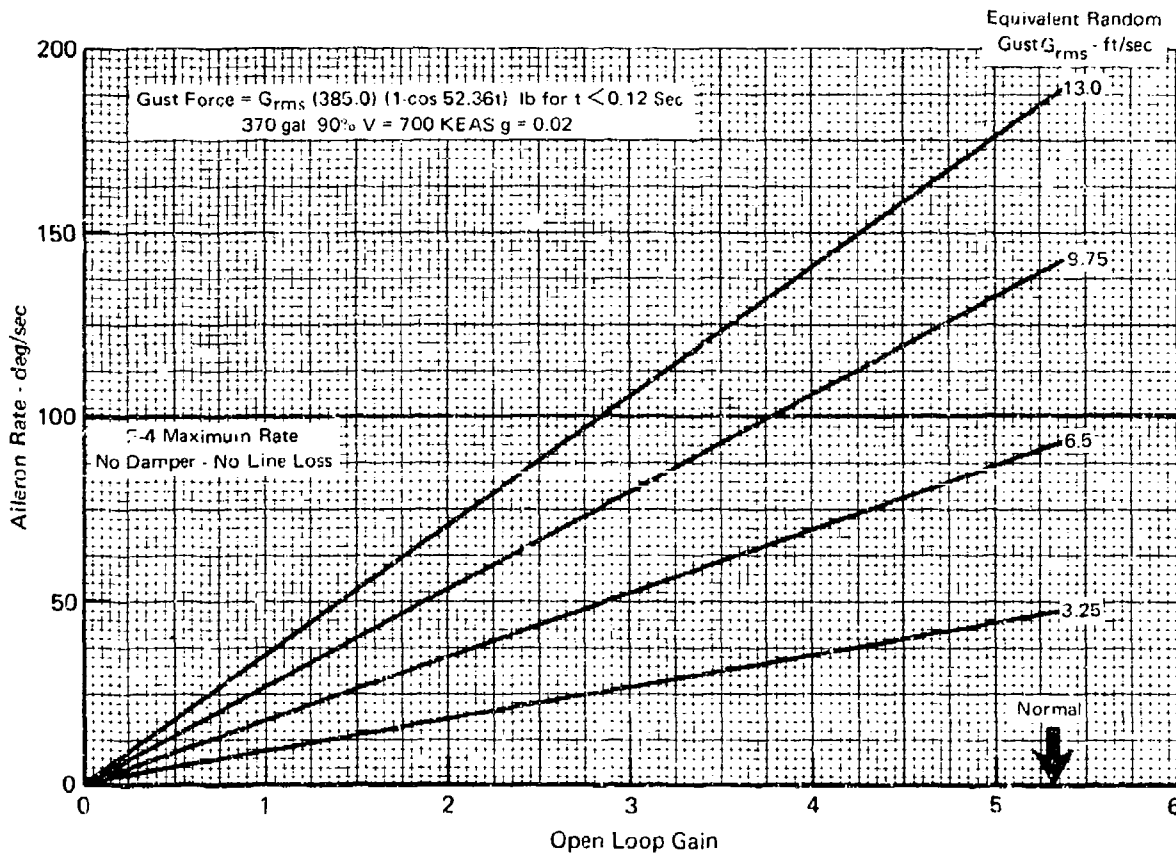
FIGURE 70 MAXIMUM AILERON RATE vs GUST LEVEL AND CONTROL
SYSTEM GAIN

for the 90% full-370 gallon tank case at 700 knots, g = .02, sea level conditions. The plot indicates a maximum aileron rate limit for the F-4 at 700 knots of about 100 deg/sec. Thus for the normal gain setting, 5.34, the flutter system can cope with about a 7 ft/sec (rms) gust without rate limiting.

Nonlinear Studies

Stability with Rate Limits - Deflection limit cases were run with the 90%-370 gallon tank case for pure aileron and aileron-spoiler control surface systems. The 700 knots, g = 0.02, sea level, 13 ft/sec gust conditions were used in these time domain studies.

Aileron Control Surfaces - Results from runs with rate limits of 100 deg/sec and 60 deg/sec are shown in Figures 71 and 72, respectively. Active control is maintained in each case even though the actuators are rate saturated over a significant portion of each oscillation cycle. The crucial factor is that there is a net dissipation of airstream energy over each cycle. These results show that this is possible even though the aileron displacement rate does not exactly conform to the command signal. There is, however, some degradation in how fast the excitation is damped out as evidenced by the effective damping coefficients:

No Limits   - g = 0.033
100 deg/sec limit - g = 0.032
60 deg/sec limit - g = 0.023

Aileron-Spoiler Control Surfaces - These studies were conducted to give a realistic simulation of the actual F-4 aircraft. The spoiler deflection was multiplied by a factor of 1-1/2 to match the F-4 gearing - 5 degrees down aileron on left wing causes a simultaneous 7.5 degrees up spoiler command on the right wing. These runs were conducted before the final control loop design was specified. The studies used a compensation based on actual unimproved F-4 actuator hardware:

Aileron Actuator: $\dfrac{1}{1 + .1S}$

Spoiler Actuator: $\dfrac{1}{1 + .06S}$
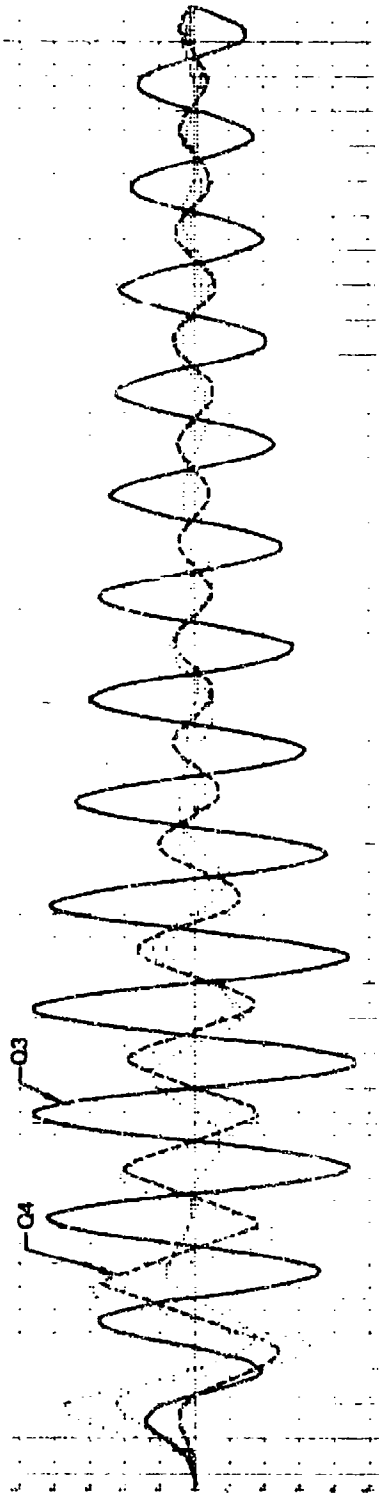
FIGURE 71 DYNAMIC RESPONSE PLOTS ILLUSTRATING EFFECTS OF AILERON
ACTUATOR RATE LIMIT - 100 DEG/SEC LIMIT

F-4 370 gal. 90% V = 700 KEAS g = 0.02 Gust RMS = 13 ft/sec

FIGURE 72 DYNAMIC RESPONSE PLOTS ILLUSTRATING EFFECTS OF AILERON
ACTUATOR RATE LIMIT · 60 DEG/SEC LIMIT

This system was found to be unstable for aileron authority limits of
3 degrees and 60 deg/sec. For the F-4 aircraft at sea level density condi-
tions the aileron deflection and deflection rates are limited to about 10
degrees and 75 deg/sec, respectively. The system was found to be stable
for aileron limits of 10 degrees and 110 deg/sec combined with spoiler
limits of 15 degrees and 150 deg/sec.

Dead Space Evaluation - Dead space, as defined in these studies, is
the result of hydraulic actuator control valve spools designed with overlap
so as to eliminate leakage flow for zero signal command. The F-4 aileron
actuator control valve is designed for zero overlap so that a finite
response occurs for any non-zero command signal. Time domain runs have been
made, however, with the F-4 wing/store data to determine levels of limit
cycle motion resulting from rather large values of dead space.

The modeling of the actuator in the time domain program is described in
Figure 73. The original formulation for the actuator transfer function in
the Laplace notation was not suitable for this purpose since variables
describing the real hardware components were not present. The more physical
loop shown in Figure 73 gives the same transfer function and also allows
for the efficient evaluation of both dead space and fluid flow limits. The
case chosen is the 370 gallon tank 90% full. Runs were made for dead space
up to 10% of the full valve travel. The resultant limit cycle motion
amplitudes shown in Figure 74 for all of the system coordinates are very small.
The amplitude at the wing tip in the flutter mode is less than 0.3 in. and
the aileron deflection less than 0.1 deg. for dead space as large as 10% of
full valve travel.

Free Play - Free play introduces lags in the response. The phenomena
arises because of "slop" in the force producer system outboard of the power
actuator control valve. The phenomena can be explained in terms of the simple
translation actuation device sketched in Figure 75. A positive input command
at block A does not result in a translation of bar B until the "slop" distance,
d, is exceeded. So far the situation looks deceptively similar to dead space.
At maximum amplitude commands, however, the phenomena is different. When
Block A reverses direction it must first cover a distance of 2d before trans-
lation of bar B is initiated in the negative direction. Sketch (b) in the
figure shows a time history of block A input translation versus bar B output

131

DEAD SPACE   LIMITING
HERE   HERE

X_C —⊕— X_E → [K] — X_V → [C] — $\dot{X}_A$ → [$\int \dot{X}_A$] — X_A →

DIFFERENTIAL EQ. $(1 + p/KC)X_A = X_C$, $p = \frac{d}{dt}$

EQUIV. TRANSFER FUNCTION $\dfrac{X_A}{X_C} = \dfrac{1}{1 + S/KC}$
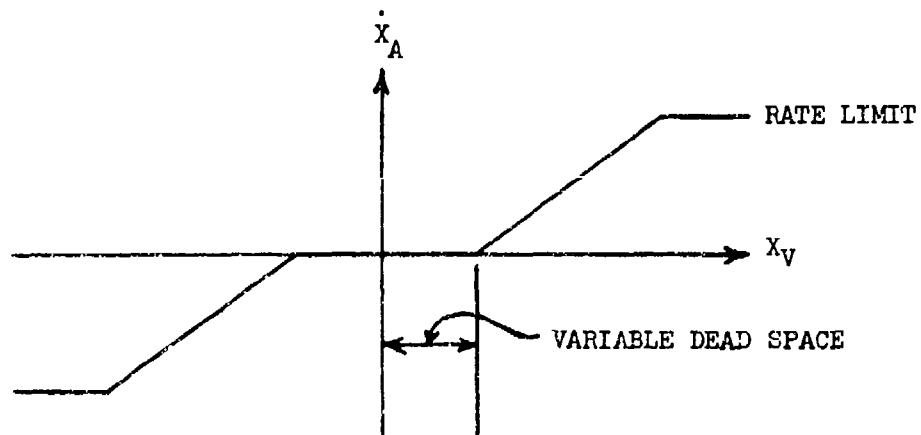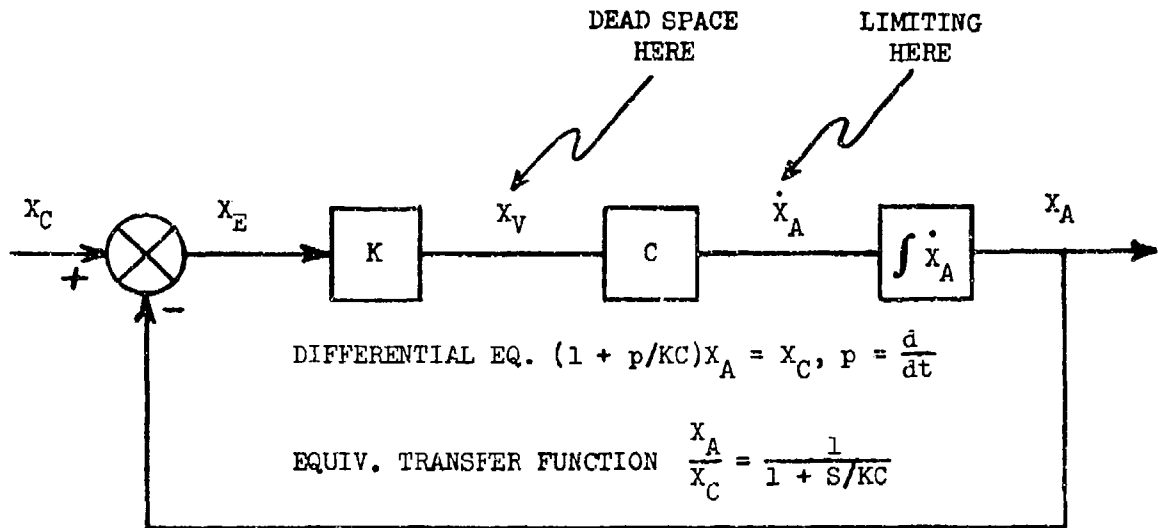
DESIRED TRANSFER FUNCTION $= \dfrac{1}{1+.016S}$

NO LOAD RATE LIMIT $\dot{X}_{A_{MAX}} = 6.67$ IN/SEC ($\dot{\delta} = 100$ DEG/SEC)

VALVE MOTION FOR FULL FLOW $X_{V_{MAX}} = .375$ IN.

VALVE GAIN $C = \dot{X}_{A_{MAX}}/X_{V_{MAX}} = 17.79$/SEC.

FORWARD LOOP GAIN $K = 1/.016C = 3.514$

FIGURE 73 ACTUATOR MODEL FOR DEAD SPACE STUDIES

132
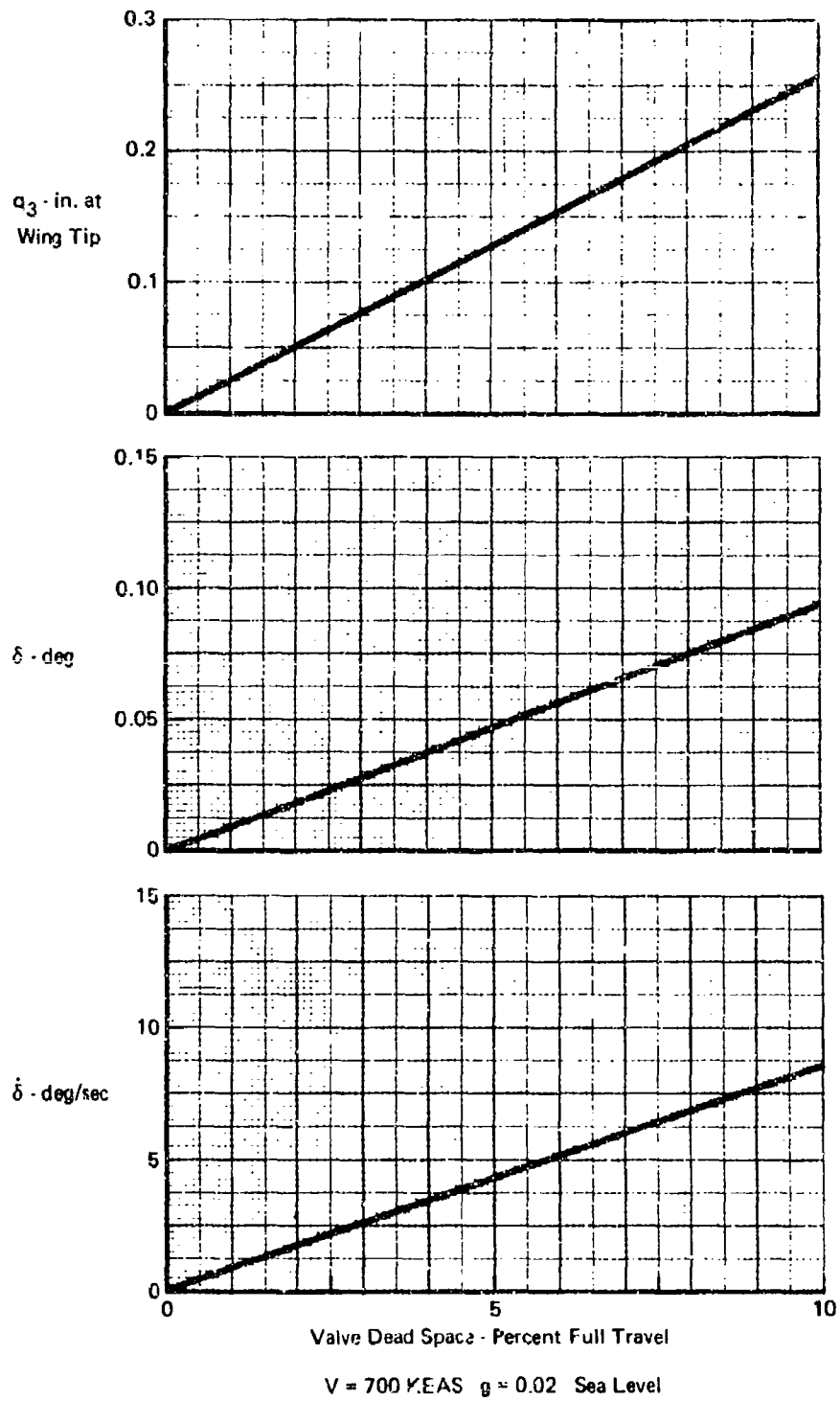
FIGURE 74 LIMIT CYCLE MOTION OF 370 GALLON TANK 90% FULL CONFIGURATION
WITH AILERON ACTUATOR DEAD SPACE

133
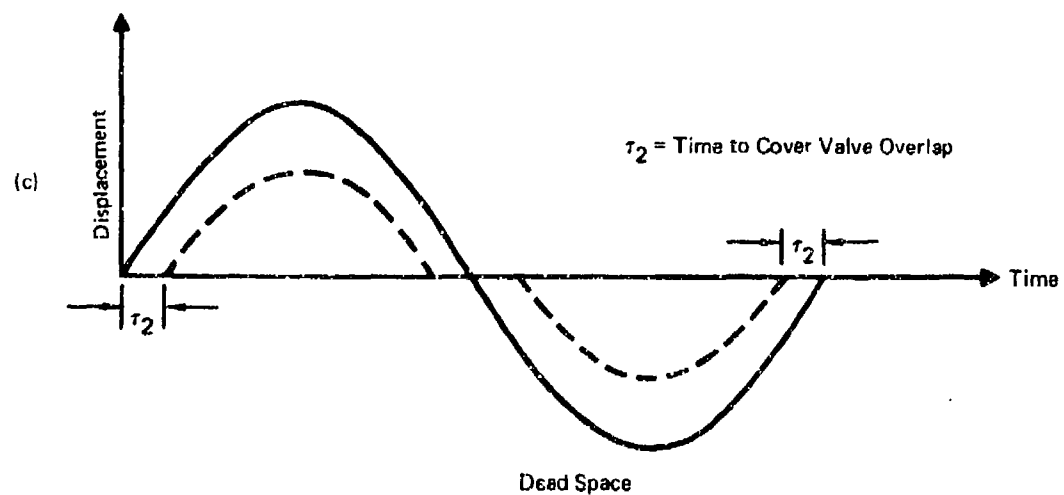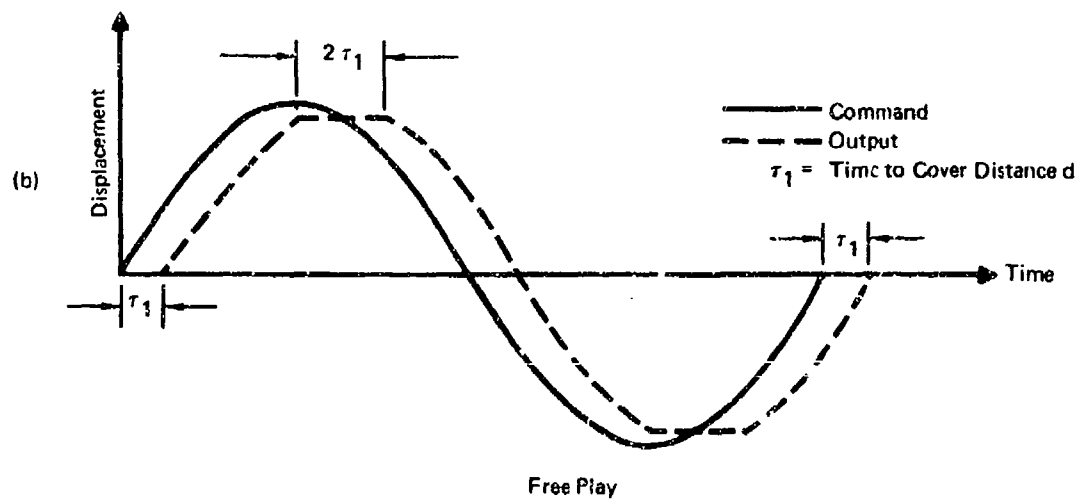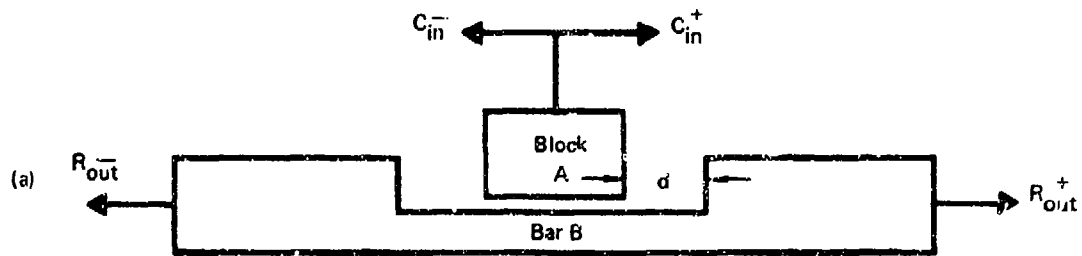
FIGURE 75   ILLUSTRATION OF FREE PLAY AND DEAD SPACE EFFECTS
ON ONE CYCLE OF AILERON MOTION

translation. It is seen that the net effect of free play is a constant time lag, τ_1, of the output amounting to the time it takes before an actuation command results in an output in either direction. The maximum displacement is also reduced somewhat as shown in the figure. Sketch (c) is a time history drawing of the dead space phenomena showing how its effect is different from free play.

A test case for the 90% full 370 gallon tank configuration with what amounted to a 3 degree lag free play effect was run on the time domain program. Stability was maintained with no significant performance degradation. The free play of the F-4 aileron has been undetectable in ground vibration tests and is much less than the military specification requirement of 1/30 of a degree.

4.1.3 Comparison of Passive-Active Control Schemes - No single flutter control scheme will stabilize flutter for several different wing/store configurations. If the store mass properties vary, the passive fix or active compensation will also vary. Active flutter suppression has been shown to offer the following advantages:

1. Ease of adjustment when stores are changed

2. Lower weight penalty

3. No redesign of the aircraft wing or store structure

Mass ballast fixes require that heavy weights be switched when the store carriage is altered. This involves either switching heavy wing masses on the order of 1000 pounds per aircraft or redesigning stores with new, and increased, mass characteristics. An active flutter control system, on the other hand, involves making two adjustments (when notch filter and high frequency lag are fixed); feedback gain, and lag phase angle. Such a system would add about 200 lb to the aircraft weight. This weight estimate is developed in Section 5.5.

The active flutter suppression scheme which utilizes a generalized electroni compensation network is the most easily adaptable to store carriage changes. The scheme will work with adequate stability margins for the full velocity range of the F-4 at sea level. If the compensation is fixed during flight, the flutter control system performance will be limited to altitudes below about 10,000 feet.

4.2 Advanced Aircraft Horizontal Tail Flutter Control

The main purposes of these horizontal tail flutter control studies were to investigate both the potential payoff of active flutter control in future aircraft and to determine if active control is possible when the control force producer motion is an integral part of the flutter mechanism. The vehicle for this effort is the advanced aircraft of Figure 6. The description of the horizontal tail mass, inertia, stiffness, and vibration properties is given in Appendix II.

4.2.1 Passive Flutter Studies - Since it was desired to evaluate active flutter control using the pitch actuator, a search was made to establish a candidate horizontal tail configuration with a well defined pitch-bending flutter mechanism. Studies were simultaneously performed to determine the optimum passive flutter solution.

4.2.1.1 Optimum Passive Flutter Solution - Studies were performed to determine the minimum weight passive flutter fixes resulting from:

1) Stiffness changes

2) Balance weight additions

3) Combined stiffness changes and balance weight additions

4) Pitch restraint variations for each case.

The COPS (Computerized Optimization Procedure for Stabilators) program, described in Reference 4, was our first attempt at automation of the steps in stabilator design. This program development considers all significant design constraints, including the aeroelastic constraint of flutter, at each step of the design process. One of the approximations built into the program is a torsional stiffness increase proportional to the fourth power of the local chord (C^4). This stiffness distribution, which has been partially verified through usage on similar stabilators, is, however, not a universally applicable optimum distribution.

A minimum modification was made to the COPS program to allow individual stiffness changes at each station along the elastic axis. The modified program was then run, in the batch processing mode, to obtain several values of the change in flutter dynamic pressure (ΔQ) for associated stiffness levels (GJ) and weight increments (ΔW) at each elastic axis station. It was determined from these runs that the highest efficiency ($\Delta Q/\Delta W$) results from initial stiffness increases in Section 7 of Figure 8. The next most efficient section is the tip section. Sections inboard of 7 are progressively less efficient.

136

A CJ stiffness distribution, based on these COPS sensitivity studies, is shown in Figure 76. A weight increase of 20.7 lbs is required for the indicated Stiffness Sensitivity Design level to achieve a speed of 575 knots. The basic COPS program, using the C^4 distribution, predicts a weight increase of 29 lbs for the same improvement in flutter velocity. The Stiffness Sensitivity Design is lighter by 8 lbs primarily because the inboard stations are not stiffened unnecessarily. The GJ levels are obtained by adding layers of boron/epoxy composite material with fibers oriented at ± 45 degrees with respect to the elastic axis. The bending stiffness (EI), resulting from GJ increases, is shown in Figure 77.

Parametric flutter studies, based on the stiffness and weight data generated by COPS, were performed using an Indicial Lift computer program. The classical aerodynamic derivatives were modified for C_{L_α} = 3.48/radian and center of pressure at 25% chord.

The results for separate variations of stiffness levels and balance weight additions using an Indicial Lift program are shown in Figure 78. These data are similar to previous results from the COPS program shown in Reference 4. The results indicate that the balance weight solution branch gives the minimum weight passive flutter solution ($\approx$ 30 lbs). The target flutter velocity is 760 KEAS. The basic COPS program had previously been applied to a stabilator with the same geometrical characteristics. Those runs determined that the balance weight located in the leading edge of the outboard section 8, as used in these more sophisticated studies, leads to the minimum weight passive flutter solution.

The effect of combined stiffness and balance weight as a function of the pitch rotational restraint is shown in Figure 79. The most important effect shown in this figure is the rapid increase in flutter velocity with pitch restraint for the Candidate Design. For the nominal pitch frequency of 20 Hz the flutter velocity for this case is 587 KEAS at a frequency of 12.5 Hz.

4.2.1.2 Candidate Design for Active Flutter Control – The Candidate Design was chosen for further study of active control because the pitch restraint dramatically affects flutter and because of the relatively low flutter frequency. A significant characteristic of this configuration is that for a pitch frequency of 20 Hz there is only one flutter mode, and for a pitch frequency of 30 Hz the surface is completely flutter-free.
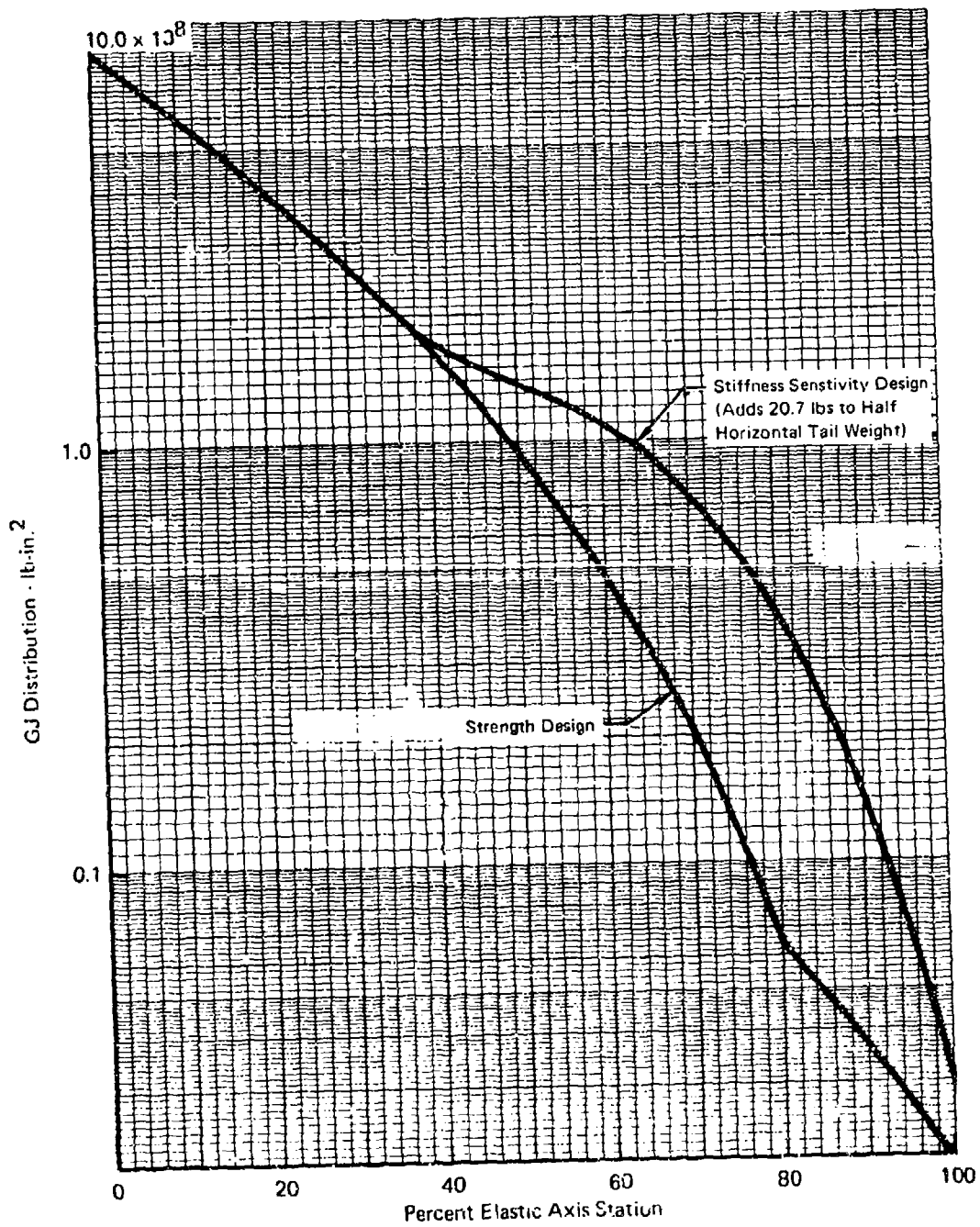
Note: Candidate Design is Strength Design with 20 lb Non-Structural Weight at Leading
Edge of Section 8.

FIGURE 76   ADVANCED AIRCRAFT HORIZONTAL TAIL - TORSIONAL
STIFFNESS DISTRIBUTION
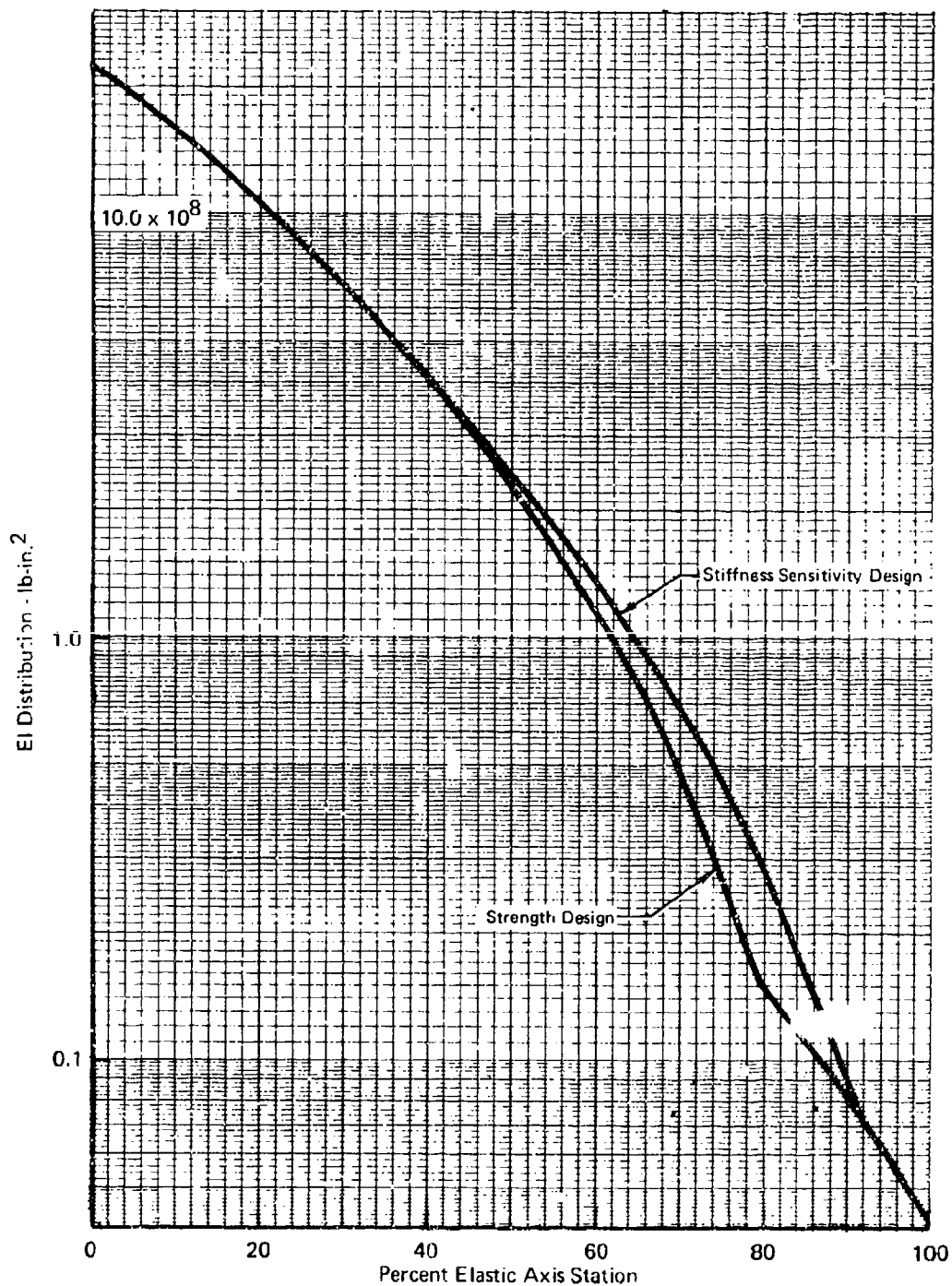
FIGURE 77 ADVANCED AIRCRAFT HORIZONTAL TAIL - BENDING
STIFFNESS DISTRIBUTION

Note: Candidate Design is Strength Design with 20 lb Non-Structural Weight at Leading
Edge of Section 8.
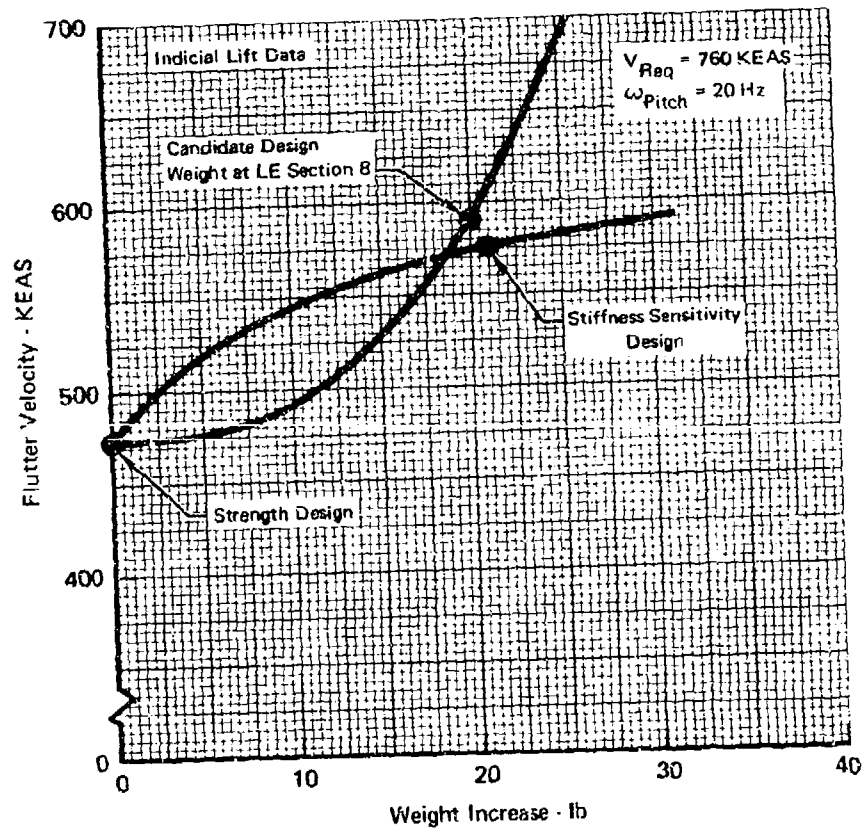
FIGURE 78   ADVANCED AIRCRAFT HORIZONTAL TAIL · COMPARISON
OF STIFFNESS AND BALANCE WEIGHT PASSIVE FLUTTER SOLUTIONS
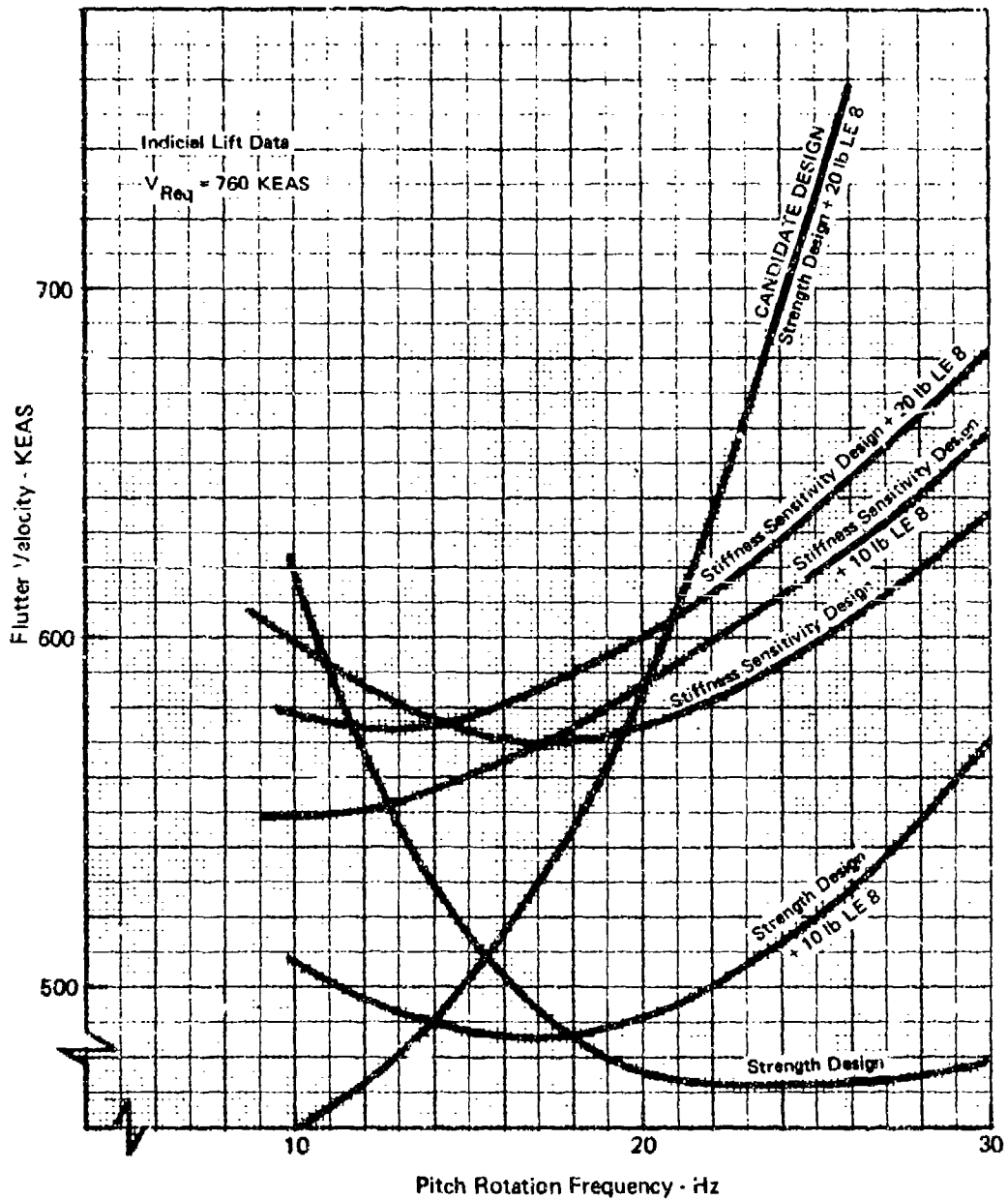
FIGURE 79   ADVANCED AIRCRAFT HORIZONTAL TAIL - FLUTTER VELOCITIES OF TRIAL SOLUTIONS AS A FUNCTION OF PITCH ROTATIONAL RESTRAINT

141

The slope of the flutter mode crossings on the V-g plots are compared in Figure 80 for each of the tail configurations with the pitch frequency of 20 Hz. Slopes for the advanced wing (covered later) and wing/store study configurations are also shown in the figure for comparison. The slope for the Candidate Design lies between those for the advanced wing and the 370 gallon tank - 90% full wing/store cases. The implication here is that a greater improvement in flutter is possible for the Candidate Design than for the other tail configurations.

The Candidate Design was chosen as the most promising candidate for active flutter control based on the following reasons:

1) flutter is a function of pitch restraint

2) frequency of flutter is relatively low

3) V-g crossing is relatively shallow

4) there is only one basic flutter mechanism.

4.2.2 Active Flutter Studies

4.2.2.1 Frequency Domain Studies - Active flutter control studies were conducted for the Candidate Design and also for most of the other designs which were tested in the search for the Candidate Design. The studies used the same data that was used in the Indicial Lift passive flutter analyses, described in Section 4.2.1.

The results of these active control test runs are summarized in Table 5. The most significant aspect of these results is that the Candidate Design is controllable with exceptionally large stability margins for the nominal pitch frequency of 20 Hz whether the bandwidth of the hydraulic actuator is extended flat to the flutter frequency or not. When the pitch frequency is reduced to 10 Hz, however, the compliance of the system causes only about 30% of the commanded stabilator deflection to be achieved, and flutter control is not possible. The case with 10 lbs ballast at the leading edge of Section 8 is controllable to about 650 KEAS with phase margins of +45 degrees or greater. The Strength Design and the Stiffness Sensitivity Design both show little promise of control. They are good examples of very small rapidly disappearing Nyquist loops which are characteristic of explosive flutter mechanisms.

The common control loop for each of these test runs included 6 degrees of freedom; the four lowest normal elastic modes, the stabilator rotation mode, and the pitch actuator deflection. A high pass filter which has unity gain

142
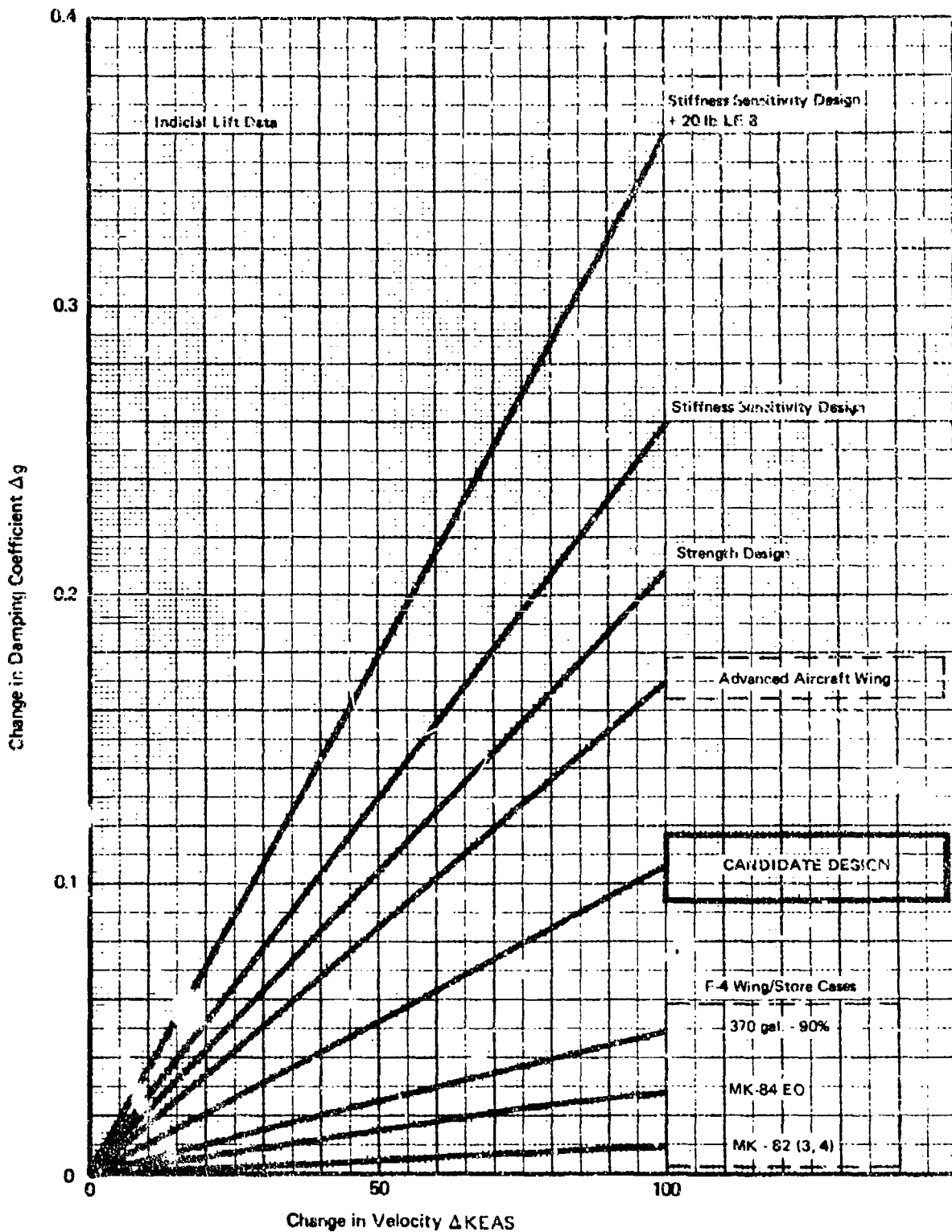
FIGURE 80 SLOPE OF FLUTTER MODE CROSSINGS FOR ALL STUDY CONFIGURATIONS

TABLE 5 ADVANCED AIRCRAFT HORIZONTAL TAIL DESIGNS TESTED FOR ACTIVE CONTROL

HORIZONTAL TAIL DESIGN	PITCH FREQUENCY Hz	ACTUATOR RESPONSE BREAK FREQUENCY Hz	REMARKS
CANDIDATE	20	15	CONTROLLABLE THROUGH 800 KEAS WITH LARGE STABILITY MARGINS
CANDIDATE	20	10	CONTROLLABLE THROUGH 800 KEAS WITH LARGE STABILITY MARGINS
CANDIDATE	20	5	CONTROLLABLE THROUGH 800 KEAS WITH LARGE STABILITY MARGINS
CANDIDATE	10	15	EXCESSIVE COMPLIANCE RULES OUT CONTROL
STRENGTH+10 LBS LE8	20	15	CONTROLLABLE THROUGH 650 KEAS WITH ACCEPTABLE STABILITY MARGINS
STRENGTH	20	15	NO PROMISE OF CONTROL
STIFFNESS SENSITIVITY	20	15	NO PROMISE OF CONTROL

144

above 10 Hz (.0159S/1 + .0159S) and a first order lag expression for the power actuator of the form (1/1 + TS) were the only control system components. The open-loop gain was set at 5.0 to guarantee good visibility with the computer generated Nyquist plots.

Consideration was given to both the location and type of sensor. The most feasible feedback signal was determined to be either the horizontal tail pitch angle or the pitch angle rate. Pitch angle feedback was chosen for the test runs of Table 5. It was obtained by double integration of the output of an angular accelerometer located at the hinge line near the horizontal tail root chord.

Nyquist plots are shown in Figure 81 for the Candidate Design for power actuator frequency response bandwidths of 15 Hz, 10 Hz, and 5 Hz. There is no significant difference between these cases except a somewhat reduced effective mechanical gain for the smaller bandwidth case and a small phase difference, among the cases, for balanced flutter control phase margins. About 45 degrees of phase lead is required to center the loop on the negative real axis for the 15 Hz bandwidth case. It takes about 75 degrees lead for the 10 Hz case and about 90 degrees for the 5 Hz case. This would seem to favor the 15 Hz case since the large phase lead angles are difficult to obtain. If we change the sign of the feedback, however, the 5 Hz case will require 90 degrees phase lag while the 15 Hz will require 135 degrees lag. From this viewpoint the 5 Hz case is preferable. The control system gain can be as large as desired for each of these cases since there is no potential control system instability to avoid. The open-loop gain, instead, will only be constrained by the rate requirements for the hydraulic actuator in a turbulent environment.

Additional studies involving compensation and pitch rate feedback were made for the Candidate Design with the actuator break frequency at 5 Hz and the pitch frequency at 20 Hz. A Nyquist plot for this case, after compensation, is shown in Figure 82. The indicated control system gain gives 6 dB margins against flutter for g = 0.0 at 750 KEAS and g = 0.02 at 800 KEAS. The phase margins are large for this configuration. Pitch rate was chosen as the feedback signal for the run of Figure 82 since the test run for this case had indicated the need for 90 degrees phase lead with pitch angle feedback. This case easily satisfies design goals for active
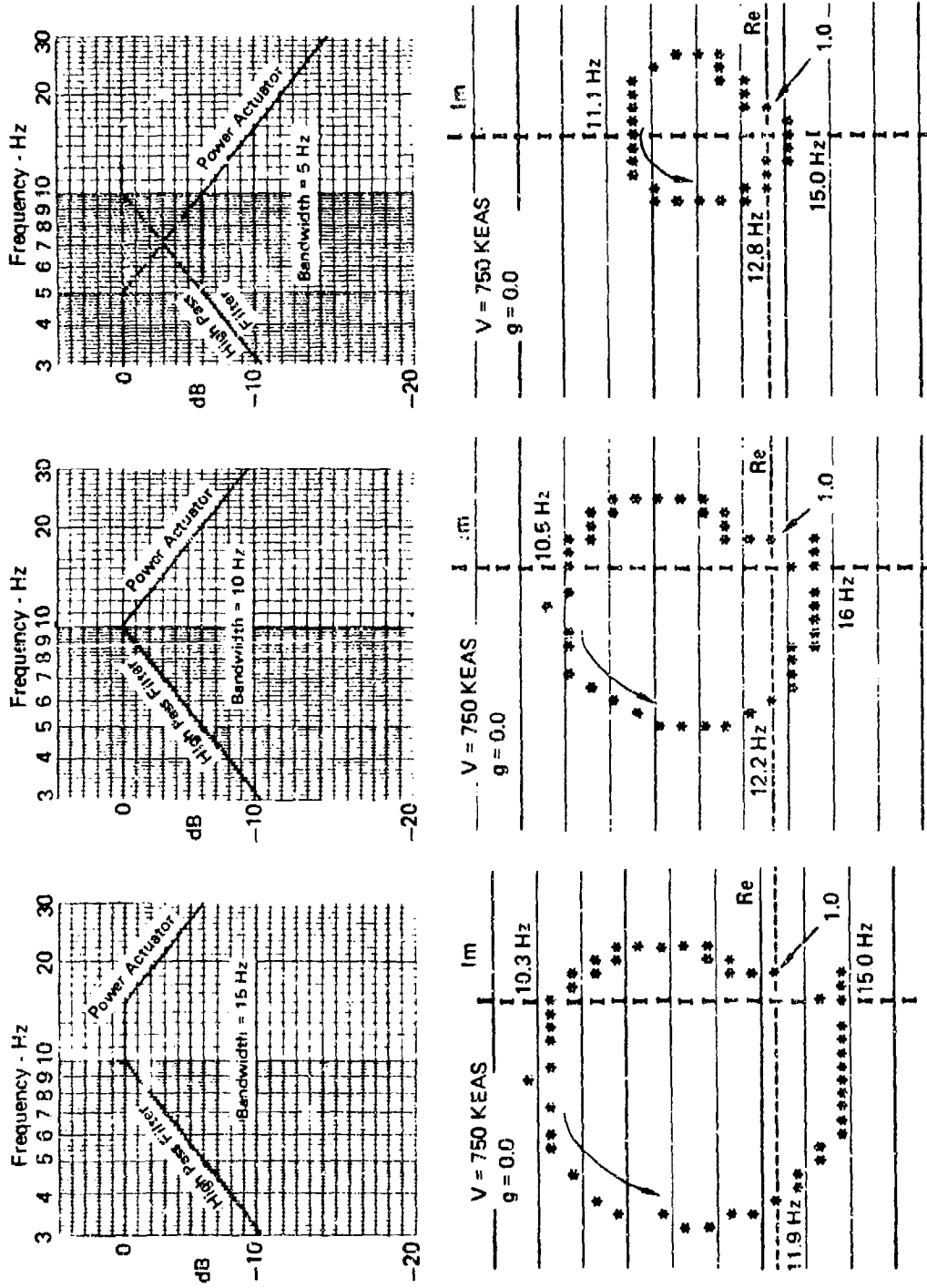
FIGURE 81 NYQUIST PLOTS ILLUSTRATING EFFECT OF VARIABLE
ACTUATOR BANDWIDTH - ADVANCED AIRCRAFT CANDIDATE
HORIZONTAL TAIL

146
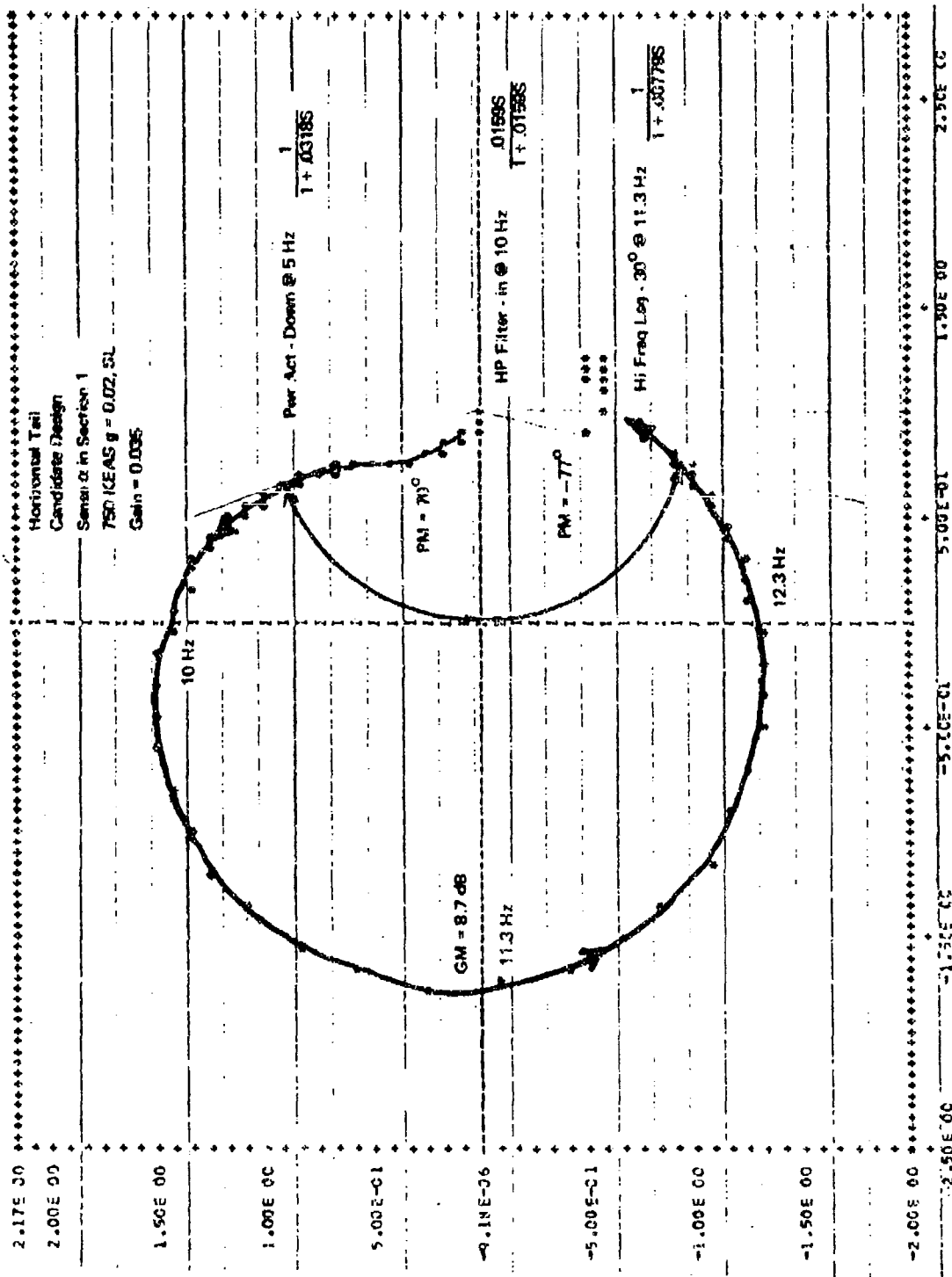
FIGURE 82 NYQUIST PLOT FOR ADVANCED AIRCRAFT HORIZONTAL TAIL
CANDIDATE DESIGN WITH COMPENSATION

147

flutter control. systems of ±6 dB gain margin and ±60 degrees phase margin. This case was thus chosen for further evaluation in the time domain.

4.2.2.2 Time Domain Studies - Runs were made using the time domain program, described in Section 3.5.2 and Appendix IV, for both velocities of 750 and 800 KEAS with $g = 0.02$ structural damping in each of the aeroelastic modes. The response of the system at 750 KEAS to a 5000 lbs $(1 - \cos \omega t)$ discrete gust at the flutter frequency of 11.3 Hz is shown in Figure 83. This gust force level is equivalent to the energy content in the bandwidth of the flutter mode for a typical random gust with 13 ft/sec rms. The motion is suppressed to near zero in about 0.5 seconds. The maximum unlimited actuator rates shown for this control are 60 deg/sec at 750 KEAS and 80 deg/sec at 800 KEAS. These rates are reasonable requirements for the short periods of demand for control surfaces of this size. As indicated in the nonlinear studies which were performed for the F-4 wing/store flutter control cases it is realistically expected that continuous control in this type of turbulent environment would be possible with rate limits as small as 30 to 40 deg/sec.

4.2.3 Comparison of Solutions

4.2.3.1 Weight for Optimum Passive Flutter Control - The minimum weight passive flutter solution uses a non-structural balance weight at the leading edge of the outermost section as shown in Figure 78. A balance weight of about 30 lbs per side added to the Strength Design will satisfy the required flutter velocity of 760 KEAS if the pitch rotation frequency is the nominal value of 20 Hz. The passive solution would only require 20 lbs per side, as shown in Figure 79, if the pitch frequency were to be as high as 26 Hz. The F-4 slotted leading edge stabilator rotation frequency is about 23 Hz. A survey of several other practical horizontal tail designs indicates a likely value for pitch frequency somewhere between 20 and 25 Hz. Thus, 40 to 60 lbs per aircraft should be sufficient to satisfy the flutter requirements for this particular horizontal tail, starting with a baseline Strength Design.

If structural stiffness increases were to be chosen as an alternative passive flutter solution the expected weight addition would be significantly greater. Even with the most advantageous use of composite material, as attempted in these studies for the Stiffness Sensitivity Design the total weight addition per aircraft would be in the neighborhood of 100 lbs or more.

148

FIGURE 83 DYNAMIC RESPONSE TO (1 - COS) GUST AT THE FLUTTER FREQUENCY - COMPENSATED ADVANCED AIRCRAFT HORIZONTAL TAIL

149

4.2.3.2 __Weight for Active Flutter Control__ - An evaluation of the weight
required for active flutter control of this horizontal tail should, in all
fairness, consider only those components which would not otherwise be
present in the aircraft. For example, the advanced aircraft being considered
in these feasibility studies, can be confidently expected to have full-time,
highly-redundant, fly-by-wire flight control systems which would be available
for cooperative use by active flutter control systems.

If we assume a triply-redundant horizontal tail flutter control system,
the additional weight items listed below would be required.

	Weight/Aircraft
Sensors 6 x 2 lbs each	12
Computers and Voters 6 x 3	18
Cockpit Displays 1 x 5	5
Wiring and Installation 1 x 10	10
	= 45 lbs

This weight is an estimate of the bare minimum weight which would be required
for active control of a controllable surface such as the Candidate Design.

It was determined in these studies, however, that a 20 lb balance
weight per side was required to arrive at the Candidate Design from the
Strength Design. Compared with this 85 lbs total penalty for active control,
it was found that only 60 lbs per aircraft was required for the optimum
passive flutter solution using balance weights. The active solution weight
of 85 lbs is very competitive, however, when compared to the passive
stiffness solution which required more than 100 lbs per aircraft.

4.3 __Advanced Aircraft Wing Flutter Control__

The main purpose of these advanced aircraft wing studies is to demon-
strate the feasibility of active suppression of bare wing flutter. Both
leading and trailing edge control surfaces acting singly or in combination
are available for active flutter suppression. Parameters such as sensor
location and type, control surface size, and control surface location are
varied to obtain the maximum stability margins.

4.3.1 Passive Flutter Studies

4.3.1.1 Baseline Design - The description of wing mass, inertia, and stiffness properties is given in Appendix III. The wing has weight additions for 15% chord leading edge flaps and 35% chord ailerons running along the entire wing span. These weight additions in each section result from control surface hydraulic lines, actuators, and local structural beef-up. Both leading and trailing edge control surfaces in any combination of wing sections are available for active flutter suppression. Two-dimensional strip theory aerodynamics with experimental aerodynamic coefficients on the eight section wing were used to model aerodynamic characteristics. The aerodynamic coefficients, $C_{L_\alpha} = 3.98$/radian and $C_{L_\beta} = 2.81$/radian, were obtained from subsonic data. The center of pressure was set at the quarter chord. Classical V-g and V-ω plots generated by an Indicial Lift computer program are shown in Figure 84. Flutter occurs in two critical modes. Mode 3 is the unstable mode in the primary flutter mechanism occurring at 540 knots, mode 4 is the unstable mode in the secondary flutter mechanism at 740 knots. An aileron with a rotation mode frequency of 60 Hz was located in Section 7 with its hingeline at the 65% chord. The aileron rotation mode does not participate in either of the two basic flutter mechanisms.

The baseline design exhibited the following characteristics:

1. Flutter of the bare wing is significantly more explosive than the F-4 wing/store configurations.

2. To achieve active stability beyond 7-0 knots two unstable modes must be simultaneously controlled.

On the average the g/V at flutter onset for the bare wing configurations was about three times that for the 90% full-370 gallon tank configuration, the minimum stability margin wing/store case. Figure 80 shows the g/V values for the wing/store, horizontal tail, and bare wing configurations. In order to control two flutter modes simultaneously, separate control surfaces must be actuated, each with its distinct feedback compensation. Multiple mode suppression, thus, doubles the number of components - hydraulic and electronic required by an active flutter control system. For these feasibility studies it was judged inadvisable to attempt multiple mode control before the practicality of single mode control was thoroughly established. The onset velocity for the second flutter mode then becomes the upper velocity

Velocity vs Damping

Advanced Aircraft Wing
EA @ 42% c C_{L_α} = 3.98/rad CP @ 25% c

C_{L_β} = 2.81/rad Aileron in Section 7

6 Elastic Modes, 1 Aileron Mode (ω_β = 60 Hz)
g = 0.0

V_F = 540 Knots V_F = 740 Knots V_F = 1080 Knots
13.7 Hz   18.7 Hz   32 Hz
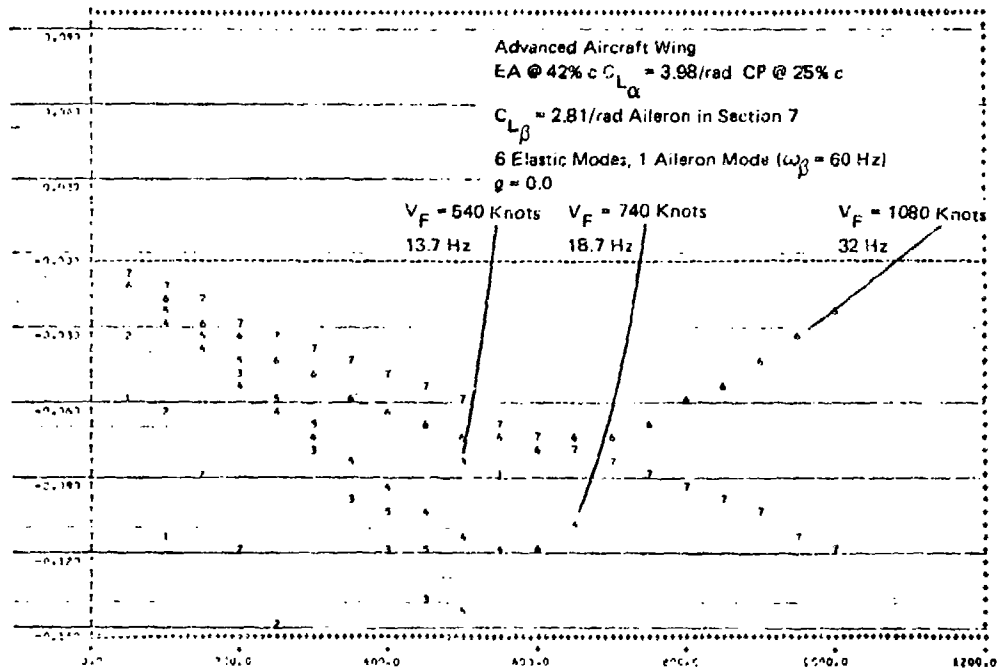
Velocity vs Frequency
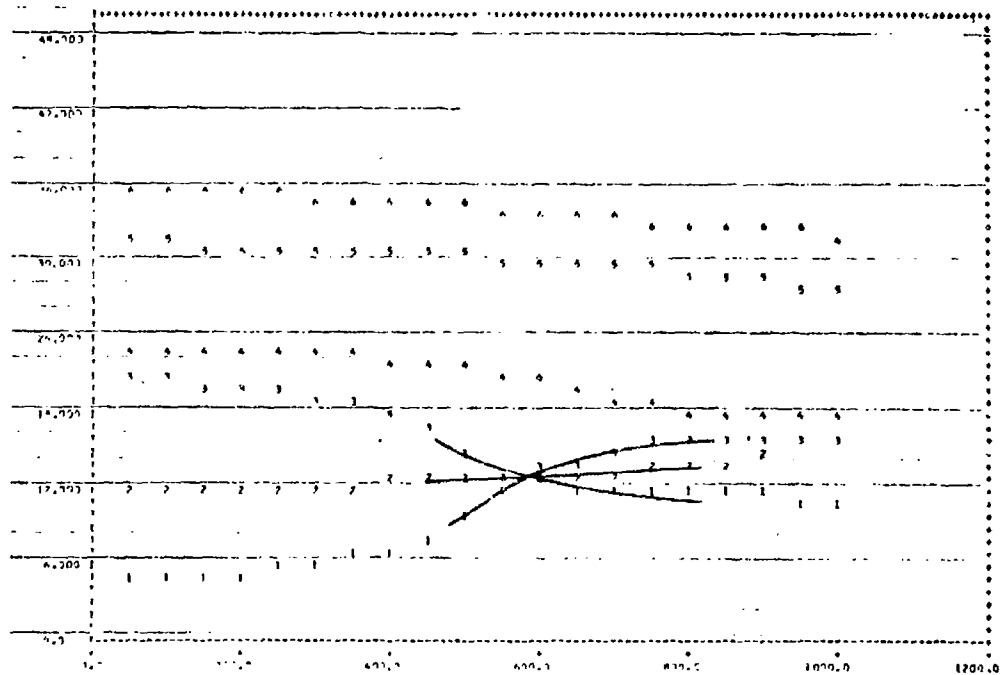
**FIGURE 84   ADVANCED AIRCRAFT WING - REFERENCE PASSIVE
FLUTTER DATA**

limit for active flutter control. The maximum velocity was found to be considerably lower because of limited stability margins.

4.3.1.2 Optimum Passive Flutter Solutions - Passive flutter studies were conducted to determine the balance weight additions and wing stiffness increases required to raise the flutter speed of the advanced aircraft wing. No combined balance weight -- stiffness increase cases were examined.

Table 6 summarizes the balance weight studies. The advanced aircraft wing can be stabilized through 740 knots (the maximum practical active control velocity) by the addition of about 200 pounds at the leading edge of Section 7 (Configuration 3). "Chord to the fourth" stiffness increases were used to determine a "stiffness fix". The stiffness increases needed to reach a flutter speed of 740 knots added about 67 lbs to the half-wing weight. This fix involved small increases in the EI and GJ values for the three most outboard wing sections.

4.3.2 Active Flutter Studies

4.3.2.1 Trailing Edge Control -- Initial frequency domain studies were run with an aileron (60 Hz frequency) in Section 7. The feedback signal was the angle of twist in Section 7. This system corresponds to either a doubly integrated perfect angular accelerometer or a structural feedback concept. These yielded the result that flutter could not be controlled beyond about 600 knots (onset at 540 knots) at sea level. This occurred because of a very rapid collapse of the unstable (CCW) loop on the Nyquist plot with airspeed. Beyond 600 knots the unstable loop vanishes, precluding flutter control through feedback compensation. Nyquist plots at several velocities are shown in Figures 85 through 87 for a feedback control loop consisting of only an uncompensated feedback gain.

The system can be stabilized at 500 and 550 knots by decreasing the feedback gain. The system is unstable at 600 knots and cannot be stabilized by changing either the gain or phase of the feedback signal because of the higher mode encirclement of the origin. Control of flutter is lost for this case between 550 and 600 knots. Notice the very restricted size of the unstable loop at 600 knots. Even if a notch filter or high frequency lag were used to eliminate high frequency modes and a 30 degree lead compensation were added, the maximum phase margins would be on the order of ± 5 degrees. Additional runs were made with pure feedback for perfect sensors

TABLE 6 SUMMARY OF ADVANCED AIRCRAFT WING BALANCE WEIGHT STUDIES

Configuration

		1 No Mass Added	2 100 lb at LE of 7	3 200 lb at LE of 7	4 200 lb at LE of 5	5 100 lb at TE of 5	6 200 lb at LE of 3
First Crossing	Velocity (KEAS)	540	608	737	474	454	516
	Frequency (Hz)	13.7	9.8	21.1	18.1	15.5	14.6
	Modes	2,3	1,2	4,5	3,4	3,2	2,3
	g/V (1/100 KEAS)	0.20	1.45	0.104	0.08	0.16	0.151
Second Crossing	Velocity (KEAS)	740	755	961	759	698	667
	Frequency (Hz)	18.7	19.1	17.6	12.5	18.3	18.0
	Modes	2,4	3,4	3,2	2,4	2,4	2,4
	g/V (1/100 KEAS)	0.19	0.23	0.08	0.61	0.08	0.07

154

FIGURE 85 NYQUIST PLOT FOR ADVANCED AIRCRAFT WING - REFERENCE CASE - V = 500 KEAS

155

Advanced Aircraft Wing
Sense α in Section 7
Feedback Gain Only
K = 5.0
Control Surface in Section 7
Hingeline @ 65% Chord
Reference Pass, Flutter Case
g = 0.0, SL
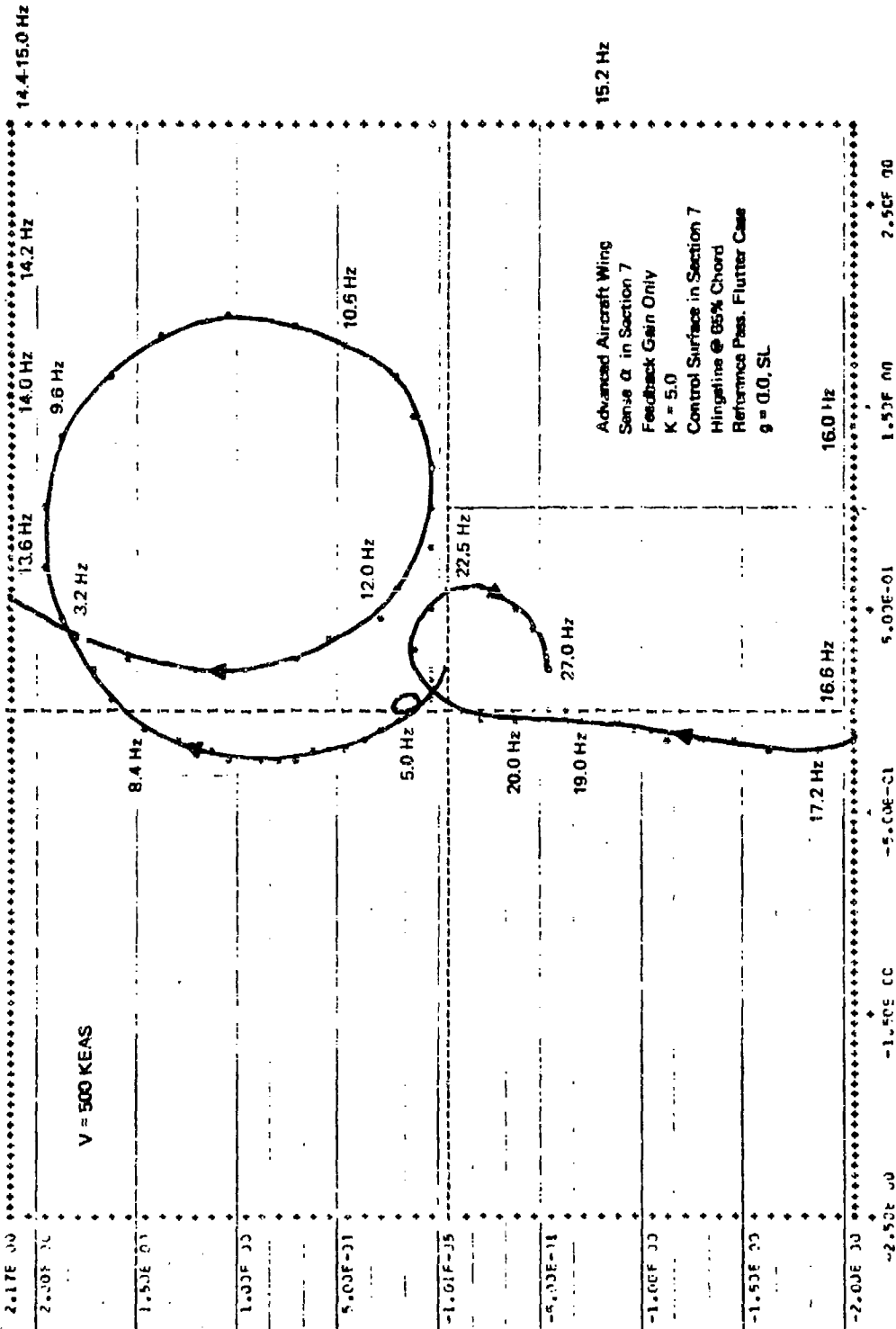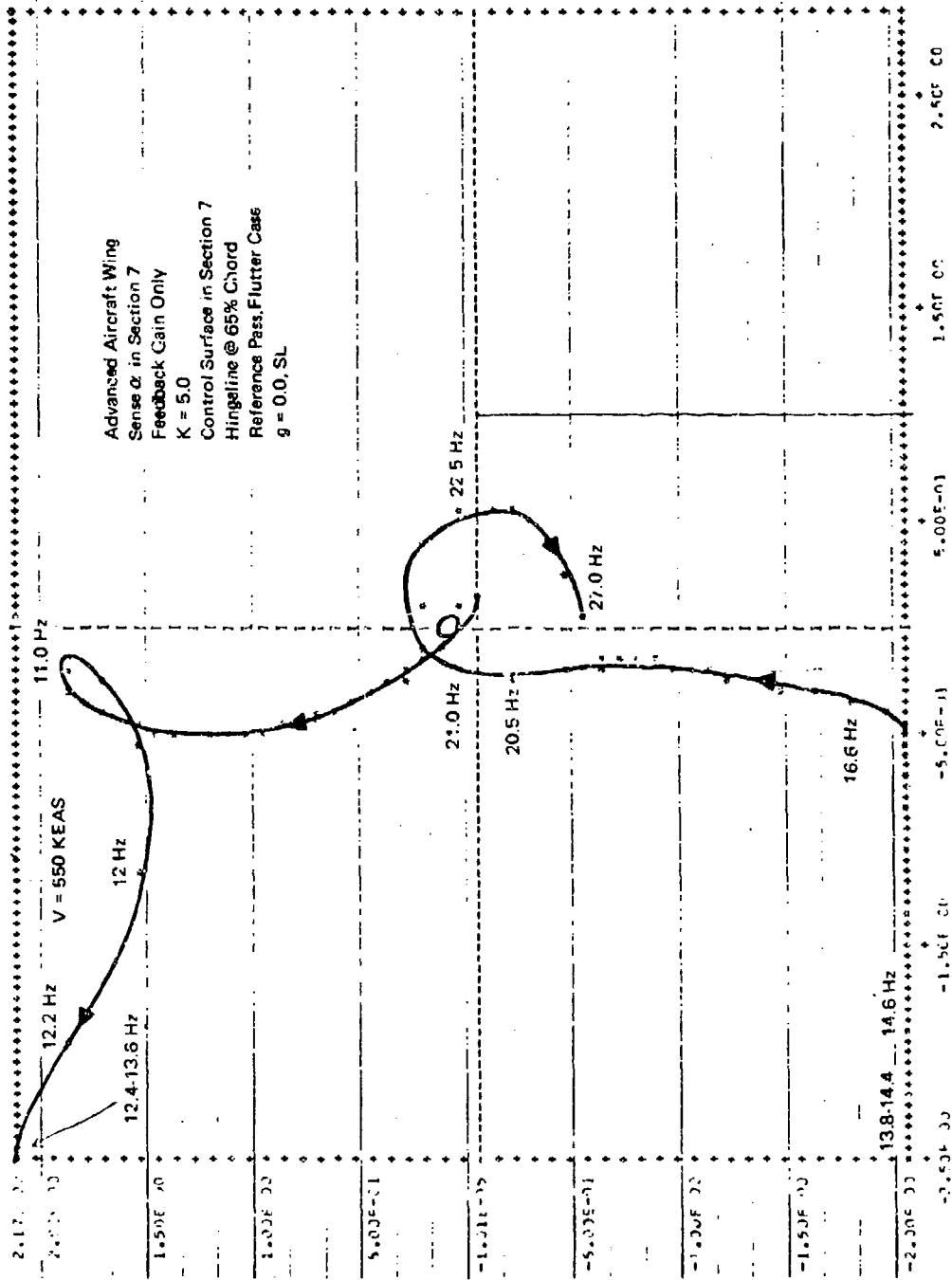
FIGURE 86 NYQUIST PLOT FOR ADVANCED AIRCRAFT WING - REFERENCE CASE - V = 550 KEAS
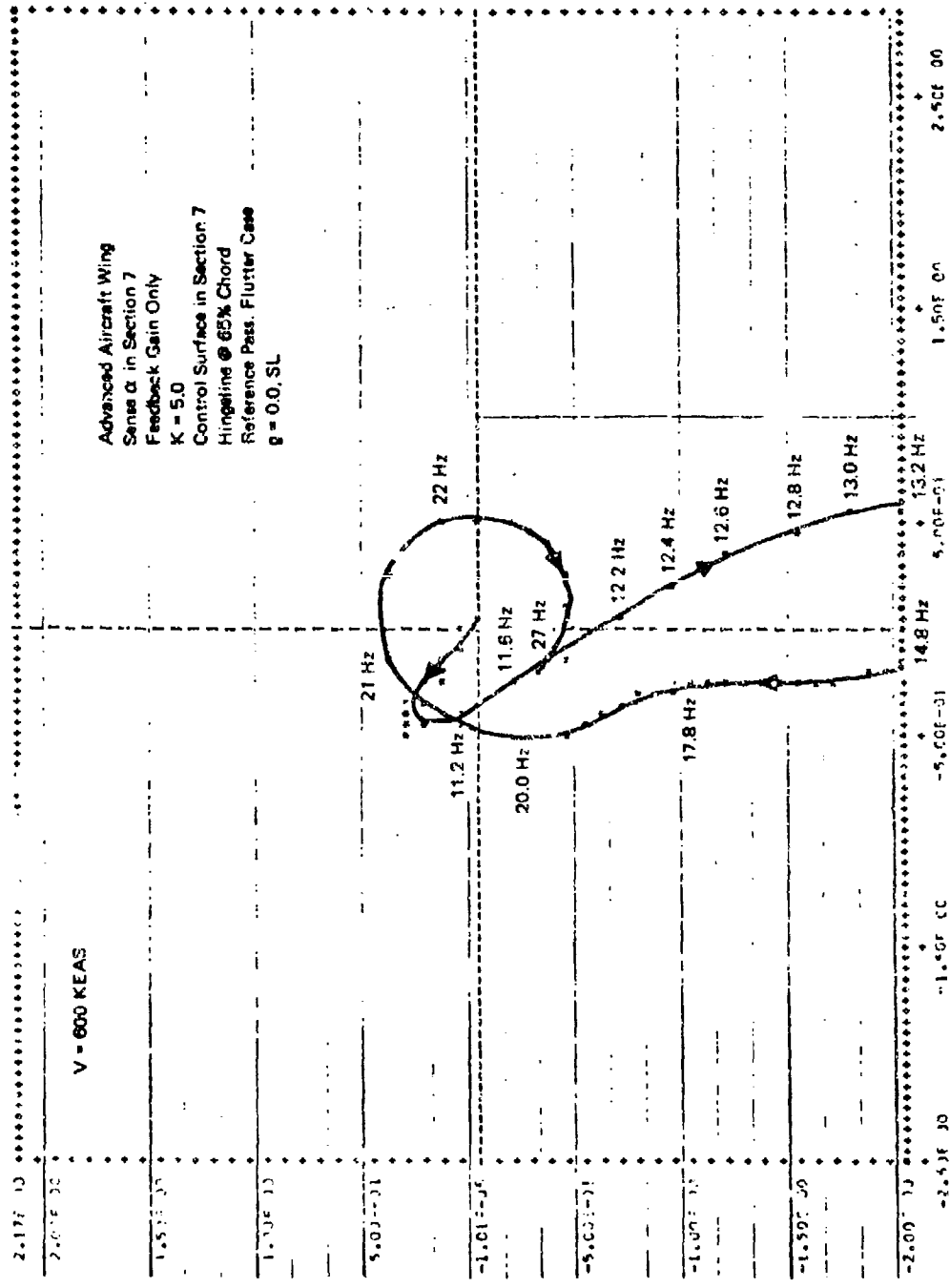
FIGURE 87 NYQUIST PLOT FOR ADVANCED AIRCRAFT WING - REFERENCE
CASE - V = 600 KEAS

157

located in Sections 4, 5, 6, and 8, and with an aileron in Section 7. The situation for each of these cases is similar to that for the Section 7 feedback sensor.

The incorporation of structural damping into the advanced aircraft wing analysis, as with the wing/store configurations, delayed flutter onset (about 10 knots) and improved stability margins. Figures 88 and 89 show Nyquist plots for the advanced aircraft wing using structural damping coefficients of $g = 0.00$ and $g = 0.02$ with identical control loops. The addition of 0.02 structural damping increases phase margins by about 50% at 560 knots (sea level). The addition of damping, however, does not improve the maximum velocity for which active flutter control is possible. The unstable loop of the Nyquist plot still disappears near 600 knots regardless of damping level.

The rapid disappearance of the unstable loop with increasing velocity might be explained by either or both of the reasons below:

1. The proximity of the two lowest flutter onset velocities (540 knots – 3rd mode and 740 knots – 4th mode).
2. The explosive nature of the flutter requires more energy dissipation capability to control the flutter than is possible with a 35% chord aileron in Section 7.

Flutter Mode Elimination Study

The first explanation was checked out by setting up a four mode study – first three elastic modes plus a 60 Hz, Section 7, aileron mode. This eliminates the second flutter mechanism resulting from the interaction of modes 3 and 4. A high pass filter and a power actuator of the forms:

High Pass Filter – $\dfrac{.0159S}{1 + .0159S}$, in at 10 Hz

Power Actuator – $\dfrac{1}{1 + .0106S}$, breaks down at 15 Hz

were also incorporated in the control loop for these limited mode studies. These elements were added to the control loop to emphasize the 13.7 Hz flutter frequency. Figures 90 through 93 show the Nyquist plots for this limited mode study with no structural damping and a gradually increasing flow velocity. Again the rapid collapse of the unstable mode is evident, even though the second flutter mechanism has been eliminated. Control capability is still lost near 600 knots.

Advanced Aircraft Wing
Sense α at Section 7, V = 500 KEAS

g = 0.0, SL

No Compensation

No High Pass Filter or Power Actuator

Gain = 5.0

Reference Pres. Flutter Case

Phase Angle Range
is 42° for Approximately
a 9dB Gain Margin

20.5Hz

12.0Hz

13.0Hz

13.4Hz
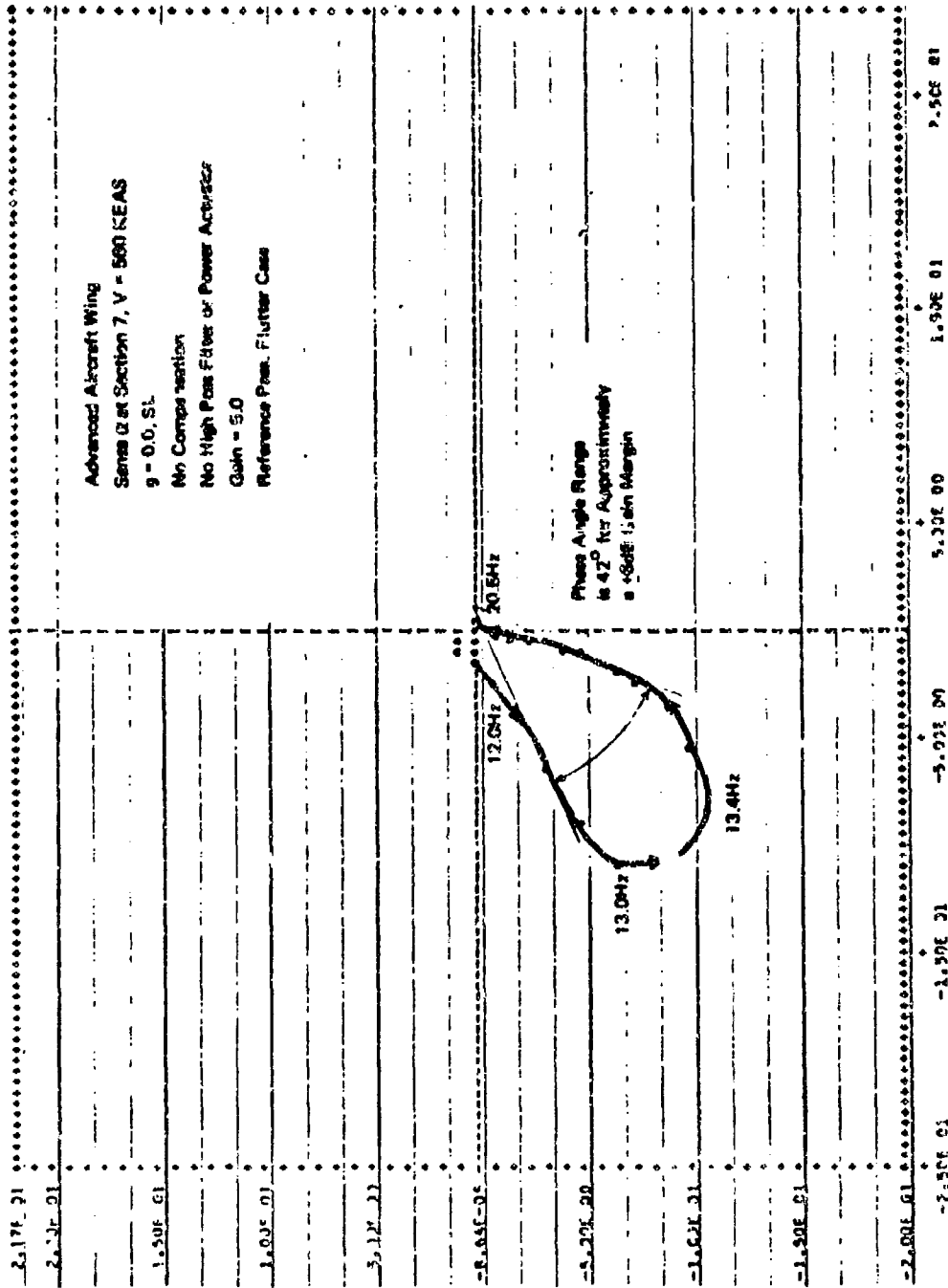
FIGURE 88 NYQUIST PLOT FOR ADVANCED AIRCRAFT WING - REFERENCE
CASE WITH NO STRUCTURAL DAMPING - V = 500 KEAS

159
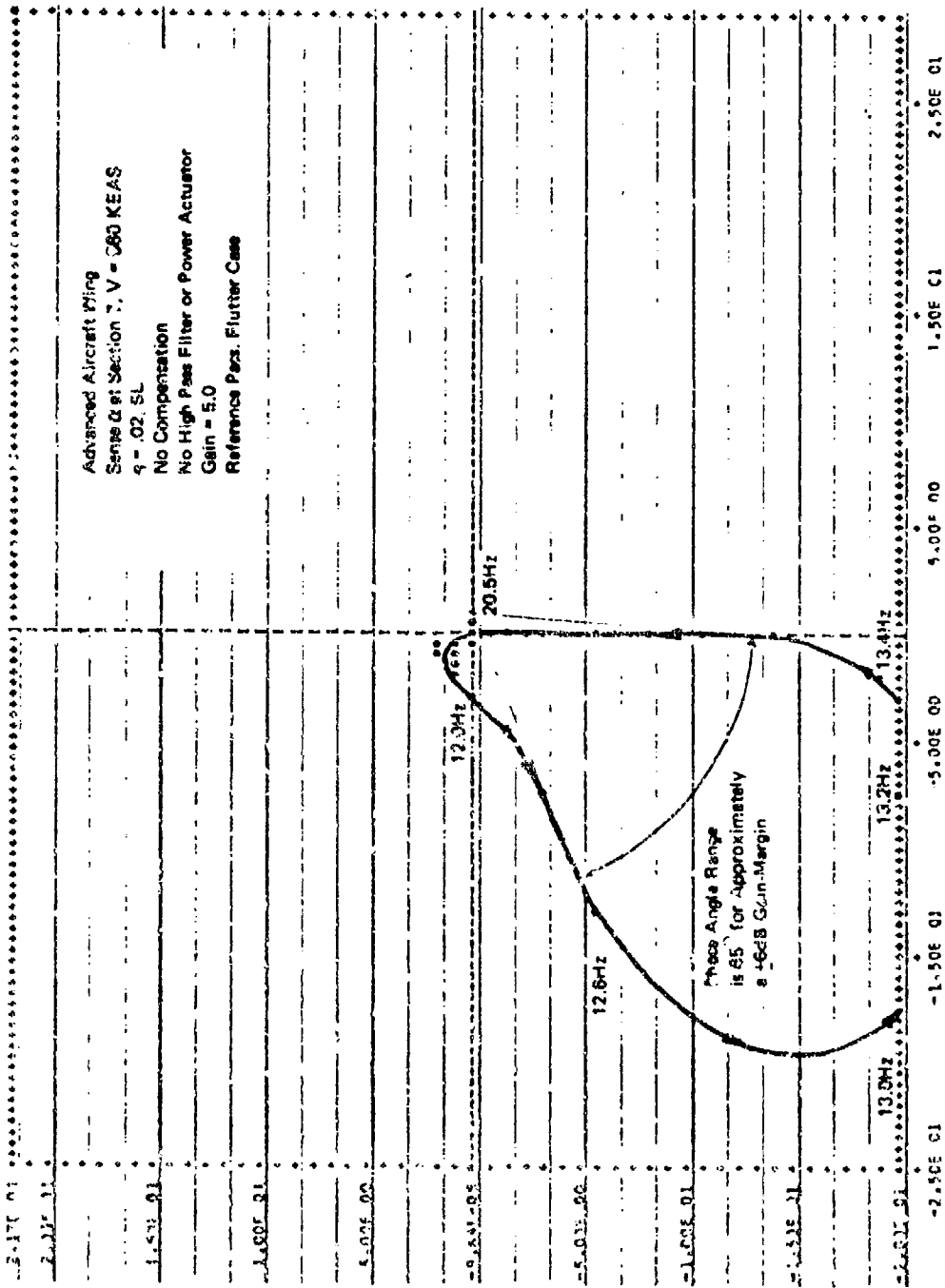
FIGURE 89 NYQUIST PLOT FOR ADVANCED AIRCRAFT WING - REFERENCE CASE WITH STRUCTURAL DAMPING - V = 560 KEAS
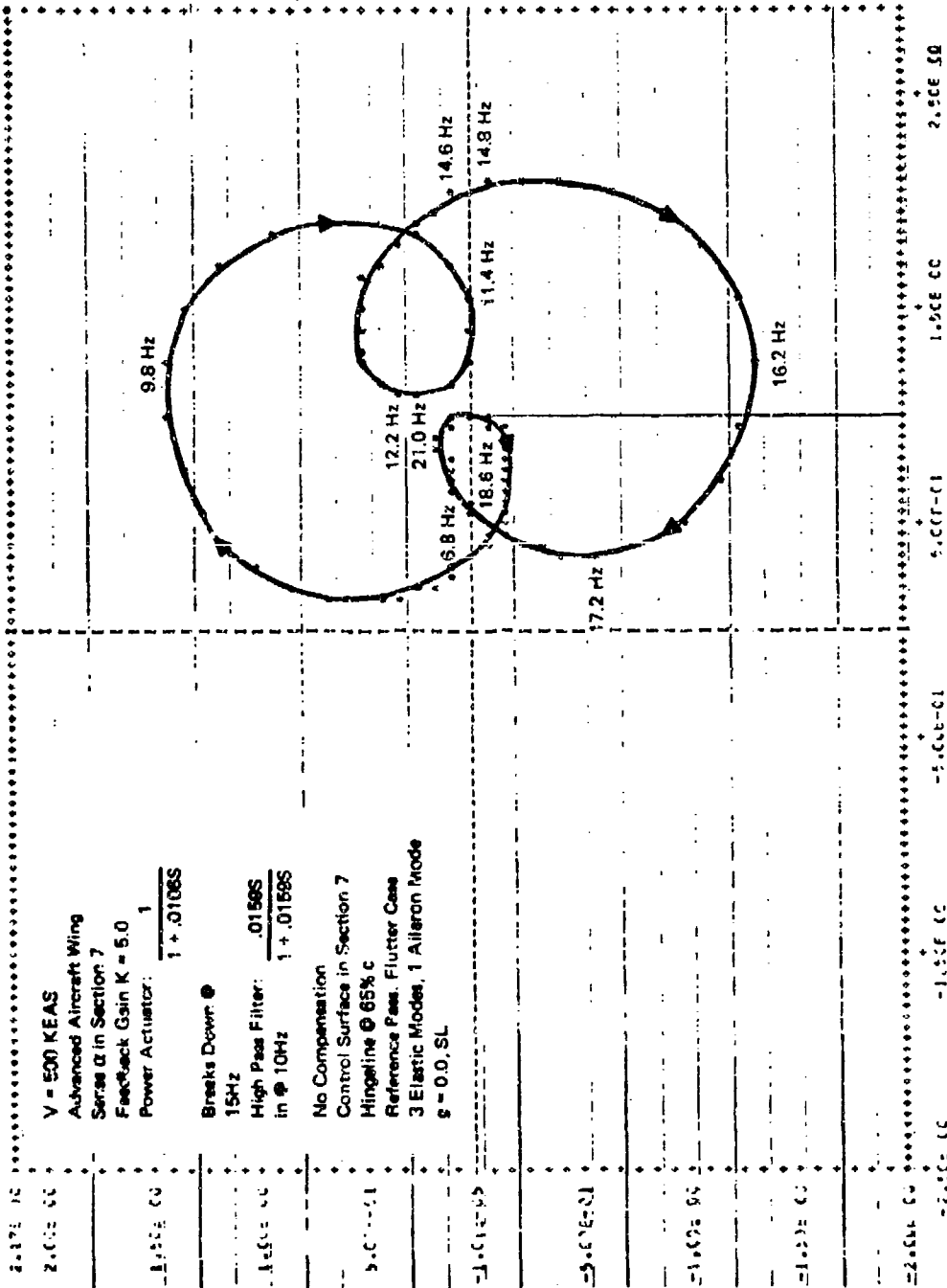
FIGURE 90 NYQUIST PLOT FOR ADVANCED AIRCRAFT WING -
THREE MODE TEST CASE - V = 500 KEAS

161
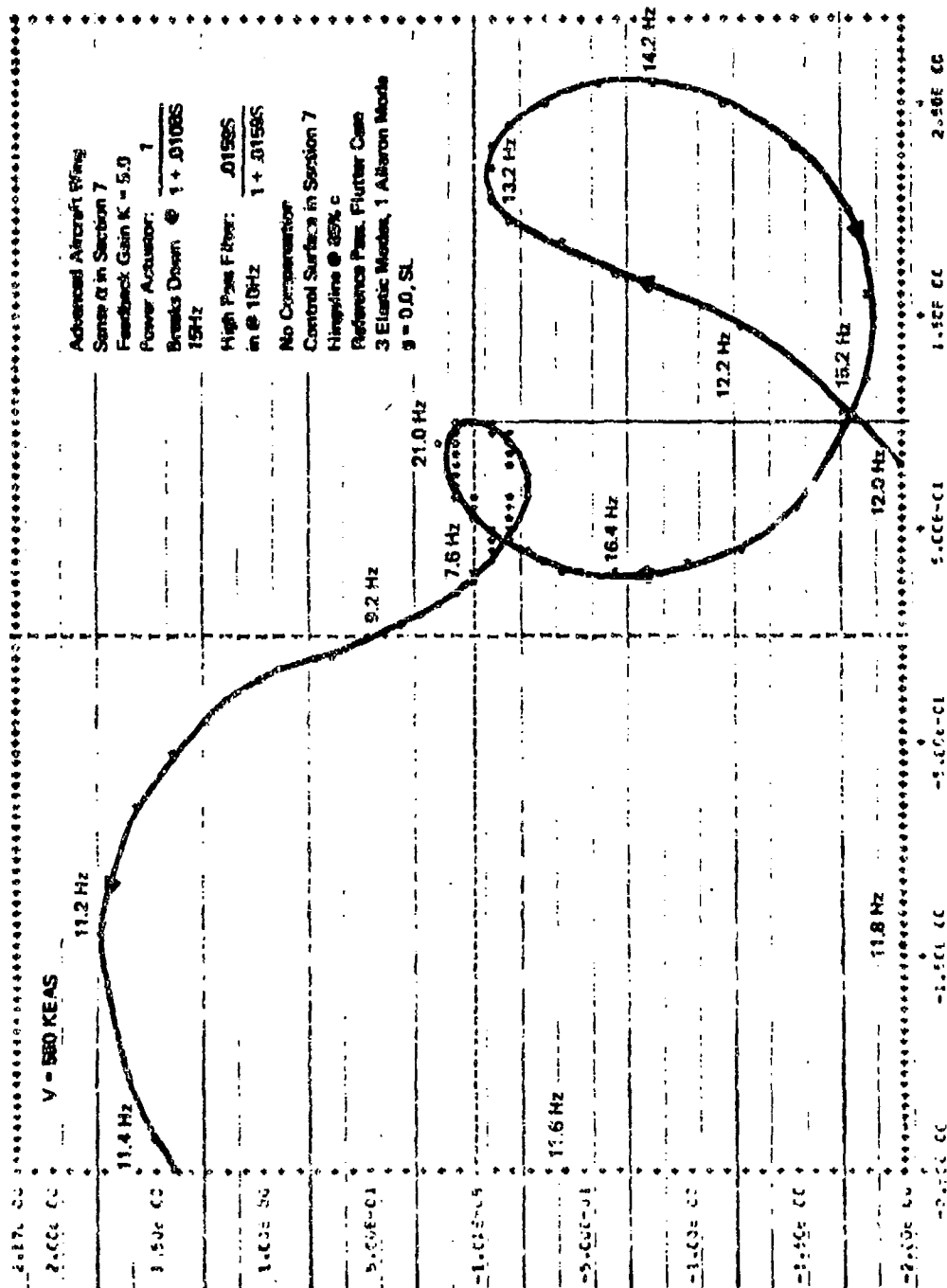
FIGURE 91   NYQUIST PLOT FOR ADVANCED AIRCRAFT WING -
THREE MODE TEST CASE - V = 550 KEAS

162
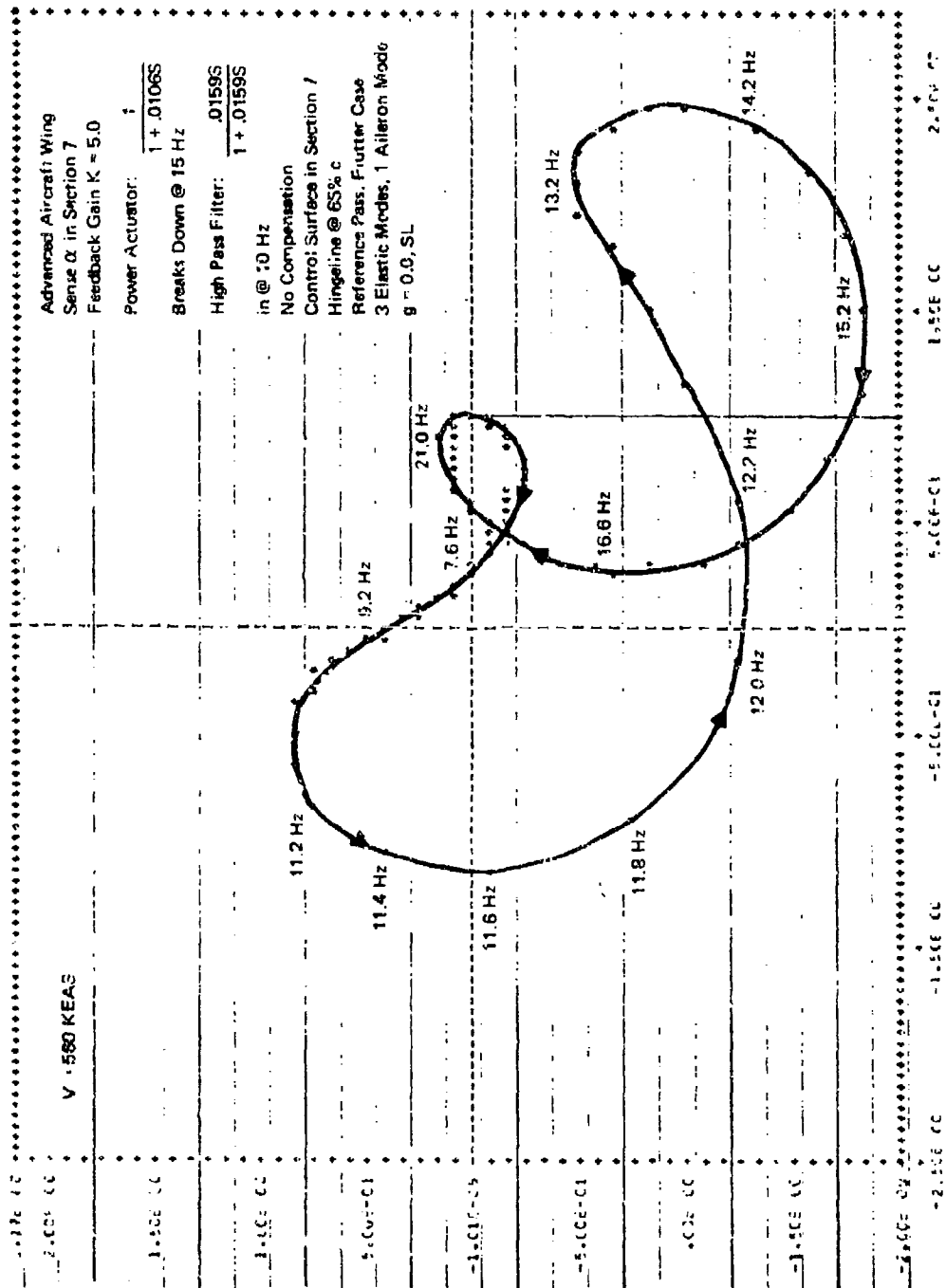
FIGURE 92 NYQUIST PLOT FOR ADVANCED AIRCRAFT WING -
THREE MODE TEST CASE - V = 560 KEAS

163
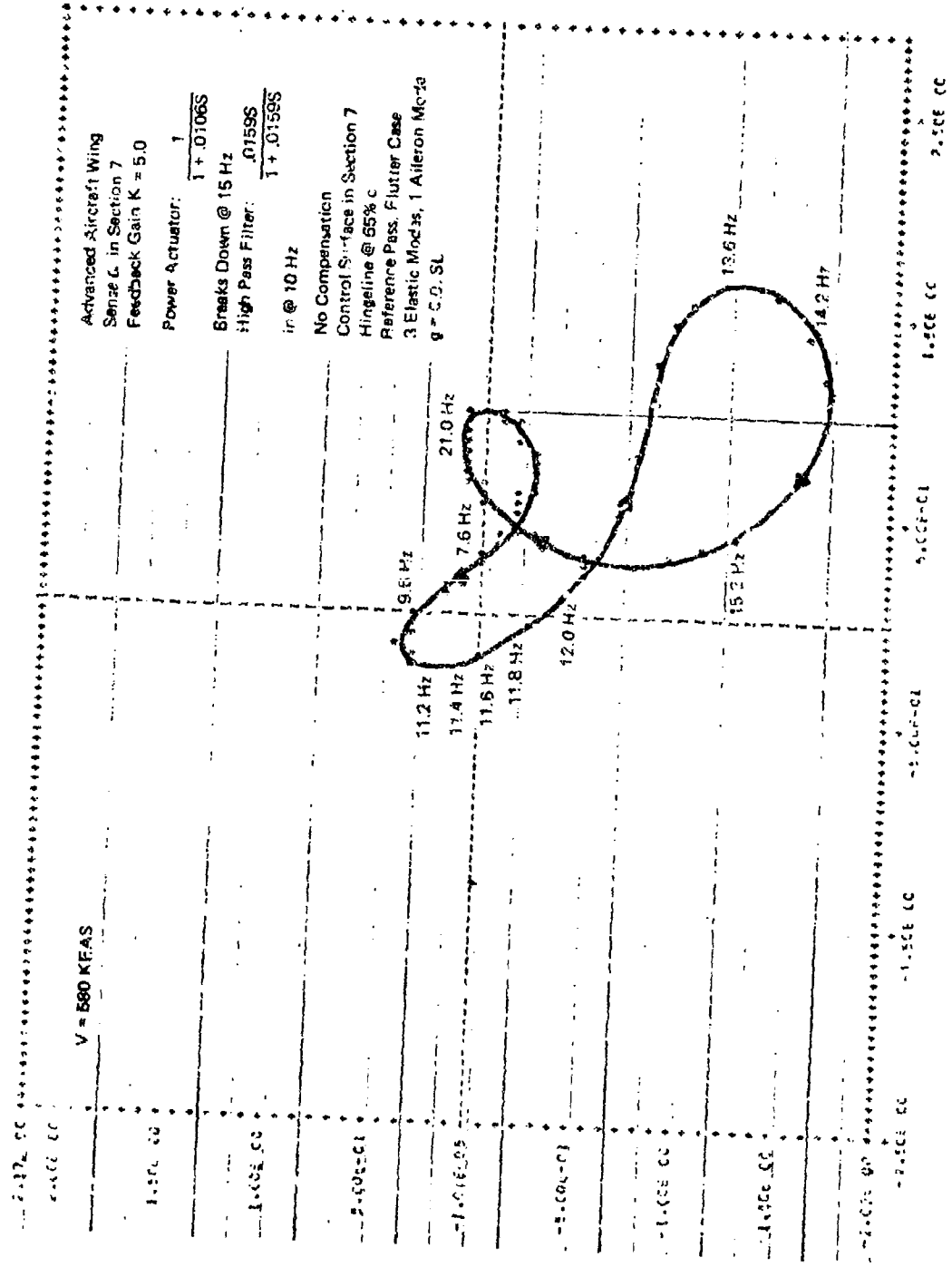
FIGURE 93 NYQUIST PLOT FOR ADVANCED AIRCRAFT WING -
THREE MODE TEST CASE - V = 580 KEAS

Aileron Sizing and Location Studies

Both the location and size of the aileron were varied in an effort to achieve flutter control beyond 600 knots. Ailerons with 35% chord depths were tried individually in Sections 8, 4, and 2. There was no improvement in the maximum stable velocity with active control. Frequency domain studies were also conducted starting with an aileron in Section 7 only and then progressively enlarging the control surface by first adding a Section 8 aileron and then adding inboard sections until the aileron ran the full wing semi-span. The wing twist at Section 7 was used as the feedback signal for all of these aileron configurations. No improvement of flutter suppression capability was achieved by enlarging the spanwise aileron dimension. The full semi-span results were actually worse than the results with the aileron in Section 7 only. A large span aileron has the problem of generating compensating aerodynamic forces and moments based on the sensed motion of a single section, say wing twist in Section 7. The wing motion at Section 4 may be out of phase with that in Section 7, especially if sizable contributions form the higher modes are present. Thus, the best aerodynamic force and moment compensation at Section 7 may worsen the situation in Section 4.

Aileron Aerodynamic Force Enlargement

In order to evaluate increased aileron effectiveness at a single section a frequency domain run was made using aileron aerodynamic coefficients which were 10 times larger than their previous values. The airfoil center of pressure was maintained at the quarter chord. The ten-fold increase in aileron coefficients is equivalent to enlarging the aileron aerodynamic forces 10 times with respect to the inertia forces. The results of this run, given in Figure 94 in Nyquist plot form, show significant improvement over the Nyquist plot shown in Figure 95 for normal aileron coefficients. It should be noted that the scale in Figure 94 is 10 times larger than that in Figure 95. The enlarged coefficient run shows a huge improvement over the normal coefficient run. The Nyquist plot in Figure 94 can be compensated above 600 knots with the addition of phase lag, a notch filter at about 16 Hz, and a feedback gain decrease. The most significant improvement as indicated by the enlarged CCW loop is the maximum phase margin range which has been increased from 10 degrees to about 120 degrees. Thus, by increasing the control surface effectiveness, flutter suppression can be achieved for velocities greater than 600 knots.

Advanced Aircraft Wing
Aileron in Section 7, No Compensation
Sense α in Section 7, V = 600 KEAS, β = 0.0, SL

Power Actuator: $\dfrac{1}{1 + .0106S}$

High Pass Filter: $\dfrac{.0159S}{1 + .0159S}$

Gain: 50

(Aileron Associated Coefficients were Multiplied by 10)

11.0Hz

10.2Hz

13.6Hz

-2.00E 01   -1.50E 01   -1.00E 01   -5.00E 00   -5.00E-02   5.00E 00   1.00E 01   1.50E 01   2.00E 01

-2.50E 01   -1.50E 01   -5.00E 00   5.00E 00   1.50E 01   2.50E 01
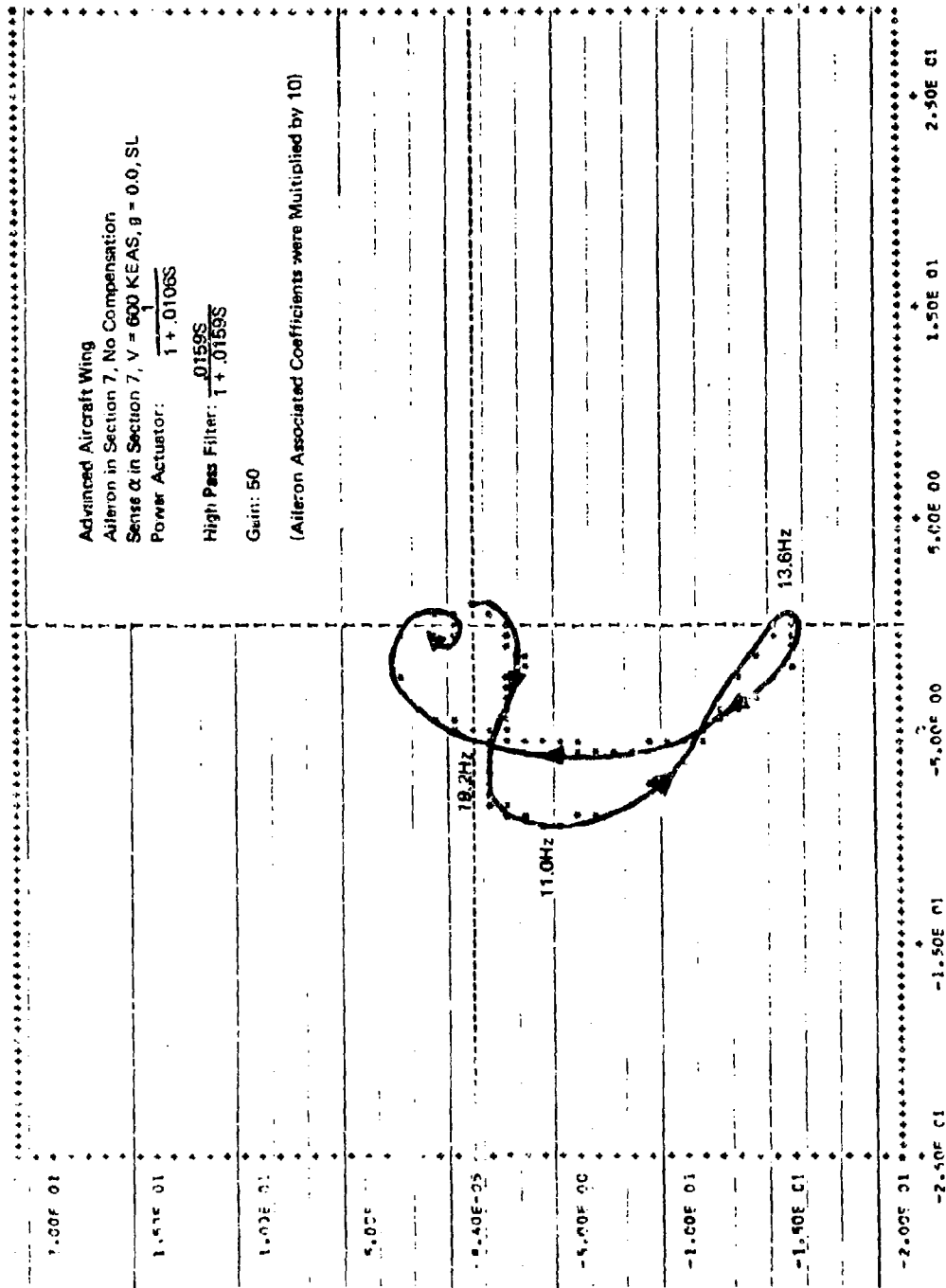
FIGURE 94   NYQUIST PLOT FOR ADVANCED AIRCRAFT WING -
AILERON AERO COEFFICIENTS X 10 - V = 600 KEAS
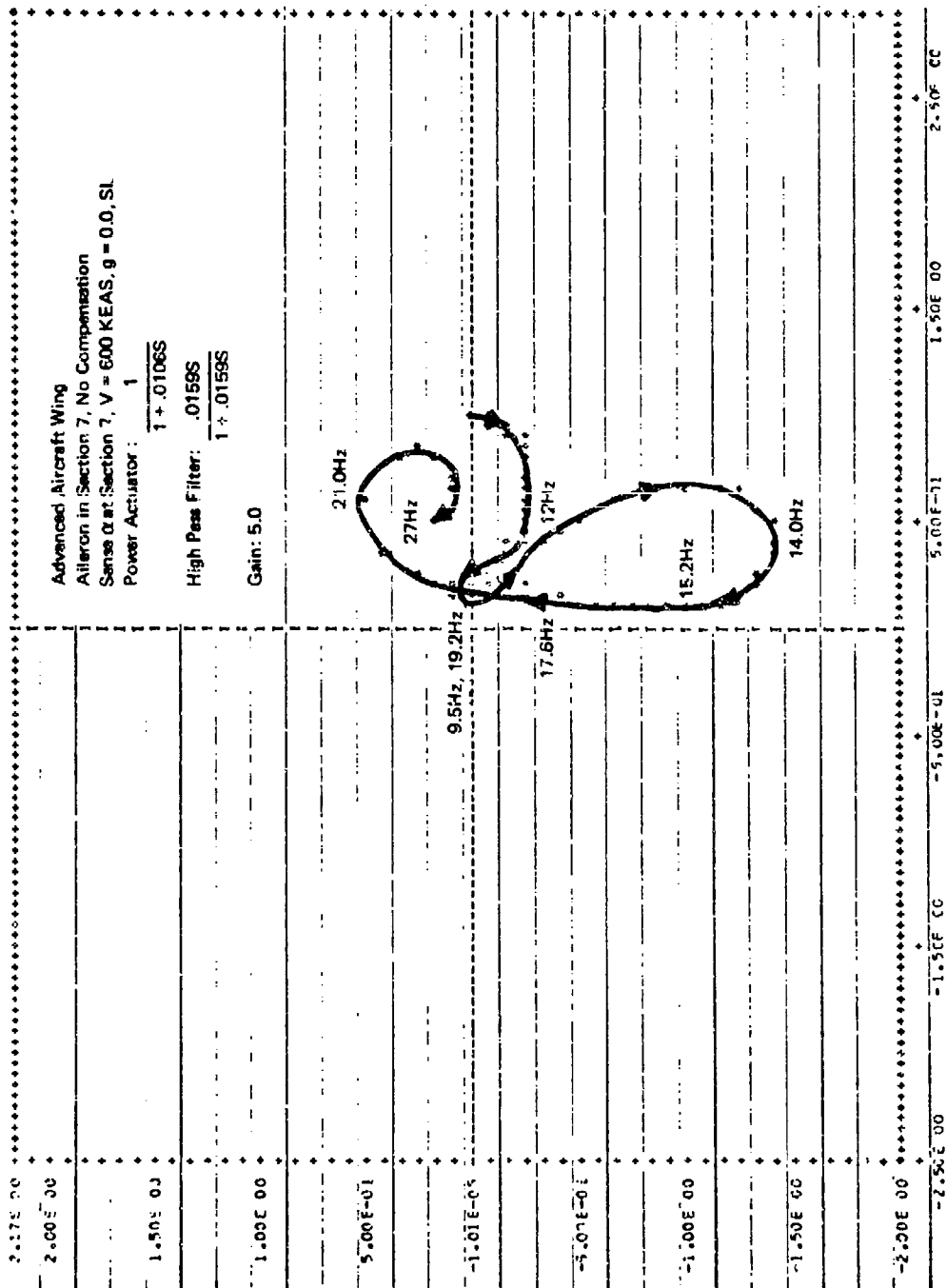
FIGURE 95 NYQUIST PLOT FOR ADVANCED AIRCRAFT WING -
NORMAL AILERON AERO COEFFICIENTS - V = 600 KEAS

167

Aileron effectiveness can be improved in the chordwise sense by two methods: leading and trailing edge control surfaces in the same wing section or an all-movable tip both of which change the relation of lift to moment from the above results.

4.3.2.2 Leading Edge Control - ACF program runs were made with a 15% chord leading edge flap incorporated in Section 7 of the baseline advanced aircraft wing. A lift-curve slope (C_{L_α}) of 2π/radian was used in the analysis rather than the previously used 3.98/radian since the currently available two-dimensional strip theory aerodynamics program with leading and trailing edge control surface capability has no C_{L_α} input option. Using the leading edge control surface program required that the ACF program be used in a form which accepted classical R + iI aerodynamics rather than the aerodynamic matrices generated at velocity by the Indicial Lift Program. This version of the ACF Program is described in Appendix IV, Section IV.2. Frequency domain studies of both leading and trailing edge control surfaces acting separately were conducted with $C_{L_\alpha} = 2\pi$ aerodynamics. Both control surface frequencies were specified at 60 Hz. The flutter onset speed of the advanced aircraft wing configuration was lowered to 390 knots at 15.54 Hz because of the increased C_{L_α}. The new C_{L_α} did not affect the flutter mechanism: modes 2 and 3 interacting explosively. Using a control loop consisting of the wing equations and an uncompensated Section 7 twist feedback, only about a 60 knot flutter speed improvement was possible with either control surface. Leading edge control appears subject to the same stability margin restrictions as trailing edge control in suppressing the explosive flutter of a bare wing.

4.3.2.3 All-Movable Wing Tip Control - This analysis used a wing identical to the baseline advanced aircraft wing for the first five sections in stiffness and inertia characteristics. The sixth wing section was different from the corresponding baseline section because 37 lbs. were added to the torque box to model the wing tip control actuator. The weight of the actuator currently in use on the F-4 stabilator is 37 pounds. The inertia properties of Sections 7 and 8 were those generated by the COPS program for these sections with no leading or trailing edge control surfaces. Appendix III summarizes the inertia and stiffness data as generated by the COPS program for a wing with/without control surfaces. In order to maximize the flutter control capability of the wing tip, the two outboard

sections were treated as a rigid (infinitely stiff) extension of Section 6 for the first six wing modes. An uncoupled pure tip mode consisting of Sections 7 and 8 rotating together about the elastic axis (EA) with no EA translation completed the 7 mode analysis. A high tip mode frequency, 30 Hz, was specified to avoid creating a new flutter mode through interaction with the lower wing modes. The consequences of assuming Sections 7 and 8 to be rigid are an increased flutter onset velocity and a better flutter control capability.

The aerodynamic simulation for this all-movable tip configuration employed C_{L_α} = 3.98/radian and CP = 25% chord. The flutter onset velocity is 692 knots at a frequency of 11.4 Hz. The passive flutter speed increase over the baseline wing configuration can be traced to changes in the mass and stiffness characteristics of the outboard sections. Active control is possible up to about 900 knots when the included angle of the unstable loop of the Nyquist plot is reduced to 9 degrees (phase margin $\pm$ 4.5 degrees). This is a 30% flutter velocity penetration.

A similar configuration with a tip section aileron was also examined to provide a basis of comparison. The tip aileron analysis was altered only in the control surface mode. An aileron in Sections 7 and 8 beginning at the 65% chordline replaced the movable tip. The wing surface portions of Sections 7 and 8 were treated as rigid extensions of Section 6. The aileron rotation mode frequency was specified to be 60 Hz. This configuration began fluttering at 742 knots and 12.49 Hz without active flutter suppression. The higher passive flutter onset velocity probably occurs because of the higher control surface frequency. Active control with an aileron suppressor is lost between 850 and 900 knots.

Nyquist plots of the wing aeroelastic, feedback control equation are given in Figures 96 and 97 for the all-movable tip and aileron control surfaces. The most striking contrast is the much larger plot when the movable tip is used as a flutter suppressor. A more crucial difference is the maximum included angle of the unstable loop, since this is equal to twice the maximum balanced phase margin. The included angle, though significantly larger with the all-movable tip case for similar flutter velocity penetrations, still allows phase margins of only $\pm 45°$ after a 40 knot flutter penetration. The reasonably large flutter penetration capability for the all-movable tip scheme is, thus, offset by restricted stability margins. This rapid reduc-
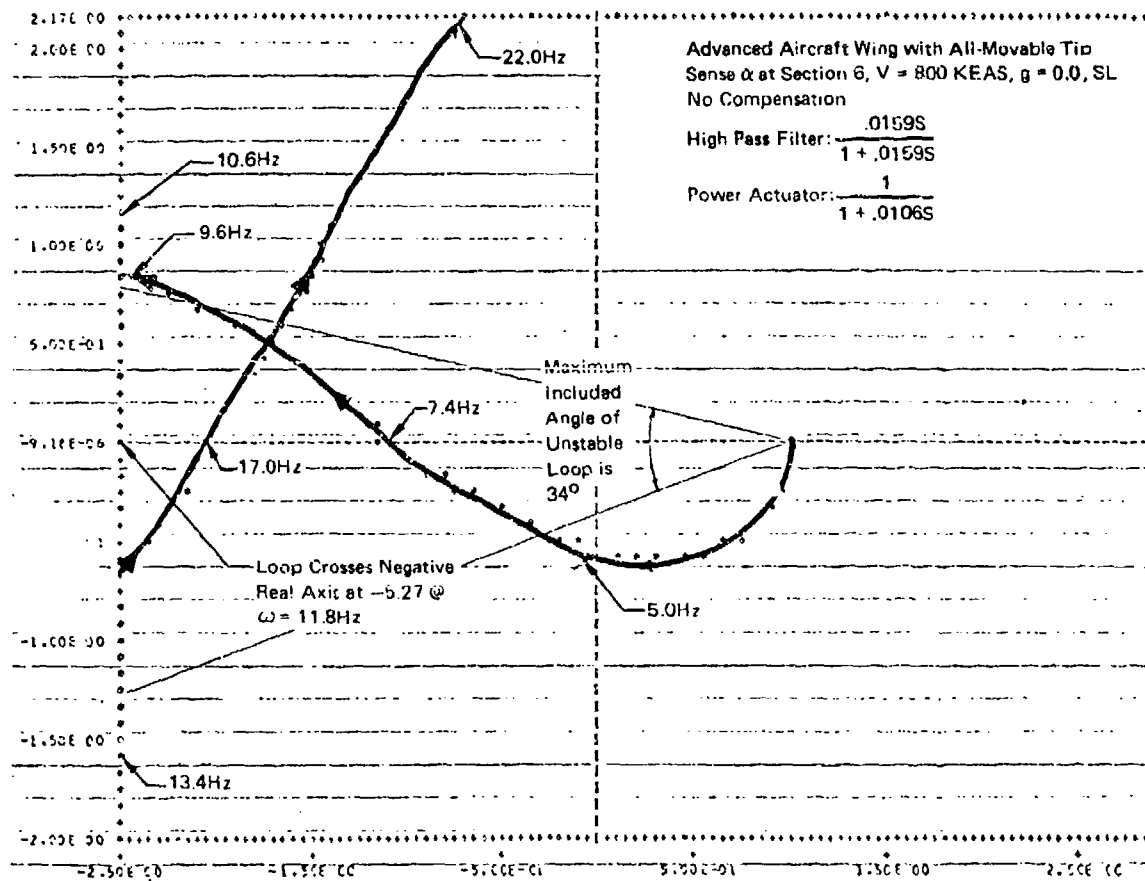
FIGURE 96 NYQUIST PLOT FOR ADVANCED AIRCRAFT WING -
ALL MOVABLE TIP CASE - V = 800 KEAS
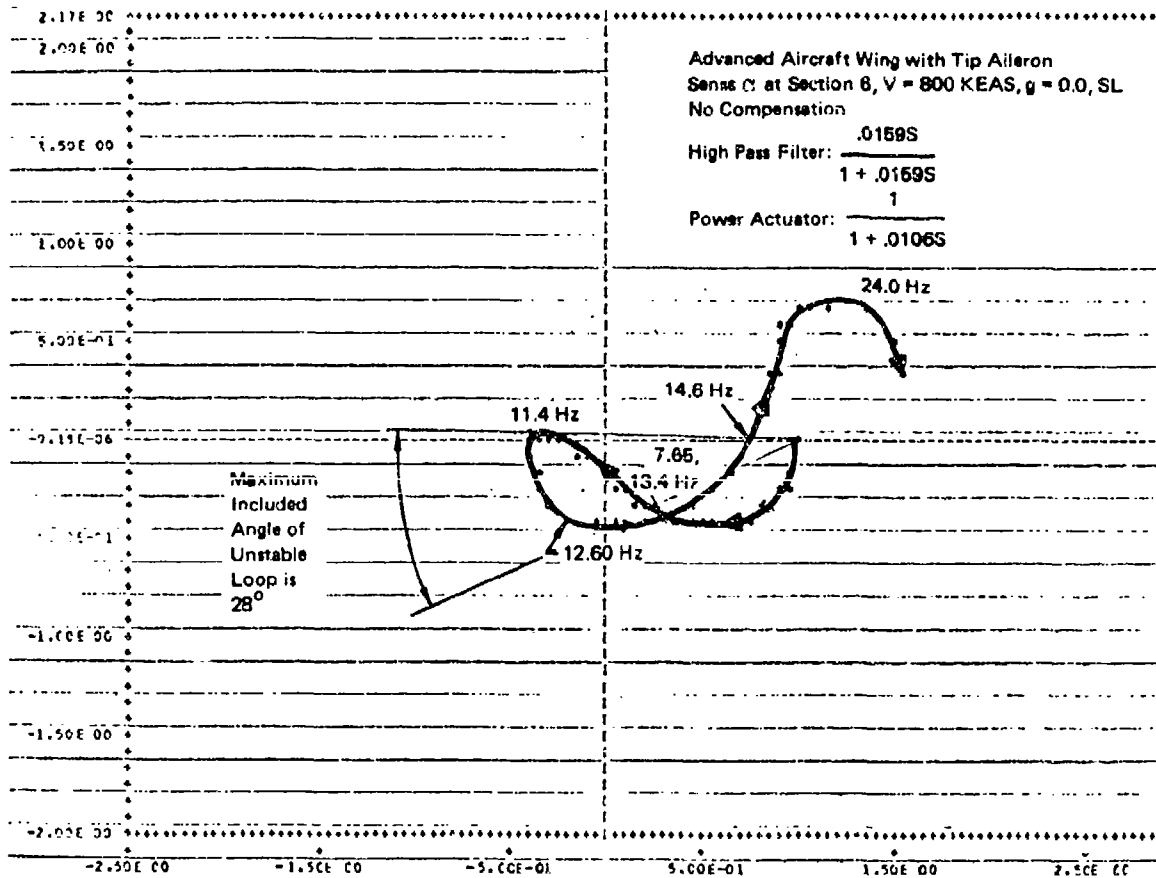
FIGURE 97   NYQUIST PLOT FOR ADVANCED AIRCRAFT WING -
TIP AILERON CASE - V = 800 KEAS

tion in phase margins with increasing velocity seems, once again, to corre-late with the relative "explosiveness" of flutter. The g/V at flutter onset for the movable tip cases was about five times that of the worst F-4 wing/store case.

Neither the use of leading edge control surfaces nor an all-movable tip permitted the realization of the large phase margins during flutter penetration suggested by Figure 94. Apparently, it is crucial that the control surface CP be maintained considerably aft of the wing elastic axis when the aerodynamic effectiveness of the surface is increased. A reaction jet with a large thrust capability mounted aft of the EA could generate (by maintaining an aft control surface CP) the moments and forces necessary to improve the flutter control phase margins.

4.3.2.4 <u>Control of Modified Configurations</u> - The relative "explosive-ness" of flutter as measured by g/V appears to be a fundamental parameter in determining the amount of penetration possible with a flutter control system. When 200 pounds were added to the leading edge of Section 5 the resulting passive study configuration had a g/V of about 1/2 of the .2/100 knots value obtained for the baseline configuration. The 200 lb mass addition configuration lowered the flutter onset velocity to 474 knots but flutter control was still possible to about 600 knots, a 26% flutter pene-tration with zero stability margin. Although the 200 lb mass balance is an unacceptable flutter fix since it lowers the flutter onset speed, it does illustrate that explosive, virtually uncontrollable, flutter mechanisms can be calmed through mass addition to permit better control. For some future designs a combination of mass addition and active flutter control may be the most efficient flutter fix.

4.3.3 <u>Advanced Aircraft Wing Concluding Remarks</u> - An active flutter suppression scheme for this configuration could provide control up to about an 11% flutter velocity penetration with very limited phase margins. The most efficient flutter fix for the aircraft wing under study is a stiffness increase of the outboard wing sections costing about 67 pounds. This com-pares with a target active system weight of 200 pounds per aircraft.

The relative "explosiveness" of the flutter mode at onset is the deciding factor as to whether or not an active system makes sense. A flutter mechanism with a value of g/V less than .1/100 knots appears to be a pre-requisite for sizable flutter velocity penetrations with an active system.

172

Some improvements in penetration can be achieved by increasing the control surface effectiveness but significant velocity improvements can be realized only if the flutter mode is first "tamed" through wing stiffening or balance weights. It should be emphasized that even though an active system is impractical for the particular study configuration; other, less explosive advanced wing configurations may be suitable for active control of flutter.

5. IMPLEMENTATION STUDIES

The vehicle considered in these active flutter control implementation studies is the F-4 Phantom and a significant amount of data is based on the SFCS (Survivable Flight Control System) fly-by-wire aircraft. The F-4 was chosen as the study vehicle rather than the advanced design aircraft because the use of a real-world data base permits a much more thorough investigation of aircraft control system components. Though the comments in this section concern the F-4 lateral control system components they should be generally applicable also to the control systems of other aircraft such as the advanced design aircraft used in the horizontal tail and wing studies.

5.1 Existing F-4 Lateral Control System

The lateral control system for the F-4 aircraft is shown schematically in Figure 98. The lateral control system allows control of the aircraft about its longitudinal axis by a combination of aileron and spoiler deflection. The system consists of one aileron and two spoilers hinged to each wing. Power is supplied by two primary 3000 psi hydraulic systems (PC1 and PC2) and one utility hydraulic system. The aileron is actuated by a single hydraulic power actuator and servo control valve, while each spoiler is positioned by a tandem hydraulic power control actuator with a remote dual control valve. Each aileron and spoiler power actuator is driven by a dual independent hydraulic system: the left wing actuators are driven by the PC1 and utility hydraulic systems while the right wing actuators are driven by PC2 and utility. If one hydraulic system fails, the remaining one is capable of driving the actuator. Also, if both hydraulic systems in one wing fail, the third hydraulic system will be available to drive the lateral power actuators in the opposite wing. The control stick is connected to the aileron power actuator and dual spoiler valves by a series of push-rods, bellcranks, and safety springs. The safety spring cartridge is contained in both the L/H and R/H system so that binding of the controls on one side will not prevent pilot inputs to the other half of the system. The output motion of the aileron actuator produces a maximum of one degree up aileron and thirty degrees down aileron. The inboard and outbord spoiler surfaces have a range of flush to forty-five degrees up motion available. The surfaces are synchronized such that all surfaces are
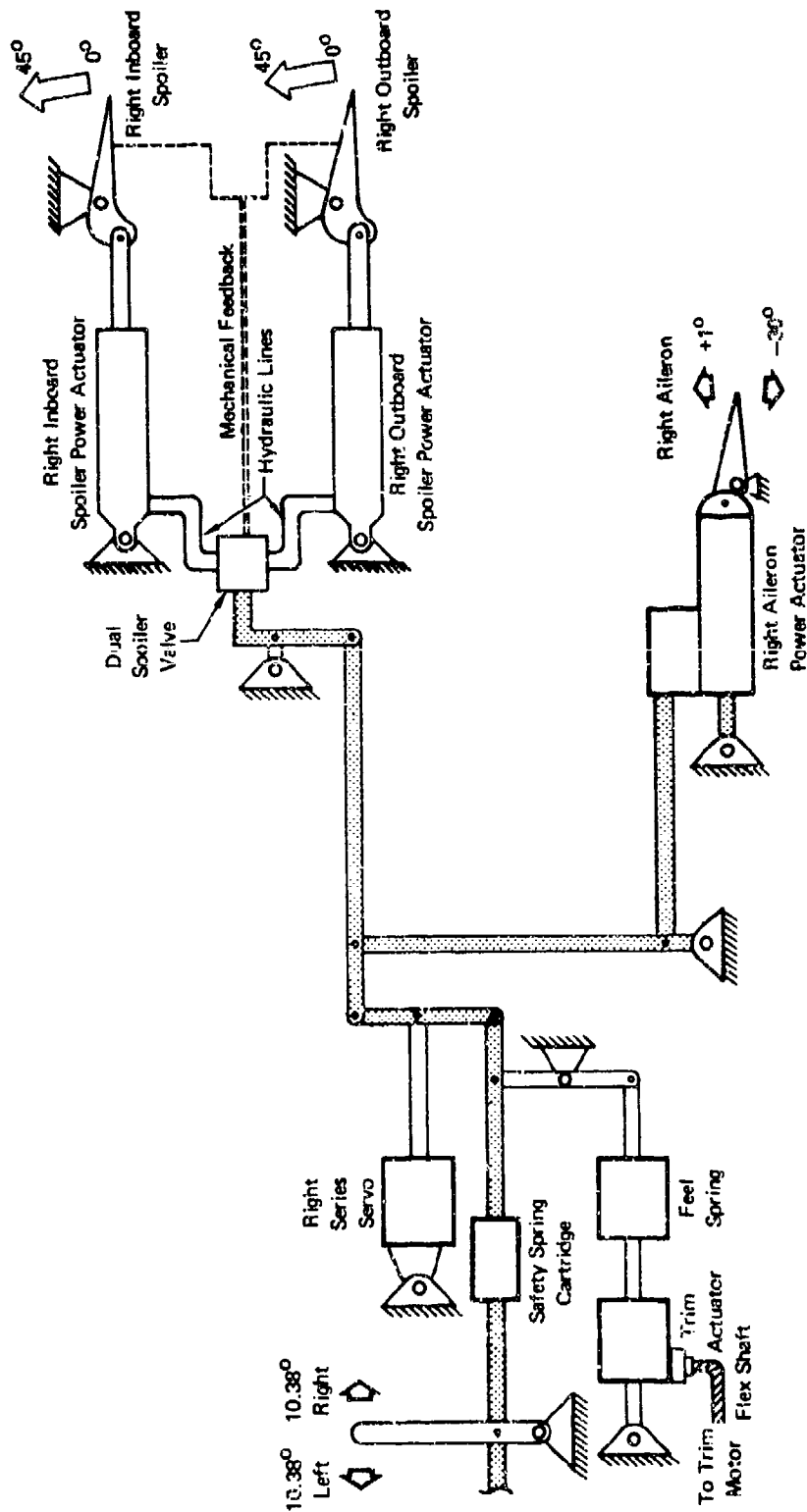
FIGURE 98 SCHEMATIC OF F-4 LATERAL CONTROL SYSTEM

175

at streamline condition simultaneously, while thirty degrees down aileron on one side is reached at the same stick deflection as forty-five degrees up spoiler on the opposite side. Aileron and spoiler motion can also result from inputs from the series servo actuator. This element implements the commands of the stability augmentation system. The series servo is powered by only the utility hydraulic system. Feel forces for the pilot are generated by spring cartridges in each wing. The feel system breakout force is approximately 2.3 pounds with full stick throw requiring approximately 12 pounds. Trim is achieved by moving the backup point for the spring cartridges. Synchronization of trim is accomplished by using a single electric actuator that simultaneously drives a screwjack in each wing through a flexible shaft. The feel spring cartridges are mounted in the wing to provide maximum backup for the servo actuators.

The aileron power actuator, shown in Figure 99, is a four barrel actuator, with the four side-by-side pistons powered by two separate hydraulic systems. The two inner pistons of the left wing actuator are powered by the PC1 system while the two outer pistons are powered by the utility system. In the right wing aileron actuator the utility system powers the inner pistons while PC2 drives the outer pistons. The connection of separate hydraulic systems to the inner and outer piston pairs prevents surface warpage in the event of loss of one hydraulic system. Position of the actuator is controlled by a servo valve mounted on the side of the actuator body. All inputs, manual and autopilot, are summed mechanically in the control system prior to the point at which the motion is split to control the spoilers and the aileron, therefore no electrical connections are made to the aileron actuator. Motion of the valve channels fluid to the pistons, and the resultant pressure differentials cause actuator case travel. This motion in turn balances the input and shuts off flow at the commanded position. For inputs which would result in motions above one degree up aileron, the aileron dampers bottom out and the aileron cylinders hold system pressure until a lower position is commanded.

The spoiler power actuators are tandem actuators powered by two hydraulic systems each: PC1 and utility power the left wing cylinders and PC2 and utility power the right wing cylinders. Both inboard and outboard actuators are required to prevent surface warpage. Motion of the two actuators in each wing is controlled by a single valve which converts

176

Retract

Pivot Point

Control Lever

Servo Valve

Aileron

Power Actuator

Pivot Point

Legend

PC 1 Pressure
PC 1 Return
Utility Pressure
Utility Return
Static
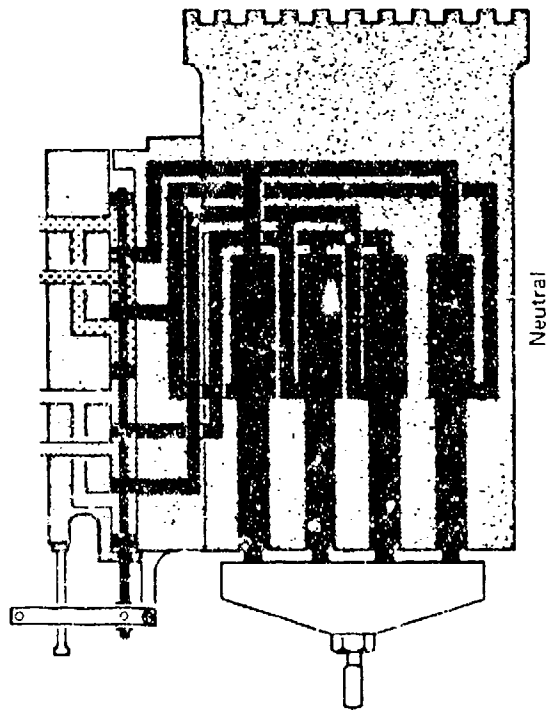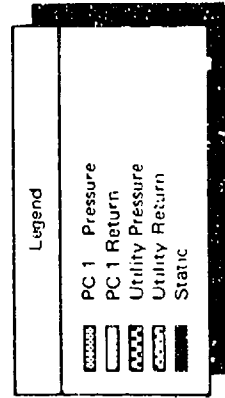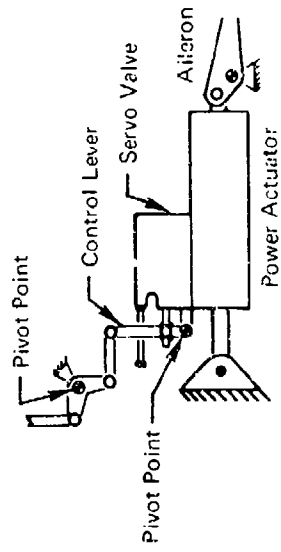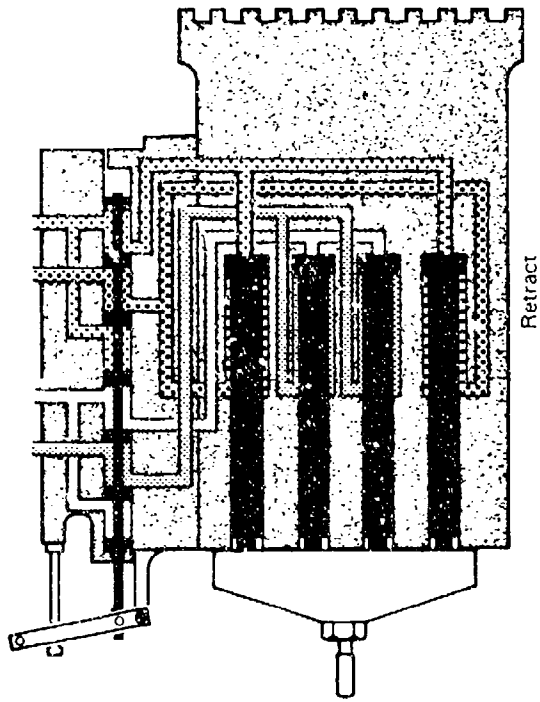
Note: The Hydraulic
Plumbing Shown
is for the Left
Wing Actuator Only.

Neutral

Extend
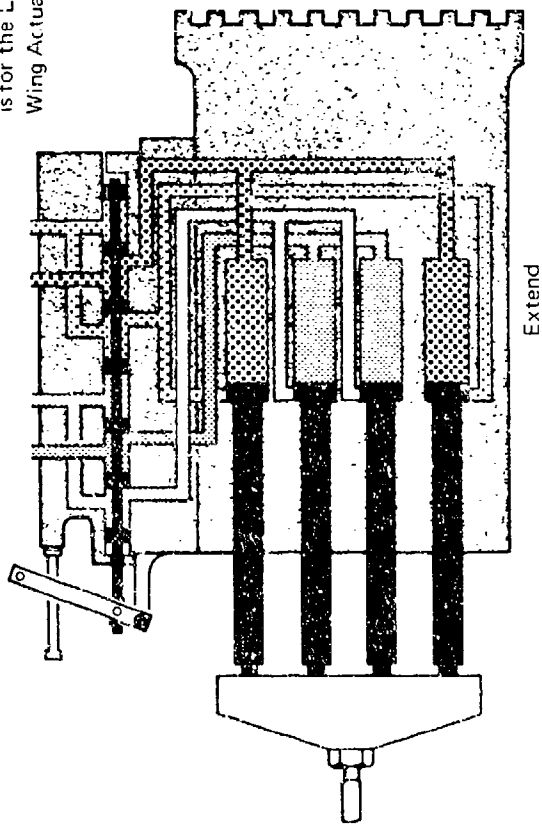
FIGURE 99 SCHEMATIC OF F-4 AILERON POWER ACTUATOR

lateral control linkage motions to hydraulic flows. Surface position linkages shut off the valve at the point where surface position corresponds to stick position. Valve openings commanding down spoiler result in a static pressure in the cylinders which holds the spoilers against the wing structure.

5.2 Control System Interaction Study

Integration of an active flutter control system with other flight control systems is desirable from many viewpoints as described in Section 3.3.2. The principal benefits are a reduction in both weight and cost compared to a dedicated flutter control system.

The general approach we have taken in the design of a flutter control system is to share selected portions of the existing aircraft flight control system. All of the flutter control elements are located in the feedback branch around elements in the forward loop which the flutter control system shares with the flight control system. The flutter control feedback loop may thus be opened at any time during flight at sub-flutter velocities with no effect on the performance of the aircraft. A high pass filter is present in the flutter feedback loop to effectively decouple the two systems for low frequency signals, such as pilot commands, when the loop is in operation.

5.2.1 Root Locus Studies with the F-4 Stability Augmentation System - Root locus runs were made to evaluate the interaction of the flutter control system with the F-4 Lateral/Directional Stability Augmentation System (SAS). The MATLOC computer program described in Appendix IV was used for this study. The control system block diagram is shown in Figure 100.

The lateral channel of the SAS uses roll rate signals from a roll rate gyro to add damping to the basic aircraft aerodynamic damping in roll. The channel is interrupted whenever the pilot maneuvers in roll so as not to obtain roll fighting action from the SAS system. The gain associated with the roll rate loop is fixed.

The directional channel of the SAS uses signals from a yaw rate gyro to add damping to the aircraft dutch roll mode. These signals are passed through a canceller (a high pass filter), which removes the low frequency portion of the signal, so the system does not oppose the pilot during maneuvers. Signals from a lateral accelerometer are used to provide

178

Definition of Symbols
a   Aircraft Yaw Acceleration
p   Aircraft Roll Rate
r   Aircraft Yaw Rate
α   Wing Twist Angle
δa   Aileron Deflection
δr   Rudder Deflection
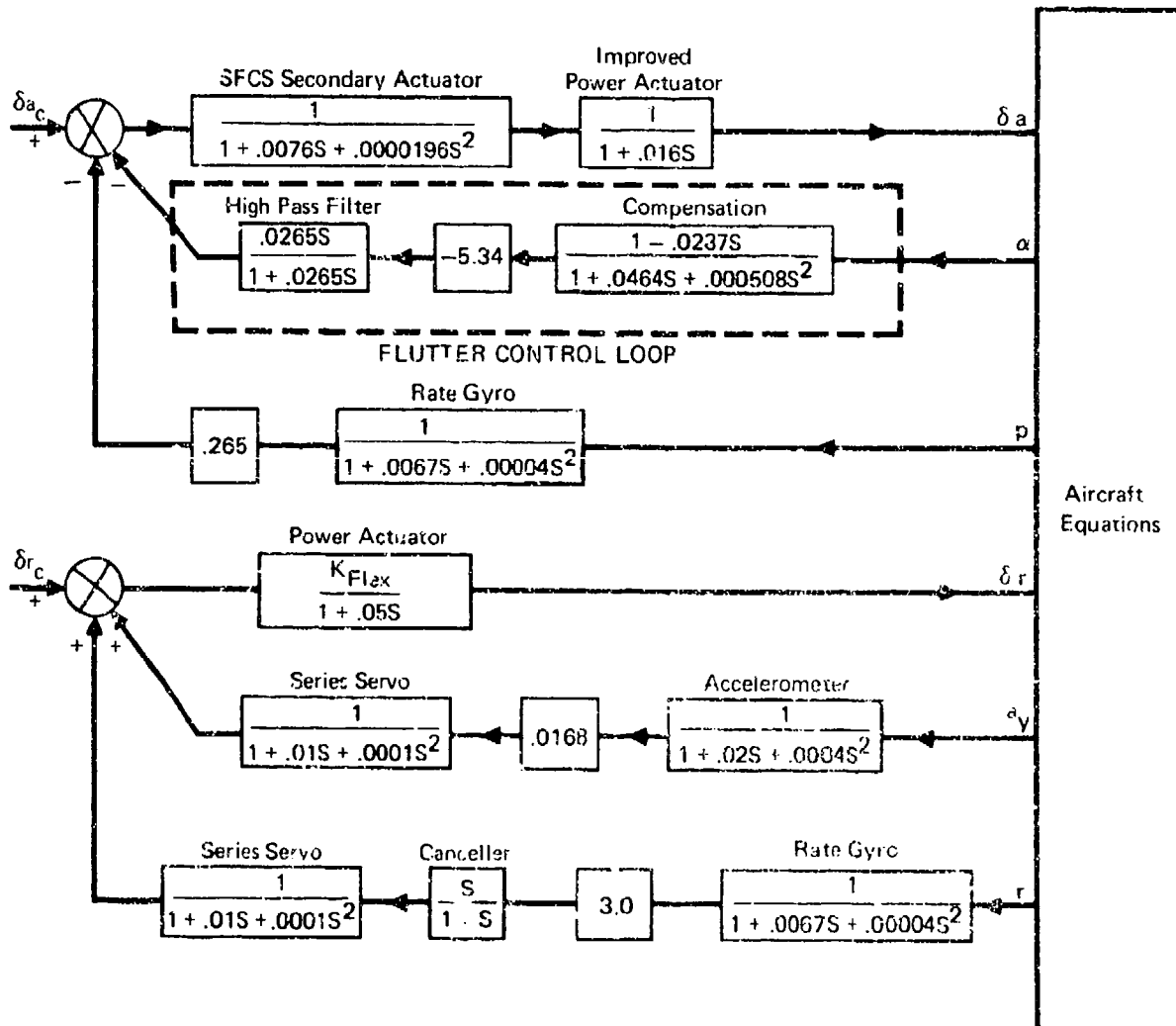
FIGURE 100 BLOCK DIAGRAM OF F-4 LATERAL/DIRECTIONAL STABILITY AUGMENTATION SYSTEM

179

coordinated turns. The gains associated with the yaw rate and lateral acceleration loops are fixed.

The flight condition chosen for these runs is Mach 0.84 at sea level. The roll rate loop gain is the root locus gain parameter. The unmodified operational F-4 lateral/directional SAS root loci are shown in Figure 101. The nominal roll rate gain for the system is $K_p = 0.265$. These data are as used in F-4 control dynamics analytical models. Figure 102 shows the root loci when the F-4 series servo actuator is replaced by the CFCS secondary actuator described in Section 5.5.1 and when the aileron power actuator bandwidth is extended flat to 10 Hertz. The operational F-4 requires these changes as the base for an active flutter suppression system. The new high frequency pole for the power actuator moves the branching point to the left on the negative real axis. The system is highly damped and very stable.

A third run introduces the flutter control system as an inner control loop. The 370 gal-90% case with 3 elastic modes was chosen for this test case. The flutter equations of motion were expressed in terms of the Laplace variable. These equations, along with the flutter control system have the effect of changing the overall control system characteristic equation from one with 11 zeros over 17 poles to one with 26 zeros over 32 poles. Figure 103 shows the root loci for this case. The situation is very similar to that shown in Figure 102, with the flutter control system turned off, except that some local pole-zero action has been introduced on the negative real axis. The system is still highly damped and very stable. The elastic modes, all of which have negative real parts, are not shown in this figure, since the primary concern here is the effect of the flutter control system on the aircraft flying qualities. These runs illustrate that the flutter control system may be effectively decoupled from the flight control system, at least for fighter type aircraft with large frequency separation, even though the forward loop control elements are shared. There may, however, be significant effects on the flight control system design if the bandwidth of the common forward control loop is increased as assumed in these studies.

5.2.2 Effects on Flight Control System Design – First, let us define some terms. Electrical signals will be generated by the sensors (i.e., rate gyros and accelerometers) in a typical aircraft flight control or stability augmentation system. These sensors, which are generally mounted
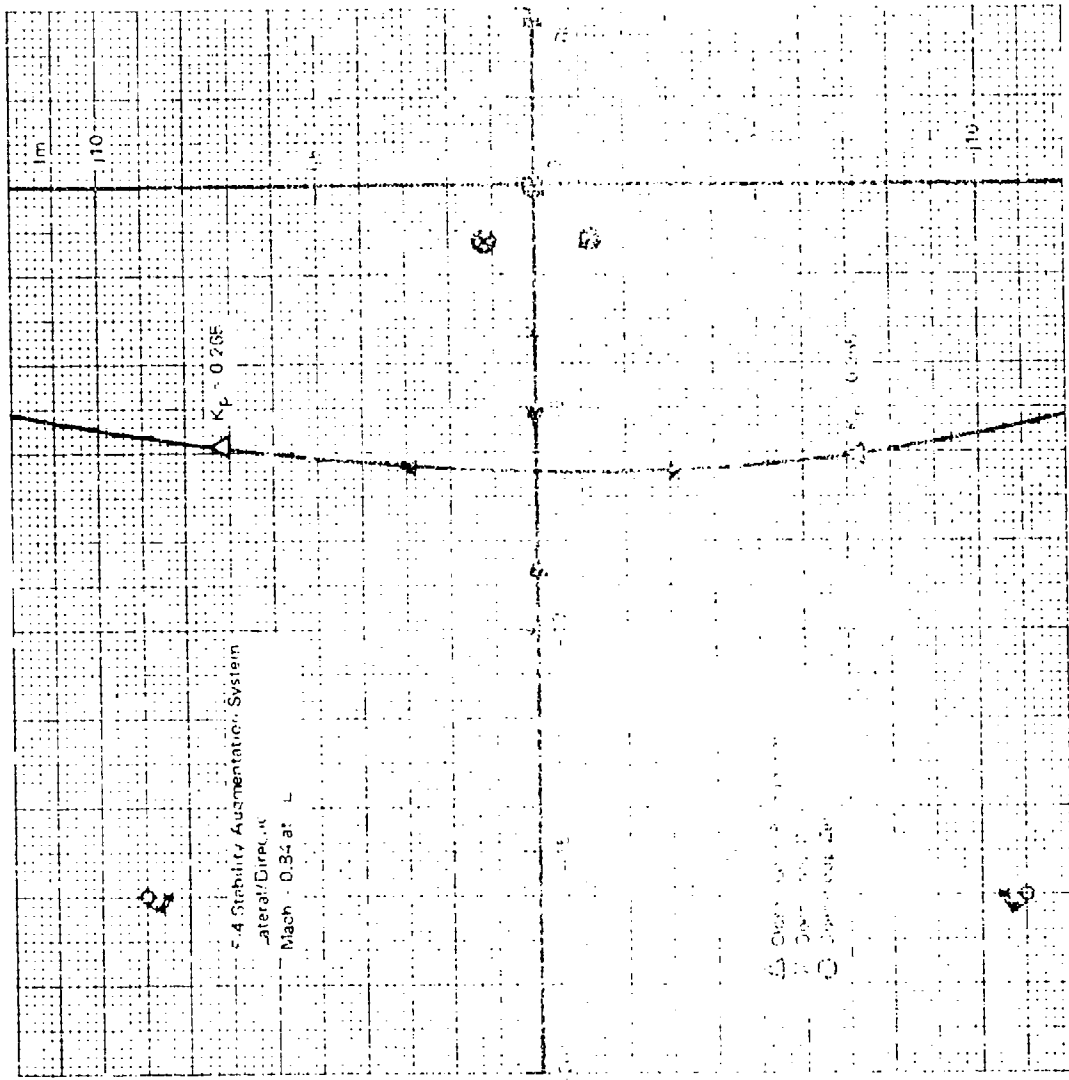
FIGURE 101 ROOT LOCI FOR F-4 LATERAL/DIRECTIONAL SAS
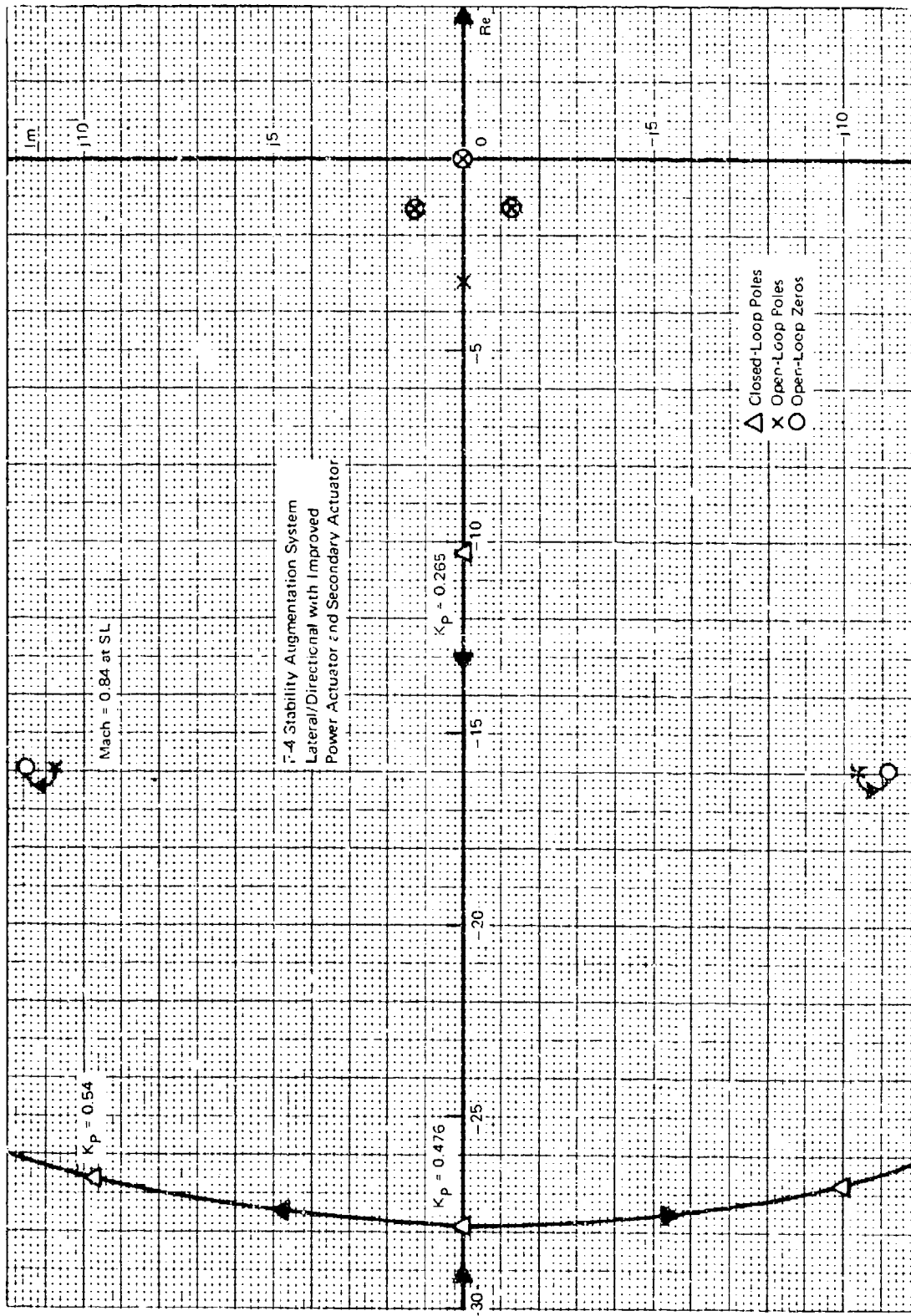
FIGURE 102 ROOT LOCI FOR F-4 LATERAL/DIRECTIONAL SAS WITH SFCS SECONDARY
ACTUATOR AND POWER ACTUATOR BANDWIDTH EXTENDED TO 10 Hz

182
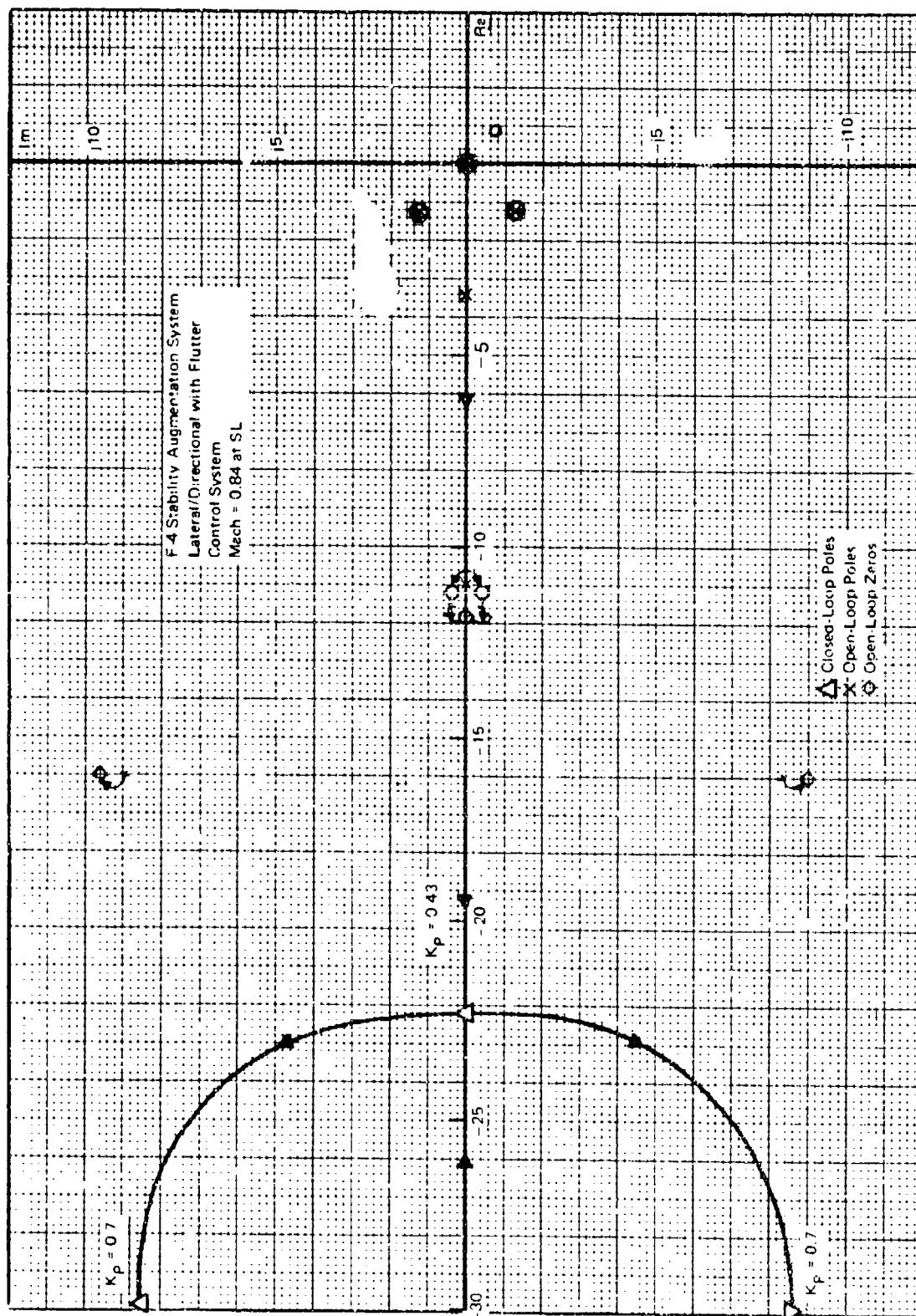
FIGURE 103 ROOT LOCI FOR F-4 LATERAL/DIRECTIONAL SAS WITH FLUTTER
CONTROL SYSTEM AND EQUATIONS OF MOTION FOR 370 GALLON - 90% CONFIGURATION

in the fuselage, will sense both rigid and elastic motion. Both types of motion signals may potentially destabilize the control system and thus create divergent oscillations.

For significant elastic modes in the low frequency range of the rigid aircraft modes it is not practical to attenuate the unwanted elastic signal since the desired rigid aircraft signals would also be attenuated. The normal design procedure instead is to use "phase stabilization" of the control system with respect to the elastic modes. This phase control procedure allows for the otherwise desirable high open-loop gains. It suffers, however, because accurate knowledge of the phasing of the elastic modes is required and this is very difficult to obtain without testing with the actual hardware.

If the significant elastic modes have frequencies which are well separated from the rigid aircraft modes it is possible to attenuate the unwanted elastic mode response by the use of electronic compensation such as notch filters and lag-lead networks. This procedure is called "gain stabilization." The elastic modes may have any phase whatsoever and the control will still be stable.

Active flutter control is inherently a "phase stabilization" process since a positive controlling force must be used. You may not "gain stabilize" or "hide from" the flutter you are trying to control.

The F-4 (and most other contemporary fighter type aircraft) is relatively stiff and its elastic modes are well separated from the rigid aircraft modes. The F-4 flight control and stability augmentation systems are gain stabilized with respect to the elastic modes. One of the easiest methods, which is customarily used, to gain stabilize aircraft flight control systems is to specify the lowest practical hydraulic actuator bandwidth. This, combined with the placement of the body mounted sensors near minimum elastic mode response points, will minimize the need for additional electronic filtering.

The Bode gain diagram of Figure 104 illustrates the effect of actuator bandwidth extension on a typical flight control system design which required a notch filter to gain stabilize an elastic mode signal. If the actuator bandwidth is extended flat to 10 Hz, as shown in the figure, it is readily apparent that a sizable increase in the depth of the notch filter
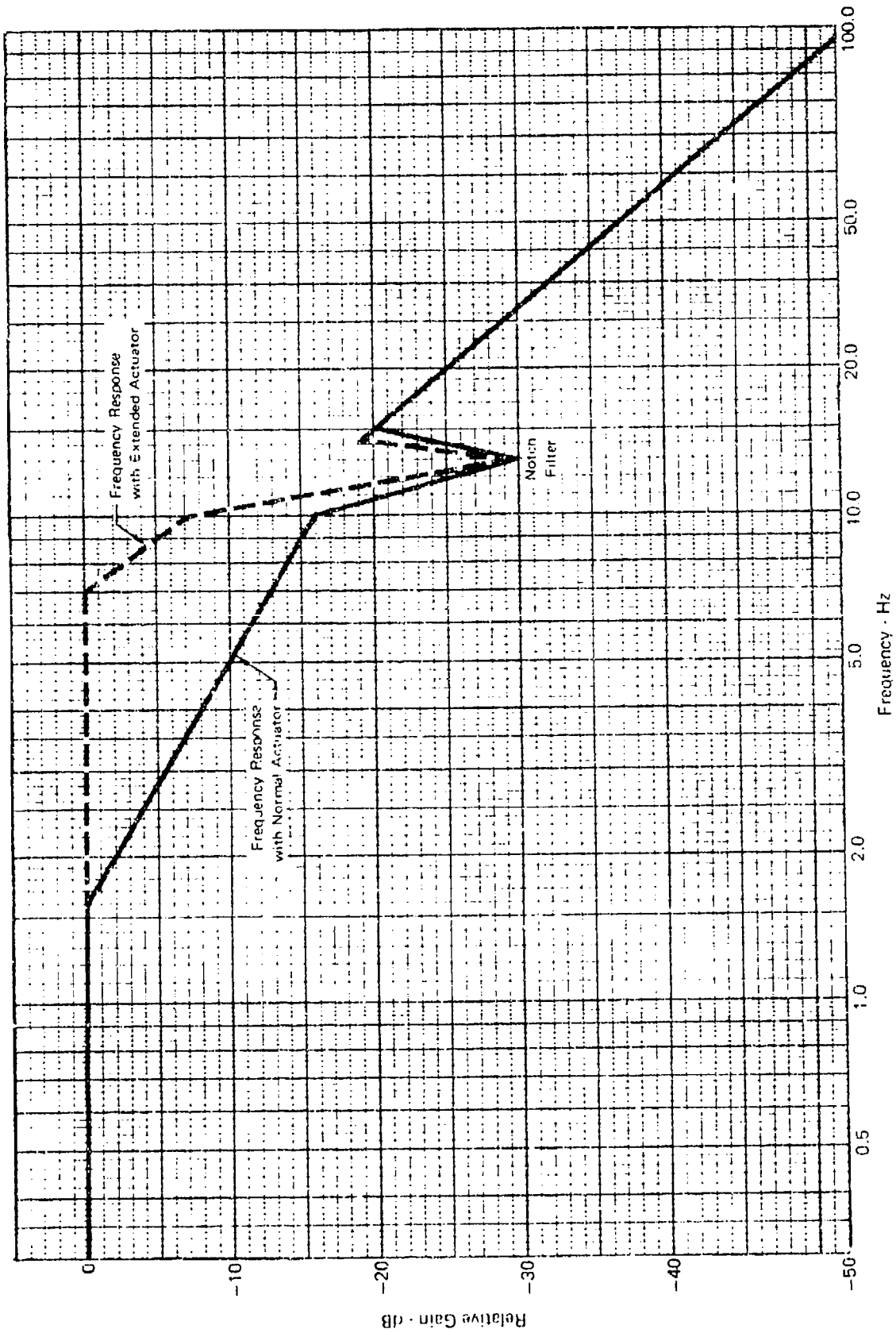
FIGURE 104 EXAMPLE ILLUSTRATING EFFECT OF ACTUATOR BANDWIDTH
EXTENSION ON FLIGHT CONTROL SYSTEM DESIGN

will be required to prevent control system induced instabilities at the elastic mode frequency. If the aircraft control system is manual or if a stability augmentation system is present, but disconnected, the problem alluded to would not exist; the pilot does the filtering naturally. Any closed-loop fly-by-wire system as implied here, however, should be designed as an integrated package with all of the interacting control systems and all significant rigid and elastic modes considered simultaneously.

5.3 Basic Active Flutter Control System Considerations

This section describes the characteristics of a basic flutter control system as it might be expected to be implemented on an F-4 aircraft.

5.3.1 Hydraulic System Modifications

5.3.1.1 Existing Hydraulic System – As described before, the hydraulic power for the F-4 is furnished by three 3000 psi systems; PC1 and PC2 and utility. The pump capacities are 25 gals/min for both PC1 and PC2, and 50 gals/min for the utility system. The pump flow rate is essentially linear with engine rotational speed (RPM).

Aileron Deflection and Rate Limits

The maximum aileron deflection limits are shown in Figure 105. These data, from published F-4 documents, show that up to 10 degrees of aileron deflection is possible throughout the entire F-4 flight domain.

The maximum aileron rate limits are shown in Figure 106. These rates were calculated for an aileron surface actuator when in the act of extending against the aerodynamic hinge moment at the given flight condition. In addition to the aerodynamic hinge moment these data include the characteristics of the actuator master control valves and the losses in the hydraulic lines between the pump and the actuators. The analysis is conservative in that the active stroke of the master control valve was used to determine the maximum actuator rates. The aileron actuator specification indicates a small rate increase for master control valve overtravel. Figure 107 shows the substantial improvement in aileron rate limit (about 40% at Mach 0.6) which is possible when hydraulic line losses are eliminated.

The deflection and rate limit plots show the common characteristics of decreasing capability with increasing Mach number. The abrupt decrease of maximum limits between Mach 0.8 and 1.0 is due to a sudden rise in the aileron hinge moment coefficient in the vicinity of Mach 1.
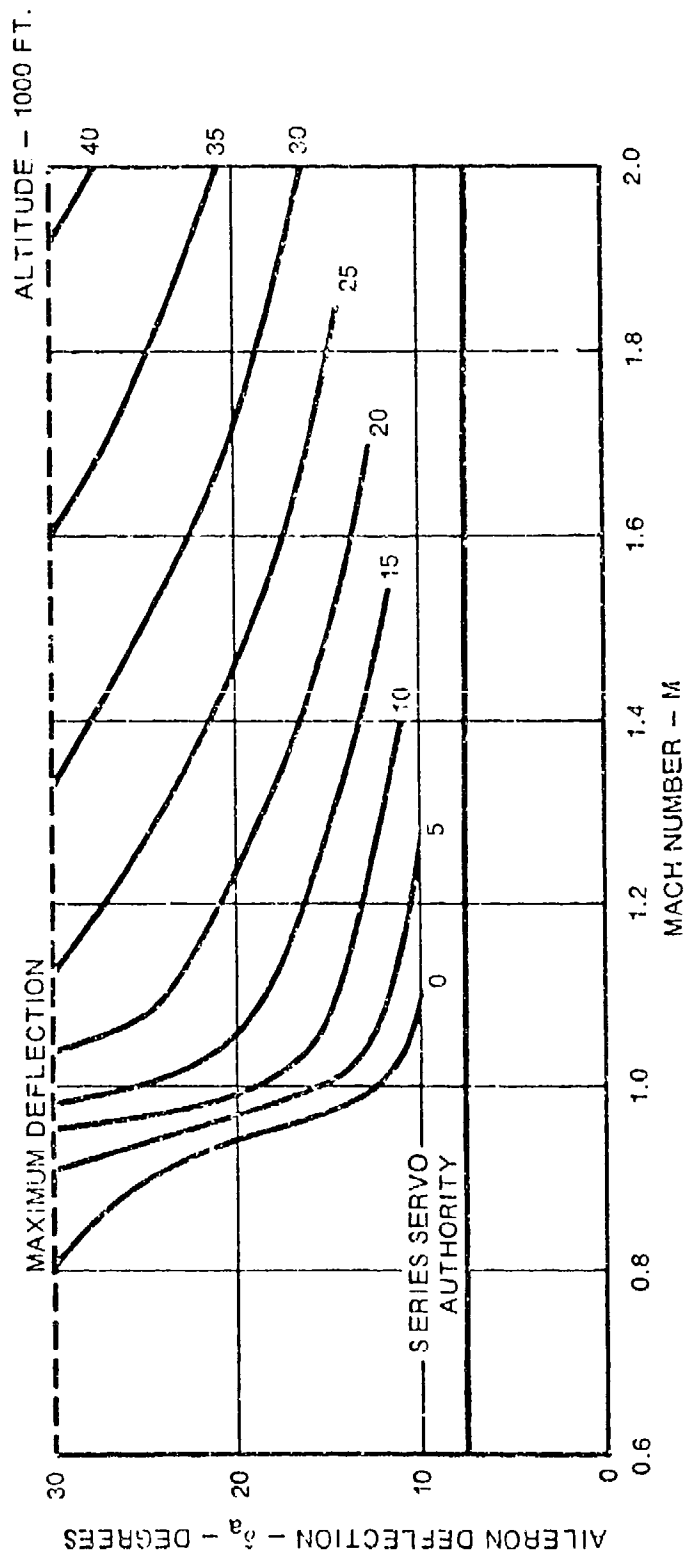
FIGURE 105 F-4 AILERON DEFLECTION LIMITS DUE TO AIRLOADS

FIGURE 106 F-4 AILERON RATE LIMITS WITH LINE LOSSES INCLUDED
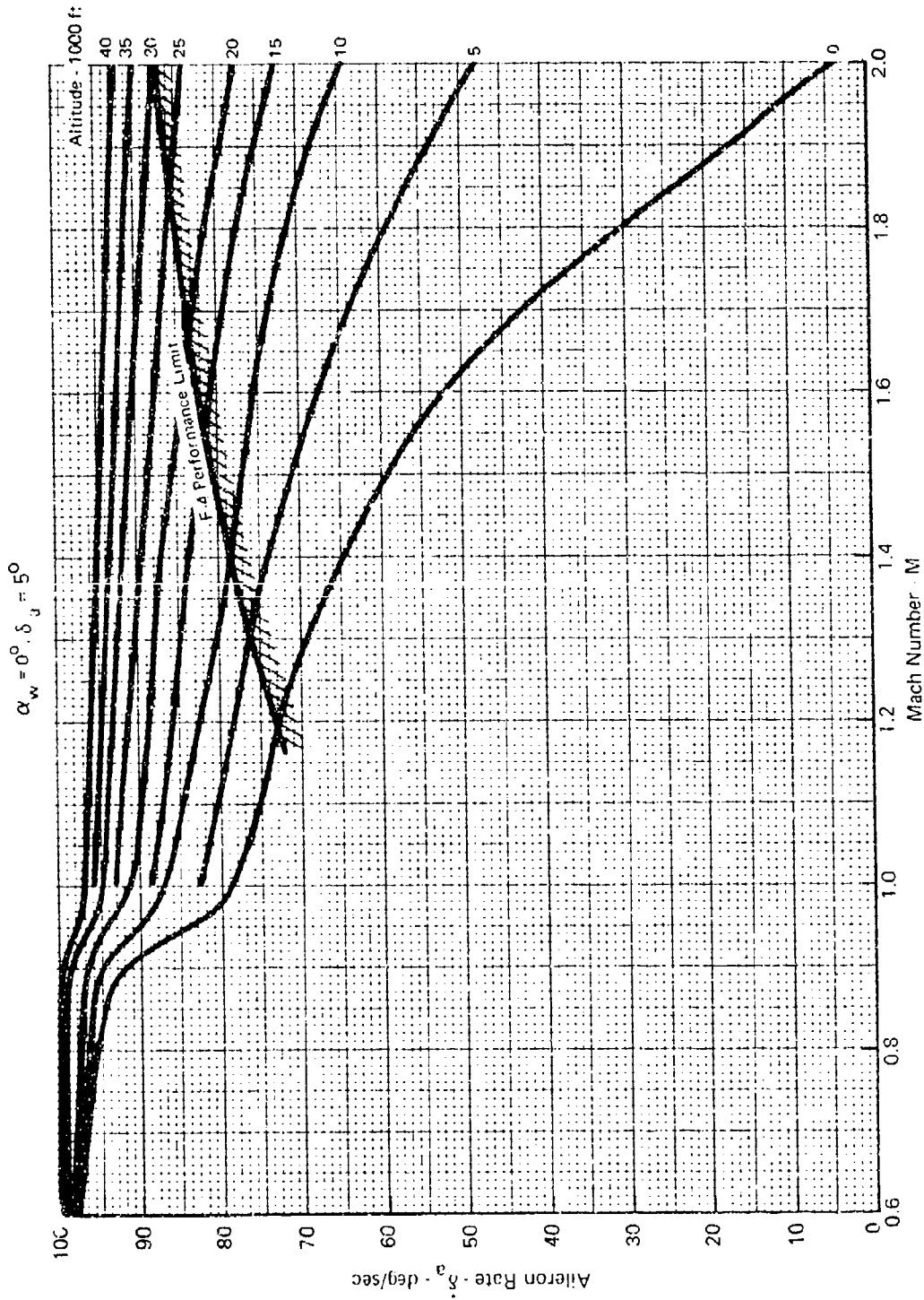
Note: Rate Limits Shown are with Flutter Damper Removed.

$\alpha_w = 0°, \delta_J = 5°$

Altitude - 1000 ft

Aileron Rate - $\dot{\delta}_a$ - deg/sec

Mach Number M

Note: Rate Limits are with Flutter Damper Removed.
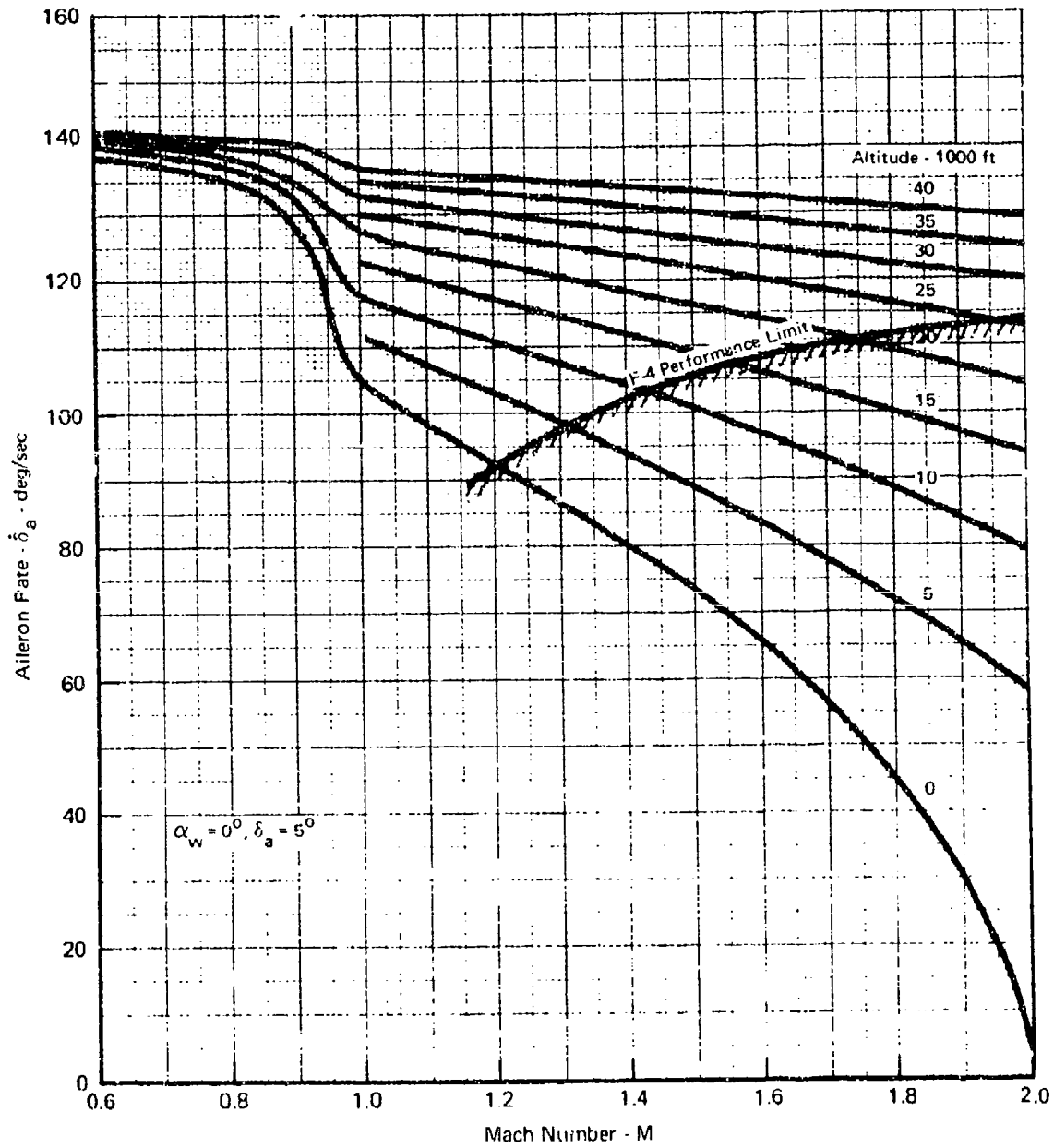
FIGURE 107 F-4 AILERON RATE LIMITS WITH NO LINE LOSSES

Spoiler Deflection and Rate Limits

The deflection limits for the spoilers are given in Figure 108.
These data show that the spoiler deflection of up to 30 degrees is possible
throughout the entire F-4 flight domain. Figures 109 and 110 give the
spoiler rate capabilities calculated in the fashion described above for
the ailerons.

Aileron Frequency Response Characteristics

The experimentally determined frequency characteristics for the
aileron power actuator are shown in Figure 111. A transfer function of
$1/1+.1S$ has been used in F-4 control system analyses to represent these
chara.ceristics. This transfer function which breaks down at 1.6 Hz is a
good approximation to the small signal character'.stic (.49 degrees double
amplitude, D.A.). A slightly larger bandwidth transfer function would better
match the larger signal characteristics (2.9. degrees D.A.).

5.3.1.2 Improvement Required for Hydraulic Systems - It is
emphasized that the improvements presented here are based on the good
engineering design rules discussed in Section 6.2. However, the
absolute necessity for these improvements for a practical flutter control
system is still an open question. It is unlikely that a final determination
can be made without subsequent wind tunnel and exploratory flight testing.

Aileron Power Actuator Bandwid h Extension

The control system design stuaies of Section 4.1 use a power actuator
frequency response transfer function of $1/1+.016S$ which is flat out to 10 Hz.
One of the possible methods of achieving this bandwidth extension is
illustrated in Figure 112. An electrical feedback loop containing an
LVDT (Linear Variable Differential Transformer) has been added around the
F-4 power actuator. An effective feedback gain of approximately 5.0 would
give the required 10 Hz bandwidth ($6.0 \times 1.6 = 9.6$).

Aileron Rate Capability Increases

The control surface rate limit is the single most critical design
constraint for a practical flutter control system. Every reasonable
system improvement which will improve these rate limits should be employed.
Some of the various system improvements possible are,

1) An accumulator

2) Orifice area increase

3) Valve redesign for larger pressure drop
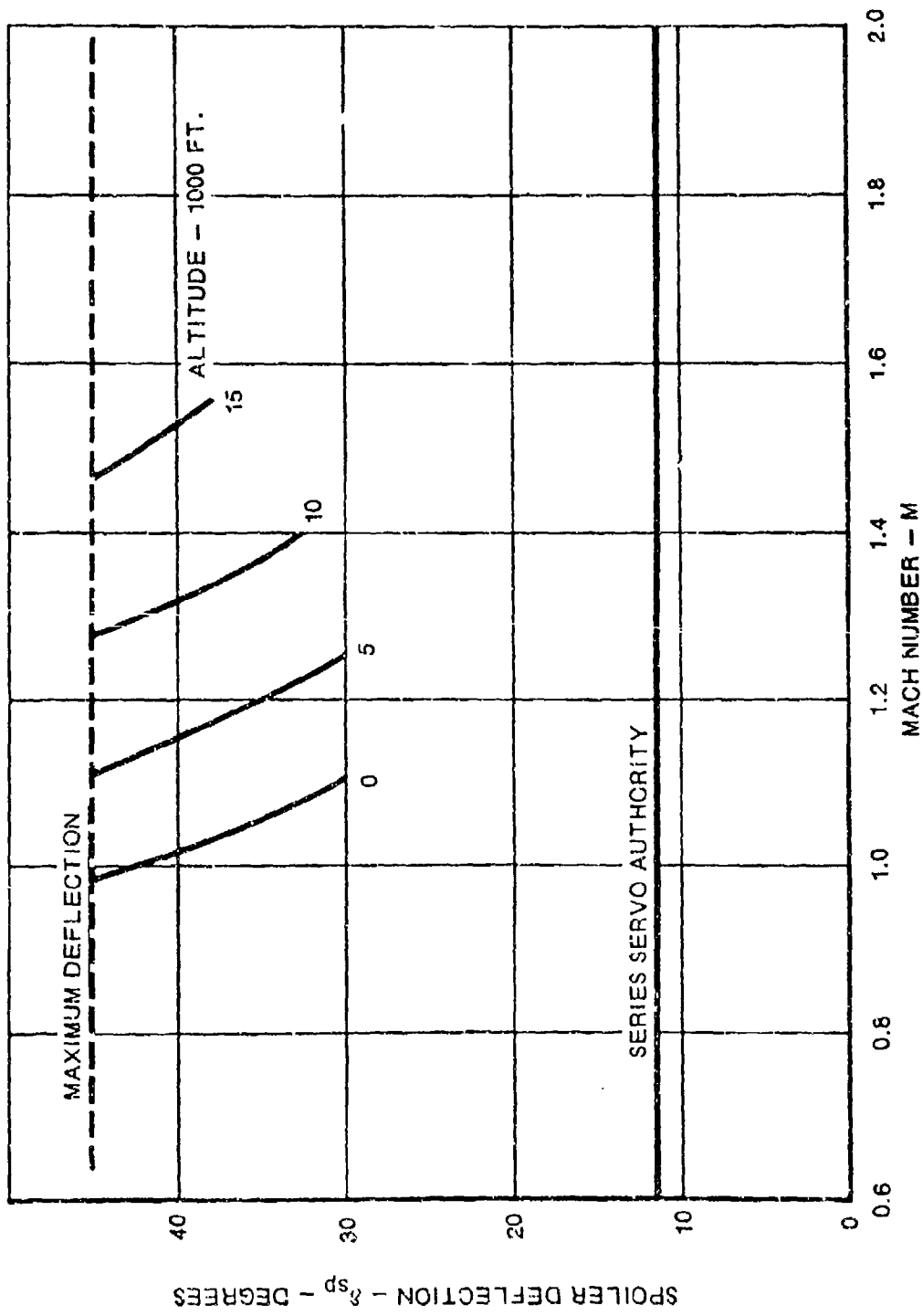
FIGURE 108 F-4 SPOILER DEFLECTION LIMITS DUE TO AIRLOADS
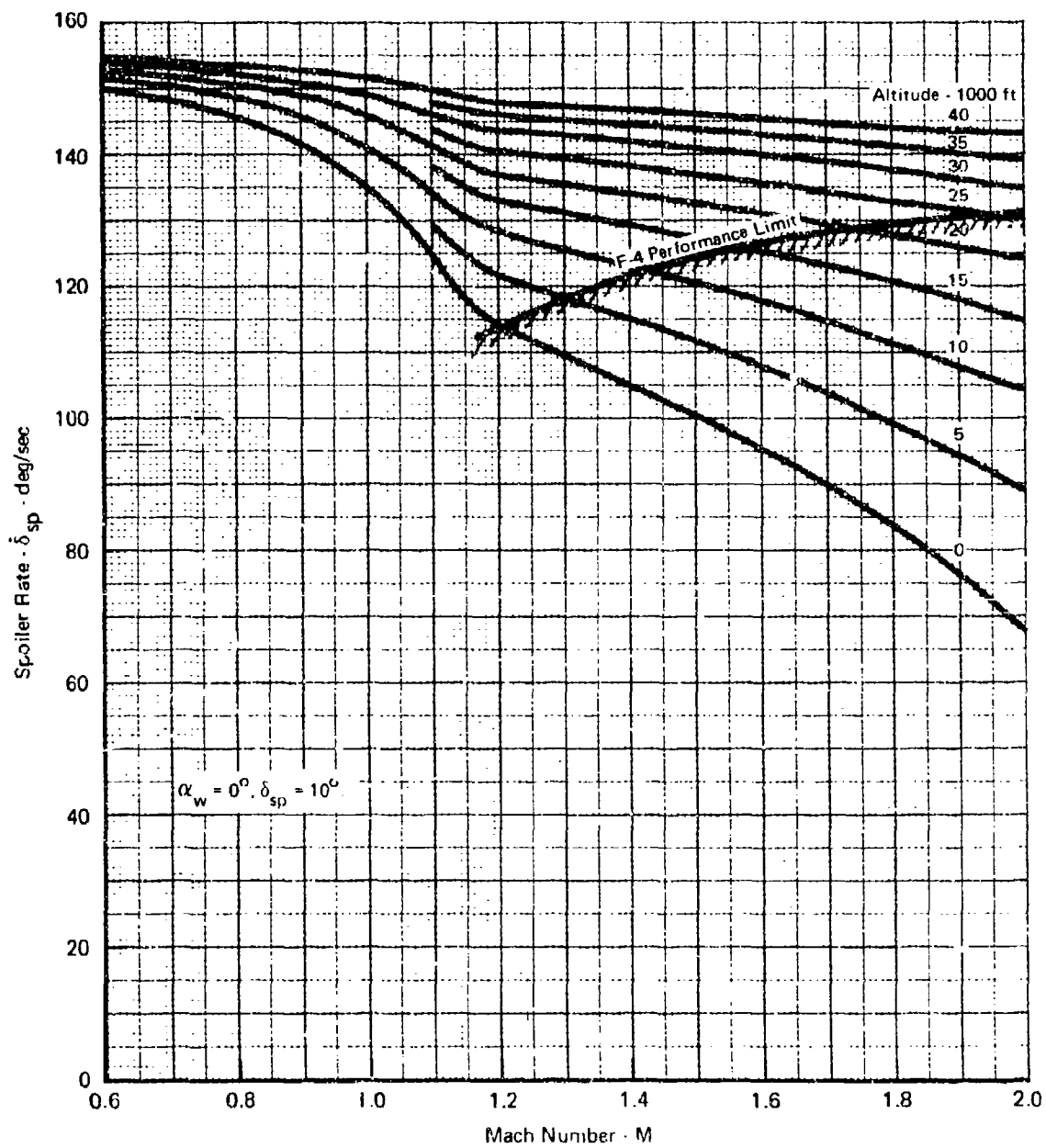
FIGURE 109   F-4 SPOILER RATE LIMITS WITH LINE LOSSES INCLUDED
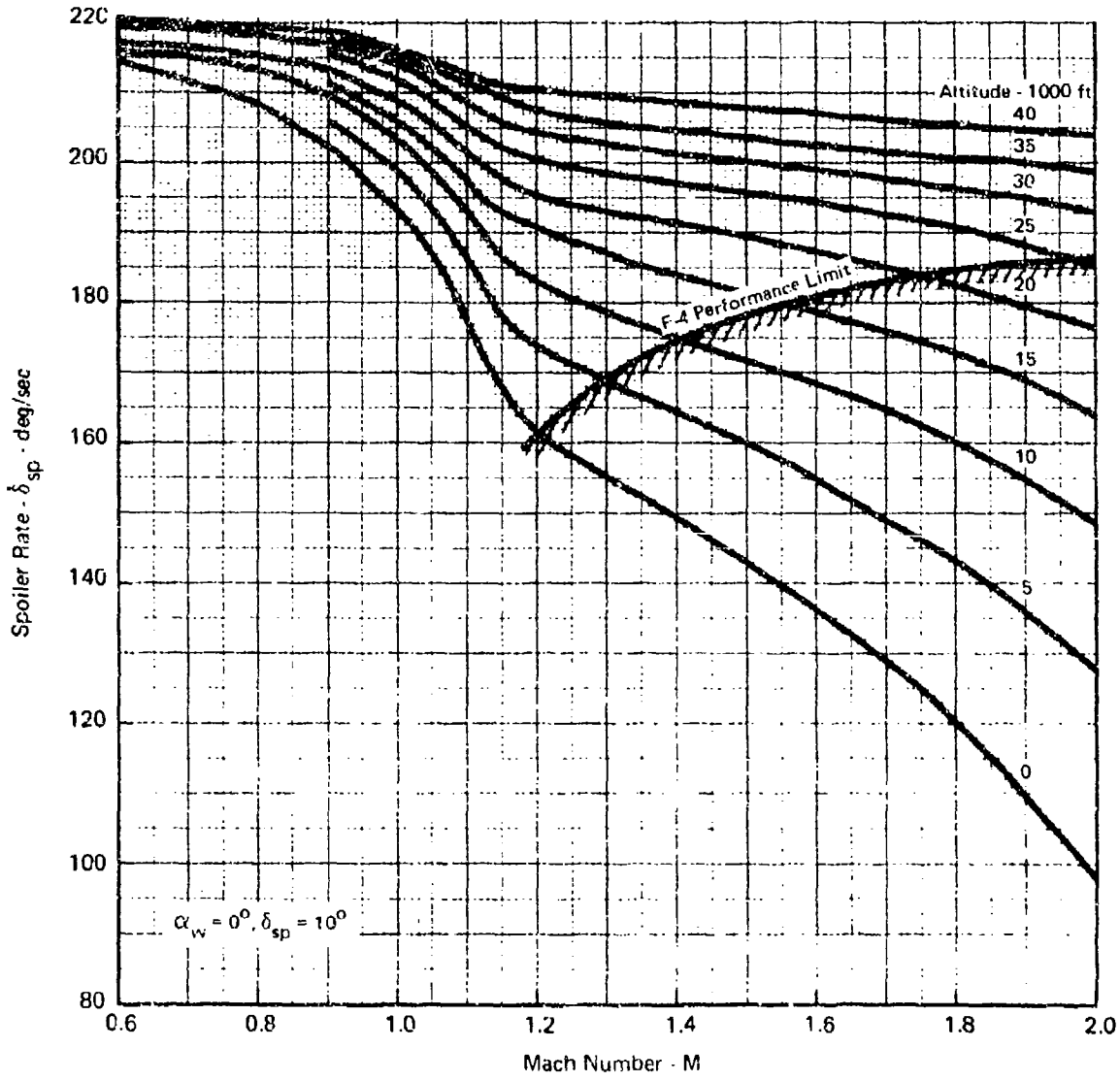
FIGURE 110   F-4 SPOILER RATE LIMITS WITH NO LINE LOSSES
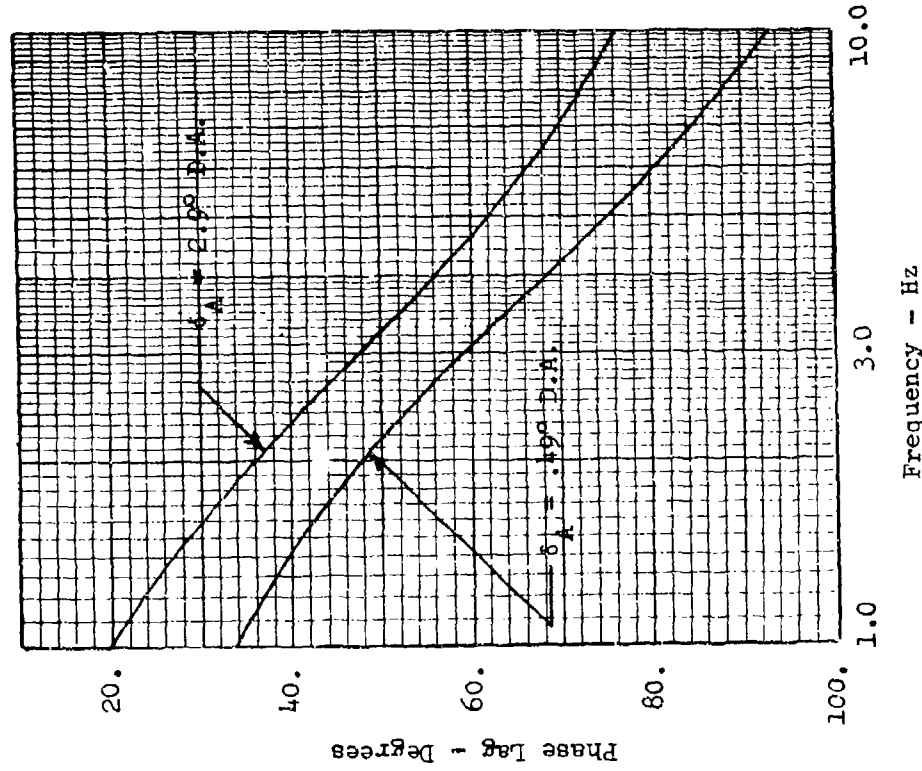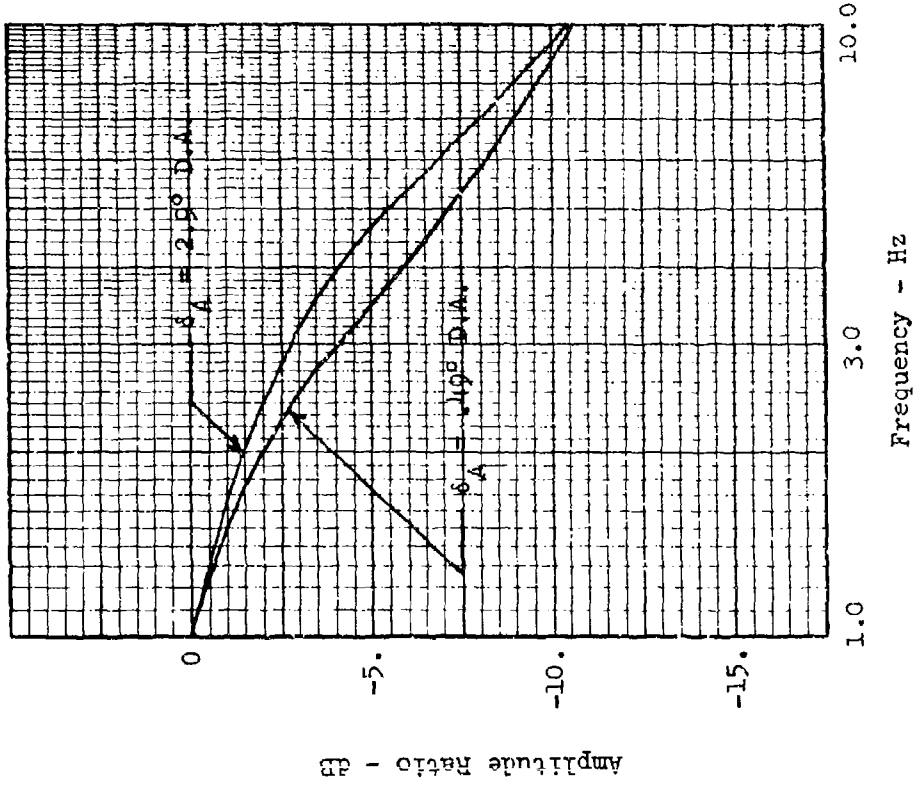
Note: Double amplitude is abbreviated as D.A.

FIGURE 111 F-4 AILERON POWER ACTUATOR FREQUENCY RESPONSE
CHARACTERISTICS ILLUSTRATING EFFECTS OF SIGNAL AMPLITUDE

194

FIGURE 112 BLOCK DIAGRAM ILLUSTRATING CONCEPT OF ACTUATOR
BANDWIDTH EXTENSION USING ELECTRICAL FEEDBACK
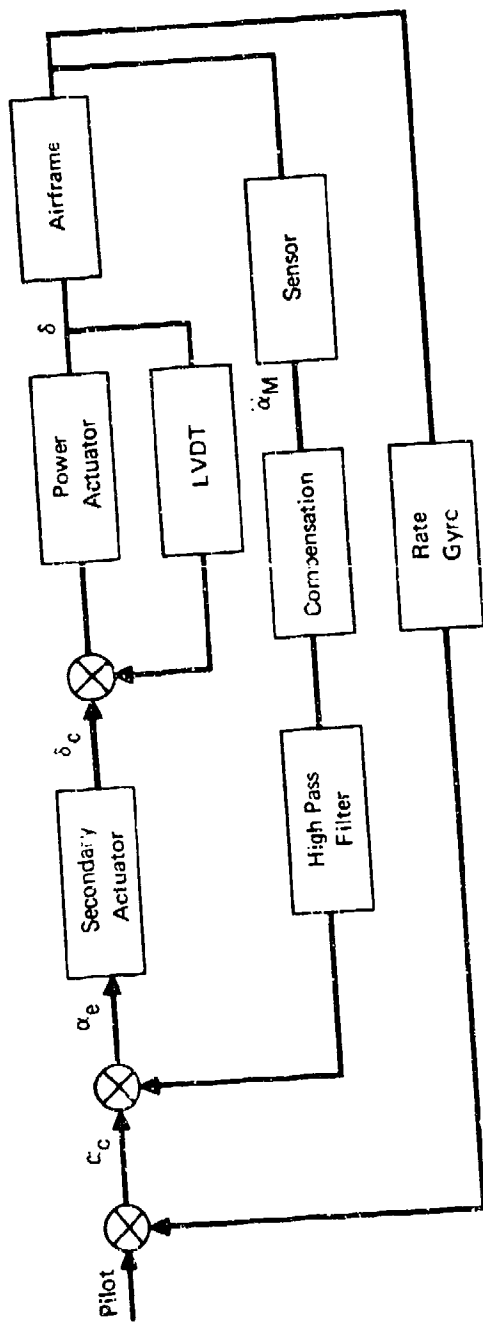
$$\frac{\delta}{\delta_{c_{w/o}LVDT}} = \frac{1}{1+\tau s} = G(s)$$

$$\frac{\delta}{\delta_{c_{w}LVDT}} = \frac{\frac{1}{1+\tau s}}{1+K\frac{1}{1+\tau s}} = \frac{1}{(1+K)+\tau s}$$

Note: K is the LVDT Gain

4) Larger hydraulic lines

5) Increased horn radius

6) Pump gear change

7) Larger pump.

These improvements are listed in a decreasing order of desirability. An accumulator, power actuator control valve redesign for a larger pressure drop,and increased orifice area are the most likely improvements which would be required for an operational flutter control system.

Replacement of Series Servo Actuators

For flight safety it is necessary to replace the F-4 series servo actuator (which would be shared by both the flight and flutter control systems) since it does not possess the redundancy/reliability required for active flutter control. A suitable substitute for the series servo actuator is the secondary actuator developed for the SFCS aircraft.

The secondary actuator is shown schematically in Figure 113. This actuator is a quadruplex, force-summing,hydraulically powered actuator which controls the aileron power actuator control valve in response to electrical signals from both the active flutter control system and the aircraft stability augmentation system. It also provides electrical information for off-line monitoring and comparison. The secondary actuator is comprised of four individual elements whose force outputs are summed through a rotary linkage as shown in Figure 113(a). This unit may be operated with three systems as considered in these studies with the F-4 aircraft. A cross section of a typical element is shown in Figure 113(b). The element is driven by a single stage jet pipe servovalve. The element has an LVDT to provide a position feedback signal.

The differential pressure across each element's piston head is monitored by a differential pressure sensor. The differential pressure is converted into an electric signal which is transmitted to the off-line monitors. When an element is in error, it will fight the other elements and its differential pressure will increase relative to the others. When the differential pressure exceeds a predetermined level, the monitor logic will indicate that the element has failed and initiate a shut down by de-energizing the element's solenoid operated shutoff valve. A more complete description of the secondary actuator is presented in References 5 and 15.

(a)

Yellow Element — Piston & Rod

Red Element

Output

Centering Mechanism

Output Arm

Black Element

Braking Mechanism

Summing Shaft

Blue Element

Rocker Arm

Mechanical Schematic

(b)

Piston
Centering Braking
Release

Pressure

Notes

1. Element output data (nominal)
   Piston area — 0.204 sq in
   Stroke — 0.500 in
   Force — 294 lb

Element
Output Piston

Position LVDT

2. Differential pressure sensor
   detection levels (nominal)
   90 psi — loss of pressure
   714 psi — normal operation
   930 psi —
   1000 psi —

3. The centering braking mechanism

4.

Differential Pressure Sensor

Differential Pressure Sensor LVDT

Hydraulic Schematic, Single Actuator Element

FIGURE 113 SCHEMATIC DIAGRAMS FOR SFCS SECONDARY ACTUATOR

197

5.3.2 <u>Structural and Flight Control System Modifications</u> - The
structural and flight control system modifications for the implementation
of flutter control systems in contemporary aircraft can be expected to be
restricted to local structural beef-up's and control system linkage changes.
In future aircraft, with full-time fly-by-wire power-by-wire flight control
systems, even these structural modifications may not be required. As developed
previously the secondary actuator of the SFCS aircraft could be used in the
flutter control system for an F-4 aircraft. The lateral control system
arrangement for the SFCS aircraft is shown in detail in Figure 114. The
secondary actuator, because of its bulk, must be located away from the
power actuator. New linkages are present between the secondary actuator
and the aileron power actuator. If a flutter control system uses this
lateral control system it is imperative that there be no structural
resonances in this linkage in the frequency range of the flutter mode. Free
play in the linkage should be kept to a minimum. The free play outboard of
the F-4 aileron power actuator is virtually zero because of the efficient
piano hinge attachment to the control surface and the relatively stiff
actuator support structure.

The feel spring cartridge has been moved to the aft cockpit area in
the SFCS aircraft as shown in Figure 114. For an active flutter control
system the feel spring should be as stiff as the pilot will accept. It
should also be located in the wing as close as possible to the summing
junction of the secondary actuator. These feel spring constraints are
required to prevent the diversion of secondary actuator mechanical signals
back to the pilot's stick instead of to the aileron power actuator spool as
desired.

Several possible control surface force producer concepts have been
shown to be feasible in the studies reported in Section 4. For implementa-
tion on the F-4 aircraft, the following four separate concepts show promise:

(1) Dropped aileron ($\approx$ 5 deg.) able to move in both directions.

(2) Existing aileron/spoiler combination.

(3) Aileron modified to move both directions with the spoiler dis-
abled.

(4) Aileron modified to move a limited amount of travel in the upward
direction ($\approx$ 5 deg.) before the spoilers are activated.
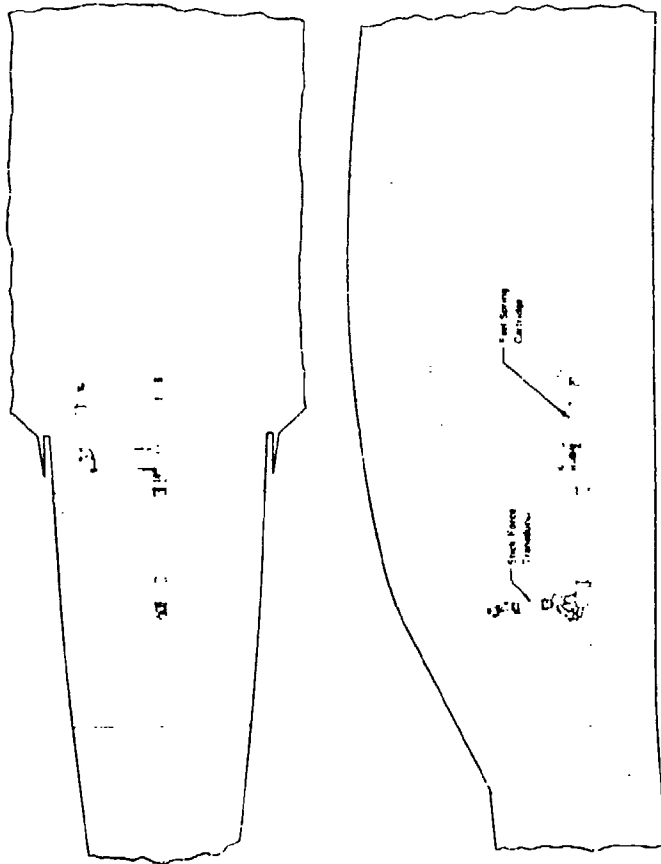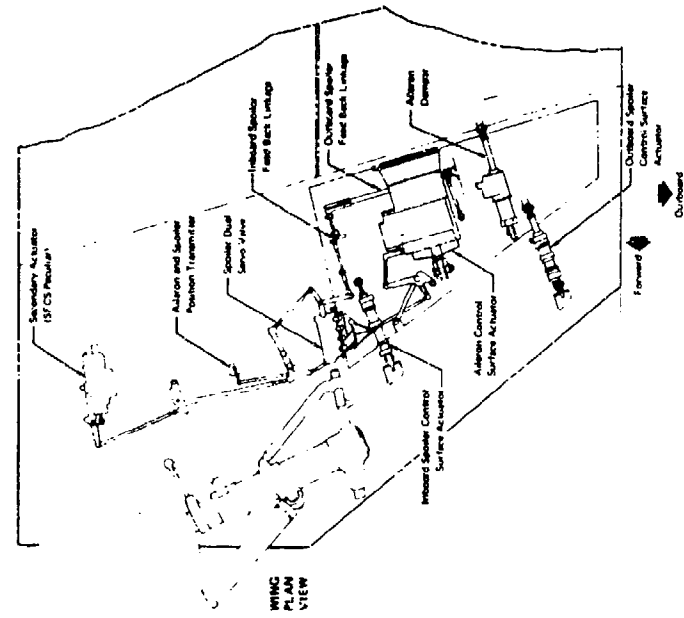
FIGURE 114 SFCS LATERAL CONTROL SYSTEM

The drooped aileron concept is the easiest to implement but is only practical for test flights, because of aerodynamic drag. The existing aileron/ spoiler combination is feasible as an operational solution. It can be expected, however, to require improvements in both backup structure and actuator hydraulics for two spoilers and one aileron actuator per side. The use of spoilers to control flutter may cause problems because spoilers possess highly nonlinear completely unknown oscillatory aerodynamic characteristics. The remaining two concepts require some structural modifications but otherwise are very promising as an operational solution since only the aileron is used in the flutter control system.

The detailed evaluation of each of these promising concepts is beyond the scope of these studies. A design engineering trade study needs to be performed to determine which concept is the preferred solution.

5.3.3 Realization of Electronic Components -- The electronic compensation networks used in the wing/store control system designs are easily assembled from passive elements such as resistors and capacitors and simple solid state operational amplifiers. The pure phase lag network used in these designs is shown in terms of operational amplifiers and potentiometers in Figure 115. The other control system components can be assembled from passive elements only and are not shown since they are adequately described in the literature for analog computers.

The detail design of the flutter control system Computer Voting Units is beyond the scope of these studies. They will contain, however, at least the following items:

(1) Analog computer circuitry to implement the flutter system control laws.

(2) Voter units.

(3) Servo amplifiers to interface with the electro-hydraulic secondary actuators.

(4) Power supplies, oscillators, and converters to generate all of the required electrical signals for the entire flutter control system.

(5) Provisions to interface with both pilot initiated and ground test circuitry.
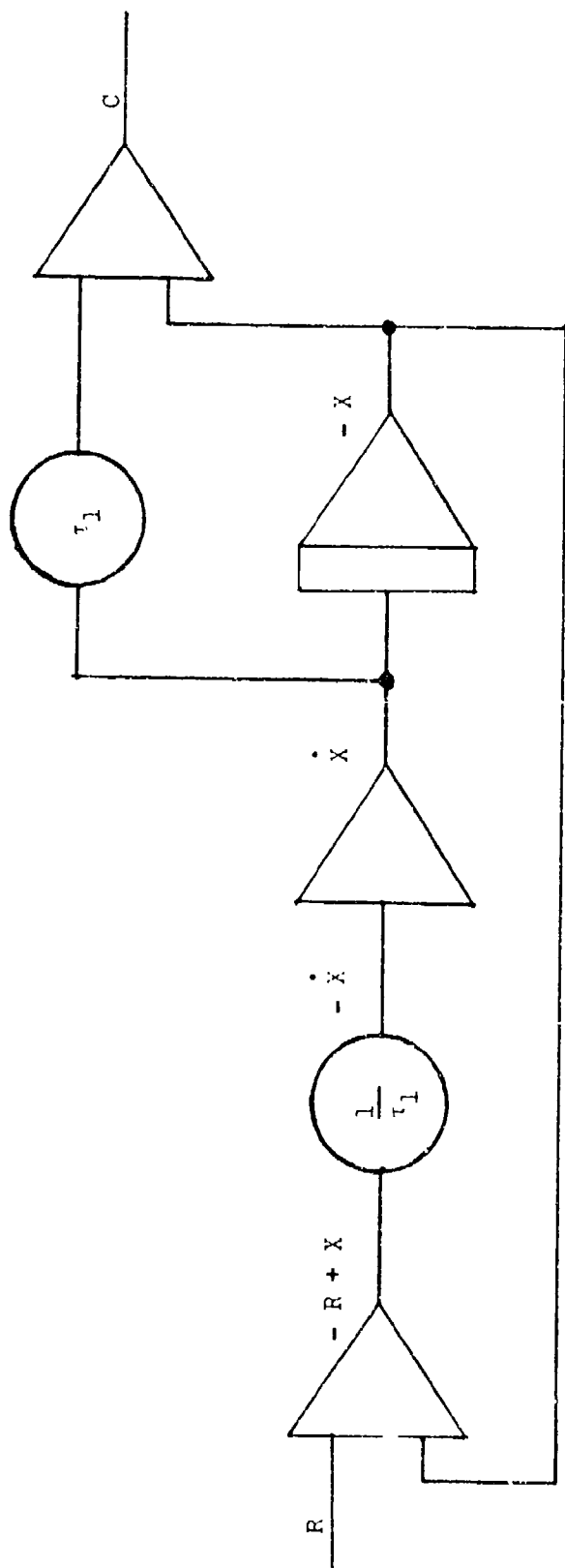
$$C = X - \tau_1 \dot{X}$$

$$\dot{X} = \frac{1}{\tau_1} (R - X)$$

$$\frac{C}{R} = \frac{X - \tau_1 \dot{X}}{X + \tau_1 \dot{X}}$$

FIGURE 115 PURE PHASE LAG NETWORK REALIZATION $-\dfrac{(1-\tau_1 S)}{(1+\tau_1 S)}$

(6) Comparators to monitor the voter units and apprise the pilot of any system failure.

(7) For flight test only, the electronic buffers required for interface with the flight test instrumentation.

5.3.4   Phase Margins and Sensitivities - MCAIR experience with fighter aircraft control systems indicates that phase margins of ±45 degrees are justified design criteria when analytical studies include control system nonlinearities. For linear analytical studies a phase margin of ±60 degrees can be justified. These phase margins have been considered as preliminary design guidelines in these flutter control studies.

Phase stabilization in one form or another is required for active flutter control. By phase stabilization we mean that a feedback signal commands a force producer with phase characteristics so that the response to the force producer has a stabilizing effect.

5.3.4.1   Control System Phase Uncertainties - The phase sensitivity to parametric variations in control system components was determined for a typical flutter control system of the general type presented in Figure 15. To guarantee a conservative evaluation, the following pessimistic tolerance values were used:

  $\pm$ 10% on gains

  $\pm$ 20% on time constants.

The control loop for the particular case considered is given in Figure 116. This is the improved power actuator case of Reference 14. The accelerometer (80 Hz), secondary actuator (36 Hz) and the lag compensation numerator (202 Hz) were not varied in this study since they are outside the frequency range of interest (0 - 25 Hz). Each parameter in the control loop was varied and the deviation from nominal of the open-loop frequency response was determined in both gain and phase. The RSS (Root Sum Square) value for these individual deviations was found to be less than 19 degrees in phase and 1.5 dB in gain for frequencies up to 25 Hz. RSS implies that the error sources are independent and hence the variance of the sum is the sum of the variances. These data indicate that somewhat less than 20 degrees phase uncertainty should be easily achieved for the general type of control systems being considered if quality components are used in the control loop electronics.
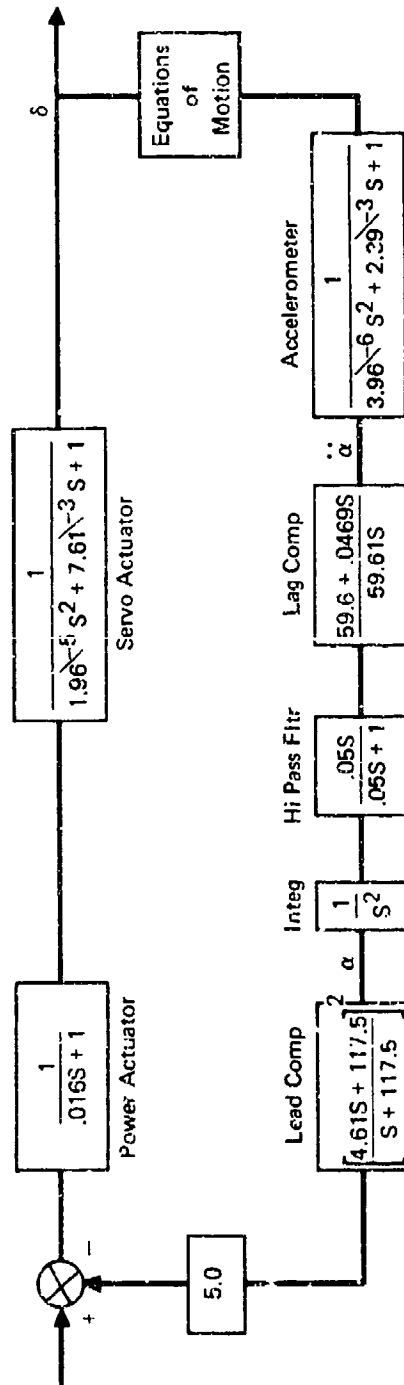
FIGURE 116 CONTROL LOOP FOR PHASE SENSITIVITY EVALUATION

203

5.3.4.2 <u>Power Actuator Sensitivities to Signal Size</u> - Experimental
frequency response test results are shown in Figure 111 for the F-4
aileron power actuator. Phase lag and amplitude ratio are shown for both
small (.49 degrees) and large (2.9 degrees) double amplitude motion. The
maximum phase variation with signal size is on the order of 15 degrees over
the entire frequency range from 1 to 10 Hz. This effect is in addition to
the previously defined RSS phase uncertainties, that is $\sqrt{19^2 + 15^2} = 24.2$
degrees. This value is still well within the study design guideline of
±45 degrees phase margin when nonlinearities are included in the analysis.
The corresponding gain variation is on the order of 1.5 dB at 4 Hz but
near zero in the vicinity of the flutter frequencies at 8-10 Hz.

5.3.4.3 <u>Flutter Mode Frequency Uncertainties</u> - Phase uncertainties
in a flutter mode can be adequately compensated for by control components
with slowly changing phase over the frequency range of the flutter mode.
For a particular dynamic configuration at a specified flight condition,
the trajectory on a Nyquist plot would be in roughly the same location
whether the flutter occurred at say 8.5 Hz or 9.5 Hz, assuming <u>all</u> other
components in the control loop have approximately the same phase angle at
both 8.5 Hz and 9.5 Hz.

A test computer run has been made to evaluate phase uncertainties caused
by flutter mode frequency uncertainties. For this test run, the zero air-
speed frequency of the mode which goes unstable was changed from 8.78 Hz to
9.78 Hz. The control system was the design of Reference 14 with the
improved power actuator and with g = 0.0. Flutter occurs for this modified
system at a frequency of 9.05 Hz compared to 8.33 Hz for the nominal case.
The appearance of the Nyquist plots is essentially unchanged and indicates
stability for all velocities through 300 KEAS just as for the nominal case.
This run demonstrates that active flutter control is feasible even if the
flutter frequency is not precisely defined provided that it is the only
unknown variable in the system. It has been previously established in
Reference 14, Figure 7, that precise knowledge of the flutter onset
velocity is not required in any case.

5.3.4.4 <u>Aeroelastic System Phase Uncertainties</u> - As developed above,
the control system electronic components can be easily made to have a very
small phase uncertainty. In addition, full-scale ground test data for both

the electronic and hydraulic components can be credibly related to flight vehicle hardware. The only unresolved phase uncertainties are those which are generated by the variable and unknown aeroelastic characteristics of the aircraft.

There is, however, a particular characteristic of the control system open-loop frequency response function which is suitable for use in eliminating virtually all of the remaining aeroelastic phase uncertainties in both wind tunnel models and operational flight vehicles. This characteristic is illustrated by the Nyquist plots of Figure 117. For flight velocities below the flutter velocity (V_F), the Nyquist loop associated with the potentially unstable mode closes in a clockwise (CW) direction. At very low velocities, the plot may look like a "can of worms" and the significant modes may be difficult to determine. As the airspeed increases, the potential flutter mode becomes the single most predominant loop. As flutter is approached, the loop becomes progressively larger. It becomes infinite, and the direction of closure changes to counter-clockwise (CCW) when flutter onset is reached. As the velocity increases further into flutter, the loop becomes progressively smaller. The most significant characteristic of this transition is that the unstable post-flutter loop is 180 degrees out of phase with the stable sub-flutter loop. This characteristic has been observed in the ACF computer program runs regardless of the number of potentially unstable modes or of the number of included degrees of freedom.

Nyquist plots such as those given in Figure 117 show at a glance the required phase change for flutter control. If the control system compensation is adjusted to locate the sub-flutter loop-of-interest with its major axis along the positive real axis, the post-flutter loop will be in the desired position with its major axis along the negative real axis. We expect that a wind tunnel test engineer can, with the use of a Nyquist Plot display of the type shown in Figure 117, eliminate the effects of the aeroelastic system unknowns.

5.4 Flight Safety Considerations

Flight safety is a paramount design consideration for active flutter control systems. It is a consideration which affects the basic system complexity and redundancy and thus ultimately its total weight and cost. Some level of system redundancy is required because of the catastrophic nature of the flutter phenomena which demands continuous control when deep in the flutter region.

$v_F + \epsilon$

$v_F - \epsilon$

Required Phase Change for Control

Sub-Flutter

Post-Flutter
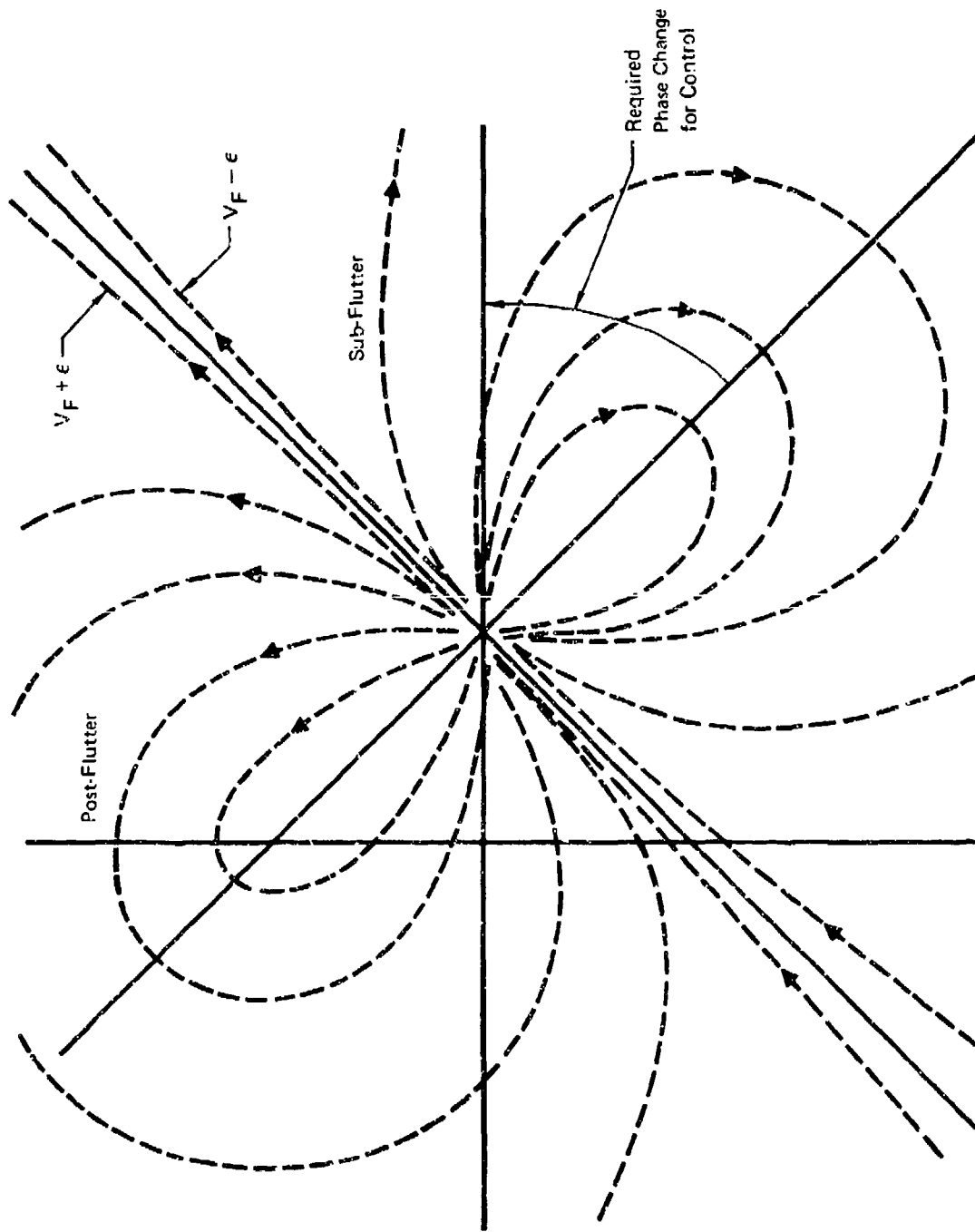
FIGURE 117 PLOT ILLUSTRATING NYQUIST LOOP CHARACTERISTICS FOR VARIABLE AIRSPEED

The order of the system redundancy is a function of the design criteria for flight safety. The design guidelines which have been considered in these studies are given in Section 3.1.3. The basic goal of these preliminary guidelines is to use a minimum number of redundant control system components to guarantee a failure rate of less than one catastrophic failure (loss of aircraft) per million flight hours. The nature of flutter is such that continuous control is required for each aileron when the aircraft is in the flutter region. This requirement is much more demanding than the SFCS fly-by-wire requirement which allows individual aileron failure.

5.4.1 Reliability Data and Analyses

5.4.1.1 Component Failure Rates - To lend credibility to the reliability assessment we have used published data for the SFCS F-4 aircraft as given in Reference 5, page 39.

The failure rates of particular significance for active flutter control on the F-4 aircraft are shown below:

	Component Failure Rate (per 10^6 Hrs.)
Aircraft AC Electrical Supplies (Dual)	14.0
Engine Flameout	30.0

If the active flutter control system on an F-4 aircraft included only the two items listed in the failure rate table above, the system failure rate would already be 44 per million flight hours. The failure of an active flutter control system during post-flutter velocity flight implies loss of the aircraft unless the flutter mechanism is disrupted. Thus, if a wing/store mechanism is being controlled, a high flutter control system failure rate might be acceptable if the stores were automatically ejected upon system failure. Alternately, the aircraft loss probability could be minimized by removing high failure components from the flutter control system.

5.4.1.2 Automatic Store Ejection - If an automatic store ejection system with a failure rate of less than 1000 per 10^6 hours were included in an active flutter control system, a 44.0 per 10^6 hours failure rate could be reduced to much lower than the target 1.0 per 10^6 hours. The failure rate for the operational F-4 store ejection systems, considering only those failures attributable to inadvertent store ejection and hung stores, is less than 20 per 10^6 hours. Store ejection would probably be impractical,

207

however, for anything other than a 1-g level demonstration test flight. Ejection placards exist for nearly every flutter restricted store configuration. These placards are required because of the tendency toward store aft-end-up rotation during ejection for some aircraft angles of attack. This motion creates the danger of impact of the store with the wing trailing edge. The adverse tail-up rotation is attributable primarily to the aerodynamic loads on the store and not the ejection impulse. Because of this, even if for no other reason, it is clear that automatic store ejection is not a satisfactory means of achieving the desired level of reliability in an operational sense.

5.4.1.3 Elimination of High Failure Rate Items

Aircraft AC Electrical Supplies

A schematic of a possible flutter control system is shown in Figure 118. As indicated in the figure the only electrical power required for the system to operate is the 28 volts DC for the Computer Voter Units and the system AC power supply. The CVU's include both the voter circuits (necessary to operate the secondary actuator) and also the flutter control system electronic components: compensators and high pass filter. The system power supply provides the AC electrical power needed by the motion sensor and the Linear Variable Differential Transformer. The flutter control system could operate for a limited time (until the aircraft was slowed to a sub-flutter velocity) on a small 28 volt emergency battery supply. The incorporation of such a battery into the flutter control system is essential to eliminate AC power failure as a critical failure mode. The aircraft AC power system normally provides the DC power to the active control system by means of transformer/rectifiers.

Engine Flameout

Engine flameout, with a failure rate of 30.0 each million flight hours, causes a loss of the hydraulic pumps so that the hydraulic systems are forced to rely on the stored energy in accumulators, power control reservoirs, and engine rotary inertia. This provides a continuous, decreasing hydraulic pressure for the aircraft which is also, because of the engine flameout, rapidly losing speed and thus stabilizing flutter. Calculations show that a clean F-4 will slow from 800 to 600 KEAS in about 20 seconds at sea level. An F-4 with external stores would decrease
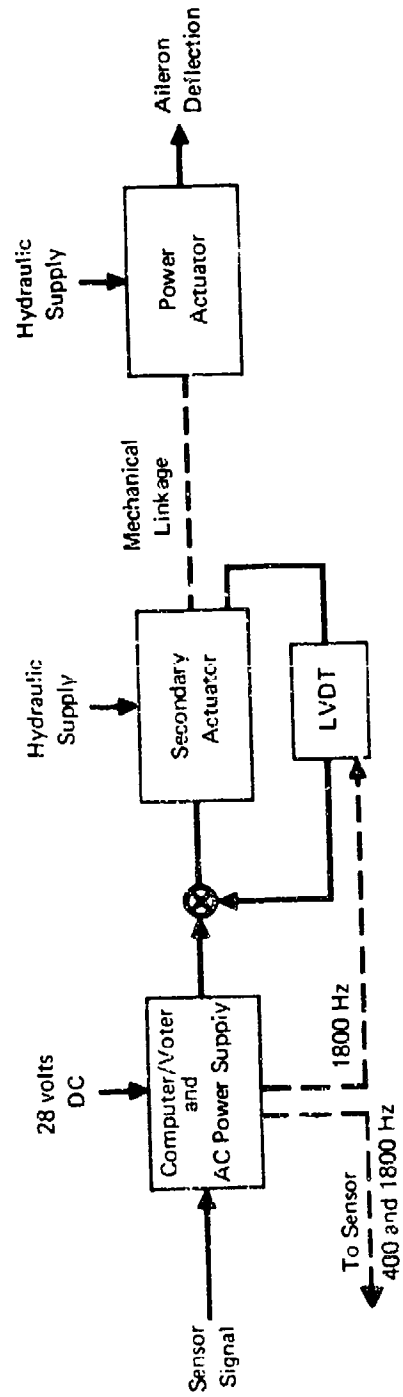
FIGURE 118 SCHEMATIC OF AILERON ACTUATION SYSTEM

speed even faster. The engine speed, as a function of time after flameout, is shown in Figure 119. This plot was taken from Reference 15.

It is seen that a minimum of 40% RPM is available to drive the hydraulic pumps 20 seconds after flameout. The pumps, which have a linear flow characteristic with speed, will thus furnish 10 gallons per minute to each hydraulic system for 40% engine RPM. If we assume that other aircraft demands are minimal, each aileron power actuator will be able to use nearly 20 gallons per minute from its two available hydraulic systems.

It has been shown (Section 4.1.2.4) in rate limited time domain runs with the 370 gallon tank-90% full case that flutter control can be maintained with aileron rate limits as low as 60 deg/sec even though the limits are invoked as much as 50% of each cycle of motion. Calculations based on the 60 deg/sec limited case give maximum flow requirements of 14 gallons per minute during the first second after the gust excitation. It may thus be concluded that flutter control will be maintained during the aircraft slowdown following engine failure provided other aircraft hydraulic demands are small while the aircraft is flying through severe turbulence.

5.4.2 Voter Logic and Redundancy Requirement

5.4.2.1 Voter System Concept - It is assumed that a practical flutter control system specification will require that the first failure in the control system loop will create a condition in which there is no critical degradation of system performance. A triply-redundant electronic configuration is required to satisfy this one-fail-operate performance criterion. This is true since it is not possible to recognize the good signal with only two signals to compare.

One procedure for voting is described in detail in Reference 5, pages 101-115. This procedure, which is based on quadruply-redundant systems, could be readily adapted to triply-redundant systems. For triply-redundant systems, however, the voting procedure can be greatly simplified by using solid-state transistor diodes (or possibly even integrated circuits) instead of the feedback operational amplifiers of the SFCS (Reference 5) voting system. A conceptual voter block diagram is shown in Figure 120. The "AND" circuit chooses the more negative of the two input signals while the "OR" circuit chooses the most positive of its three input signals. If any failure should occur, the failed signal will be greatly different from the other two signals and will thus be either the most positive or the

210

The chart shows Engine Speed % RPM (vertical axis, 0 to 100) versus Elapsed Time after Flameout - Sec (horizontal axis, 0 to 100).

Labels on chart:
- Ground Idle Speed
- Generator Drop Out
- Variation in Decay Rate Observed Inflight
- Effect of Extracting 10 Additional HP
- Nominal Minimum Restart
- 51 Sec
- 63 Sec
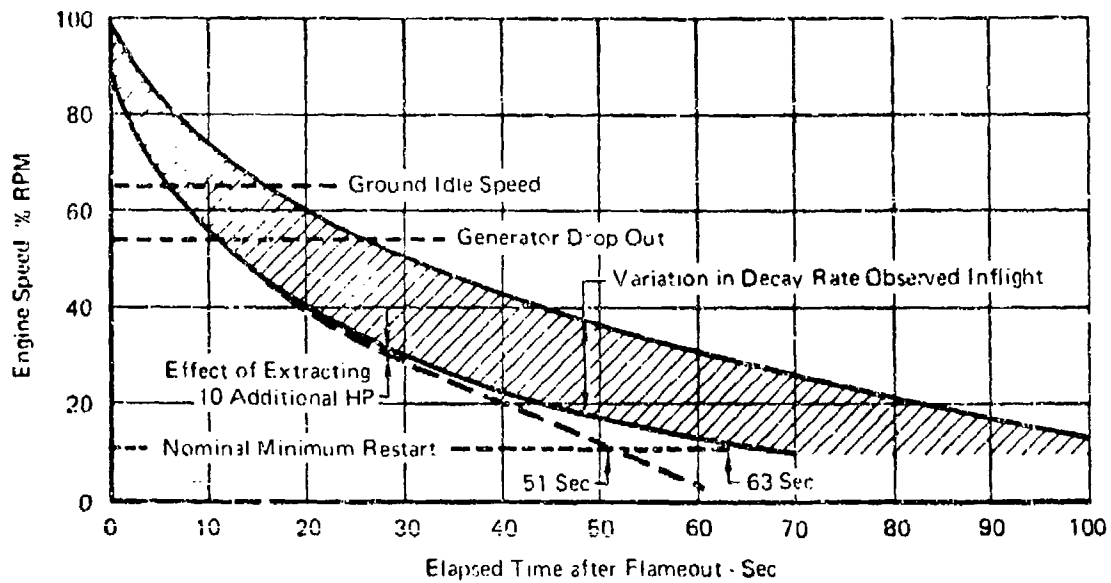
Altitudes = 5,000 Ft thru 55,000Ft.
Mach No. = .3 thru 1.2

FIGURE 119 ENGINE WIND-DOWN CHARACTERISTICS
FOR F-4 J-79 ENGINES

most negative of the signals. Since the failed signal cannot be the mid-value signal, it is instantaneously rejected whether it be a hardover in either direction, an open circuit, or just an out-of-tolerance partial failure. Since the failed channel is voted out on an instantaneous basis, uninterrupted, undegraded, full-signal performance is assured and no transient is experienced in the loop even without detection of the failure.

5.4.2.2 <u>Off-Line Comparator Concept</u> - The pilot, however, must be apprised of the failure to allow him to respond to the warning and reduce the speed of the aircraft. Off-line comparators, which show an output only when the difference of two signals being compared is greater than a preset tolerance amplitude, are suitable for this monitoring requirement. Although there are other possible schemes for failure detection, the cross-voter monitoring concept illustrated conceptually in Figure 121 is the most appropriate for this application. In this concept, a signal failure will be detected by the off-line comparators in the same channel in which the failure occurs. For example, consider the case where all three signals are initially within the preset tolerance band of the comparators. If now any one of the three signals leaves the tolerance band, one of the two remaining signals still within the band will become the common mid-value output signal. The voltage across the comparator in the failed channel will thus exceed the tolerance and cause the failure signal to be initiated.

5.4.3 <u>Practical Multiply-Redundant Flutter Control System</u>

5.4.3.1 <u>System Description</u> - In the previous section an argument was made that a triply-redundant electronic configuration would be adequate for a flutter control system. A conceptual flow diagram for such a system is shown in Figure 122. The control loop is triply-redundant from the sensors through the secondary actuators. It becomes a single path at the secondary actuator force-summing output shaft. The mechanical linkage which adds the pilot's commands to the flutter control system commands is part of this single path section. The loop becomes doubly-redundant at the aileron actuator to complete the circuit. Individual DC electrical sources and hydraulic power supplies are required for the operation of the flutter control system. The additional components shown in this figure, referenced to an operational F-4 aircraft, are the sensors, computers, secondary

"And" Chooses the More Negative of the Two Signals

"Or" Chooses the Most Positive of the Three Signals

Output is the Instantaneous Mid-Value Signal
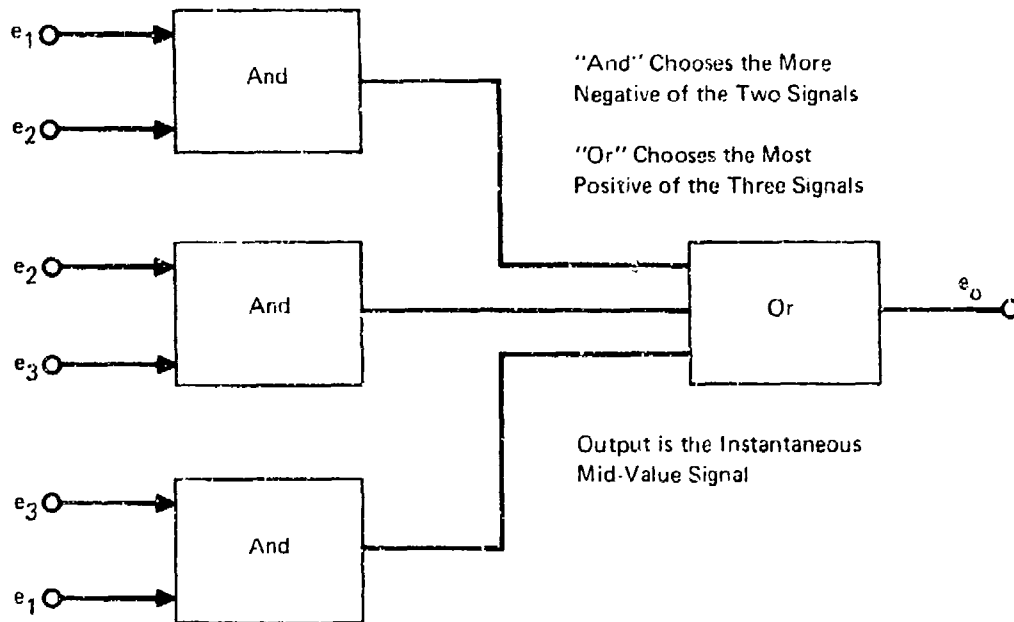
FIGURE 120 VOTER CONCEPTUAL BLOCK DIAGRAM
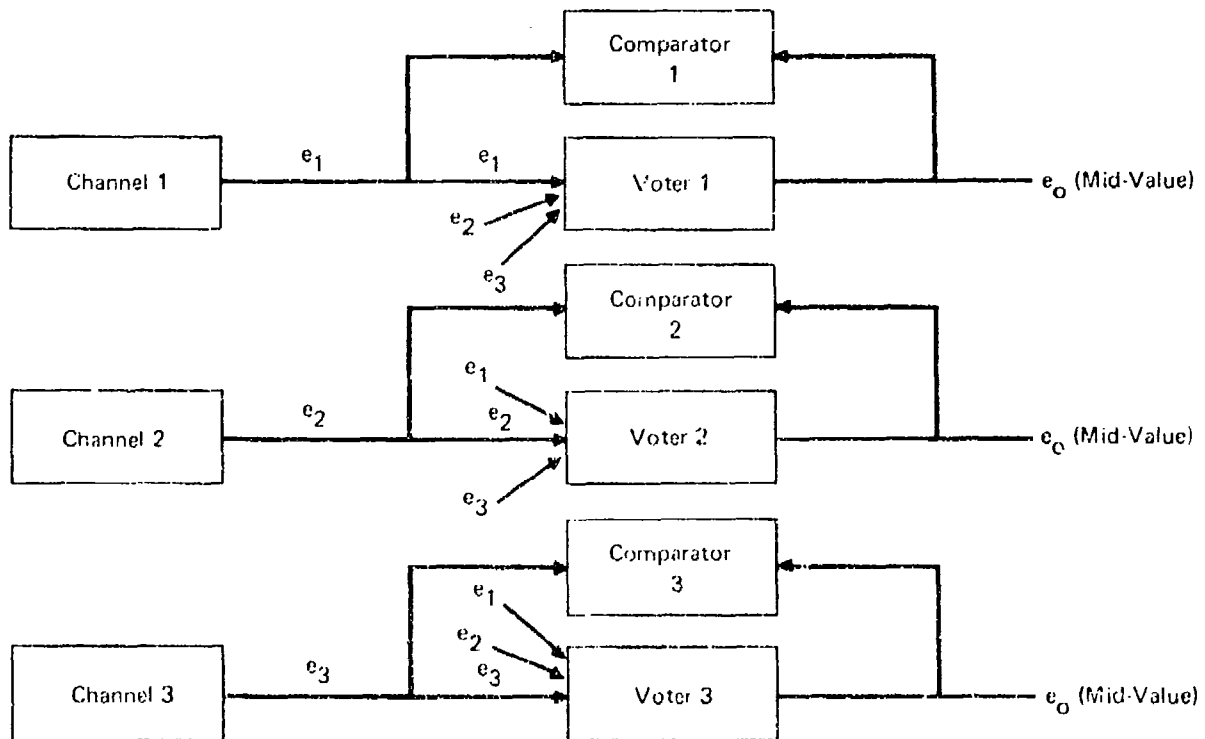
FIGURE 121 CROSS-VOTER MONITORING CONCEPT
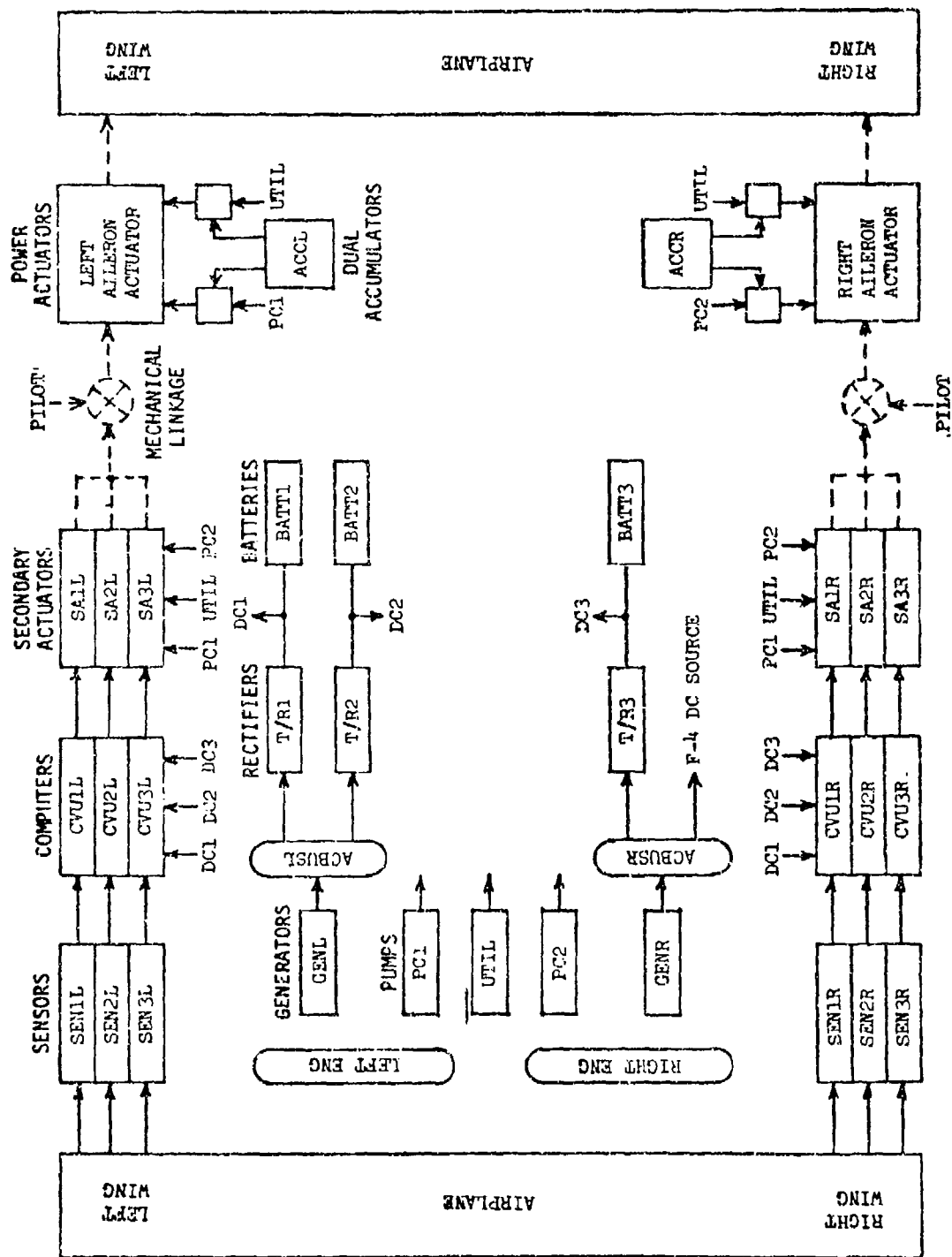
FIGURE 122 CONCEPTUAL FLOW DIAGRAM FOR WING/STORE FLUTTER CONTROL SYSTEM

214

actuators, transformer/rectifiers, batteries, and accumulators. The batteries, which furnish the emergency DC power to the Computer Voting Units, must be maintained by rigidly scheduled inspection and servicing to ensure their availability as the backup system.

Switching is provided in this system which would automatically connect the remaining good bus to the failed bus in the case of a single generator failure. This eliminates the need for battery power, except possibly during the switching process, for anything other than complete loss of aircraft AC power.

5.4.3.2 <u>Failure Analysis</u> - The complete catastrophic failure table for the conceptual system sketched in Figure 122 is shown in the table below. Notice that AC electrical supply failure and engine flameout have been eliminated.

CATASTROPHIC FAILURE RATE TABLE PER SIDE FOR ACF SYSTEM

Component Description	Number of Channels	Failure Rate per Channel (per 10^6 Hrs.)	Collective Component Failure Rate (per 10^6 Hrs.)
Secondary Actuator	3	250	.00002
All Mechanical Linkages	1	.01	.01
Aileron Actuator	1	.10	.10
Hydraulic Power Loss	2	NA	.004
Sensors & CVU's	3	10,000*	<u>1.000</u>
		Total/Side =	1.114
		Total/Aircraft =	2.228

* Sensor and <u>C</u>omputer <u>V</u>oting <u>U</u>nit Failure Rate, computed below.

Component Description	Number of Elements	Failure Rate per Element (per 10^6 Hrs.)	Collective Channel Failure Rate (per 10^6 Hrs.)
Passive elements	40	125	5,000
Active elements	10	500	<u>5,000</u>
		Total =	10,000

All of the failure rates shown, except those for the sensors & CVU's, are taken from Reference 5, page 39. The sensor & CVU failure rate computation was made according to the assumed model given below the table. Sensors, operational amplifiers, and Linear Variable Differential Transformers are considered to be active elements while resistors, capacitors, and

215

transistors are considered to be passive elements. The one failure per 100 hours for the Sensor-CVU combination (10,000 failure/10^6 Hrs.) is really a quite conservative figure. For example, Reference 5 lists the failure rate of the SFCS pitch computer channel, which is at least as complex as the flutter control CVU-Sensor channel and includes more active elements, as one failure every 40,000 hours! Obviously, by using either fewer or better quality components, the reliability of the Sensor-CVU channel can be dramatically improved to easily satisfy the one catastrophic failure per million flight hours reliability criterion.

Based on the consideration of this section, it appears possible to achieve overall failure rates for an active flutter control system on the order of one failure per million flight hours.

The reliability guidelines are believed to be conservative for several reasons. The principal reason is that an active flutter control system would be used in only a small (unknown) percentage of the actual flight time of the aircraft. In addition, it is recognized that the control system would be pretested at a sub-flutter velocity before penetration of the flutter region. If the test indicated trouble anywhere in the system, the pilot could leave the system off and avoid penetration. After any single system failure, when in the flutter region, the pilot would also have an opportunity, after being apprised of the failure, of reducing the airspeed to a stable velocity prior to the occurrence of a second failure. Flight safety requirements for flutter control systems which can be turned off when not needed, pre-tested before use, and which allow a stabilizing pilot response for any single failure should not be required to have the same level of reliability as for full-time fly-by-wire aircraft flight control systems, such as used in the SFCS aircraft, which must work successfully from take-off to touch-down.

5.5 Weight Estimate for an Active Flutter Control System

The following list of component weights is based on the conceptual flow diagram of Figure 122 and relies heavily on data from both the SFCS aircraft of Reference 5 and the MCAIR in-house advanced CCV fighter studies.

		Weight (per aircraft) lbs.
Secondary Actuators	2x40.0 = 80.0	70
– Series Servo Actuators	-2x5.0 = 10.0	
Accumulators	2x9.5 = 19.0	0
– Flutter Dampers	-2x9.5 = -19.0	
Computer Voting Units	6x10	60
Racks for CVU's	6x2	12
Sensors	6x2	12
Cockpit Displays and Test Control Board	1x30	30
Transformers/Rectifiers	3x9	27
Wiring and Electrical Mods.	1x30	30
Installation, hydraulic lines, linkage, etc.	1x20	20
Batteries	3x3	9
Estimated total additional weight	=	270

This estimate does not include weight for a Built In Test (BIT) unit. It is assumed that ground test equipment will be used instead of a BIT for pre-flight checkout.

The system is based on the F-4 lateral flight control loop with the series servo replaced by the multiply-redundant SFCS secondary actuator. In future aircraft it is expected that flight control systems will use much more compact actuation concepts. Examples of such schemes are:

(1) Electro-hydraulic secondary actuators mounted directly on and mechanically driving the control valve of the primary hydraulic power actuator, and

(2) Completely integrated fly-by-wire, power-by-wire, multiply-redundant primary electro-hydraulic power actuators.

Either of these two actuation concepts would effectively eliminate the need for both the heavy SFCS type secondary actuators and the associated mechanical linkage. This would reduce the estimated total weight to approximately 200 pounds per aircraft, assuming that none of the weight for the primary actuation system is chargeable to the flutter control system. If the flutter control system were to require separate dedicated components the weight would be significantly greater than the 200 pounds per aircraft.

217

6. DISCUSSION

This section discusses the most significant results obtained in these studies.

6.1 Payoffs for Active Flutter Control

The promised benefits from active flutter control are of two types,

(1) expansion of flight envelope for contemporary and future aircraft by removal of flutter placards,

(2) weight savings in future aircraft.

The studies indicate that the increase in flutter speed through active control is a direct function of the severity of the flutter mode. The more explosive the flutter mechanism, the less flutter speed increase is possible. For speed increases greater than 10% the necessary condition is that the flutter mechanism have a damping coefficient change (in a classical V-g sense) at passive flutter onset which is less than 0.1/100 knots. Most F-4 wing/store flutter cases satisfy this requirement. The advanced aircraft horizontal tail and wing designs considered in these studies required passive modifications to "calm" the flutter mode before active control was feasible.

The specific payoffs for active flutter control for the study configurations are given in the paragraphs below.

F-4 Wing/Store Configurations

Gain margins greater than ±6 dB were determined for each of the F-4 wing/store cases for velocities up to the maximum velocity of the F-4 with stores (730 knots) for sea level aerodynamic data and g = 0.02 structural damping. Phase margins for the same cases are ±60 degrees or greater except for the 370 gallon tank - 90% full, which has phase margins of approximately ±45 degrees. The studies determined that the flutter control system stability margins, both gain and phase, decrease with increasing velocity and increasing altitude. The margins were found to be nearly the same for both subsonic (M = .9) and supersonic (M = 1.2) aerodynamic theory. As a result of the decreasing gain and phase margins operation of both the MK-84 EO and the 370 gallon tank cases with an active flutter control system is restricted to altitudes below about 10,000 feet. The MK-82 case was not analyzed.

The removal of store flutter placards is a benefit for which there is no realistic weight trade off. The benefit is operational in that the aircraft can fly lower and faster than before and it will thus be more effective with enhanced survivability. These are very real benefits and can easily justify

the 200 lbs or more required for the active control system. The 200 lbs is based on a triply-redundant control system designed for less than one catastrophic failure per million flight hours. This weight figure also assumes that existing control surfaces and hydraulic actuation devices are available for cooperative use so no weight has been included for those components. The studies have indicated that such cooperative use is feasible.

Advanced Aircraft Horizontal Tail

A flutter speed increase of more than 30% was achieved with gain margins greater than ± 6 dB and phase margins greater than ± 60 degrees for the Candidate Design configuration. The horizontal tail Candidate Design consisted of the baseline Strength Design with 20 pound ballast weights added to each tip at the leading edge. The ballast weights were necessary to make the horizontal tail flutter mode less explosive and, hence, more controllable. The total projected weight penalty for active flutter control of the baseline Strength Design, including ballast weights and flutter control system components not shared with the aircraft flight control system, was 85 pounds. This is 25 pounds more than the passive flutter solution using ballast weights and at least 15 pounds less than the solution using stiffness increases.

Advanced Aircraft Wing

The flutter mode of the baseline Strength Design of the advanced aircraft wing was much more explosive than any of the wing/store configurations studied or the horizontal tail Candidate Design. Ballast weights in excess of 200 pounds per aircraft were required to make the primary flutter mode reasonably controllable. Without ballast weights the baseline wing flutter velocity could be improved by about 10% when an aileron was used as the flutter suppressor. A 30% flutter velocity improvement was obtained with an all-movable tip flutter suppressor. This all-movable tip case, however, exhibited unacceptable stability characteristics after only a 6% flutter velocity improvement. A 30% flutter velocity improvement was obtained passively for the baseline configuration with less than a 100 pound weight penalty.

6.2 Hardware Considerations

Hydraulic System Requirements

The studies have generally assumed that the hydraulic actuator frequency response bandwidth is extended past the flutter frequency being controlled. If this is not done it becomes difficult to decouple the flutter control system from the flight control systems when force producers are shared. In

addition, the forward loop of the flight control system may begin to exhibit many of the characteristics of the feedback loop if the forward loop is highly attenuated in the frequency range where the feedback loop is highly amplified. For example, consider a simple feedback control system in which the magnitude of the forward loop transfer function G(S) (the plant) is much smaller than that of the feedback transfer function H(S) (the flutter control loop). H(S) is also assumed large with respect to unity. The closed-loop transfer function is thus

$$\frac{G(S)}{1 + (G(S) \; H(S))} = \frac{G(S)/H(S)}{1/H(S) + G(S)} \approx \frac{1}{H(S)}$$

The flight control plant would, therefore, not be expected to respond as it was originally designed.

If exclusive dedicated control surfaces are available for the flutter control system it appears from the results of the studies reported in Reference 14 that existing low bandwidth force producers are feasible for flutter control. The concept in that case is to trade off the loss of gain in the control force producer with increased gain in the control system electronics so that the net gain level around the complete closed loop is held constant at the required level for the flutter control.

Control valves must be designed for high flow rates. This is because of the requirements for cycling in the high frequency range of flutter. This frequency varies from 7 to 11 Hz for F-4 wing/store flutter. Frequencies higher than this can be expected for fighter aircraft wings and horizontal tails. An accumulator must be included to ensure continuity of the desired flow rate if other aircraft systems are potentially able to starve the flutter control system for short periods of time.

Aileron rates on the order of 200 deg/sec are required for the tested F-4 wing/store control system designs when the open-loop gain is set for a gain margin of 6 dB against the g = 0.0 structural damping passive flutter boundaries when in region of extreme turbulence (G_{RMS} = 13 ft/sec). If the open-loop gain is reduced to give 6 dB against the g = 0.02 structural damping flutter boundary, the aileron rates are all less than 100 deg/sec, which is within the capability of the F-4 aircraft. The equivalent damping in the flutter mode, after excitation, is reduced, however, when the open-loop gain is reduced, as illustrated in Figure 69.

For a given configuration and flutter mode the control surface rate is proportional to,

(1) the input excitation level,

(2) the control system open-loop gain.

If a flutter control system is required to operate in a region where there is a significant amount of excitation energy at the flutter frequency (i.e., a well developed thunderstorm), rate requirements will be high. On the other hand, if clear air turbulence and maneuver loads are the only excitation sources the rate requirements will be somewhat reduced. If, in the future, clear air turbulence sensing becomes practical, hydraulic rate requirements for active flutter control could be dramatically reduced. Results given in Reference 14 show rate requirements of less than 10 deg/sec for high intensity, low frequency maneuver loads and discrete wind gusts such as would be expected in demonstration test flights.

It is questionable whether any fly-by-wire system should ever be flown in thunderstorms because of the danger of lightning strikes. This is not as serious a consideration for flutter control systems as it is for full-time flight control systems since flutter control systems can be turned off when the aircraft velocity is less than the flutter velocity.

This area of hardware capability demands the most attention in any further investigation of active flutter control. As more information is obtained from wind tunnel or flight tests some of the more restrictive design guidelines may be reliably and confidently relaxed so as to reduce the demands on the control system hardware.

Effects of Nonlinearities

Control system nonlinearities have been evaluated in these studies. The major considerations are summarized in the following paragraphs.

The deflection limit for control surfaces is never reached, or even remotely approached, by an active flutter suppression system. Since the pilot's use of the control surface is restricted to small angles in the high Q region, there is very little or no chance of the control system to reach its limit deflection while flutter is being controlled.

The rate limit, on the other hand, is the single most critical design constraint and affects the system gain and available power for flutter control. Control is maintained, however, even though hydraulic actuators are rate limited over a significant portion of each oscillation cycle. The effec-

221

tive damping of the aircraft response is reduced if the maximum rate limit of the control surface power actuator is lowered. If the maximum rate limit is too low, control of the flutter mode is lost.

Dead space and free play have been evaluated and found to be acceptable for a control system such as the F-4 aileron actuation system If these non-linearities are present, and measurable, the flutter control system design could be modified slightly to accommodate the additional control system lags.

Hydraulic control valve friction and inertia have not been evaluated. These effects can be evaluated most realistically through hardware bench tests. Control valve inertia can be expected to be an important design consideration in a flutter control system for wing or horizontal tail flutter modes which are at higher frequencies than the wing/store flutter modes. Very light control valve spools may be needed for control of very high frequency flutter modes.

The effects of resonances, free play, and alternate force paths for the mechanical linkage between secondary actuators and the power actuator control valves needs special attention in any detail design for a flutter control system. For example, free play in this linkage has the same effect as power control valve dead space. A hard point must be provided also to prevent force transmitted back to the pilot's stick in any "walking stick" arrangement such as used in most operational fighter aircraft.

6.3 Operational Benefits

A study was performed to determine the nature of some of the operational benefits likely to occur because of active control of fighter aircraft wing/store flutter. The F-4 aircraft, as a typical case, carries two basic types of external stores, either fuel tanks or weapons. The feasibility studies to date have emphasized the fuel tank configuration primarily because it provides a verified flight demonstratable design with a convenient method for changing the dynamic configuration in flight. The operational benefits likely to result from fuel tank flutter control are undefined since most of the typical missions for the F-4 specify dropping the fuel tanks as soon as they are empty. The 4810 lbs of fuel in the external tanks is sufficient for from 4-12 minutes of flight at the maximum power setting, depending on Mach number and altitude. For the military power setting, the flight time varies from 15-75 minutes. The stylized missions for the F-4 use up the external fuel supply within the first 100 miles of flight. The reason for this short range is that 2400 lbs of fuel is used from the external tanks for warm-up and take-off.

Data contained in the USAF Aircrew Weapons Delivery Manual (Reference 16) may be used to establish some of the likely benefits to be obtained from increased aircraft velocity at low altitudes. The reduced release altitude may result in a significant increase in weapon effectiveness. The lateral displacement of the weapon delivery footprint is reduced because of the shorter trajectory for the weapon. The longitudinal displacement footprint may also be reduced but here there is a trade off between reductions due to shorter trajectories and increases due to an uncertainty increase in the weapon release timing. A case can also be made for the expansion of the flight envelope for certain flutter critical stores, such as ECM (Electronic Counter-Measures) pods, which should not be jettisoned because of expense or security. To evaluate these payoffs in depth and to determine other additional benefits requires a far more detailed operations analysis than for this preliminary study.

6.4 Survivability-Vulnerability Considerations

The Air Force Tactical Air Command has a standing requirement for the capability to carry and deliver conventional munitions supersonically. It has been argued that supersonic delivery will provide increases in survivability. As the attacking aircraft drop to lower altitudes to avoid radar directed guns and missiles they are subjected to enemy ground fire. A high-

speed low-altitude approach would significantly decrease the enemy's ability and time to acquire and fire on the attackers.

These flutter control studies have been concerned primarily with the establishment of feasibility and have not specifically assessed the combat vulnerability of a particular active flutter supression system. Nevertheless, certain general comments can be made concerning the system vulnerability.

Cat strophic battle damage failure can occur in a flutter control system either by:

1) Direct impact of projectiles on critical control system elements, or
2) A battle damage failure of some other element in the aircraft which propagates to and causes the failure of a critical control system element.

Each of these two battle damage modes will be considered for the conceptual control system design for F-4 wing/store flutter control shown in Figure 122. The components shown in the figure are required for a practical flutter control system designed for less than one catastrophic failure, from causes other than battle damage, each million flight hours. The additional components, referenced to an operational F-4, are the sensors, computers, secondary actuators, transformer/rectifiers, batteries, and possibly the indicated accumulators.

Direct Impact Damage

The aileron, aileron power actuator, and mechanical linkages have the same individual damage probabilities as an operational F-4. However, an F-4 equipped with an active flutter suppression system requires the continuous functioning of both ailerons to avoid a catastrophic failure, while the unmodified F-4 allows the failure of individual ailerons.

Similar comments apply to the spoilers if they are used in the flutter control system. The accumulators would be in the immediate vicinity of the aileron power actuator and can be expected to experience similar damage effects. The triply-redundant secondary actuator is also a single point battle damage item since it is contained in one package.

The sensors must be located at a single point on the wing in order to give the same signal in all three channels. They are thus more susceptible to catastrophic damage than would be the case if they were dispersed. All of the electrical wiring, computers, transformer/rectifiers and batteries,

however, may be separately packaged and widely dispersed to minimize the battle damage effects of direct projectile hits.

Induced Failures

The single most critical battle damage induced failure is caused by the loss of the hydraulic power supplies. The F-4 aircraft is typical of contemporary aircraft in that hydraulic lines of the separate systems are in close proximity in several locations, such as the wing and empennage areas. In these regions a single projectile could cause loss of all hydraulic power. The loss of either primary system combined with the loss of the utility system will cause loss of flutter control for one or the other of the aircraft wings.

Vulnerability Reduction Concepts

Automatic failure isolation in aircraft hydraulic systems to reduce the probability of a single hit causing loss of the complete system can be accomplished by a number of methods as described in References 17 and 18. Several of the most promising concepts are being further developed for use on advanced aircraft. The requirement for flutter control systems is such that some of the more attractive concepts, such as reservoir level sensing, may not be suitable because of excessive time lags between sensing of the failure, determination of the failure location, and isolation of the damaged section. A set of continuously functioning in-line hydraulic logic devices to quickly isolate damaged sections of the hydraulic system would be very attractive for flutter control systems.

Power-by-wire actuation promises a dramatic improvement in flight control system survivability. Because the hydraulic power supply is integrated into the actuator package the induced failures resulting from projectile hits in other parts of the aircraft are minimized. The only external components in such a system are the electrical wiring which may be both redundant and widely separated. Heat rejection, which is a measure of the hydraulic losses to the system in the form of heat, however, is significant for such systems as described in Reference 19. The additional duty cycle associated with flutter control may significantly increase cooling requirements.

Under AFFDL sponsorship (Reference 20) criteria and guidelines are being developed for vulnerability indices which could be used to comparatively evaluate candidate flight control system mechanization concepts in an earlier stage of design. Definitive battle damage mode and effects analyses can be performed when specific detail design data becomes available.

6.5 Wind Tunnel and Ground Testing

6.5.1 <u>Wind Tunnel Tests</u> - The lack of verified knowledge of control surface and spoiler unsteady aerodynamics leads to a requirement for wind tunnel testing, particularly in the transonic region. However, both low speed and transonic tests are recommended. The bulk of data and electronics checkout would be performed in the relatively inexpensive and efficient low speed tests. The unknown effects caused by compressibility would be evaluated in the transonic tests. It is premature, however, to recommend the exact nature of wind tunnel models. Additional study is required to evaluate the trade offs among available tunnels, model types, model support concepts, model scaling and the closely related hydraulic system requirements. The available tunnels prohibit using the same model for both subsonic and transonic tests.

Recent experience at McDonnell Aircraft Company has demonstrated the practicality of using miniature hydraulic actuators for the excitation of a typical subsonic flutter model. Actuator bandwidths of 20 Hz with amplitudes on the order of ± 4 degrees are obtainable from the miniature linear actuators used in these tests. Similar type actuators would be appropriate for transonic testing if the model envelope was not prohibitive because of an overly small model scaling.

In particular, an F-4 wing/store flutter control model suitable for low speed testing could consist of a single wing with stores and a partial fuselage section cantilevered from the side wall of the tunnel. Sensors, such as accelerometers, would be mounted on the wing panel and furnish signals through a cable to an electronic compensation module located on the outside of the tunnel. The compensation module would be designed to permit easy adjustment of feedback gain and phase margin and permit filtering. All feedback compensation would be performed by the compensation module. Instrumentation for the test engineer initiated, open-loop frequency response tests as described in Section 5.3.4.4 would also be present. These frequency response tests would be performed prior to entry into the flutter critical region. The servo valve, which accepts signals from the compensation module, would be located as close to the aileron power actuator as the design permitted to minimize hydraulic line losses. A small linear power actuator mounted on a wing spar near the control surface hinge line would drive the surface through a bellcrank linkage.

Actuation should be performed at the control surface location with the shortest and tightest linkage possible to minimize drive mechanism wrap-up and control surface free play. Excessive amounts of either of these two items can destroy the credibility of the results and may even preclude testing altogether. In this regard, miniature hydraulic actuators are preferable to electric torque motors for active flutter control model testing. Electric torque motors, in general, have dynamic problems, such as drive mechanism wrap-up, mechanical linkage free play, as well as potential instabilities caused by the high gains required in the torque motor feedback loop to increase bandwidths.

The frequency scaling for the largest practical model should be kept as low as possible to allow for reduced demands on the model hydraulic system design and to establish the maximum credibility in relating wind tunnel hydraulic system data to flight test vehicle data.

Wind tunnel tests to measure oscillatory aerodynamic data from a distributed set of pressure sensors, might be appropriate if unexpected behavior is seen in the functional tests. These measured data, in conjunction with the data generated in the functional tests could provide guidance for corrective measures.

6.5.2 Ground Tests - Design confidence testing will be required for the flutter control system hardware prior to flight evaluation. The required testing falls into several general categories.

Open-Loop Tests

Component evaluation testing will be required for each of the flutter control system components with special emphasis devoted to the hydraulic actuators and the electronic computer voting units. Component transfer functions and response characteristics should be determined for each of the components. These transfer functions would allow for updating the analysis.

Closed-Loop Tests

Component integration testing, which includes hybrid simulation and iron bird tests, will be required to verify component functional and compatibility relationships and the closed-loop response characteristics.

Installed System Tests

Functional, and both open and closed-loop control system response tests should be performed for the flutter control system installed in the aircraft prior to first flight. Selected installed system tests should be performed before each succeeding test flight.

227

Dynamic Structural Tests

Ground vibration tests will be required to substantiate the theoretical and wind tunnel flutter predictions. These tests will be necessary for the evaluation of the dynamic characteristics for each of the specific test configurations. Tests should be conducted with the control system both on and off.

6.6 Rationale for Stability Margins

One of the engineering judgment decisions which must be made for any flutter control system is the specification of stability margins. This decision is especially difficult since there will always be unknowns in any practical feedback control system. For flight control systems which are unstable if tested to the margin, the stability margins themselves are among the unknowns. All we really know, in general, about flight control systems is whether or not the system works.

As developed in Section 5.3.4, the electronic and hydraulic components of a flutter control system can be made to have very small, and measurable, phase and gain uncertainties. There are, however, at least three unpredictables which must be considered in an operational flutter control system:

1) Analytical inadequacies of the servo-aeroelastic (control system, structure, inertia, and aerodynamics) model,

2) Uncertain variations in store inertial characteristics,

3) Operational changes in the wing-pylon-rack systems caused by use and environment.

In addition to these unpredictables, the inevitable Murphy's law becomes a factor also. Stability margins must either be very large to accommodate these unpredictables or else some type of operational test to eliminate the uncertainties must be performed before using the system.

It has been McDonnell Aircraft Company experience with fighter aircraft flight control and stability augmentation systems that the stability margins listed below are reasonable:

	Phase Margins	Gain Margins
Linear Studies	±60 deg	±6.0 dB
Nonlinear Studies	±45 deg	±4.5 dB

These stability margins have been considered as preliminary guidelines for flutter suppression systems. They are considered to be applicable to the

limit velocity (V_L) of the aircraft and are not superimposed on the normal 15% flutter margin required by the current military specifications. As component hardware, wind tunnel, and flight test data become available, these stability margin guidelines can be confidently modified to become realistic design specifications for future aircraft applications.

7. CONCLUSIONS AND RECOMMENDATIONS

The following general conclusions have been justified by these studies.

1. Mild flutter is controllable with an active system. Nearly all cases of F-4 wing/store flutter are in this category.

2. Hardware is available for the implementation of an active flutter control system.

3. Existing control surfaces can be used for fighter type aircraft, where frequency separation allows for the sharing of components among flight control systems and flutter control systems.

It is recommended that additional effort be directed toward the detail design evaluation of an active flutter control system for an F-4 aircraft with external stores. This effort should also be directed toward the generation of program plans for wind tunnel testing and should include specific design requirements for the necessary hardware and models.

APPENDIX I

ANALYTICAL MODELS FOR F-4 WING/STORE CONFIGURATIONS

The analytical models used in these studies of wing/store flutter control are described in the following paragraphs. These models have been validated by experiment and are in current use for the F-4 flutter analyses.

I.1 Wing Idealization

The analytical model of the F-4 wing is shown in Figure 123. This representation consists of a 28 degree-of-freedom lumped mass model. This includes two aircraft rigid body degrees-of-freedom: vertical translation, and pitching rotation. A matrix of influence coefficients was derived on the CEAC analog computer to match measured ground vibration data. The weight associated with each of the influence coefficient control points is shown in Table 7.

I.2 MAU-12 Pylon Idealization

The MAU-12 pylon supports the MK-84 EO Laser Guided Bomb directly, or supports six MK-82 500 lb. bombs with the MER rack. The mathematical model for the MAU-12 pylon at BL 132.5 is shown in Figure 124. This analog was developed by matching two experimental single store configurations, the Walleye and the SUU-16 dummy gun pod. Figure 124 shows the wing and pylon geometry and locates the equivalent springs used in the model. The complete matrix of CEAC derived influence coefficients for the F-4 wing cantilevered at the aircraft centerline, in combination with the MAU-12 pylon is given in Reference 21, Appendix D. Store cg's are referenced to point 6 of the pylon model.

I.3 MER Rack Idealization

The development of a mathematical model of the MAU-12 pylon – MER rack combination was much more complicated than that for the MAU-12 pylon alone. The problems, which arise because of structural redundancies at the rack attachment points, are discussed on pages 19, 20, and 21 of Reference 21. Figure 125 shows a sketch of the complete MAU-12 pylon-MER rack combination analogy. Rack stiffness values were furnished by the manufacturer and were verified analytically at MCAIR.

I.4 370 Gallon Tank Pylon Idealization

The 370 gallon tank is attached at BL 132.5 by its own pylon. The spring and weight data for the tank simulation is given in Figure 126. As

231
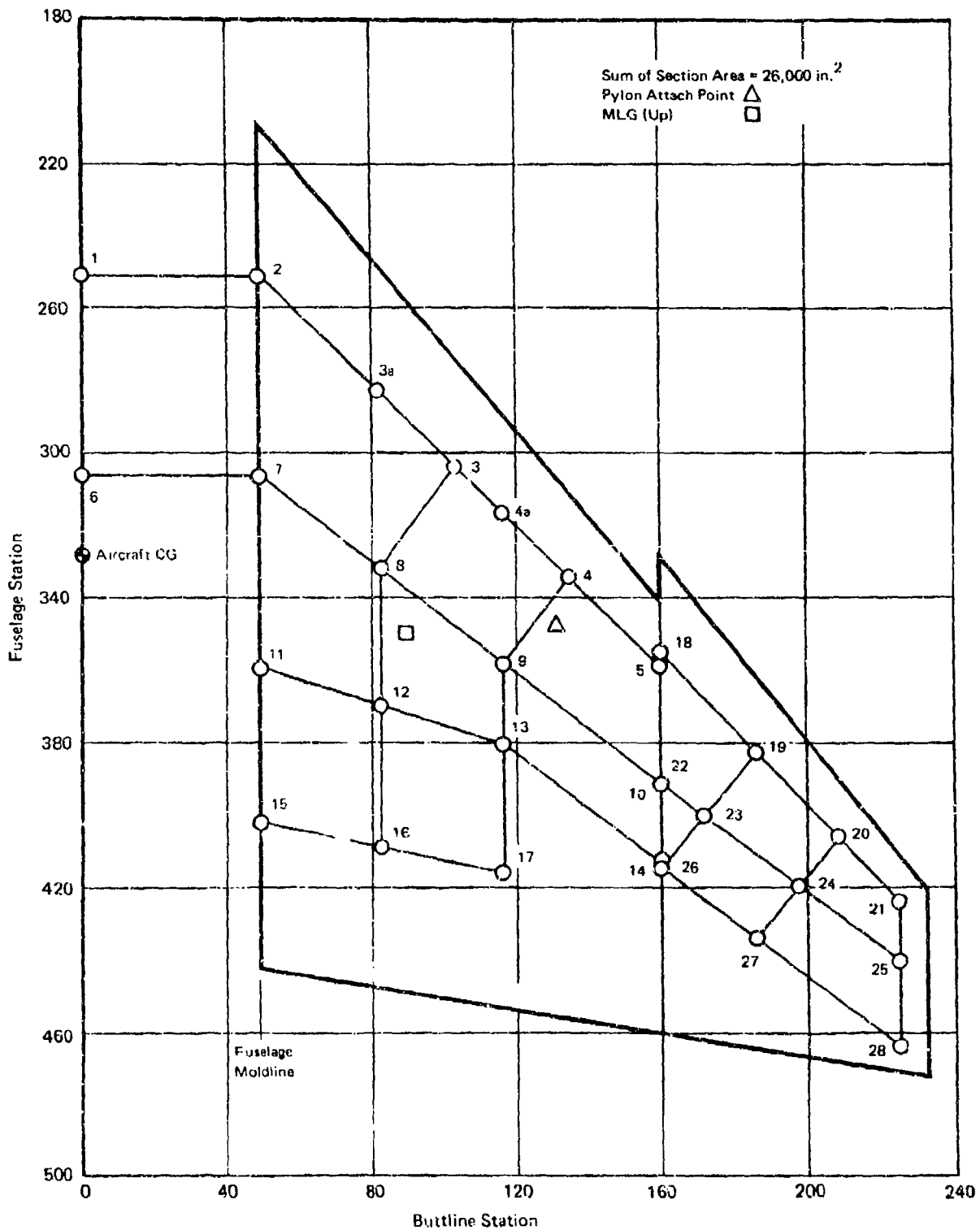
FIGURE 123   F-4 WING IDEALIZATION

TABLE 7 WEIGHT ASSOCIATED WITH F-4 WING CONTROL POINTS

WING CONTROL POINTS	WING WEIGHT ASSOCIATED WITH CONTROL POINT (lt.)	1/2 FUSELAGE WEIGHT LUMPED AT CONTROL POINTS (lb)
1	88.099	
2	293.278	3,542.515
3a	0.0	
3	295.210	
4a	0.0	
4	250.774	
5	192.814	
6	88.099	
7	201.701	
8	160.742	
9	136.786	
10	106.646	
11	99.691	10,535.969
12	142.195	
13	121.330	
14	94.282	
15	0.0	
16	71.870	
17	61.824	
18	0.0	
19	27.821	
20	30.912	
21	19.552	
22	0.0	
23	26.739	
24	30.912	
25	14.954	
26	0.0	
27	34.003	
28	8.733	
MLG Up	498.456	

Notes:

1. 1/2 wing weighs 2,422.8 lbs. without fuselage points and MLG
2. Pitch inertia of 1/2 aircraft (minus wt. of 1 wing) about CG is 535,557 mug-in^2. Aircraft pitch slope defined by line joining control points 7 and 2.

233

FIGURE 124 MAU-12 PYLON IDEALIZATION
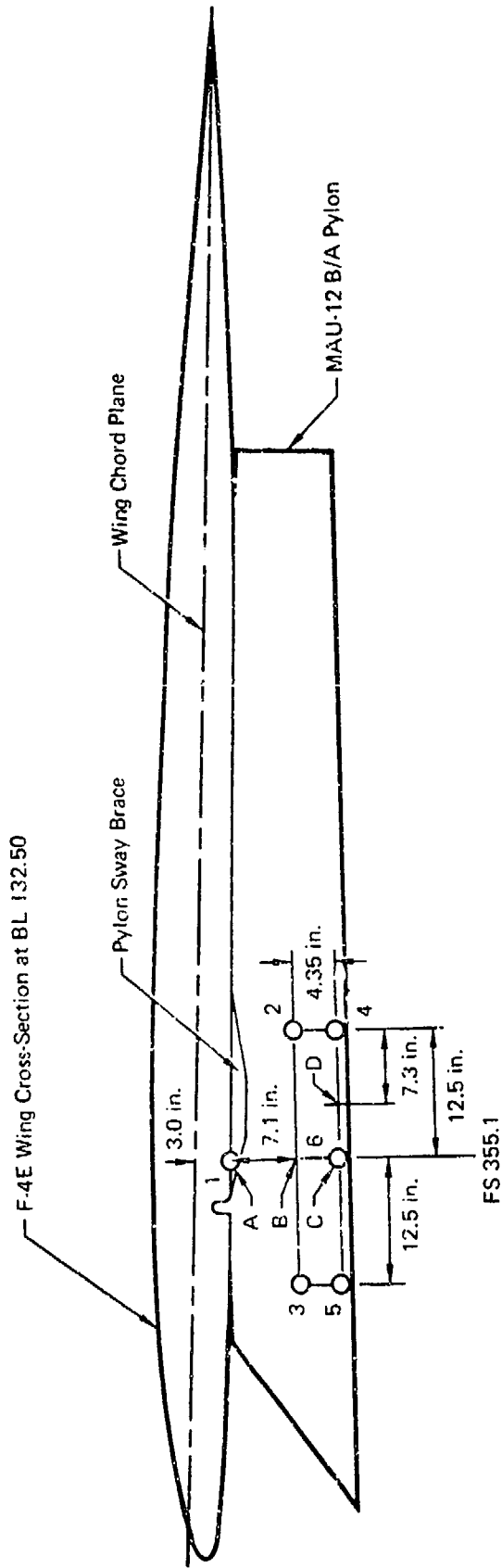
Point	Weight - lb
1	56.0
2	48.0
3	8.6
4	64.0
5	11.5
6	—

Pylon Spring Constants

Name	Location	Value
Upper Pylon Sway Brace Spring	A	15.0×10^6 in.-lb/radian
Pylon Roll Spring	B	30.0×10^6 in.-lb/radian
Rack Sway Brace Spring	C	10.0×10^6 in.-lb/radian
Pylon Yaw Spring	A	28.0×10^6 in.-lb/radian
Pylon Pitch Spring	D	55.0×10^6 in.-lb/radian

234

Note: All dimensions are given in inches.

**FIGURE 125 AFT-SHIFTED MER RACK/MAU-12
PYLON IDEALIZATION**
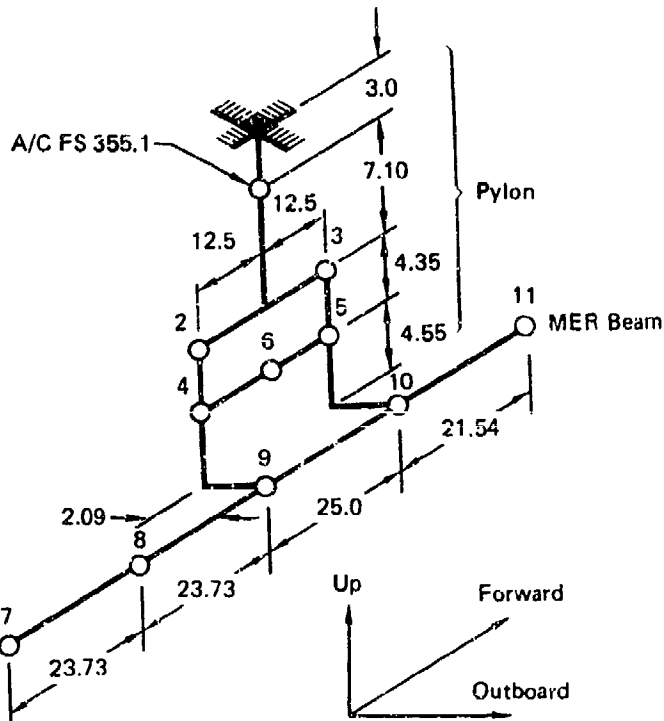
Point	Weight (lb)
7	60.0
8	33.0
9	33.0
10	34.0
11	60.0

A/C CG at FS 327.7

A/C FS 354.8

Note: All dimensions are given inches.

Point	Weight (lb)
2	46
4	23
5	23
6	0
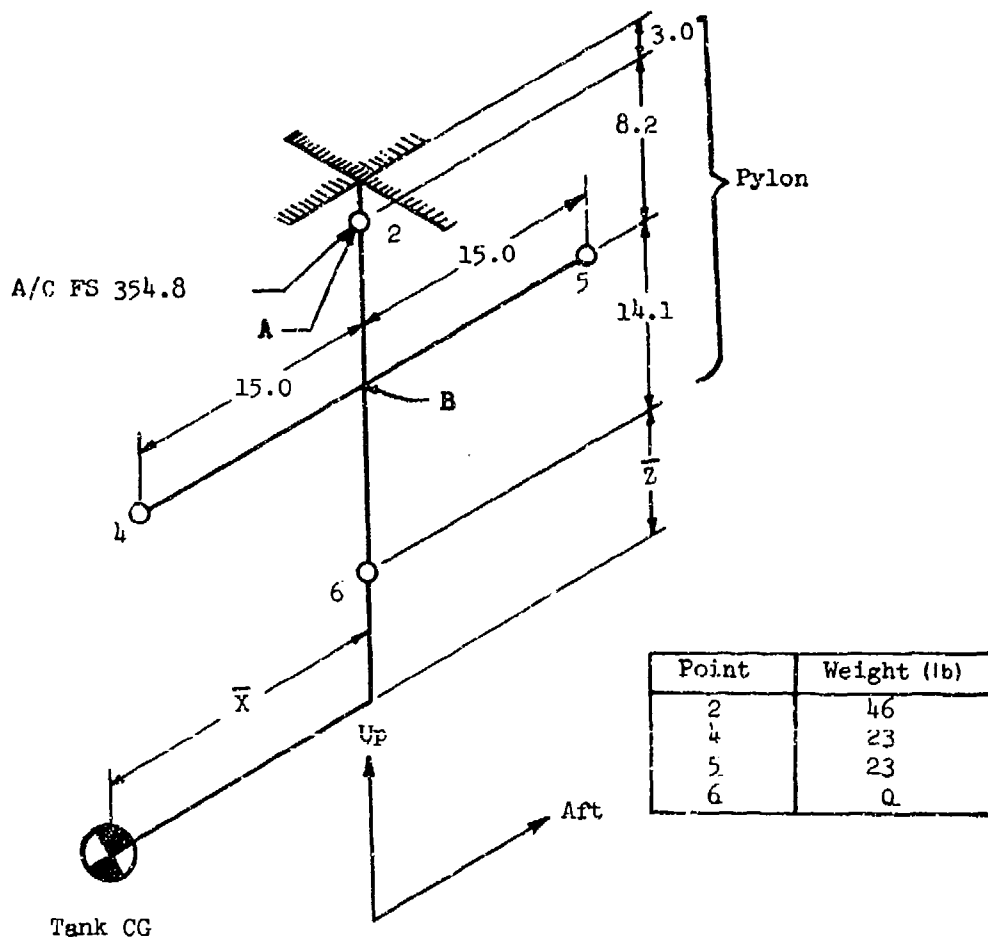
Pylon Spring Constants		
Name	Location	Value
Pylon Pitch Spring	A	100.0×10^6 in-lb/radian
Pylon Yaw Spring	A	92.0×10^6 in-lb/radian
Upper Pylon Roll Spring	A	9.65×10^6 in-lb/radian
Lower Pylon Roll Spring	B	10.30×10^6 in-lb/radian

$\overline{X}$ varies between 4.5 and 20.8 inches and $\overline{Z}$ varies between -4.3 and .1 inches depending on the fuel load.

FIGURE 126 370 GALLON TANK AND PYLON IDEALIZATION

236

with the MAU-12 pylon, point 6 serves as the store c_g reference point.

I.5 Correlation of Math Models with Hardware

A good measure of the adequacy of a mathematical model is the correlation of theoretical vibration frequencies (zero airspeed) with the corresponding hardware frequencies. Tables 8 through 11 show the frequency correlations obtained for the bare wing, wing/MAU-12 pylon, wing/MAU-12 pylon/rack, and wing/tank pylon configurations. No store flexibility was modelled in obtaining theoretical frequencies. In the first three tables there is good agreement shown for all modes except the rack lateral bending mode of the MAU-12/MER/Pod configuration. The store loading for this case consisted of two 350 lb pods mounted on the forward shoulder stations of the MER rack. The pitch inertia for these pods is 594,000 lb-in^2 about the pod center of gravity. The reason for the poor lateral mode comparison is believed to be the assumption that bending moments in the MER rack are not transferred thru the attachment points. This assumption is equivalent to neglecting rotary moments of inertia in a beam vibration analysis. The rack lateral bending mode, however, does not affect the flutter mechanism. Table 11 compares experimental 370 gallon tank, 90% full frequencies from Reference 11 with their theoretical counterparts. Good agreement is shown except for the tank pitch/1st wing torsion mode whose experimental frequency is just over 1.5 hertz below the theoretical value.

I.6 Wing/Store Vibration Mode Shapes

Normalized still-air mode shapes are shown in Figures 127 and 128 for the mode pairs which coalesce to cause the primary flutter mechanism of the 370 gallon tank, 90% full wing/store combination. The stores under study in this report are attached at BL 132.5 between sections C-C (BL 118.25) and D-D (BL 160). The store motion indicated in the figures is absolute and include motion of the store attach points. The still-air mode shape which most closely resembles the flutter mode of the other wing/store combinations is given in Figures 129 through 131.

TABLE 8 COMPARISON OF THEORETICAL AND EXPERIMENTAL MODAL FREQUENCIES FOR BARE F-4 WING

Mode Description	Frequency – Hz	
	Experimental	Theoretical
Wing First Bending	8.2	8.4
Wing Second Bending	18.9	19.6
Wing Torsion	28.8	29.1

TABLE 9 COMPARISON OF THEORETICAL AND EXPERIMENTAL MODAL FREQUENCIES FOR SINGLE STORES INSTALLATION ON BL 132.50 MAU-12B/A PYLON

Configuration	Mode Description	Frequency – Hz	
		Experimental	Theoretical
Walleye	Wing First Bending	7.0	7.0
	Pylon Roll	12.9	12.9
	Wing Second Bending	16.4	16.3
	Pylon Pitch	17.5	17.3
	Pylon Yaw	17.8	18.0
Dummy SUU-16A Gun Pod	Wing First Bending	6.5	6.5
	Pylon Roll	9.3	9.2
	Pylon Pitch	10.6	10.7
	Pylon Yaw	12.8	12.5
	Wing Second Bending	15.7	15.9

TABLE 10 COMPARISON OF THEORETICAL AND EXPERIMENTAL MODAL FREQUENCIES FOR AN AFT-SHIFTED MER INSTALLATION

Configuration	Mode Description	Frequency – Hz	
		Experimental	Theoretical
Two 350-lb Pods On Forward Shoulder Of Rack	Rack Lateral	5.6	6.4
	Wing First Bending	7.3	7.4
	Rack Vertical	7.8	7.9
	Pylon Yaw – Roll	14.2	14.9
	Wing Second Bending	18.6	18.4
	Rack Twist	21.5	22.5
	Pylon Pitch	24.4	25.4
	Wing Torsion	27.9	28.8

TABLE 11 COMPARISON OF THEORETICAL AND EXPERIMENTAL MODAL FREQUENCIES FOR A 90% FULL 370 GALLON EXTERNAL FUEL TANK

Mode Description	Frequency – Hz	
	Experimental	Theoretical
Wing First Bending	6.8	7.2
Tank Pitch/1st Wing Torsion	7.2	8.78
Wing Second Bending	16.8	15.6

239

Spanwise Deformation

Chordwise Deformation

Section G-G

Section H-H

Section A-A

Section B-B
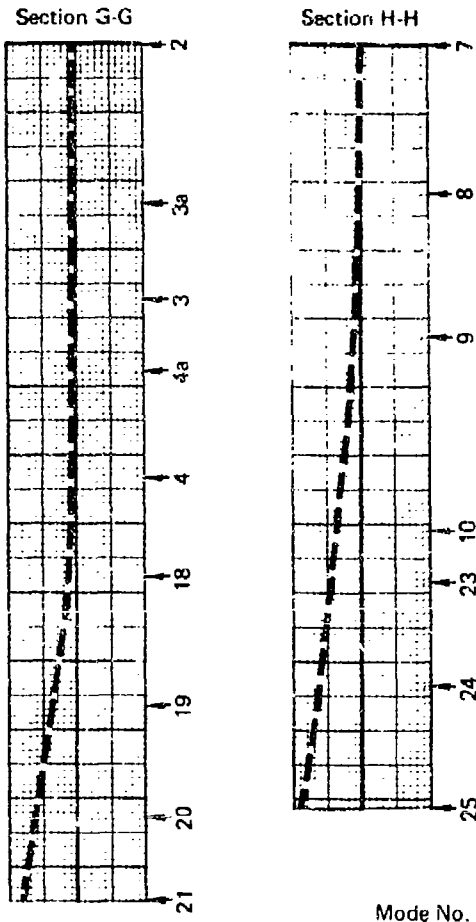
Section C-C

Section D-D

Section E-E
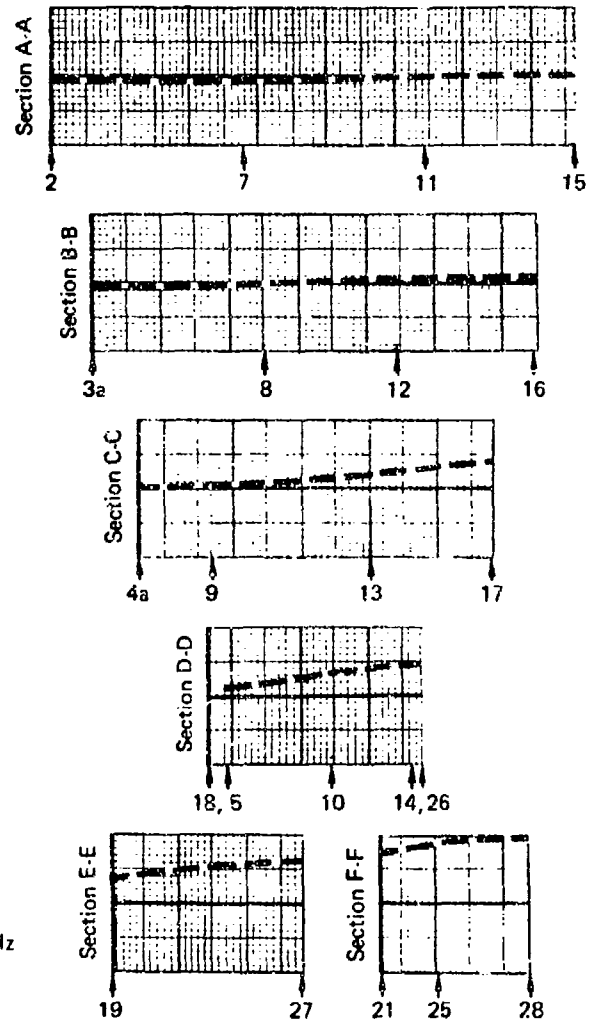
Section F-F

Mode No. 2
Frequency 7.18 Hz

Freestream
Velocity

F-4 Wing Sectioning

+ Outboard   + Up   + Aft

Lateral   Vertical   Fore-Aft
Store-Pylon Mode
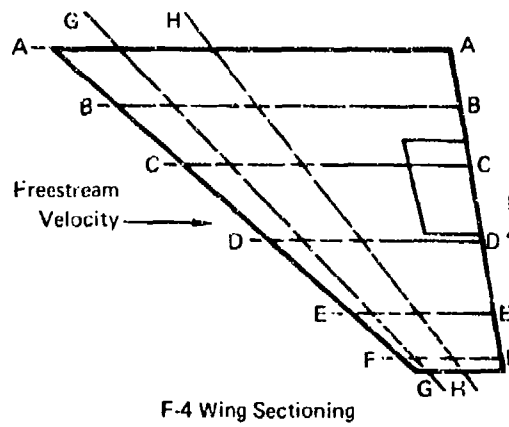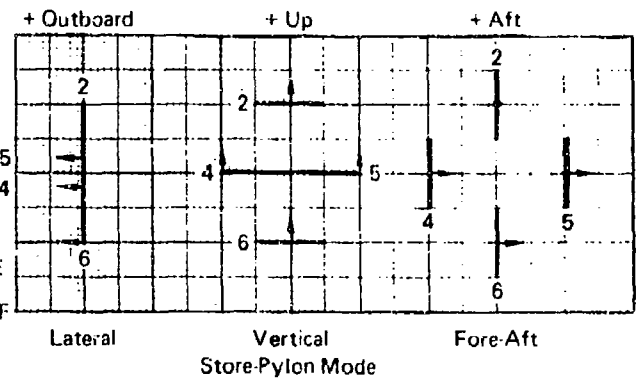
FIGURE 127 F-4/370 GALLON TANK - 90% FULL, SECOND
NORMAL VIBRATION MODE

240

Spanwise Deformation

Section G-G   Section H-H

Chordwise Deformation

Section A-A

2   7   11   15

Section B-B

3a   8   12   16

Section C-C

4a   9   13   17

Section D-D

18, 5   10   14, 26

Section E-E

19   27

Section F-F

21   25

Mode No. 3
Frequency 8.78

F-4 Wing Sectioning

+ Outboard   + Up   + Aft

Lateral   Vertical   Fore-Aft

Store-Pylon Mode
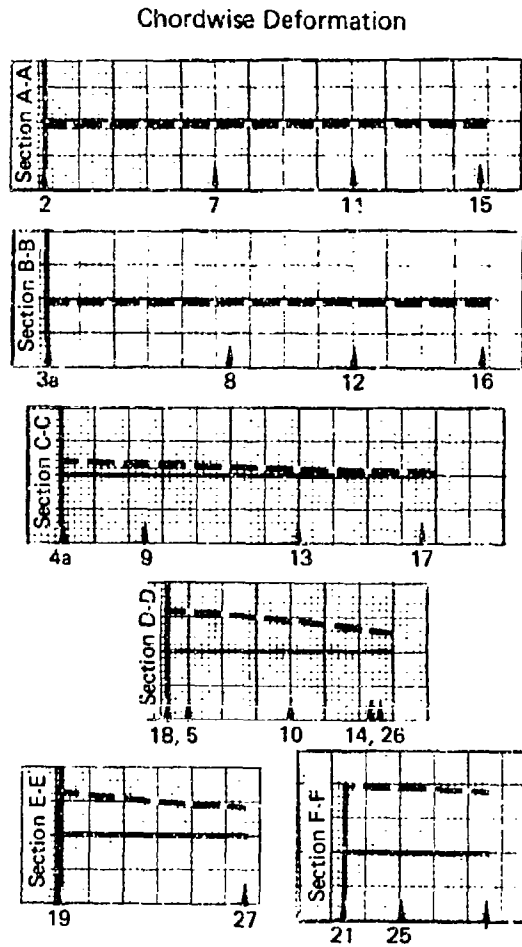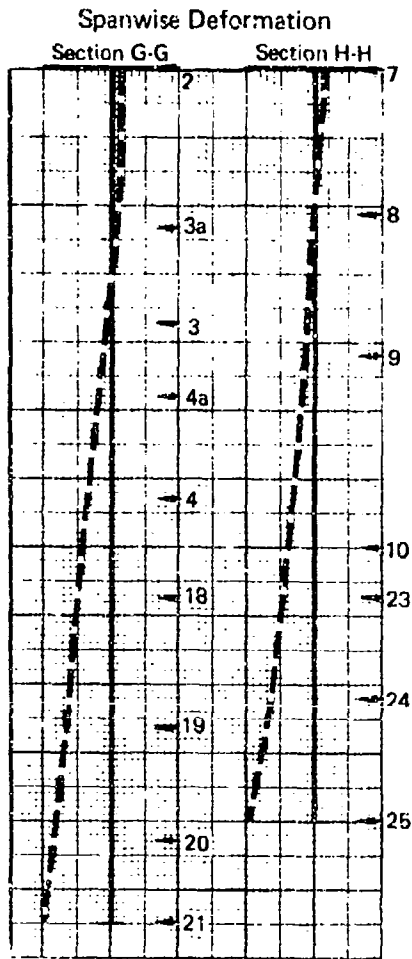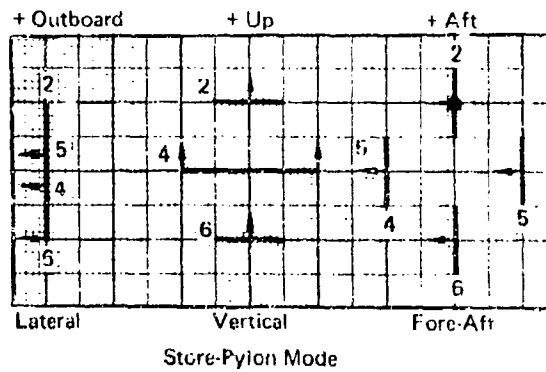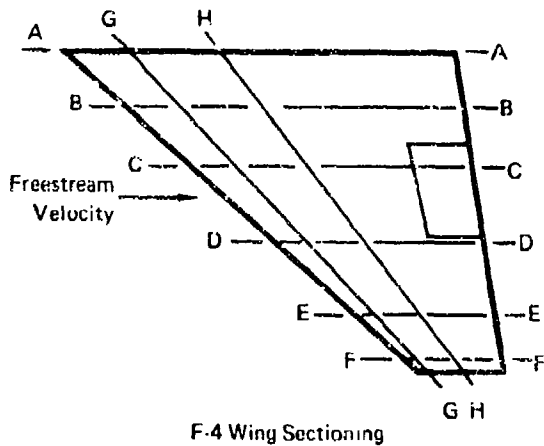
FIGURE 128 F-4/370 GALLON TANK - 90% FULL, THIRD
NORMAL VIBRATION MODE

241

Spanwise Deformation

Chordwise Deformation

Section G-G

Section H-H

Section A-A

Section B-B

Section C-C

Section D-D

Mode No. 2
Frequency 8.46 Hz

Section E-E

Section F-F

G   H

A -   A

B -   B

Freestream
Velocity

C -   C

D -   D

E -   E

F -   F

G   H

F-4 Wing Sectioning

+ Outboard   + Up   + Aft

Lateral   Vertical   Fore-Aft

Store-Pylon Mode

FIGURE 129 F-4/370 GALLON TANK - 62% FULL, SECOND
NORMAL VIBRATION MODE

Spanwise Deformation

Chordwise Deformation

Section G-G | Section H-H

Section A-A

Section B-B

Section C-C

Section D-D

Section E-E

Section F-F

Mode No. 3
Frequency 10.85 Hz

Freestream
Velocity

F-4 Wing Sectioning

Lateral
+ Outboard

Vertical
+ Up

Pylon Mode

Pylon Idealization
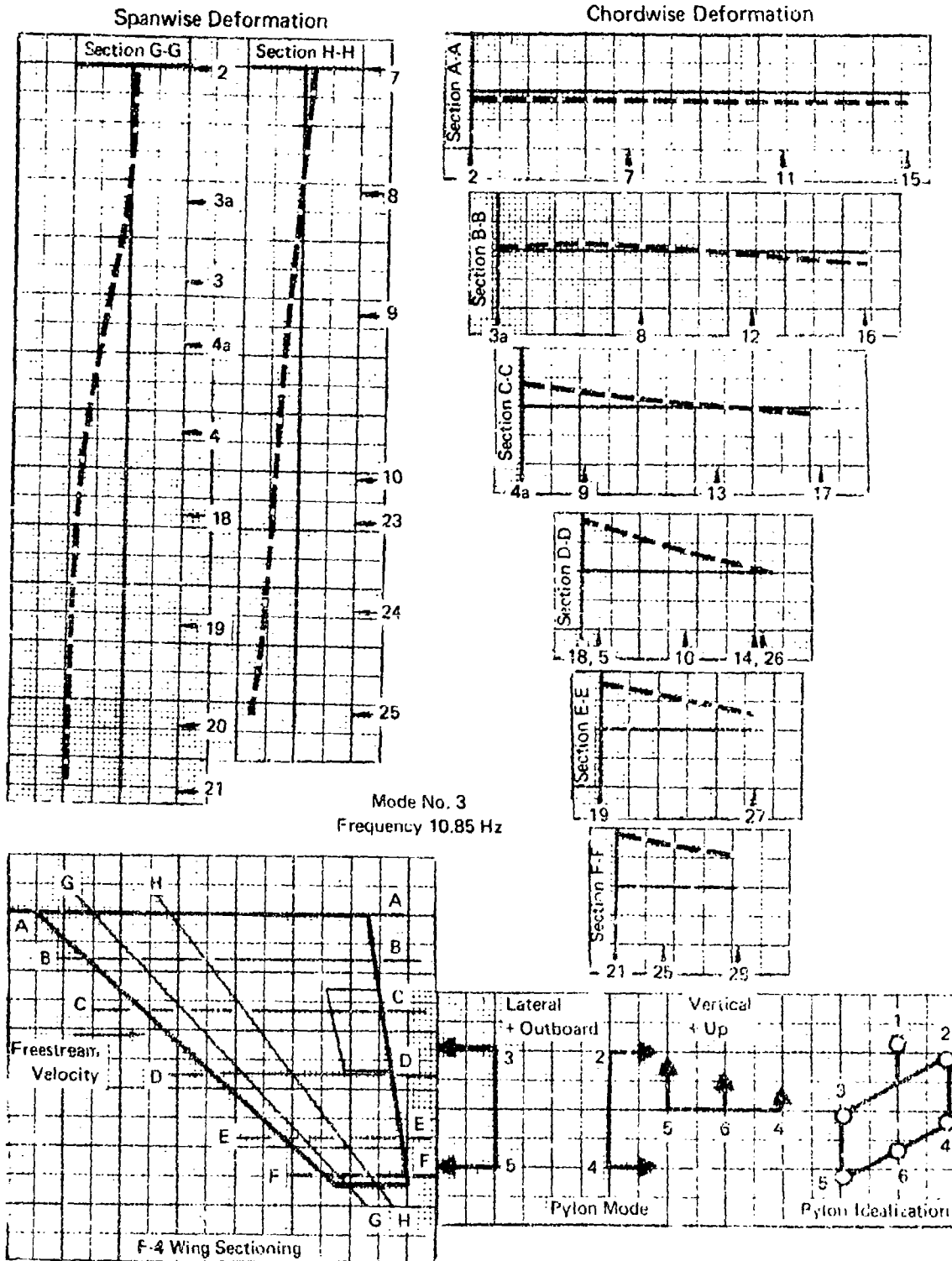
FIGURE 130 F-4/MK-84 EO, THIRD NORMAL VIBRATION MODE

243

Spanwise Deformation

Section G-G   Section H-H

Chordwise Deformation

Section A-A

Section B-B

Section C-C

Section D-D

Section E-E

Section F-F

Mode No. 3
Frequency 7.73 Hz

F-4 Wing Sectioning

Freestream
Velocity

+ Outboard

Lateral

Vertical, + Up

Rack Mode

Pylon-Rack Idealization
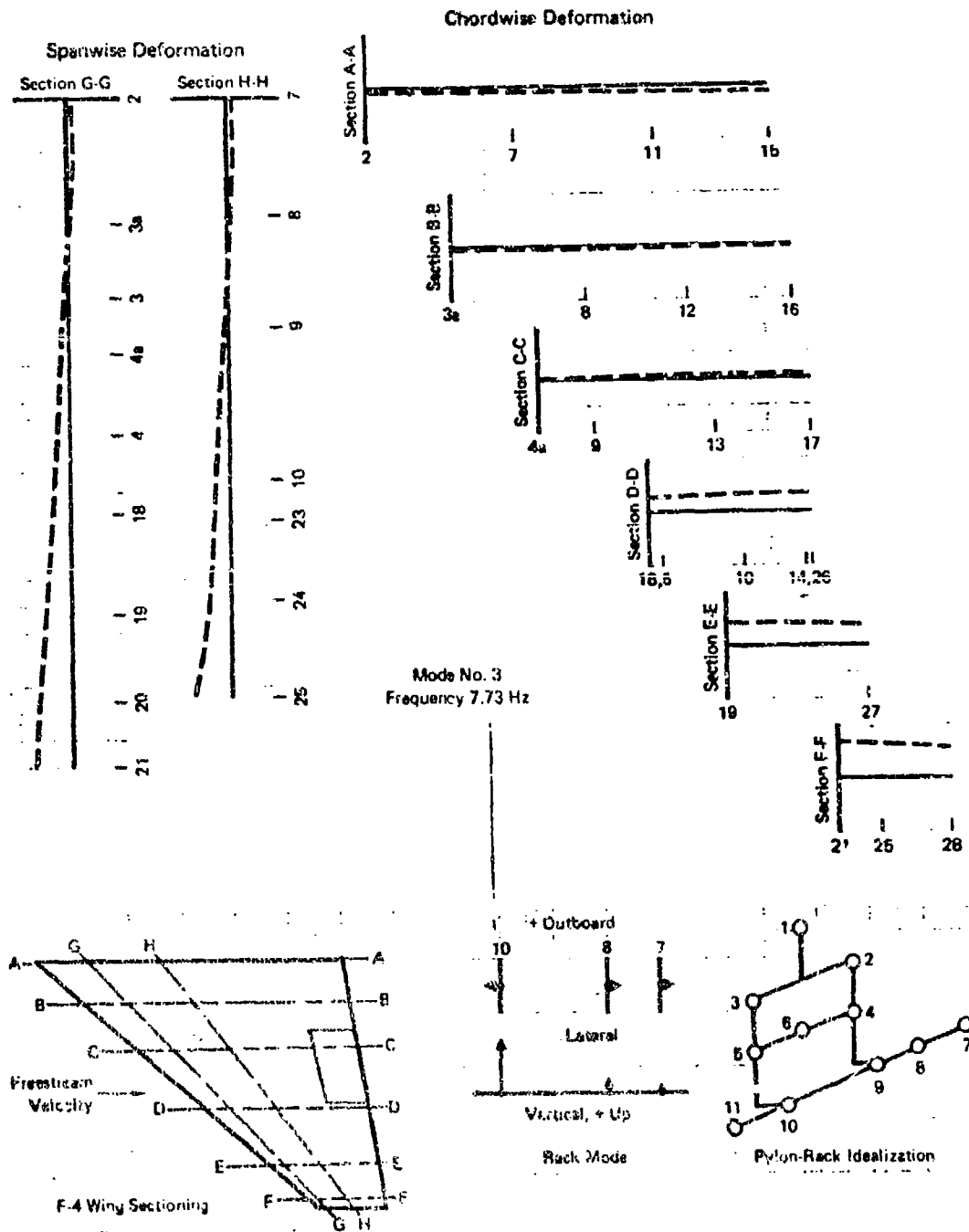
FIGURE 131 F-4/MK-82 (3, 4) THIRD NORMAL VIBRATION MODE

244

APPENDIX II

ANALYTICAL MODEL FOR ADVANCED AIRCRAFT HORIZONTAL TAIL

The Computerized Optimization Procedure for Stabilators (COPS) of Reference 4 has been used to generate the detailed structural description for the advanced aircraft horizontal tail. A general matrix computer program was used to evaluate the dynamic matrix and perform the eigenvalue (vibration) solution.

II.1 Geometrical Data

The overall characteristics for this surface are given in Table 2 of the main report. The analytical model generated by COPS is shown in Figure 8. The forward spar is at 32.2% chord, the aft spar is at 57.5% chord and the elastic axis is at 45% chord. Each of the eight discrete rigid chord sections is further divided into leading edge, torque box, and trailing edge components. A linear variation of thickness ratio from root to tip and the four digit NACA airfoil shape were used by the COPS program to calculate the airfoil thicknesses.

II.2 Air Load Data

The design tail load is specified at 61,000 lbs. This value is based on a 5g (limit) aircraft. An elliptical air load distribution obtained from the design load generates the bending moment and torque data used in the strength analysis.

II.3 Strength Data

The structural material is boron/epoxy composite. A composite layup for a feasible strength design torque box skin is specified with 70% of the fibers at 0 degrees, 20% at ± 45 degrees and 10% at 90 degrees. The allowable tension stress is specified at 80,000 lb/in^2 and the minimum skin thickness at 0.04 in. The composite material layup for the spars has 100% of the fibers at ± 45 degrees. The allowable shear stress is 50,000 lb/in^2 and the minimum spar thickness is 0.04 in. The GJ and EI stiffness distributions for the feasible Strength Design horizontal tail are given in Figures 76 and 77. Also shown in the figures are data for the Stiffness Sensitivity Design calculated as described in Section 4.2.1.1 of the main report.

II.4 Weight Data

The weight assessment is made in accordance with the basic idealization shown in Figure 8. The weight data in Table 12 is for the Strength Design. The Stiffness Sensitivity Design, which differs from the Strength

TABLE 12 WEIGHT DATA FOR ADVANCED AIRCRAFT HORIZONTAL TAIL

CANDIDATE DESIGN

Leading Edge

X-BAR	Y-BAR	IOY	IOX	IOXY	WEIGHT
28.38	5.66	2231.50	149.79	153.96	13.27
40.34	17.30	1578.76	125.62	129.11	11.13
52.30	28.93	1088.75	104.76	107.05	9.23
64.26	40.57	728.86	85.19	87.55	7.56
76.21	52.20	471.24	68.53	70.49	6.09
88.16	63.82	292.60	54.51	56.02	4.81
100.11	75.44	172.06	41.28	42.45	3.70
112.03	87.05	95.75	30.67	31.73	22.74

Torque Box

X-BAR	Y-BAR	IOY	IOX	IOXY	WEIGHT
66.95	5.66	4887.13	450.47	331.13	39.91
75.49	17.28	3493.13	375.77	276.16	33.32
84.02	28.83	2380.81	301.43	221.52	26.76
92.63	40.47	1524.75	229.04	168.38	20.39
101.02	52.23	896.06	161.16	118.50	14.41
109.48	63.54	465.14	102.59	75.44	9.08
118.12	75.26	213.75	59.76	44.22	5.42
126.93	87.13	107.00	43.36	31.86	3.84

Trailing Edge

X-BAR	Y-BAR	IOY	IOX	IOXY	WEIGHT
112.60	5.68	2766.75	114.12	44.48	10.11
117.13	17.32	1979.63	98.07	38.23	8.69
121.67	28.86	1378.06	83.50	32.56	7.40
126.71	40.59	927.63	70.29	27.41	6.23
130.74	52.28	599.13	58.38	22.77	5.18
135.27	63.86	366.81	47.88	18.69	4.22
139.80	75.48	209.13	37.70	14.70	3.36
144.33	87.08	108.33	29.21	11.41	2.59

TOTAL WEIGHT =   279.44 LBS.

Units
Length - Inches
Weight - Pounds
Inertia - Pound - Inch^2

Design only in the torque box regions, has weight data as shown in Table 13.

II.5 Vibration Data for Candidate Design

Vibration mode shapes for the four lowest normal modes of the Candidate Design of Section 4.2.1.2 of the main report are shown in Figures 132 to 135.   Support flexibility in roll is included in these modes, but pitch is excluded since it is desired to include the pitch restraint in a separate uncoupled mode. This uncoupled pitch rotation mode is then inertially coupled with the normal vibration modes for the flutter solutions.

The principal mode of interest is the second mode shown in Figure 133. This normal mode may be arbitrarily labeled the first torsion mode.   Its frequency decreases with airspeed and it is the unstable mode in the flutter mechanism.   The mode is coupled with the first bending motion of the surface. Note that both Mode 1 (Figure 132) and Mode 2 (Figure 133) have only first bending combined (in and out of phase) with first torsion.

Node lines of the second normal mode are shown in Figure 136 for three stabilator configurations. Both the Strength Design and the Stiffness Sensit vity Design have node lines for flutter near the aft portion of the surface. These node lines show the influence of second bending mode coupling. Both of these designs are more prone to flutter than the Candidate Design which has a favorable node line near the leading edge of the surface over the entire span so that its frequency does not decrease with increasing airspeed.

TABLE 13 WEIGHT DATA FOR ADVANCED AIRCRAFT HORIZONTAL TAIL - STIFFNESS SENSITIVITY DESIGN TORQUE BOX

TORQUE BOX SECTION	X-BAR IN.	Y-BAR IN.	IØY LB-IN^2	IØX LB-IN^2	IØXY LB-IN^2	WGT. LB.	ΔWGT. LB.
1	66.95	5.66	4887.13	450.47	331.13	39.91	0
2	75.49	17.26	3493.13	375.77	276.16	33.32	0
3	84.02	28.88	2380.81	301.43	221.52	26.76	0
4	92.53	40.17	1622.33	318.18	179.16	21.70	1.31
5	101.02	52.03	1187.28	213.54	157.01	19.09	4.68
6	109.48	63.54	830.81	182.96	134.66	16.21	7.13
7	118.12	75.26	433.06	121.07	89.59	10.98	5.56
8	126.93	87.18	164.35	66.60	48.94	5.90	2.06

$$\Sigma \Delta WGT = 20.74$$
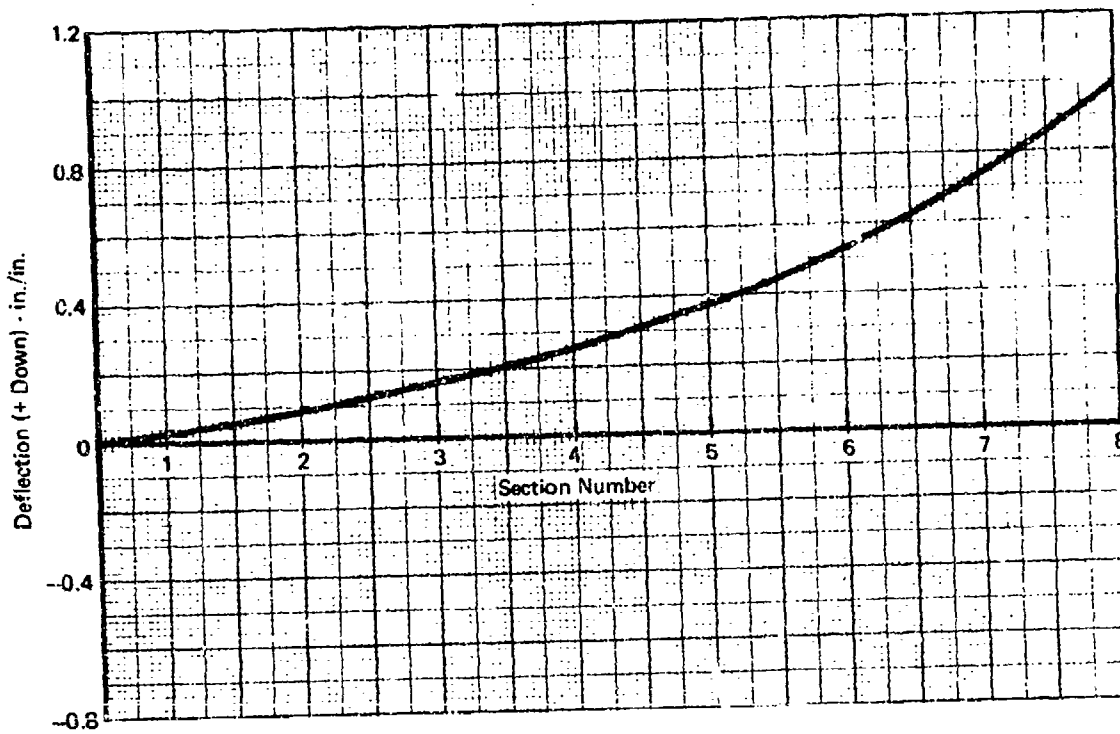
Frequency = 12.7 Hz
Generalized Mass = 0.154 lb sec^2/in.
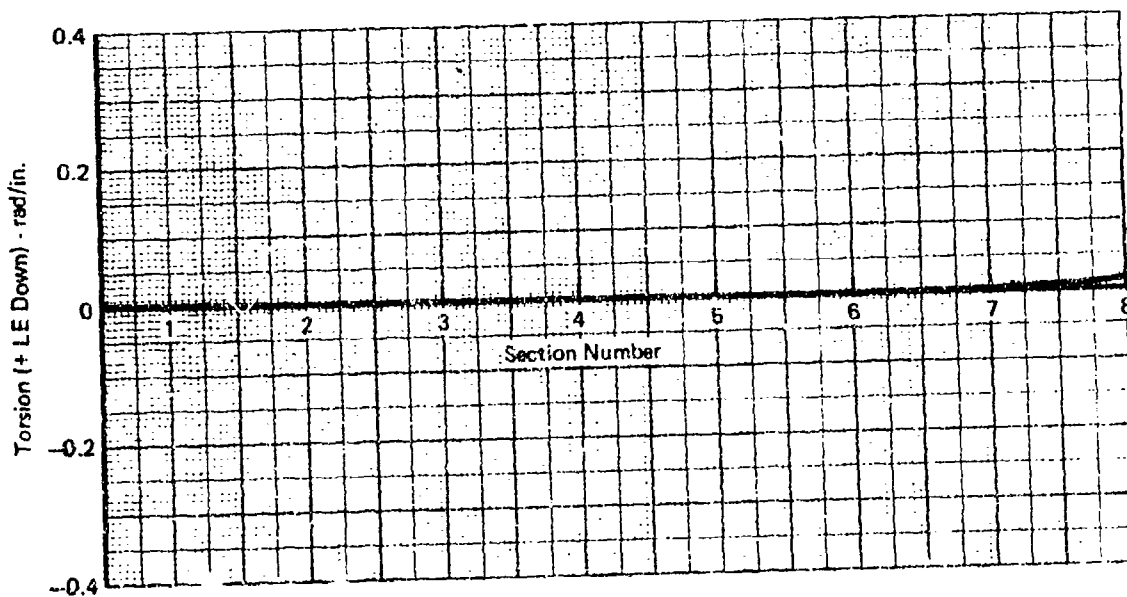
FIGURE 132 ADVANCED AIRCRAFT HORIZONTAL TAIL-CANDIDATE
DESIGN FIRST NORMAL VIBRATION MODE

Frequency = 21.58 Hz
Generalized Mass = 0.227 lb sec^2/in.
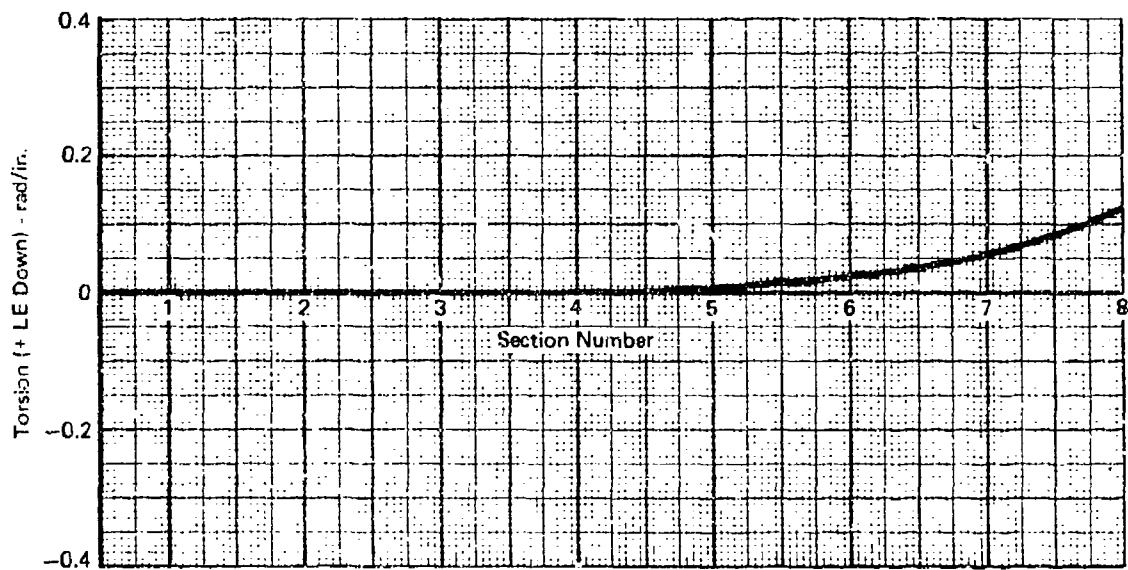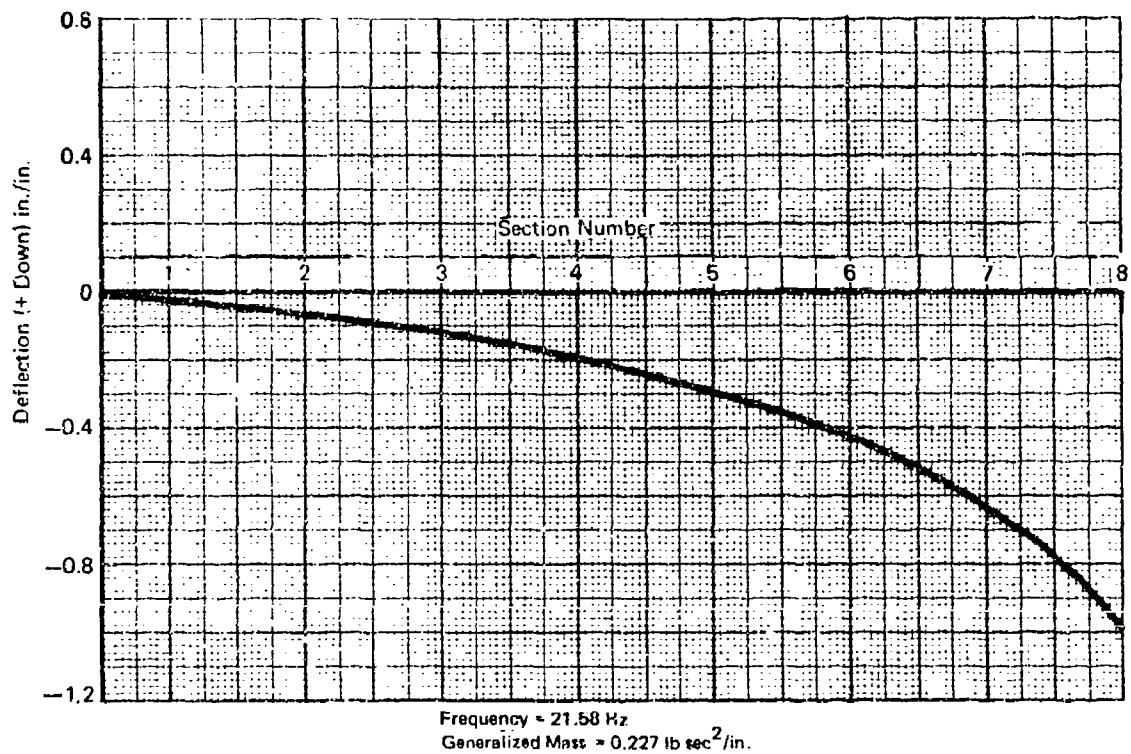
FIGURE 133 ADVANCED AIRCRAFT HORIZONTAL TAIL - CANDIDATE
DESIGN SECOND NORMAL VIBRATION MODE
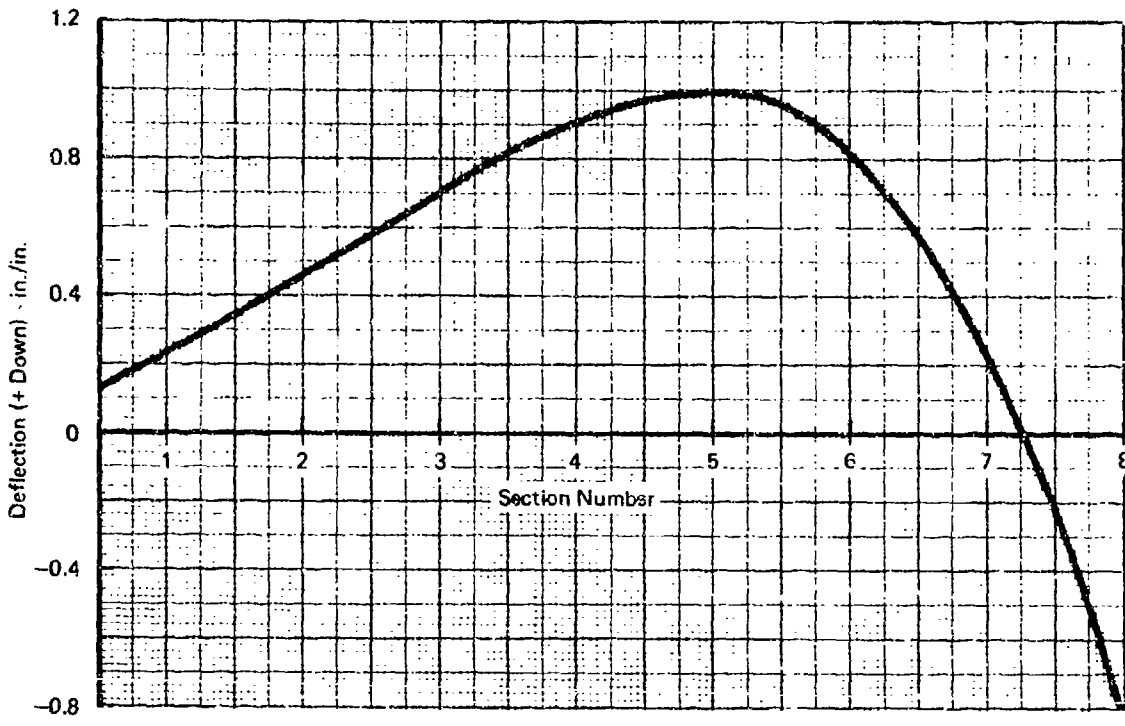
Frequency = 37.03 Hz
Generalized Mass = 0.557 lb sec^2/in.
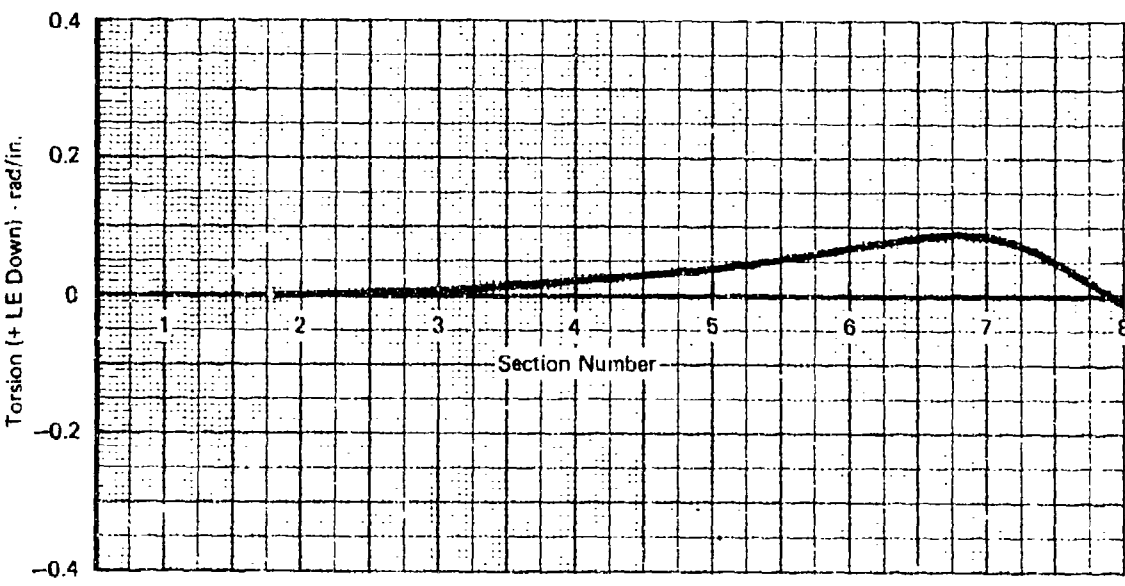
FIGURE 134 ADVANCED AIRCRAFT HORIZONTAL TAIL - CANDIDATE
DESIGN THIRD NORMAL VIBRATION MODE
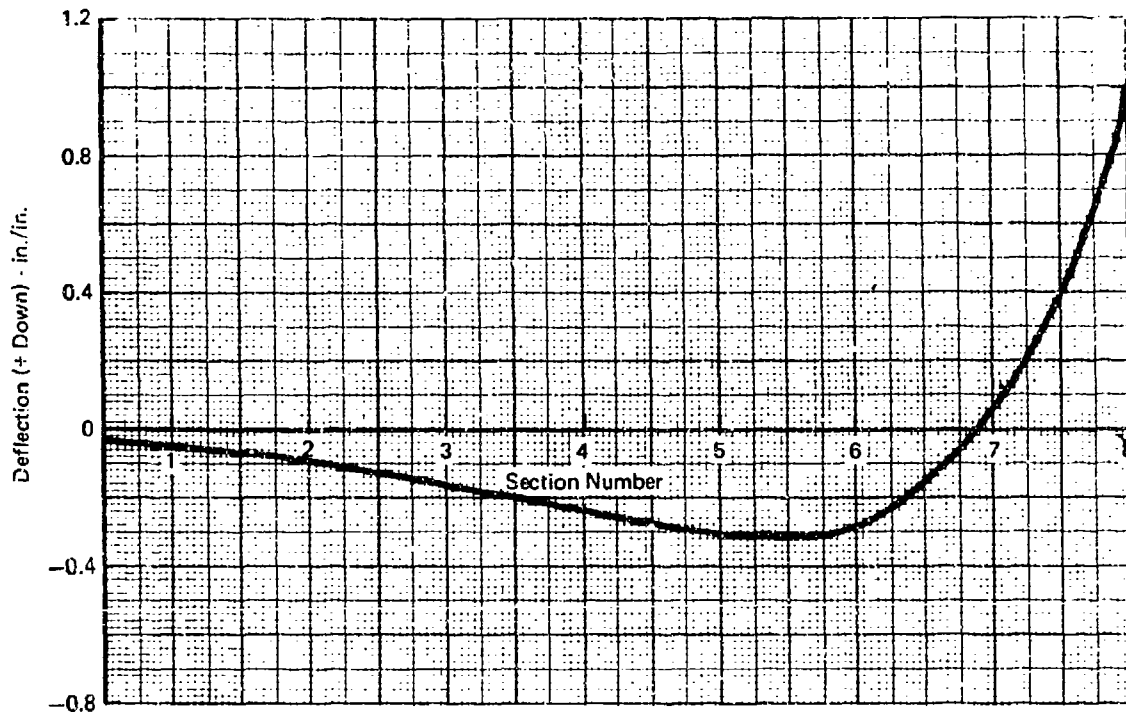
Frequency = 44.02 Hz
Generalized Mass = 0.151 lb sec^2/in.
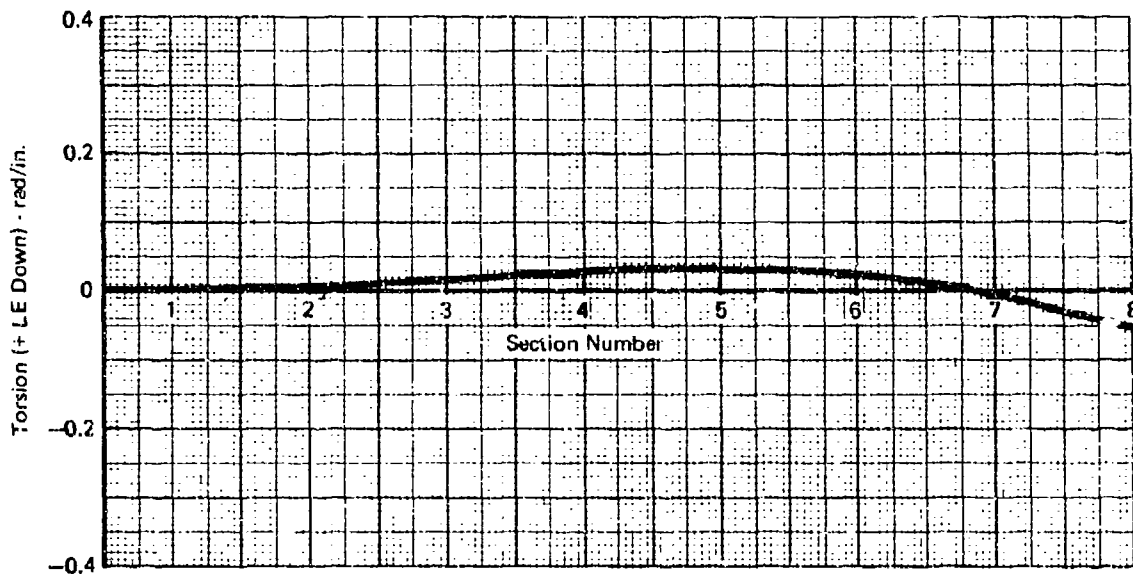
FIGURE 135 ADVANCED AIRCRAFT HORIZONTAL TAIL - CANDIDATE
DESIGN FOURTH NORMAL VIBRATION MODE
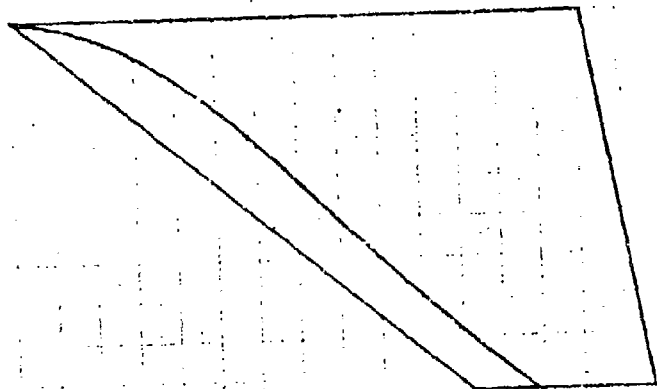
STRENGTH DESIGN

STIFF. SENS. DESIGN
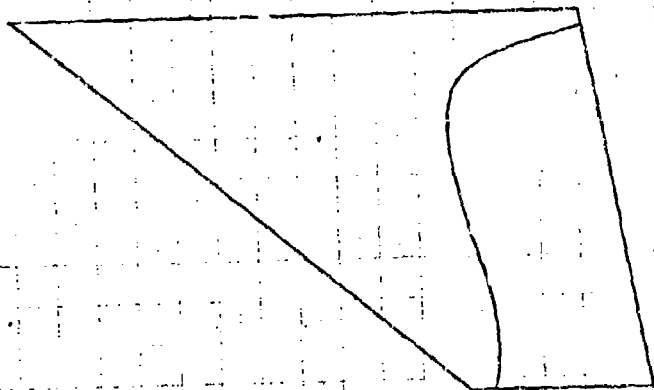
CANDIDATE DESIGN
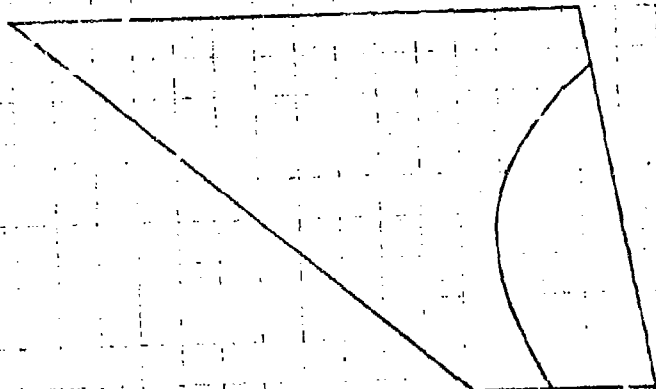
FIGURE 136 ADVANCED AIRCRAFT HORIZONTAL TAIL - NODE LINES OF SECOND NORMAL VIBRATION
MODE FOR TRIAL CONFIGURATIONS

253

APPENDIX III

ANALYTICAL MODEL FOR ADVANCED AIRCRAFT WING

The Computerized Optimization Procedure for Stabilators (COPS) of
Reference 4 has been used to generate the detailed structural descrip-
tion for the advanced aircraft wing.

III.1 Geometrical Data

The overall characteristics for this wing are given in Table 2 of the
main report. The analytical model generated by COPS considers only the ex-
posed area of the wing as shown in Figure 9. The model consists of eight
discrete rigid chord streamwise sections. Each section is further divided
into leading edge, torque box, and trailing edge components; thus creating
24 planform areas. A linear variation of thickness ratio from root to tip
and the four digit NACA airfoil shape are used by the program to calculate
the airfoil thicknesses.

III.2 Air Load Data

The design load for the exposed wing panel is 110,000 lbs. This value,
which is 72% of the overall design load for this 5g (limit) aircraft, was
obtained by weighted integration of the airload distribution for the theore-
tical wing. An elliptical air load distribution based on the exposed wing
design load generates the bending moment and torque data used in the strength
analysis.

III.3 Strength Data

The structural material chosen for this wing is boron/epoxy composite.
A feasible strength design layup for the torque box skin is specified with
70% of the fibers at 0 degrees, 20% at ± 45 degrees and 10% at 90 degrees.
This layup is uniform over the span. The allowable tension stress is speci-
fied at 80,000 lbs/in^2 and the minimum skin thickness at 0.04 in.

The composite material layup for wing spars has 100% of the fibers at
± 45 degrees. An allowable shear stress of 50,000 lbs/in^2 and a minimum
thickness of 0.04 in. are specified for the spars.

The leading and trailing edge sections are given skin thicknesses which
vary from 0.06 in. at the root chord to 0.02 in. at the tip chord. Both sec-
tion cores are filled with titanium honeycomb. The honeycomb weight was
included in the analysis; but its stiffness characteristics were omitted.

The EI and GJ distributions resulting from the described wing structure
are given in Figure 137.

254
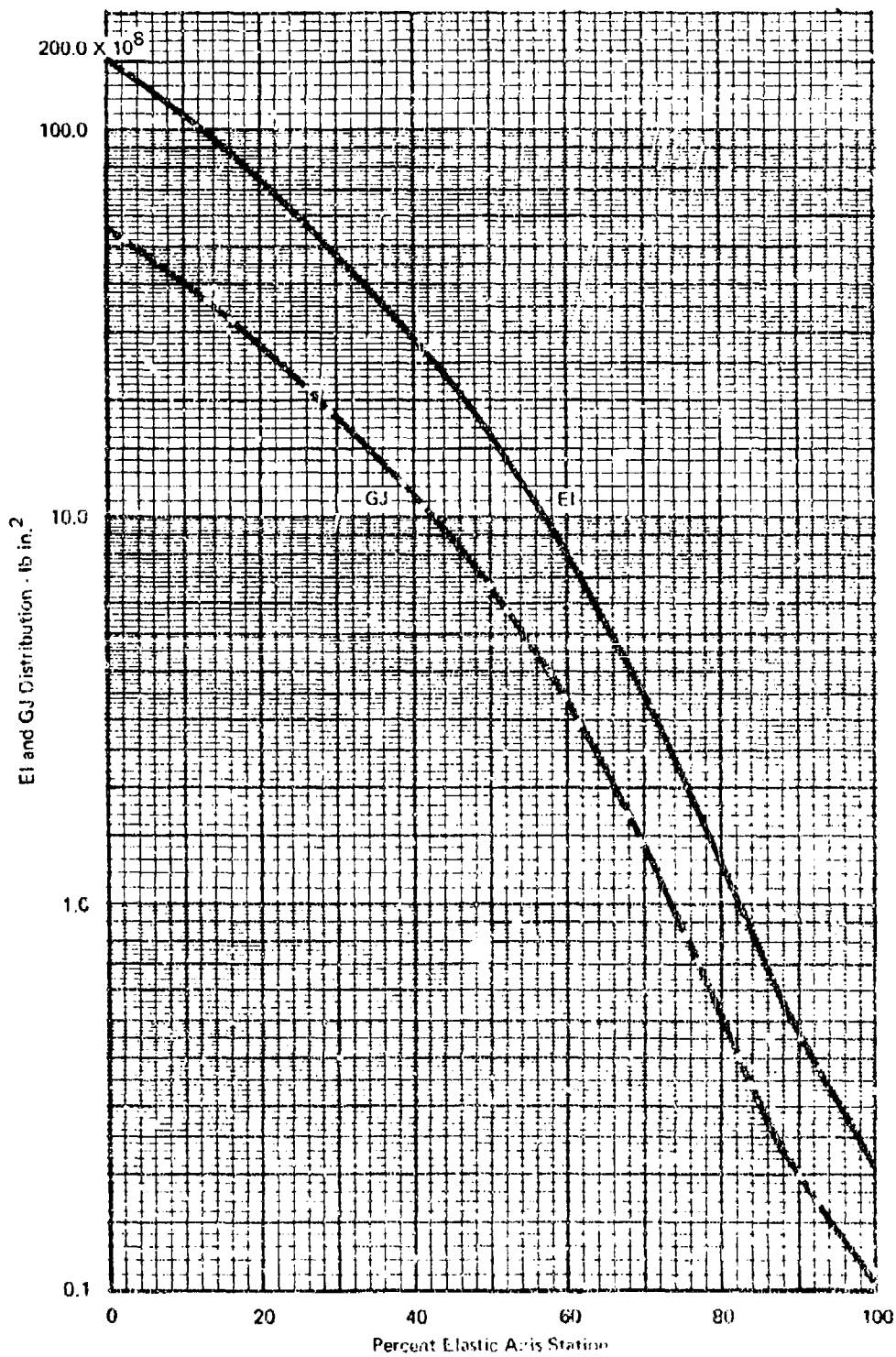
FIGURE 137 EI AND GJ DISTRIBUTION FOR ADVANCED AIRCRAFT WING

The EI and GJ for the torque box carry-through structure are constant at the exposed wing root chord values from the fuselage moldline to the aircraft centerline.

III.4 Weight Data

The weight assessment for the exposed wing is made in accordance with the basic idealization shown in Figure 9. Local weight data for each of the 24 planform areas are given in Table 14 for the strength design wing. This distribution has no aerodynamic control surfaces on either the leading or trailing edges. The location of the planform area center of gravity is given by X-BAR and Y-BAR. The local pitch inertia, roll inertia, and product of inertia are given by IOY, IOX and IOXY.

A similar weight distribution is given in Table 15 for the wing with control surfaces in each section of both leading and trailing edges. The torque box weight is unchanged. By combining selected parts of these two separate weight distributions the user is able to specify whether or not a control surface is to be included in each of 8 leading and 8 trailing edge sections.

III.5 Wing Vibration Data

The six lowest zero airspeed wing vibration modes are given in Figures 138 through 143. The bending deflections are for points on the elastic axis (42% chord) and are defined as positive downward. The torsion deflections are in the streamwise direction and are positive for the leading edge down. Bending slope about the streamwise axis is also included in the analysis. Each of these normal coupled elastic vibration modes is normalized to the maximum bending deflection.

TABLE 14 WEIGHT DATA FOR ADVANCED AIRCRAFT WING - NO AERODYNAMIC CONTROL SURFACES

LEADING EDGE

X-BAR	Y-BAR	IOY	ICX	IOXY	WEIGHT
27.27	11.67	1992.90	767.40	966.72	16.08
57.35	35.6C	1582.58	454.01	822.19	13.71
87.05	59.27	1160.00	612.11	643.93	10.75
117.67	83.42	829.31	391.48	492.31	8.22
147.52	107.33	428.50	315.50	397.06	6.65
177.00	130.76	419.50	222.25	280.25	4.73
207.52	155.05	205.75	150.19	167.63	3.14
237.48	178.85	179.19	104.30	132.00	2.23

TORQUE BOX

X-BAR	Y-BAR	IOY	ICX	IOXY	WEIGHT
79.38	11.6C	133794.00	10165.65	10753.38	213.25
104.63	35.46	92198.00	8267.61	8741.50	173.56
129.84	55.32	60122.00	6432.81	6801.50	135.23
155.02	83.13	36453.00	4705.50	4975.00	99.25
180.11	106.07	19995.00	3149.06	3326.00	66.78
205.07	130.46	9481.00	1839.81	1942.00	39.35
230.50	154.52	4054.00	991.88	1051.00	21.17
256.62	179.18	2019.00	656.31	693.06	13.75

TRAILING EDGE

X-BAR	Y-BAR	IOY	IOX	IOXY	WEIGHT
147.90	11.7C	6393.75	1037.10	925.74	21.72
166.95	35.63	4683.50	900.57	716.88	18.87
185.70	55.15	3076.50	704.5	560.80	14.86
205.03	83.46	1914.06	535.3	429.44	11.31
224.07	107.39	1277.25	445.7	354.88	9.35
243.66	130.72	725.09	315.15	251.06	6.68
262.09	155.12	372.36	210.44	167.63	4.42
281.07	178.97	211.06	154.50	123.13	3.27

TOTAL WEIGHT = 918.34 LBS

Units

Length ~ Inches
Weight ~ Pounds
Inertia ~ Pound - Inch^2

TABLE 15 WEIGHT DATA FOR ADVANCED AIRCRAFT WING - AERODYNAMIC CONTROL SURFACES IN EACH LEADING AND TRAILING EDGE SECTION

LEADING EDGE

X-BAR	Y-BAR	IOY	ICX	IOXY	WEIGHT
26.01	11.77	4463.72	1674.99	2346.14	39.54
56.32	35.72	3593.75	1631.65	2034.55	34.40
86.02	59.45	2712.25	1238.24	1662.11	28.25
116.17	83.84	2127.13	7079.84	1341.81	22.72
146.13	107.55	1699.94	908.25	1125.28	18.85
176.56	131.31	1200.09	705.89	867.55	14.51
206.81	155.49	899.97	555.02	675.47	11.34
237.75	179.47	633.40	386.51	485.40	8.11

TORQUE BOX

X-BAR	Y-BAR	IOY	IOX	IOXY	WEIGHT
79.38	11.60	133794.00	10169.69	10753.38	213.25
104.63	35.48	92198.00	8267.81	8741.50	173.56
129.84	59.32	60122.00	4432.01	6801.50	135.23
155.02	83.13	36453.00	4705.50	4975.00	99.25
180.11	106.87	19595.00	3149.06	3326.00	66.78
205.07	130.48	9481.00	1835.81	1942.00	39.35
230.50	154.52	4054.00	591.88	1051.00	21.17
256.82	179.18	2019.00	456.31	696.06	13.75

TRAILING EDGE

X-BAR	Y-BAR	IOY	ICX	IOXY	WEIGHT
140.55	11.70	20801.71	1893.23	1508.96	54.55
159.91	35.63	15554.30	1807.24	1429.53	52.77
176.77	59.18	5581.75	1203.36	1369.68	52.92
196.54	83.46	8802.93	1894.43	1314.10	50.63
215.65	107.38	7433.81	1550.38	1282.51	48.58
237.63	130.72	3153.63	771.46	615.65	29.42
257.86	155.12	2141.31	711.31	584.56	27.01
277.61	178.97	1294.74	639.73	530.55	20.61

TOTAL WEIGHT = 1285.53 LBS

Units

Length ~ inches
Inertia ~ pound - inch^2
Weight ~ pounds
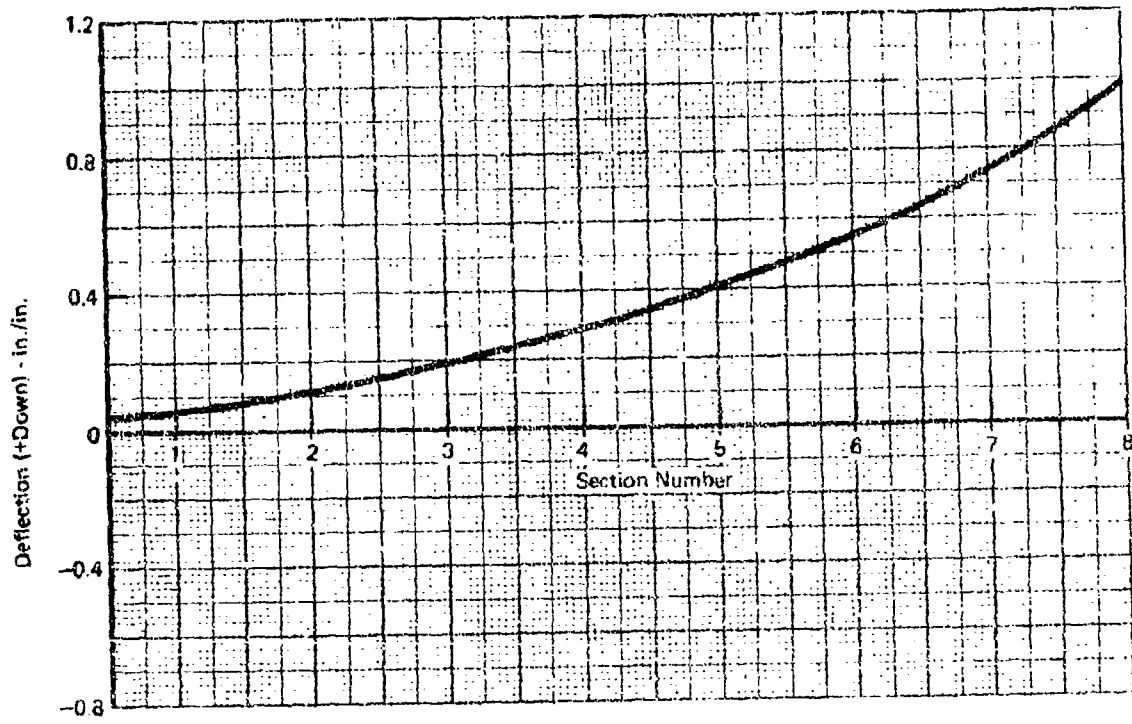
Frequency = 5.02 Hertz
Gen. Mass = .407 lb sec^2/in.
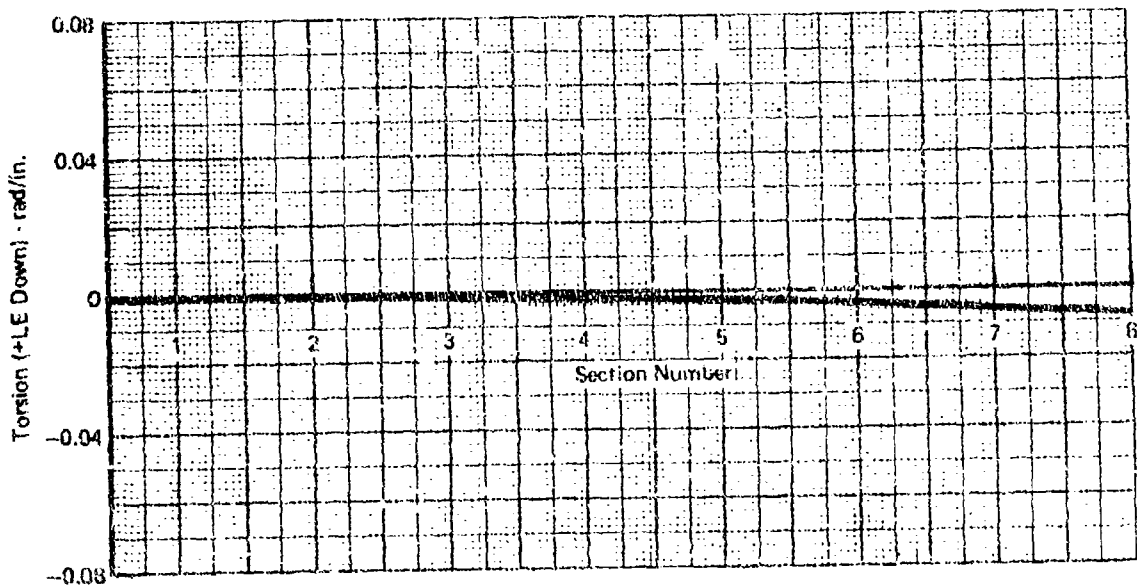
FIGURE 138 ADVANCED AIRCRAFT WING - FIRST VIBRATION MODE
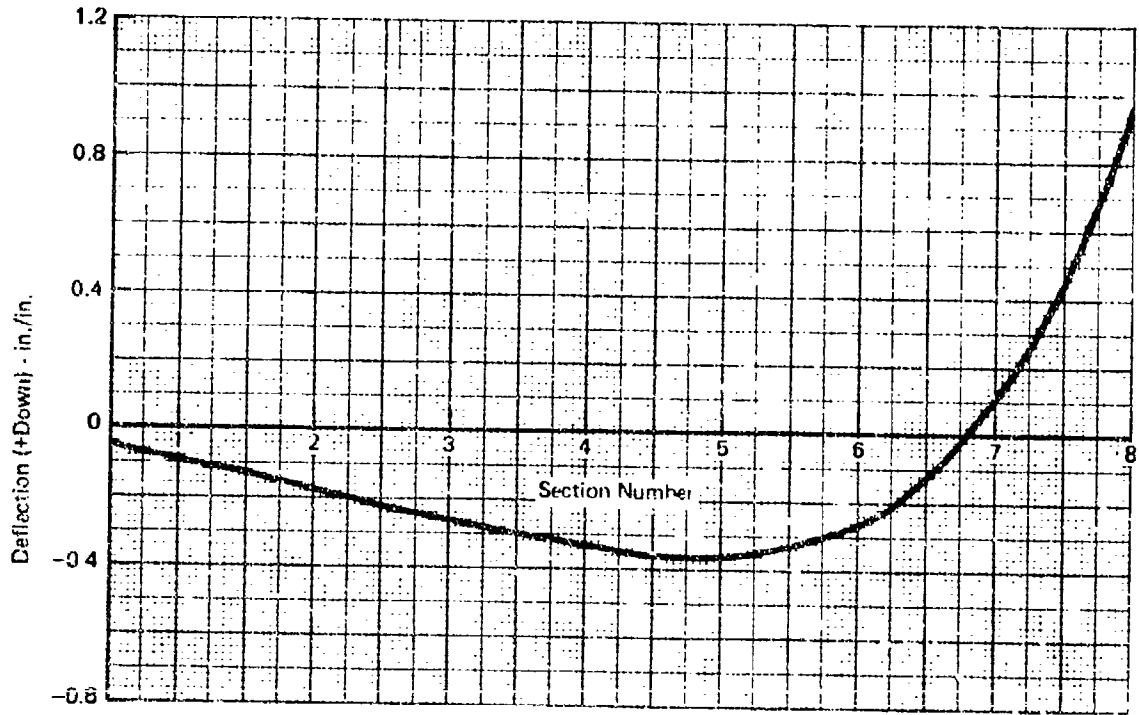
Frequency = 12.11 Hertz
Gen. Mass = .445 lb sec^2/in.
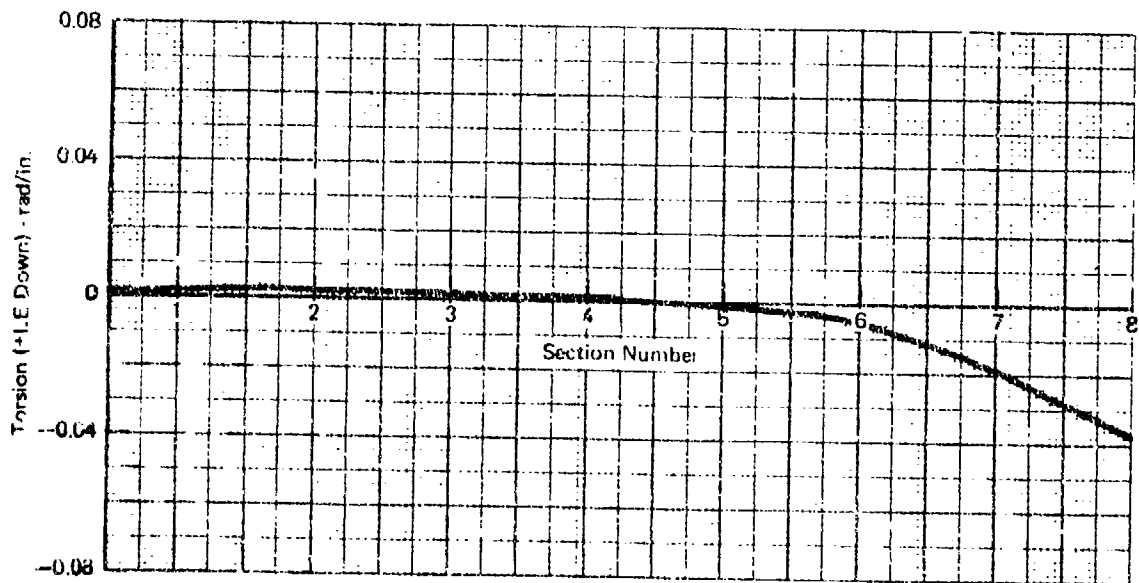
FIGURE 139 ADVANCED AIRCRAFT WING - SECOND VIBRATION MODE
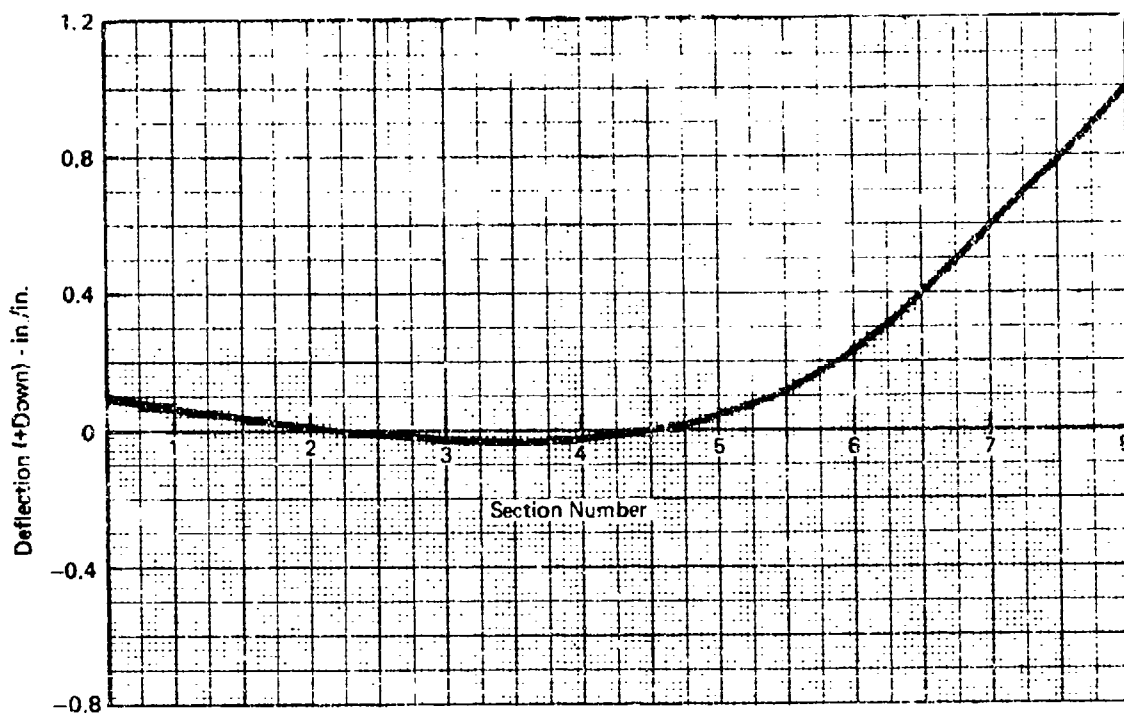
Frequency = 21.14 Hertz
Gen. Mass = .699 lb sec^2/in.
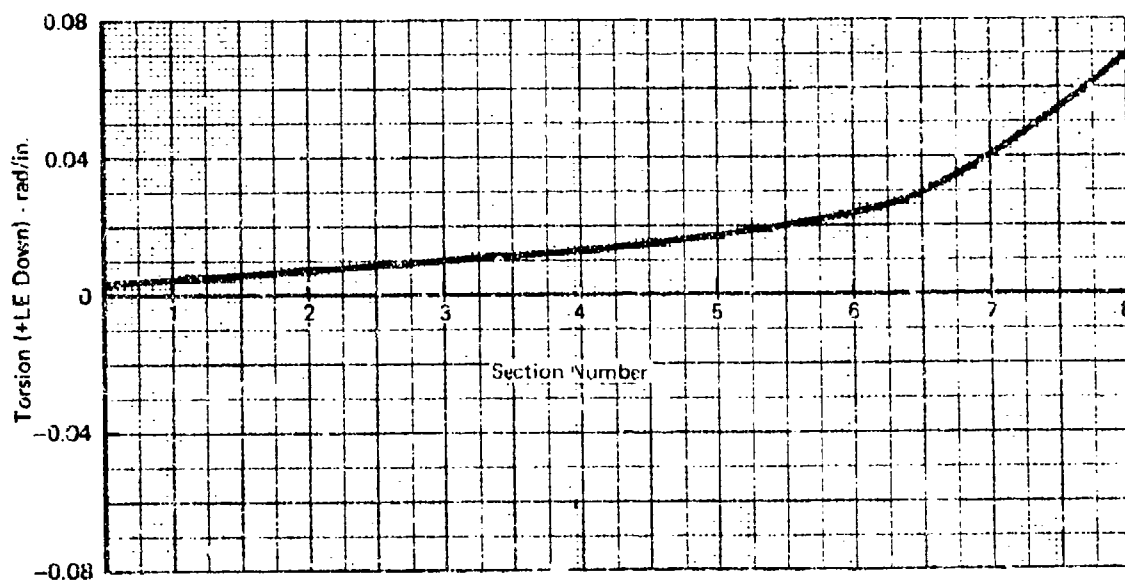
FIGURE 140 ADVANCED AIRCRAFT WING - THIRD VIBRATION MODE
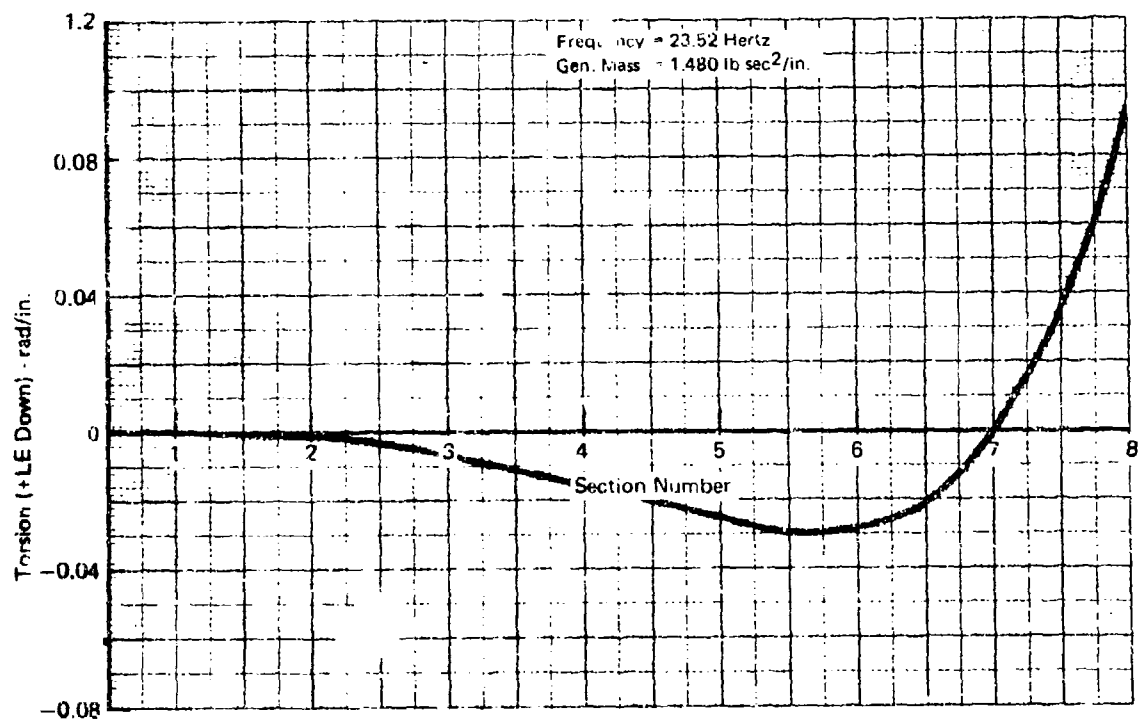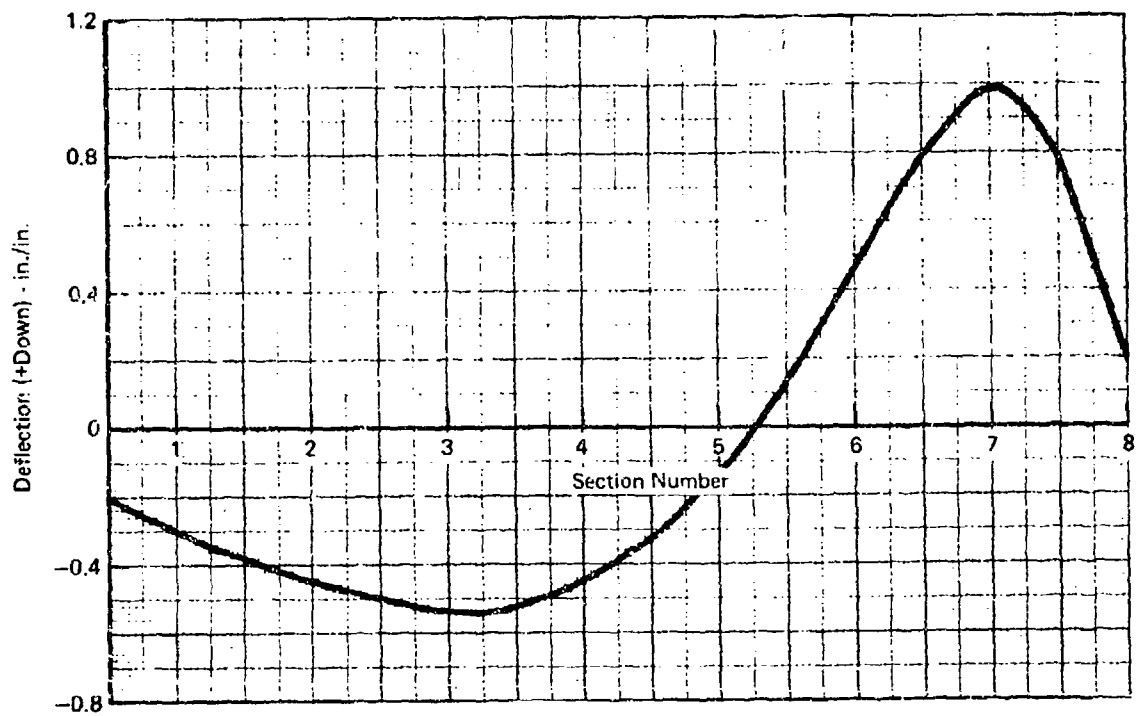
FIGURE 141 ADVANCED AIRCRAFT WING - FOURTH VIBRATION MODE
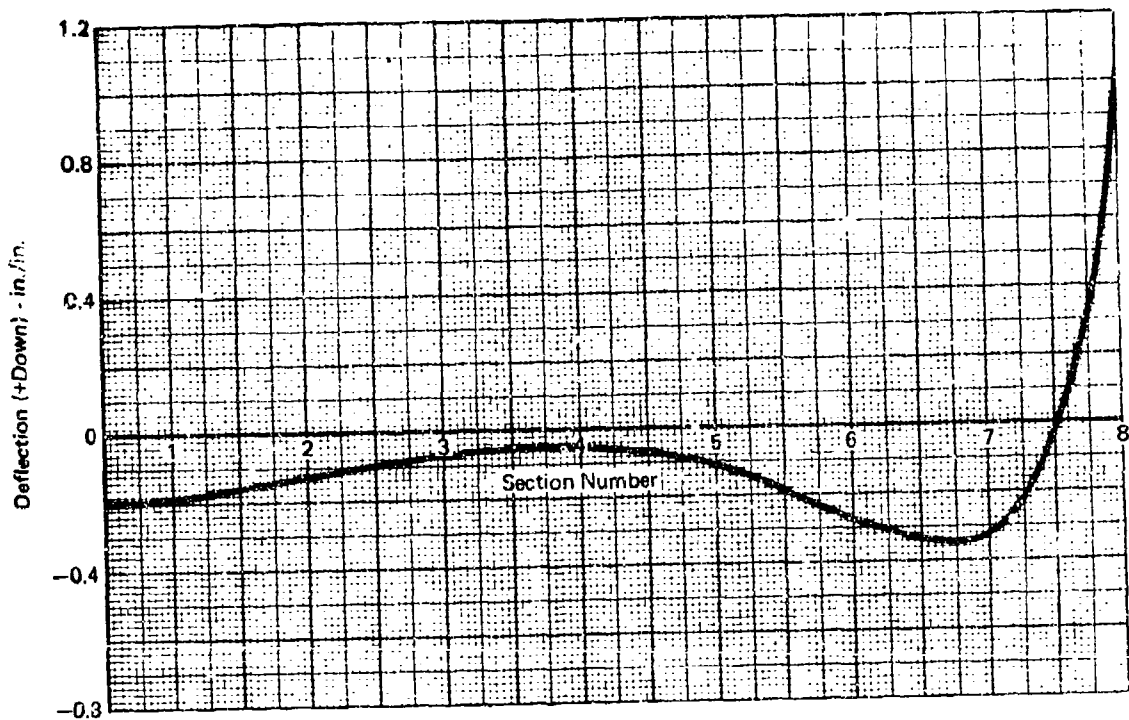
Frequency = 32.19 Hertz
Gen. Mass = .884 lb sec^2/in.
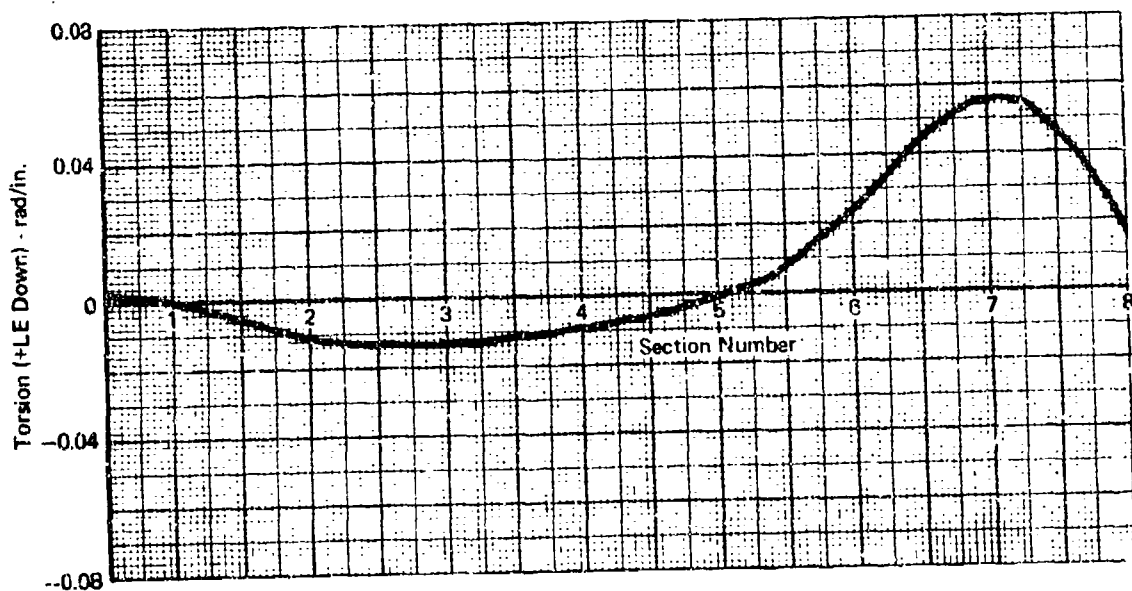
FIGURE 142 ADVANCED AIRCRAFT WING - FIFTH VIBRATION MODE
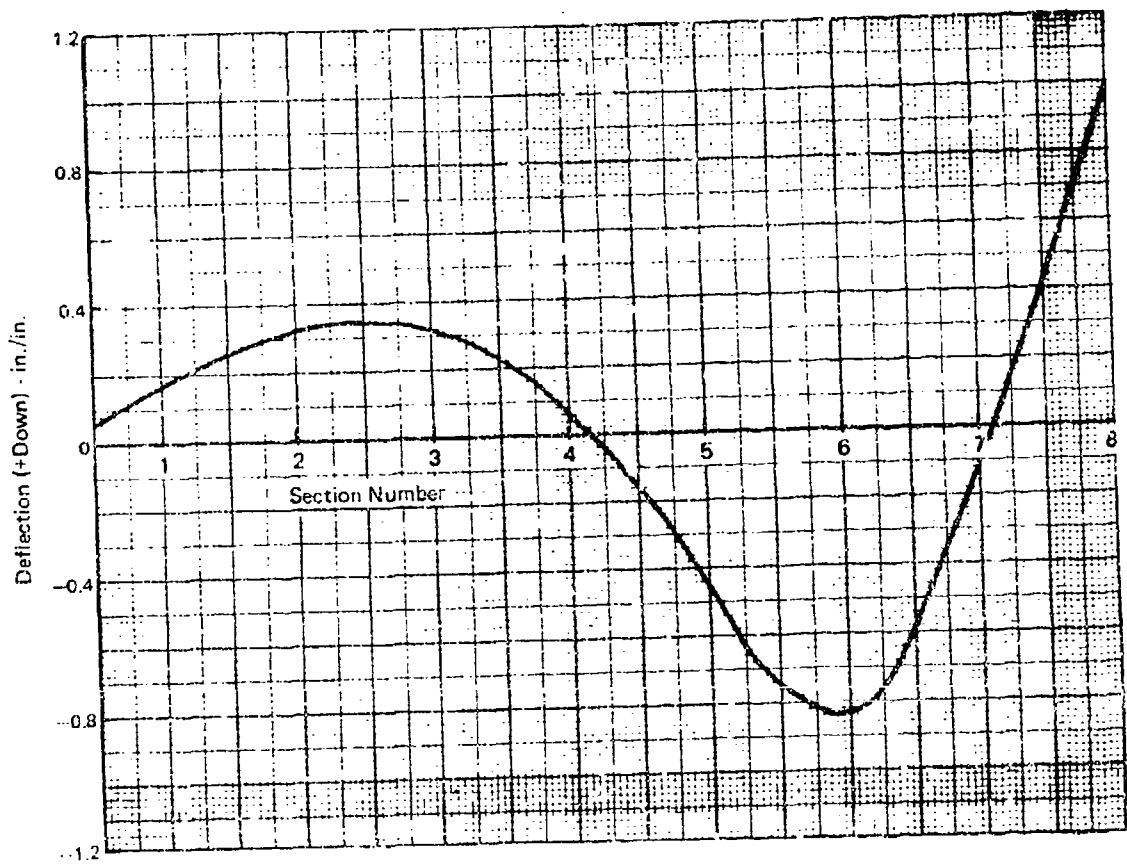
Frequency = 36.56 Hertz
Gen. Mass = 1.318 lb·sec²/in.
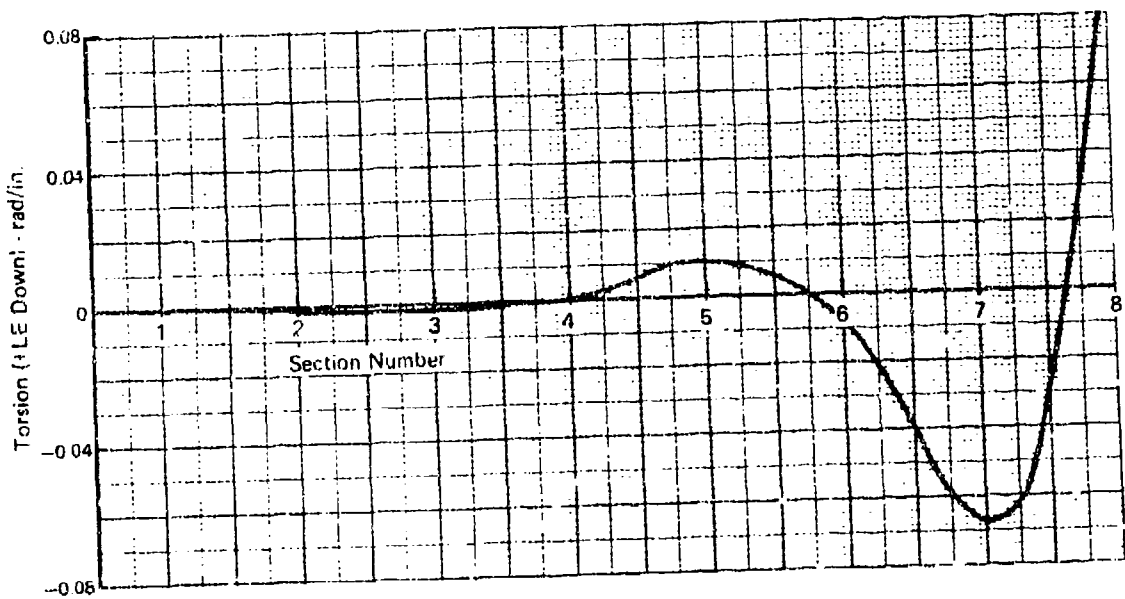
FIGURE 143 ADVANCED AIRCRAFT WING - SIXTH VIBRATION MODE

264

COMPUTER PROGRAM DESCRIPTIONS

IV.1 Active Control of Flutter Computer Program – Time Domain

IV.1.1 Unforced Aeroelastic Equations of Motion – The unforced equations of motion for a general aeroelastic system may be expressed in the form,

$$M\ddot{q} + C\dot{q} + Kq + Q_A q + \frac{Q}{V} B\dot{q} + \frac{Q}{V^2} I\ddot{q} + QA_c \left[q_o \, \phi(s) + \int_o^s \frac{dq}{d\sigma} \phi(s - \sigma) \, d\sigma \right]$$

$$+ \frac{Q}{V} B_c \left[\dot{q}_o \, \phi(s) + \int_o^s \frac{d^2q}{d\sigma^2} \phi(s - \sigma) \, d\sigma \right] = 0$$

The Wagner lift growth function is given by,

$$\phi = 1 - A_1 e^{-B_1 s} - A_2 e^{-B_2 s}$$

and the non-dimensional time variables are defined as,

$$s = \frac{V}{b} t \quad \text{and} \quad \sigma = \frac{V}{b} \tau$$

Consider now the individual convolution integral terms,

$$QA_c \left[\int_o^s \frac{dq}{d\sigma} \phi(s - \sigma) \, d\sigma \right] \leftrightarrow QA_c \left(\dot{q}(S) * \phi(S) \right)$$

and

$$\frac{Q}{V} B_c \left[\int_o^s \frac{d^2q}{d\sigma^2} \phi(s - \sigma) \, d\sigma \right] \leftrightarrow \frac{Q}{V} B_c \left(\ddot{q}(S) * \phi(S) \right)$$

where $\phi(S)$ is the Laplace transform of $\phi(t)$

Let,

$$C_1 = B_1 \frac{V}{b} \quad \text{and} \quad C_2 = B_2 \frac{V}{b}$$

so that

$$\phi(t) = 1 - A_1 e^{-C_1 t} - A_2 e^{-C_2 t}$$

in terms of real time t.

The Laplace transform is then,

$$\phi(S) = \frac{1}{S} - \frac{A_1}{S+C_1} - \frac{A_2}{S+C_2}$$

which may be reduced to the equivalent expression,

$$\phi(S) = \frac{R}{S} \left[\frac{(1 + \tau_1 S)(1 + \tau_2 S)}{(1 + \tau_3 S)(1 + \tau_4 S)}\right] = \frac{1}{S} \ y(S)$$

where

$$\tau_i = f \ (A_1, \ A_2, \ C_1, \ C_2)$$

and

R = effective gain of the transfer function y(S)

The free $1/S$ in the expression is used to reduce the order for the generalized coordinates in the convolution integrals to allow for the subsequent recasting of the equations of motion into standard form. Thus, the convolution terms become,

$$QA_c \ (\dot{q}(S)*\phi(S)) \rightarrow QA_c \ (q(S)*y(S))$$

and

$$\frac{Q}{V} B_c \ (\ddot{q}(S)*\phi(S)) \rightarrow \frac{Q}{V} B_c \ (\dot{q}(S)*y(S))$$

This procedure is similar to the usual method for representation of the Theodorsen (Wagner) function on passive analog computers (i.e., CEAC). The function y(S) is well behaved in the time domain and may be programmed in the MIMAC computer language, a MCAIR form similar to the AFFDL MIMIC, just as we would program an operational analog computer.

IV.1.2 Forced Aeroelastic Equations of Motion - The forced equations of motion may be expressed as,

$$M\ddot{q} + C\dot{q} + Kq + QAq + \frac{Q}{V} B\dot{q} + \frac{Q}{V^2} I\ddot{q} + QA_c \ (q(S)*y(S)) + QA_c q_o \phi(s)$$

$$+ \frac{Q}{V} B_c \ (\dot{q}(S)*y(S)) + \frac{Q}{V} B_c \ \dot{q}_o \phi(s) = \{\frac{\partial F}{\partial q_{F_1}}\} \ q_{F_1}$$

The column matrix on the right is symbolic notation for the generalized force in each generalized coordinate mode in response to the excitation coordinate q_{F_1}. Figure 144 gives simplified examples of two equivalent idealizations for the excitation procedure. The rigid actuator deflection is defined as δ in both idealizations. The excitation is through the spring and damping terms for idealization No. 1 where the flexible deflection coordinate β is defined with respect to a fixed reference. The excitation is through the inertia (and aerodynamic) terms for idealization No. 2 where β is defined relative to the rigid actuator deflection.

Idealization No. 1

$$M\ddot{\beta} + C(\dot{\beta} - \dot{\delta}) + K(\beta - \delta) = 0$$

$$M\ddot{\beta} + C\dot{\beta} + K\beta = C\dot{\delta} + K\delta$$

Idealization No. 2

$$M(\ddot{\beta} + \ddot{\delta}) + C\dot{\beta} + K\beta = 0$$

$$M\ddot{\beta} + C\dot{\beta} + K\beta = M\ddot{\delta}$$
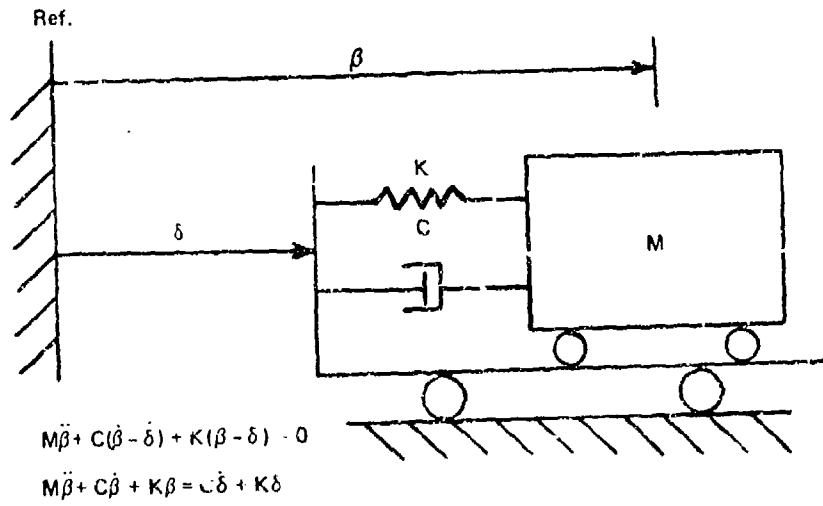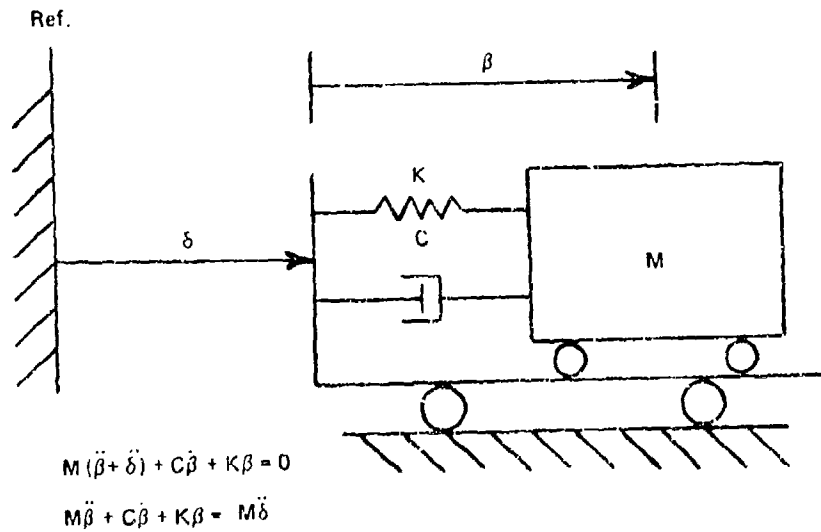
FIGURE 144   EXAMPLE OF IDEALIZATIONS FOR FORCED EXCITATION OF EQUATIONS OF MOTION

Consider now N generalized coordinates, including the flexible control surface coordinate (β), so that the state vector for the aeroelastic system will be,

$$q = \left\{ \begin{array}{c} q_1 \\ \vdots \\ \vdots \\ \vdots \\ q_{N-1} \\ \hline \beta \end{array} \right\}$$

The matrices M, C, K, A, A_c, B, B_c, and I are based on these generalized coordinates. Note that, although the equations of motion are cast in the modal form, we have not specified the types of modes. Complete freedom is allowed in choice of generalized coordinates and the formulation of various derivative matrices.

Idealization No. 1 – For idealization No. 1 (excitation through the spring) the left hand side of the equations are as shown above and the right hand side will appear as

$$\{\frac{\partial F}{\partial q_{F_1}}\} q_{F_1} + \left\{ \begin{array}{c} 0_1 \\ \vdots \\ \vdots \\ 0_{N-1} \\ \hline C_\beta \end{array} \right\} \dot{\delta} + \left\{ \begin{array}{c} 0_1 \\ \vdots \\ \vdots \\ 0_{N-1} \\ \hline K_\beta \end{array} \right\} \delta$$

This is the formulation which has been used in all of the MIMAC runs referred to in this report. In this formulation the data input is simplified since only two numbers (C_β, K_β) are required for the excitation matrices. This is the preferred method when the elastic rotation mode of the control surface is included in the analysis. It is particularly important to include the control surface back-up flexibility in the time domain solutions even if the mode does not interact with the flutter modes of interest. The flexible surface will "give" under air loads and thus allow for more realistic (larger) deflection requirements for flutter control than would be the case for an equivalent rigid control surface representation. In this regard, it is also important to include any potential control surface warpage in the analysis.

<u>Idealization No. 2</u> - For idealization No. 2 (excitation through inertia and implied aerodynamics) the left hand side of the equations is the same as for idealization No. 1. The right hand side will appear, however, as,

$$\{\frac{\partial F}{\partial q_{F_1}}\} \, q_{F_1} \rightarrow - \, \{M\} \, \ddot{\delta} - Q\{A\}\delta - \frac{Q}{V} \, \{B\}\dot{\delta} - \frac{Q}{V2} \, \{I\} \, \ddot{\delta}$$

$$- \, Q \, \{A_c\} \, \delta_o \phi(s) - Q \, \{A_c\}(\delta(S)*y(S))$$

$$- \frac{Q}{V} \, \{B_c\} \, \dot{\delta}_o \phi(s) - \frac{Q}{V} \, \{B_c\}(\dot{\delta}(S)*y(S))$$

where $\{{}_{\text{A}}\}$ etc. denotes the last column of each matrix of coefficients.

Note that with idealization No. 2 the spring and damper are not essential to the formulation and thus may be eliminated completely from the analysis if so desired.

IV.1.3 <u>MIMAC Equation Formulation</u> - The complete set of equations of motion allowing for either idealization No. 1 or No. 2 appear in the MIMAC program in standard form as.

$$\ddot{q} = [M + \frac{Q}{V2} \, I]^{-1} \, \{-[C + \frac{Q}{V} \, B] \, \dot{q} - [K + QA] \, q - QA_c \, q_o \phi(s) - QA_c(q(S)*y(S))$$

$$- \frac{Q}{V} \, B_c \dot{q}_o \phi(s) - \frac{Q}{V} \, B_c \, (\dot{q}(S)*y(S)) - [\{M\} + \frac{Q}{V2}\{I\}]\ddot{\delta} - [\{C\} + \frac{Q}{V} \, \{B\}]\dot{\delta}$$

$$- [\{K\} + Q \, \{A\}]\delta - Q\{A_c\}\delta_o \phi(s) - Q\{A_c\}(\delta(S)*y(S)) - \frac{Q}{V} \, \{B_c\} \, \dot{\delta}_o \phi(s)$$

$$- \frac{Q}{V} \, \{B_c\} \, (\dot{\delta}(S)*y(S)) + GUST + \ldots\ldots\}$$

<u>Atmospheric Turbulence Input</u> - The gust input shown above is symbolic only. The program, as written, has the option of either discrete gust or equivalent random turbulence inputs.

Discrete gusts such as an impulse or a (1 - cos) shape may be represented by straightforward functions of time.

Random turbulence is represented as an "equivalent deterministic input" by the procedure of Reference 22. The turbulence is described by the spectral shape,

$$\phi_{u_g \, u_g} \, (\omega) = \frac{2\omega_b \, \sigma_{u_g}^2}{\omega^2 + \omega_b^2}$$

where,

u_g – random gust velocity

$\phi_{u_g u_g}(\omega)$ – gust input power spectral density

ω_b – break frequency of the gust input spectrum

σ_{u_g} – standard deviation of the gust disturbance and is given by:

$$\sigma_{u_g}^2 = \frac{1}{2\pi} \int_{-\infty}^{\infty} \phi(\omega) \, d\omega$$

The input gust is assumed to have a Gaussian amplitude probability distribution with zero mean. The equivalent deterministic input (or transient analog) is obtained by the expression,

$$\phi_{u_g u_g}(S) = \left| U_g(S) \, U_g(-S) \right|_{S=i\omega} = \left| \frac{u_g(0)}{S+\omega_b} \quad \frac{u_g(0)}{-S+\omega_b} \right|_{S=i\omega}$$

where

$$u_g(0) = \sigma_{u_g} \sqrt{2\omega_b}$$

Therefore,

$$U_g(S) = \frac{\sigma_{u_g} \sqrt{2\omega_b}}{S + \omega_b}$$

The inverse Laplace transform gives,

$$u_g(t) = \sigma_{u_g} \sqrt{2\omega_b} e^{-\omega_b t}$$

which is the specific deterministic input that represents the gust spectra in question. With this input, the integral of any squared parameter of interest becomes the variance of that parameter when steady-state conditions are reached. This method of gust representation is well suited for the fast repetitive operations of an analog computer, or this equivalent MIMAC program since no time averages or repeated trials are required. It should be pointed out that the time histories of the responses are of no significance and are merely tools used to obtain the correct statistical answers.

I" 1.4 MIMAC Control Loop Formulation – The equations of motion developed above represent the aeroelastic airframe in a closed-loop feedback

control system as shown schematically in Figure 23. The control blocks
accept a second order ratio of Laplace transforms of the form

$$\frac{a_{10} + a_{11}S + a_{12}S^2}{b_{10} + b_{11}S + b_{12}S^2}$$

The MIMAC program uses a solution technique based on standard form where
the highest derivative of each variable is expressed in terms of lower
order derivatives of the same variable and other known variables. For
example,

$$\ddot{Y}_7 = \frac{1}{b_{72}}(-b_{71}\dot{X}_7 - b_{70}X_7 + a_{72}\ddot{X}_6 + a_{71}\dot{X}_6 + a_{70}X_6)$$

is the expression for block No. 7. Because of this solution technique,
the coefficients b_{i2} may not be equal to zero. If, for example, block 7
is to be unity it must be expressed as

$$\frac{a_{72}S^2}{b_{72}S^2} \quad \text{where } a_{72} = b_{72} = 1.0$$

Similar logic applies for other transfer functions.

The transfer function block for the aeroelastic airframe allows for
the feedback of a linear weighted combination of the generalized
coordinates and their derivatives obtained from the current value of the
forced aeroelastic equations of motion. The expression in the program is

$$\ddot{X}_5 = C_1\ddot{q}_1 + C_2\ddot{q}_2 + \ldots\ldots + C_n\ddot{q}_n$$

The numerator of control block 6 is then used to indicate the order of the
response being sensed by the expression

$$\ddot{X}_6 = \frac{1}{b_{62}}(-b_{61}\dot{X}_6 - b_{60}X_6 + a_{62}\ddot{X}_5 + a_{61}\dot{X}_5 + a_{60}X_5)$$

where $a_{62} = 1.0$ gives acceleration feedback

$a_{61} = 1.0$ gives rate feedback

$a_{60} = 1.0$ gives deflection feedback.

IV.2 Active Control of Flutter Computer Program - Frequency Domain

IV.2.1 Unforced Aeroelastic Equations of Motion - Indicial Lift

Formulation - The equations of motion for the Indicial Lift formulation are expressed in the form.

$$M\ddot{q} + C\dot{q} + Kq + Q\,(A + A_c C^{-1}(k))\,q$$

$$+ \frac{Q}{V}\,(B + B_c C^{-1}(k))\,\dot{q} + \frac{Q}{V2}\,I\ddot{q} = 0$$

where $C^{-1}(k)$ is a symbolic expression for the time domain equivalent for the Theordorsen function of reduced frequency $k = \frac{b\omega}{V}$; $C(k)$.

$$q_j = q_{jo}e^{i\omega t}\quad,\ i = \sqrt{-1}$$

The equations of motion then appear as,

$$(-\omega^2\,[M + \frac{Q}{V2}\,I] + \{K + Q\,(A + A_c C\,(k))\}$$

$$+ i\omega\,[C + \frac{Q}{V}\,(B + B_c C(\lambda))]\}q = 0$$

for

$$C(k) = F(k) + iG(k)$$

$$F(k) = \frac{J_1\,(J_1 + Y_0) + Y_1\,(Y_1 - J_0)}{(J_1 + Y_0)^2 + (Y_1 - J_0)^2}$$

and

$$G(k) = \frac{J_0 J_1 + Y_0 Y_1}{(J_1 + Y_0)^2 + (Y_1 - J_0)^2}$$

where J_0, J_1, Y_0, Y_1 are the J and Y Bessel Functions of the first and second kind.

Further development of these equations leading to the classical V-γ (equivalent g) and V-ω solutions is presented in detail in Reference 23. The theory is essentially based on the incompressible, two-dimensional, unsteady flow theory of Reference 24 with sweep effects accounted for by the relationships of Reference 25. As formulated, however, the parameters reflecting aerodynamic lift, moment and aerodynamic center are specifically factored out so

272

that theoretical, experimental, or empirical data may be used to account for three-dimensional and/or compressibility effects. This idealization is based on the work presented in References 26 and 27. The Indicial Lift passive flutter analyses presented in this report have used this particular formulation.

The equations of motion, as programmed here, are written as,

$$\{(-\omega^2 [M + \tfrac{\rho}{2} I] + K + \tfrac{\rho}{2} V^2 A + \tfrac{\rho}{2} V^2 A_c F - \omega \tfrac{\rho}{V} VB_c G)$$

$$+ i (\omega C + \omega \tfrac{\rho}{2} VB + \omega \tfrac{\rho}{2} VB_c F + \tfrac{\rho}{2} V^2 A_c G)\} \{q\} = 0$$

These complex equations are evaluated repeatedly by a simultaneous solution technique for a specified airspeed (V) and parametric frequency (ω). The method for determining the passive flutter velocity with this procedure, using the Mikhailov Criterion, is described in Section 3.5.1.4.

IV.2.2 Unforced Aeroelastic Equations of Motion - Classical V-g (R+iI) Formulation - The equations for this alternate formulation are expressed in the form,

$$[M + \tfrac{\rho}{2} I] \ddot{q} + [C - \tfrac{\rho}{2} VB] \dot{q} + [K - \tfrac{\rho}{2} V^2 A] q = \{F\}$$

where for flutter $\{F\} = 0$

A and B are now complex functions of reduced frequency $k = \dfrac{b\omega}{V}$ instead of being matrices of constants as is the case with the Indicial Lift formulation.

The harmonic motion constraint of the form,

$$q_i = q_{i_o} e^{i\omega t}$$

is assumed where the real part of q_j is of interest and the imaginary part is ignorable. This substitution leads to the equations,

$$([K + i\omega C] - \tfrac{\rho}{2} V^2 [\text{Re } A + i \text{ Im } A]$$

$$+ \tfrac{\rho}{2} V\omega [\text{Im } B - i \text{ Re } B] - \omega^2 (M + \tfrac{\rho}{2} I)) \{q\} = 0$$

The classical V-g procedure now divides by,

$$\pi \rho b_o^4 \omega^2$$

replaces the viscous damping matrix

$$\omega C$$

273

by an equivalent diagonal structural damping expression,

$$gK$$

which is proportional to displacement and inphase with velocity, and recognizes that,

$$\frac{V}{b_o \omega} = \frac{1}{k}$$

This leads to the equations,

$$[\frac{1 + ig}{\pi \rho b_o^4 \omega^2} K - \frac{1}{2\pi b_o^2 k^2} (Re\ A + i\ Im\ A)$$

$$+ \frac{1}{2\pi b_o^3 k} (Im\ B - i\ Re\ B) - \frac{1}{2\pi b_o^4} I - \frac{1}{\pi \rho b_o^4} M]\ \{q\} = 0$$

Define now,

$$\Omega = \frac{1}{\pi \rho b_o^4 \omega_o^2}\ K$$

$$\lambda = (\frac{\omega_o}{\omega})^2\ (1 + ig)$$

$$\sigma_o = \frac{1}{\pi \rho b_o^4}\ M$$

and the aerodynamic matrices,

$$R = \frac{1}{\pi b_o^2} [- \frac{1}{2k^2} Re\ A + \frac{1}{2b_o k} Im\ B - \frac{1}{2b_o^2} I]$$

$$I = \frac{1}{\pi b_o^2} [- \frac{1}{2k^2}\ Im\ A - \frac{1}{2b_o k}\ Re\ B]$$

The R+iI matrices are calculated by aerodynamic subroutines of a general flutter deck according to the above expressions to fit the equation as,

$$[\lambda \Omega + R - \sigma_o + iI]\ \{q\} = 0$$

or in terms of an eigenvalue formulation,

$$[R - \sigma_o + iI]\ \{q\} = -\lambda \Omega\ \{q\}$$

The solution is for the eigenvalues λ from which are obtained the V-g and V-ω data as,

274

$$g \quad = \operatorname{Im} \lambda / \operatorname{Re} \lambda$$

$$\omega \quad = \omega_o / \sqrt{\operatorname{Re}\lambda}$$

$$V_{KEAS} = \frac{1}{k} \, \gamma \omega$$

where

$$\gamma = .5921 \, b_o \, \sqrt{\frac{\rho}{\rho_{SL}}}$$

(.5921 is the conversion factor from ft/sec to knots)

We can recast these equations in a form suitable for a frequency response type solution by multiplying through by $\pi \rho b_o^4 \omega^2$ and replacing gK by ωC since we no longer have any need for a diagonal damping matrix. This leads to the equations,

$$[K + i\omega C - \omega^2 M + \pi \rho b_o^4 \omega^2 (R + iI)] \{q\} = 0$$

which can be evaluated in a manner similar to the previous formulation using the Indicial Lift expressions.

Any aerodynamic theory subroutine such as those for strip theory, kernel function, doublet lattice or Mach box may be executed to write a tape of $R+iI$ data for from 100 to 200 values of $1/k$. An interpolation procedure is required with the kernel function, doublet lattice and Mach box theories in order to be economically acceptable. The strip theory formulation is competitive even without interpolation.

For a judiciously chosen list of k_1 and a specified V and b_o the ACF program calculates a parametric frequency,

$$\omega_i = \frac{V k_i}{b_o}$$

for each ki.

The aerodynamic matrices are calculated as,

$$\pi \rho b_o^4 \omega_i^2 [R]$$

and

$$\pi \rho b_o^4 \omega_i^2 [I]$$

for each ω_i.

There is a complete change of the coefficients in the aerodynamic matrices for each value of the parametric frequency. The general approach is illustrated conceptually in Figure 145 where the lines of constantly changing slope represent the classical V-g eigenvalue approach and the constant velocity cuts represent the ACF frequency response technique. The Mikhailov stability criterion applies to this alternate R+iI procedure just as it does with the constant coefficient Indicial Lift formulation.

IV.2.3 <u>Frequency Response Functions for Forced Aeroelastic Equations of Motion</u> - The complex equations of motion for either of the preceding aerodynamic formulations are solved simultaneously for the specified airspeed (V) and frequency (ω) to obtain the response of each generalized coordinate to the forcing function. The method used for the forcing function excitation is the same as described in Section IV.1.2 for the time domain program.

The frequency response functions for the forced aeroelastic system are sensed by sensors located at any point in the aeroelastic system. The sensor output is calculated by the weighted sum of the individual generalized coordinates response by the general symbolic equation,

$$\left(\frac{\theta_{out}}{q_{F_1}}\right) = S^n \left[\phi_1 \frac{q_1}{q_{F_1}} + \phi_2 \frac{q_2}{q_{F_1}} + \ldots \ldots\right]$$

where n denotes the response type,

n = 0 gives deflection

n = 1 gives rate

n = 2 gives acceleration

To explain the use of this equation more explicitly let us consider a simple example. Figure 146 defines three generalized coordinates for an aircraft or missile.

q_{00} - Rigid body translation - ft.

q_{02} - Rigid body pitch - radian

q_{51} - First normal body bending mode - ft.

The diagram also applies for higher order aircraft elastic modes in the same sense as for q_{51}. The vibration modes for this system are assumed to be orthogonal with both themselves and the rigid body degrees of freedom. Thus, at zero airspeed there is no modal coupling. There is, of course, always aerodynamic coupling in the case of an airborne vehicle.
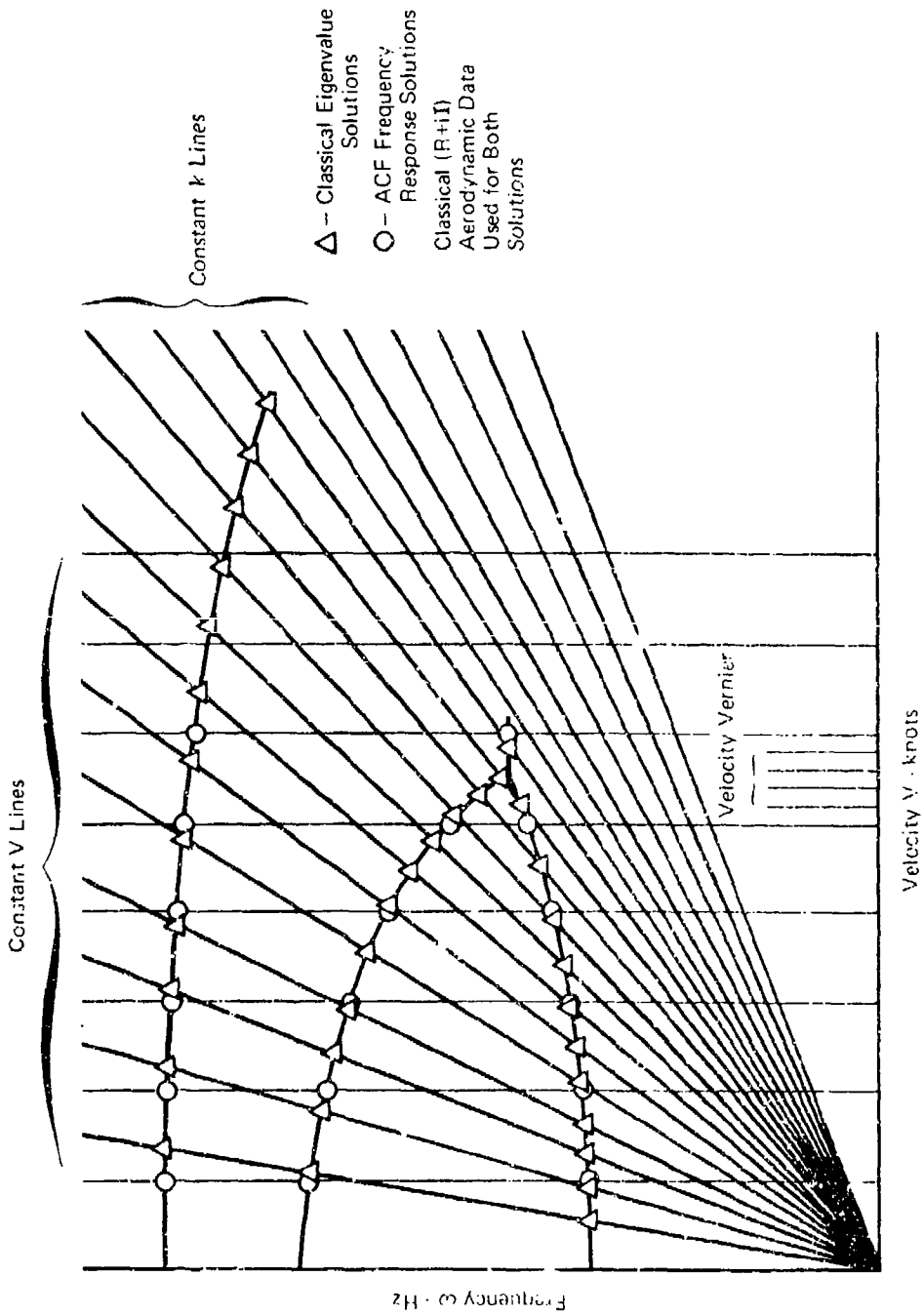
FIGURE 145 COMPARISON OF CLASSICAL EIGENVALUE AND FREQUENCY
RESPONSE FLUTTER SOLUTION TECHNIQUES
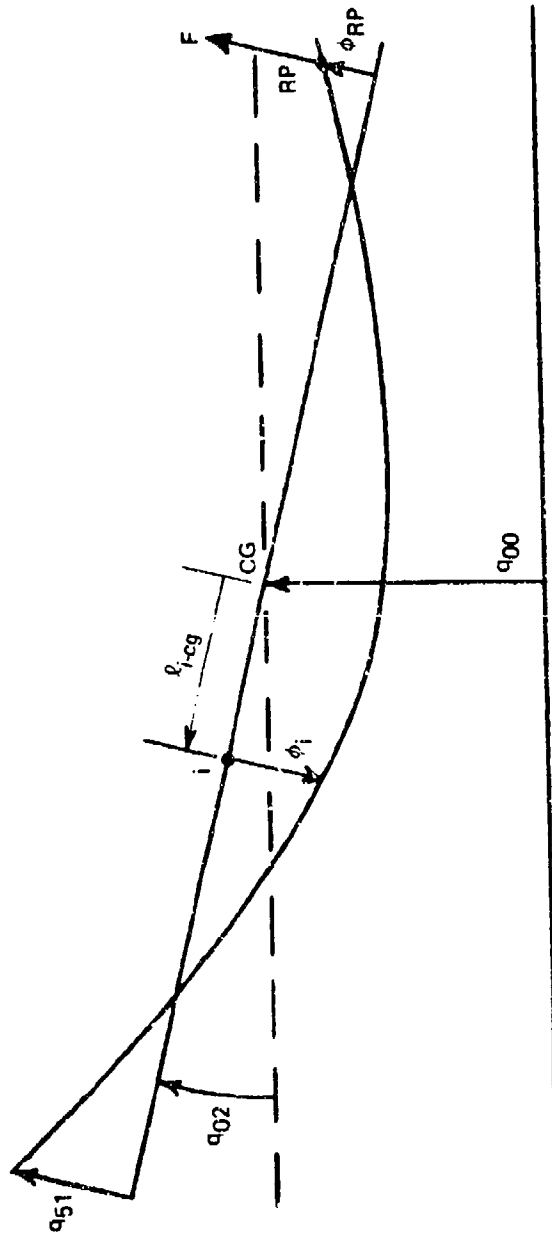
FIGURE 146 COORDINATE DEFINITION FOR EXAMPLE ILLUSTRATING USE OF
GENERAL RESPONSE EQUATION

278

For a harmonically oscillating system, it is easy to show that the total acceleration of the body at point i is,

$$a_i = -\omega^2 [q_{oo} + \ell_{i-cg} \, q_{02} + \phi_i \, q_{51}]$$

In terms of transfer functions, the acceleration in g's sensed by a body mounted accelerometer at point i in response to an excitation force F is,

$$\frac{g_i}{F} = \frac{-\omega^2}{32.2} \left[\frac{q_{oo}}{F} + \ell_{i-cg} \, \frac{q_{02}}{F} \, + \, \phi_i \, \frac{q_{51}}{F}\right]$$

A similar expression for a rate gy sensing at point i is,

$$\frac{\dot{\theta}_i}{F} = i\omega \left[\frac{q_{02}}{F} + \frac{d\phi}{dx_i} \, \frac{q_{51}}{F}\right]$$

An application of Lagranges equation to this system leads to the matrix equations of motion,

$$-\omega^2 \begin{bmatrix} \sum\limits_i m_i & 0 & 0 \\[2ex] 0 & \sum\limits_i m_i \, \ell_{i-cg}^2 & 0 \\[2ex] 0 & 0 & \sum\limits_i m_i \, \phi_i^2 \end{bmatrix} \begin{Bmatrix} q_{oo} \\[2ex] q_{02} \\[2ex] q_{51} \end{Bmatrix}$$

$$+ \begin{bmatrix} 0 & 0 & 0 \\[2ex] 0 & 0 & 0 \\[2ex] 0 & 0 & \omega_{51}^2 \sum\limits_i m_i \phi_i^2 \end{bmatrix} \begin{Bmatrix} q_{oo} \\[2ex] q_{02} \\[2ex] q_{51} \end{Bmatrix}$$

$$= \begin{Bmatrix} 1.0 \\[2ex] \ell_{cg-RP} \\[2ex] \phi_{RP} \end{Bmatrix} F$$

where F is a force acting at reaction point RP. These equations may be easily solved for the transfer functions,

$$\frac{q_{00}}{F} = \frac{1}{-\omega^2 M}$$

$$\frac{q_{02}}{F} = \frac{\ell cg - RP}{-\omega^2 I}$$

$$\frac{q_{51}}{F} = \frac{\phi_{RP}}{-\omega^2 m_{51} + K_{51}}$$

where

$$M = \sum_i m_i \qquad \text{- total vehicle mass}$$

$$I = \sum_i m_i \, \ell_{i\text{-}cg}^2 \qquad \text{- total vehicle moment of inertia about the center of gravity}$$

$$m_{51} = \sum_i m_i \, \phi_i^2 \qquad \text{- generalized mass for vibration mode } q_{51}$$

$$K_{51} = \omega_{51}^2 \, m_{51} \qquad \text{- effective spring constant for vibration mode } q_{51}$$

It is seen in the last transfer function why it is customarily said that m_{51} is a generalized mass located at the mode normalization point. The effective spring K_{51} is also realistically viewed as being there.

Nothing has been said concerning the basic nature of the excitation force F. In general, this force may be any reasonable function of ω. There is, however, an implicit assumption in this simple example that F is not a function of the generalized coordinates q_{00}, q_{02}, and q_{51}. If aerodynamics is considered or if a feedback control system commands F in response to one of the sensor outputs then the force does become a function of the generalized coordinates. The resultant equations of motion are highly coupled and the transfer functions are best found by simultaneous numerical solutions of the equations of motion. Section IV.1.2 discusses the forced equations of motion in more detail.

IV.2.4 <u>Control Loop Calculations</u> - The sensor output functions represent the airframe dynamics in the two-loop control system shown in conceptual form in Figure 18. Blocks 5, 9 and 10 accept numerical data for each value of the parametric frequency ω. The control loop calculations are performed as described in Section 3.5.1.3. The assessment of dynamic stability by the Nyquist criterion is described in Section 3.5.1.4.

IV.3   MATLOC Computer Program

IV.3.1   _Description_ - MATLOC is a FORTRAN computer program which calcu-
lates and plots the closed-loop root locus over any parameter in a system
even when the open-loop poles and zeros are not known. MATLOC is unique
in that open-loop poles and zeros as well as plant gain are calculated
exactly. The user merely inputs (1) the equation of the system in matrix
form and (2) the locations of the locus parameter in the matrix. With this
information the open-loop poles and zeros are calculated and passed to a
root locus calculation program. This program subroutine is very efficient
since it uses a branch following technique and thus seeks locus points only
in a small neighborhood of the actual locus. Angle correction between itera-
tions is accomplished by a Newton-Raphson algorithm which seldom requires
more than two iterations between points. The MATLOC program plots the root
locus over any specified area of the S-plane, for any specified locus para-
meter.

IV.3.2   _Technique_ - Given a closed-loop system:
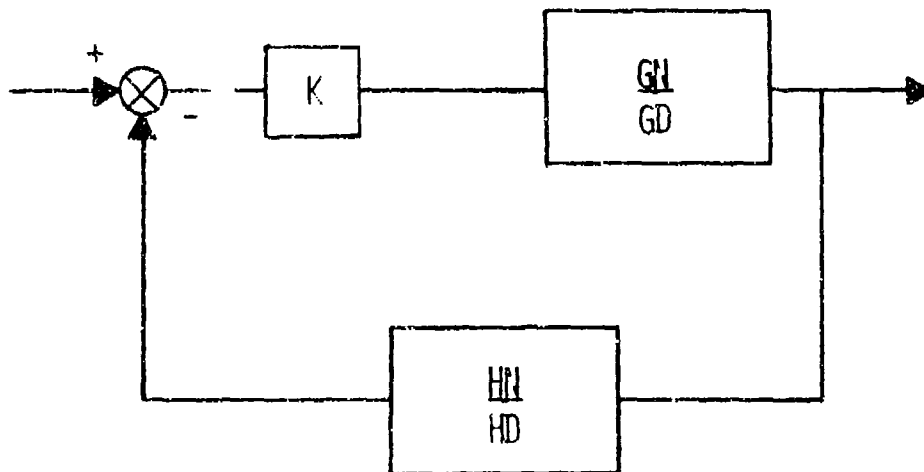
one can find the roots of the characteristic equation, (GD) (HD) + (K) (GN) (HN) = 0, as they vary over the parameter, K. This is done with the root locus technique by knowing the open-loop poles (roots of (GD) (HD) and the open-loop zeros (roots of (GN) (HN)). These open-loop poles and zeros are usually easy to determine. However, for complex multi-loop systems, these open-loop poles and zeros are usually not known and the root locus must be found by the inefficient process of finding the characteristic equation for a range of gains and solving for the roots.

These complex systems can be easily described by writing a set of simultaneous equations in the complex variable, S, and putting these equations in matrix form

$$\underline{A} \, \underline{X} = \underline{B} \, \underline{u}$$

where $\underline{X}$ is the vector of system variables and $\underline{u}$ is the vector of system inputs. Up to twelve (12) equations may be written to describe the system.

The determinant of the $\underline{A}$ matrix gives the characteristic equation of the system. By taking this determinant with the locus parameter set to zero, we obtain the open-loop pole polynomial, (GD)(HD) + (1) (GN) (HN). Subtracting the previously calculated pole polynomial, GD HD, from the new polynomial, (GD) (HD) + (1) (GN) (HN), gives the open-loop zero polynomial (GN)(HN).

In this way, it is only necessary to find the characteristic equation for two values of gain (0 and 1). This yields the open-loop poles and zeros so that the efficient Newton-Raphson circular algorithm may be applied to find the root locus. In addition, since the open-loop pole and zero polynomials are calculated exactly by this method, we can determine the system plant gain and divide it out if desired.

REFERENCES

1. "Aircraft Load Alleviation and Mode Stabilization (LAMS)", AFFDL-TR-68-158, The Boeing Company and Honeywell,Inc., December 1968.

2. Wykes, John H., and Mori, Alva S., "An Analysis of Flexible Aircraft Structural Mode Control", AFFDL-TR-65-190, Part 1, June 1966.

3. Wykes, John H., Nardi, Louis U., and Mori, Alva S., "XB-70 Structural Mode Control System Design and Performance Analyses", NASA CR-1557, July 1970.

4. Triplett, William E. and Ising, Klaus, D., "Computer Aided Stabilator Design Including Aeroelastic Constraints", Journal of Aircraft, Vol. 8, No. 7, July 1971.

5. Hooker, D. S., Kisslinger, R. L., Smith, G. R., Smyth, M. S., "Survivable Flight Control System Interim Report No. 1 Studies, Analyses, and Approach", Technical Report AFFDL-TR-71-20, May 1971.

6. Mikhailov, A. V., "Harmonic Analysis in the Theory of Automatic Control", Automatika i Telemkhanika, Moscow, 1938.

7. Landahl, M. T., "Graphical Technique for Analyzing Marginally Stable Dynamic Systems", Journal of Aircraft, Vol. 1, No. 5, 1964.

8. Nyquist, H., "Regeneration Theory", Bell System Journal, Vol. II, January 1932.

9. Katz, Henry, "Flutter of Aircraft with External Stores", Presented at the USAF Aircraft/Stores Compatibility Symposium, Fort Walton Beach, Florida, November 1969.

10. "Transonic Wind Tunnel Tests on a 13 Percent Semispan Model of the F-4E Airplane to Investigate Aerodynamic Loads on the Outboard Wing Panel and Leading Edge Slats", TR CAL-No. AA-4010-W-1, Cornell Aeronautical Lab, Inc., March 1970.

11. "Ground Vibration Test and Flight Flutter Test Results of the F-4 Aircraft with the MAC 370 Gallon Tank", McDonnell Aircraft Company Report E104, May 1969.

12. Harris, Cyril M., and Crede, Charles E., Shock and Vibration Handbook, Volume I, McGraw-Hill Book Company, New York, New York, 1961.

13. Houbolt, John C., Steiner, Roy, and Pratt, Kermit G., "Dynamic Response of Airplanes to Atmospheric Turbulence, Including Flight Data on Input and Response", NASA TR-R-199, June 1964.

14. Triplett, William E., "A Feasibility Study of Active Wing/Store Flutter Control", Journal of Aircraft, Vol. 9, No. 6, June 1972.

15. Amies, Gerald E., Clark, Cecil, Jones, Charles L., Smyth, M.S., "Survivable Flight Control System Interim Report No. 1 Studies, Analyses, and Approach, Supplement 3", Technical Report AFFDL-TR-71-20, May 1971.

16. "Aircrew Weapons Delivery Manual, USAF Series F-4C, F-4D, and F-4E Aircraft", Air Force Document No. T.O. 1F-4C-34-1-1, March 1970.

17. Taylor, Frederick R., "Designs to Reduce Aircraft Flight Control Vulnerability", AFFDL/FGL-TM-71-3, September 1971.

18. Pierce, N. J., and Thurston, C.T., "Hydraulic Circuit Breaker for Aircraft Hydraulic Systems", AFAPL-TR-70-50, Part 1, August 1970.

19. Becker, K.F., and Pedersen, N.F., "Research and Feasibility of an Integrated Servo Pump Actuator Package for Aircraft Flight Control, AFFDL-TR-71-19, January 1971.

20. "Survivability Assessment Guidelines for Flight Control Systems", AFFDL Contract F33615-73-C-3021, dated 1 October 1972.

21. Katz, Henry, Carlton, L.A., Clark, H.T., et al, "Investigation of an ECM Pod Installation for the Model F-4C Aircraft", SEG-TR-67-2, March 1967.

22. Magdaleno, Raymond and Wolkovitch, Julian, "Performance Criteria for Linear Constant-Coefficient Systems with Random Inputs", Systems Technology, Inc., ASD-TDR-62-470, January 1963.

23. Ferman, M.A., Burkhart, T.H., and Turner, R.L., "First Quarterly Report for Conceptual Flutter Analyses", BuWeps Contract NOw 66-0298-C, McDonnell Aircraft Company Report No. E549, March 1966.

24. Theodorsen, Theodore, "General Theory of Aerodynamic Instability and the Mechanism of Flutter", NACA Report 496, 1935.

25. Barmby, J.G., Cunningham, H.J., and Garrick, J.E., "Study of the Effects of Sweep on the Flutter of Cantilever Wings", NACA Report 1014, 1951.

26. Yates, C.E., Jr, "Calculation of Flutter Characteristics for Finite-Span Swept or Unswept Wings at Subsonic and Supersonic Speeds by a Modified Strip Analysis", NACA RM L57L10, March 1958.

27. Ferman, M.A., Burkhart, T.H., and Turner, R.L., "Final Report for Conceptual Flutter Analyses", BuWeps Contract NOw 64-0332-C, McDonnell Aircraft Company Report No. E350, December 1965.

DOCUMENT CONTROL DATA - R & D

(Security classification of title, body of abstract and indexing annotation must be entered when the overall report is classified)

1. ORIGINATING ACTIVITY *(Corporate author)*	2a. REPORT SECURITY CLASSIFICATION
McDonnell Aircraft Company McDonnell Douglas Corporation	Unclassified
	2b. GROUP N/A

3. REPORT TITLE

Active Flutter Suppression Systems for Military Aircraft
A Feasibility Study

4. DESCRIPTIVE NOTES *(Type of report and inclusive dates)*

Final Report - April 1971 - August 1972

5. AUTHOR(S) *(First name, middle initial, last name)*

Triplett, William E.   Landy, Robert J.
Kappus, Hans-Peter F.

6. REPORT DATE	7a. TOTAL NO. OF PAGES	7b. NO. OF REFS
February 1973	286	23

8a. CONTRACT OR GRANT NO. F33615-71-C-1481	9a. ORIGINATOR'S REPORT NUMBER(S)
b. PROJECT NO. 1370	AFFDL-TR-72-116
c.	9b. OTHER REPORT NO(S) *(Any other numbers that may be assigned this report)*
d.	

10. DISTRIBUTION STATEMENT

Distribution limited to U.S. Government agencies only: test and evaluation;
statement applied 27 Sept 72. Other requests for this document must be referred to
AF Flight Dynamics Laboratory, (FYS), Wright-Patterson AFB, Ohio 45433.

11. SUPPLEMENTARY NOTES	12. SPONSORING MILITARY ACTIVITY
	Air Force Flight Dynamics Laboratory Air Force Systems Command Wright-Patterson Air Force Base, Ohio

13. ABSTRACT

This analytical study of active flutter suppression systems for military aircraft was directed toward the accomplishment of two broad objectives:
1. Establish flutter modes, configurations, and flight conditions where active flutter control can show an advantage.
2. Formulate design guidelines and criteria to implement and test active flutter suppression systems.

To accomplish these broad objectives the study effort was divided into the three separate investigations listed below:
1. Wing/store flutter control study - to assess the practicality of extension of flutter boundaries for several store combinations.
2. All-movable horizontal tail flutter control study - to investigate both the potential payoff in future aircraft and the unique problems and difficulties when one of the participants in the flutter mechanism is used as the flutter control force producer.
3. Wing flutter control study - to parametrically evaluate the potential payoff in future aircraft by active flutter control of flutter critical primary lifting surfaces.

The studies showed that active flutter suppression systems are feasible and practical for any flutter mode which can be classified as mild or moderate flutter. Nearly all wing/store flutter cases are in this category. The advanced aircraft wing and horizontal tail configurations can be actively controlled if the aeroelastic system is first "tamed" by balance weight. It was found that the flutter control system could work successfully despite realistic hardware limitations and system nonlinearities in a tur-

13. ABSTRACT (Cont'd)

bulent environment. It was also determined that a fighter aircraft
flight control system and the flutter control system can share components
and coexist with minimal interference.

14. KEY WORDS	LINK A		LINK B		LINK C	
	ROLE	WT	ROLE	WT	ROLE	WT
Flutter						
Active						
Passive						
Control						
Suppression						
Aircraft						
Wing/Store						
External Store						
Primary Surface						